Spatial and temporal patterns in Holocene wildfire responses to environmental change in the northern extratropics

David Kesner

A thesis presented for the degree of
Master of Philosophy

School of Archaeology, Geography and
Environmental Science
University of Reading
United Kingdom

August 2022

Spatial and temporal patterns in Holocene wildfire responses to environmental change in the northern extratropics

David Kesner

Abstract

Fire is an important environmental process in the northern extratropics (NET), with various regions predicted to experience the highest magnitude increases in fire activity compared to other global regions in future. Previous NET palaeofire studies are limited by poor data availability and a lack of quantitative methods. A synthesis of charcoal records is conducted to reconstruct sub-continental-scale Holocene fire histories across the NET (>45°N) and to understand their environmental controls. A circum-NET-scale analysis, and a more spatially resolved analysis at the European scale (n of 21 regions) are conducted. At the NET scale, simulated palaeo climate and plant productivity data are used in a novel clustering method to define a stratification that delineates spatial units of coherent fire-relevant environmental change. At the European scale, this is done using pollen-based reconstructions of Holocene forest cover, summer temperature and precipitation change. Fire histories are reconstructed by aggregating charcoal records from the Reading Palaeofire Database within clusters. Fire reconstructions are correlated with climate and land cover reconstructions at 4000-year intervals. Fire responses of 20 regions show correlation values of >= |0.75| with at least one environmental variable for at least one 4000-year interval. Across Europe, fire increased over the Holocene, initially in response to the Fennoscandian Ice Sheet collapse and associated climate drying and forestation. Mid-to-late Holocene fire increases were caused by forest compositional shifts, human deforestation, and agricultural expansion. Across North America, the early-Holocene collapse of the Laurentide Ice Sheet caused continent-wide productivity increases leading to fire increases. A subsequent long-term moisture increase drove late-Holocene fire declines across most of the continent. In central Asia, a general Holocene-wide moisture increase drove a long-term fire decline. The results support previous study showing that sub-continental palaeofire histories in the NET are explained by variations in climate variables influencing fuel moisture and load, but that these effects can be modulated by land cover processes influencing fuel structure and composition. The results provide a basis for spatial prediction of fire regime changes in response to future climate, vegetation and human land use processes.

Declaration

I confirm that this is my own work and the use of all material from other sources has been properly and fully acknowledged.

David Kesner

Acknowledgements

I thank Patrick Bartlein (https://geography.uoregon.edu/profile/bartlein/) for calculating the variables needed to conduct this analysis (VPD and MI anomalies), and consistently providing useful advice and suggestions regarding the analysis design.

Contents

List of Figures

List of Tables

Introduction

Wildfire is a globally important environmental process influencing ecosystems, carbon cycling and human societies [1–3]. In many ecosystems, wildfire acts as an ecological disturbance, and is considered to have been important in shaping the evolution of various plant and ecosystem traits [4–6]. On a continental scale, fire is considered important for regulating biome distributions, for example by reducing tree cover, thereby limiting the distribution of forests [7, 8]. In modern times, changes in wildfire activity are threatening biodiversity in multiple habitats worldwide such as savannas, shrublands and forests, including through facilitating biological invasions [1, 9]. Wildfires are therefore of global conservation importance.

Recent model estimates show that the presence of fire in the earth system reduces global vegetation carbon storage by 10%, and by 17% in savanna systems [7]. Wildfire carbon emissions are also an important contributor to atmospheric carbon levels: the average annual mass of carbon emissions from wildfires between 1997-2009 has been estimated as $\sim$2 gigatons [2]. Fire carbon emissions are predicted to increase by 15% by 2100 relative to a 2016 baseline under a moderate emissions scenario as global fire probability is expected to increase in the coming decades [10–12]. Fire is therefore likely to have an increasingly important role to play in global carbon cycling in the 21st century.

Humans obtain a range of societal functions from the use of fire, including the facilitation of hunting, the prevention of future fires, pest elimination, pasture maintenance, and field preparation for agriculture [13, 14]. In recent times, wildfires have had severe negative consequences for human societies, with wildfire smoke being a major public health and economic concern [3, 15–17]. In a study investigating mortality risk associated with wildfire-related particulate pollution across 43 countries between 2000-2016, it was estimated that acute wildfire-related particulate exposure resulted in an average annual all-cause mortality of 33,510 [3]. Additionally, recent megafires are estimated to have caused billions of dollars in economic losses [16, 17]. For example, the 2016 Fort McMurray wildfire in northern Alberta, Canada, led to insured losses estimated at 3.58 billion dollars [17].

Given the current and probable future effects that wildfires will have on ecosystem dynamics, global carbon cycling, and social and economic systems, it is important to develop a reliable predictive understanding of wildfire in the earth system to be able to effectively manage present and future wildfires.

Modern wildfire controls

The current predictive understanding of wildfire in the Earth system has been developed mainly from studying wildfires in the modern era (e.g. [18, 19]). Weather conditions, climate, vegetation properties, and human activities are all shown to be important controls on modern fire activity [18, 19]. These

control fire across a range of temporal and spatial scales, may influence different characteristics of fire regimes, and interact with one another [4, 18, 20, 21]. This makes their combined effect on fire at any given scale a complex process to understand and predict.

On instantaneous to daily timescales, weather is considered an important control on fire because it determines fuel moisture, ignition probability, and fire spread [22–24]. In agreement with this, the weather variables shown to be important predictors of fire include measures of temperature, moisture, and wind speed: spatial patterns in observed 21st-century global burned area exhibit strong positive independent relationships to the number of dry days per month and vapour pressure deficit [18]. Furthermore, fire spread rate is shown to increase with wind speed and decrease with air moisture content in multiple ecosystems [22, 25, 26]. Humans and lightning strikes are important agents of modern wildfire ignitions [27, 28]. One study looking at 1.5 million fire occurrences across the United States between 1992-2012 found that human-ignited wildfires accounted for 84% of all fires and tripled the fire season length [28], while over the same period, the number of lightning-caused summer fires showed a significant positive trend.

On monthly to yearly timescales, variables indicative of fuel moisture, load, and continuity are shown to be important predictors of fire [18]. Annual net primary productivity (NPP), soil moisture deficit, and shrubby and herbaceous vegetation cover show positive independent relationships with global burned area [18]. Additionally, the aggregate of the various fire-related human activities at the global scale are thought to fragment and reduce fuel loads and therefore decrease fire, which is evidenced by studies showing that population density, an index of human presence and activity, relates negatively to global spatial patterns in fire [18, 19]. Human activities have also been implicated as the driver of an observed global decreasing trend in burned area between 1998-2015 [29]. However, a later study that assessed the spatiotemporal robustness of modern observed trends in burned area showed that the 1998-2015 burned area decline is not statistically significant and its magnitude varies strongly when varying the start and end years of analysis by a handful of years [20]. While these results imply that humans have not been driving a significant decline in global fire activity in recent decades, they are evidently an important control on its modern state through land use effects. This is supported by a recent multi-model assessment of fire effects on tree cover, which estimated that in the absence of land use, the global reduction in tree cover caused by fire between 2001-2012 would increase from 10% to 16% [7].

One study suggests that humans have had important effects on global fire trends at the centennial scale [30]. This study produced a charcoal-based reconstruction of global fire activity spanning the past 1000 years, showing a positive trend in burning from ∼1750-1870. This corresponds to evidence of widespread increases in population and land conversion for agriculture [31, 32]. However, from ∼1870 to the present, there is a global decline in burning, which occurs despite general increases in global temperatures during the 20th century [30, 33, 34]. This has been interpreted as the effect of human-induced vegetation fragmentation and fuel reduction from the previous century and their continued intensification from ∼1870 onwards [30–32]. While the evidence for human influences on global fire trends over the past ∼250 years is not quantitative or causative, the correspondence of the observed negative fire trend from ∼1870 onwards and the negative spatial human-fire relationship seen in modern modelling studies [18, 19] supports the argument that humans can be important agents of temporal variation in wildfire on a global scale. Indeed, one model estimate shows that human

population density alone accounts for a decline of 14% in global burned area between 1800-2005 [19].

In reality, controls on fire have important interactions, and this is evident when contrasting their independent and emergent fire relationships at the global scale [18, 35]. For example, annual logarithmic NPP exhibits a positive independent relationship with burned area, while its emergent relationship is unimodal [18]. This is attributed to the spatial relationship between productivity and moisture, the latter of which also shows a unimodal relationship with fire (annual precipitation in the tropics [36]). These patterns occur because high-productivity vegetation occurs in wet, humid regions where fuel is too moist to burn, while in low-productivity regions there is a low or discontinuous fuel load that cannot sustain high levels of fire activity [18]. This mechanistic explanation for the similarity between the emergent fire-moisture and fire-productivity relationships is known as the intermediate fire-productivity hypothesis [37]. Similarly, the emergent relationship of logarithmic population density with burned area is unimodal, despite its independent relationship being negative [18]. This is attributed to low-productivity regions generally being unable to support high population densities, and is therefore considered an artifact of the effect of fuel load (and, by extension, the mechanism described by the intermediate fire-productivity hypothesis) on burned area [18].

It is hypothesised that differences in plant morphological, biochemical, and structural characteristics result in differences in flammability among vegetation types, which exerts independent control on fire regimes [4, 5, 38, 39]. This is empirically supported by the positive independent relationship observed between burned area and shrubby and herbaceous vegetation cover [18]. Bistinas et al. [18] explained this pattern as due to the much faster decay rate of grass litter relative to woody litter [40], which results in a faster accumulation of dry fuel. Furthermore, a study of modern fire regimes in the circum-boreal region found a strong link between continental-scale patterns in fire regimes and tree species composition, which was not reflected in fire weather and fuel moisture indices [41]. In (coniferous) pines, thick bark and self-pruning are evolutionarily correlated traits which allow them to persist in flammable plant communities with low-intensity, fast-spreading fires by limiting the extent to which fire can reach their crowns [42–44], and insulating the base of the tree against fire damage [5]. Other pine species show a different set of adaptations in which they retain their lower branches and accumulate seed banks that are released after fire, indicating adaptation to the promotion of high-intensity crown fires [42, 43, 45]. This strategy is also exhibited by the dominant *Picea* species in the American boreal region, *P. mariana* [41, 44, 46, 47]. In the study by Rogers et al. [41], forests dominated by taxa with thick bark and self-pruning corresponded to a less intense, less severe fire regime relative to coniferous forests with species with no fire adaptations or with the *P. mariana* fire strategy, while broadleaf deciduous forests showed the lowest fire intensity measures of all forests studied [41]. These results agree with a study investigating effects of forest properties on fire occurrence across Canada, which separated forests into categories along a gradient from coniferous to deciduous dominance [48]. The study found that fire occurrence increased with coniferous tree representation in a given forest, with deciduous stands showing the lowest fire occurrence. These results highlight the important influence that plant composition can have on fire regimes.

Despite the insights gained from modern fire study, this knowledge is insufficient for comprehensively understanding and predicting fire in the earth system because it has been obtained using datasets that generally span less than 20 years [18, 20, 29, 35]. This time interval samples only a limited temporal subset of global burned area dynamics and its relationships to environmental change.

Furthermore, the wildfire patterns measured by these datasets are influenced by modern land management and settlement patterns, making it difficult to infer fire regimes that would occur in the absence of human influences or under different human land use patterns [49]. The fact that the observed recent decline in burned area is not statistically robust [20, 29] highlights that modern burned area datasets are too short to capture strong temporal variation in fire and its controlling variables that may be expected under future global change.

Data that spans longer timescales (e.g. millennia), over which the range of climate variability is much greater than on interannual timescales, and in which modern global-scale human effects on fire can be partitioned from background variability, are needed to gain a more robust understanding of the controls on fire in the Earth system. This is illustrated by Harrison et al. [50] who used millennial-scale (1-1700 CE) global biomass burning data to derive a statistically significant relationship between biomass burning emissions and land temperature, which did not emerge with a modern (2000-2014) biomass burning dataset. This demonstrates the implications of long-term data for the efficacy of future models because it enables the derivation of robust parameter estimates where modern data fails to do so. Using long-term datasets to understand fire is especially important for high-latitude environments with fire return intervals on the order of decades to centuries (e.g. [51]), where interannual datasets capture little to no information regarding their fire regimes.

Earth system dynamics on palaeo timescales

In order to contextualise changes to fire regimes and their controls that occur over palaeo timescales, it is necessary to understand the processes governing environmental variability on these timescales. Changes to environmental conditions on earth are fundamentally governed by changes to the global heat budget, which are principally influenced by insolation variability [52]. Changes to the global heat balance cause cascading effects on various earth system components, such as land ice cover and biogeochemical cycling, that ultimately result in changes to climate and vegetation controls on fire. Response times of the various components to the initial insolation changes differ substantially and depend on one another, thus they can be seen as independent forcing at different timescales [52].

Changes to insolation are caused by changes to orbital parameters (eccentricity, obliquity, and precession), which alter the seasonal and latitudinal distribution of insolation across the earth's surface on multi-millennial timescales [52]. From the last glacial period ∼22 thousand years ago (kya) to the modern period, the earth has undergone one precessional oscillation [53]. The precessional maximum occurred at ∼10kya, while obliquity reached a maximum at ∼11kya [53]. This led to a summer insolation maximum at the high latitudes between ∼11-10kya and a subsequent decline to the present day. Despite this insolation oscillation, which may be expected to result in an inverse pattern in ice cover, there has been a consistent decreasing trend in global ice cover from ∼22kya to the present day [54]. This counterintuitive pattern occurs because ice sheets take multiple millennia to respond to insolation changes, as feedbacks that regulate ice cover must first respond. For example, ice cover itself has control on the global heat balance through albedo forcing (and thus is to an extent self-regulating) [55–57]. Assuming a perfectly white ice sheet with maximum albedo, increased insolation striking the ice sheet will not accumulate more heat on its surface. The ice sheet will decline only in response to the accumulation of sufficient ambient heat in the climate and/or ocean systems.

Heat accumulation in the earth system (e.g. in the oceans) from insolation increases leads to

reductions in ice cover, hence inducing a positive feedback on global heat accumulation through reductions in planetary albedo. Global heat balance is coupled with atmospheric CO_2 concentrations, evidenced by temperatures and CO_2 being shown to closely covary on palaeo timescales [52, 58, 59]. Changes to greenhouse gas concentrations are an important influence on the earth's energy balance through their radiative forcing properties [60], hence CO_2 increases further intensify the positive feedback of global heat accumulation. The CO_2-temperature coupling can explain why ice sheets continue to decay despite multi-millennial declines in insolation. Indeed, both temperature and CO_2 are inversely related to global ice volume at the multi-millennial timescale [52, 61], and palaeo environmental indicators of temperature and CO_2 show a general increasing trend over the past 22 thousand years (ky) while global ice volume has continuously decreased [54, 58, 59].

Land-ice sheet declines involve freshwater inputs into the ocean in the form of ice or meltwater [62, 63]. Freshwater injection events since the last glacial period have been identified as resulting in and exacerbating slowed Atlantic meridional overturning circulation (AMOC) due to their effect on ocean salinity and temperature [64–67]. Major global cooling events have been attributed to this mechanism due to it resulting in reduced oceanic heat circulation to the high latitudes [65–68], which typically occurs centuries to millennia following freshwater inputs [52]. A major event associated with this mechanism happened between ∼17.5-15kya, during which freshwater events are thought to have caused a near cessation of AMOC by causing cold, shallow ocean water to trap deeper, warmer water below it, thus maintaining cold conditions in the North Atlantic [65]. The Bølling–Allerød warming event between ∼14.6-13kya in the northern hemisphere is associated with the restart of AMOC [66], as warm deep water that accumulated in previous millennia was recirculated to the high latitudes [69].

Millennial-scale changes to climate affect the spatial distribution of suitable climate space for plant types, which leads to vegetation-biome distribution shifts across continents [52, 70]. This is evidenced by observed differences in the global distribution of plant types at the last glacial period compared to the mid-Holocene [71]. Vegetation responses to climate change typically occur on centennial timescales [52], evidenced by pollen-based vegetation observations over the Bølling–Allerød interstadial [72]. These show that the boreal forest greatly expanded in Eurasia within a 15-14kya time interval, suggesting that the climate warming of the Bølling–Allerød starting ∼14.6kya alleviated limits on forest distribution and that a substantial range shift occurred within a few centuries.

In summary, major centennial-to-millennial-scale climate and vegetation changes have occurred in response to the multiple earth system changes that have followed insolation variability since the last glacial period ∼22kya. Given the understanding of climate and vegetation controls on fire (e.g. [18]), these changes are likely to have led to extreme changes to global and regional fire regimes over palaeo timescales, with no analogues in the modern remote-sensing era.

The palaeofire observational record

There are multiple environmental indicators that have been used to study how fire responds to Earth system dynamics over palaeo timescales (methane: [73]; carbon monoxide: [74]; levoglucosan: [75]; black carbon: [76]; vanillic acid: [76]; tree-ring scars: [77]; charcoal: [78]). Each indicator has strengths and weaknesses with respect to the spatial and temporal resolution and accuracy with which they record palaeofire activity. Methane, carbon monoxide, levoglucosan, black carbon and vanillic acid are derived from ice-core records, which provide a geographically integrated fire signal

over continental scales. Furthermore, methane and carbon monoxide are well-mixed atmospheric gasses [79] and therefore are limited to being used to infer palaeofire activity at the global scale. Fire histories reconstructed from tree rings are spatially limited to forested areas. Unlike ice-core and charcoal records, which can record fire activity over multiple glacial cycles, tree-ring-based fire histories are temporally limited by the lifespan of the recording tree and/or the time taken for dead recording material to decay unless fossilised or preserved in some way.

Charcoal accumulation in sediments is sensitive to fires that burn both within and outside of the catchment of the depositional environment, but is shown to be more responsive to fires that are in closer proximity to the site of deposition [80–83]. This facilitates investigation of spatial patterns in biomass burning from the catchment to the global scale through the aggregation of individual records. Charcoal therefore stands out as the most suitable indicator for studying millennial patterns in fire evolution at sub-continental scales, because it overcomes the spatial and temporal limitations of other palaeofire indicators. Charcoal has been validated as a reliable palaeofire index at multiple spatial scales and in different regions, exhibiting high correlations with independent fire evidence such as: historical documentation (Alaska [51]; Western United States [77]; southern Switzerland [84]); tree-ring burn scars (Yellowstone National Park, United States [85]; Western United States [77]); and the global methane fire record [50].

Global palaeofire controls

Sedimentary charcoal records have contributed greatly to the understanding of palaeofires and their controls at the global scale [78, 86, 87]. Multiple global palaeo charcoal syntheses have shown that there has been a general increase in global biomass burning between 21-0kya, consistent with the shift from glacial to interglacial conditions and accompanying increases in CO_2, temperatures, and plant productivity [78, 86, 87]. Daniau et al. [87] used a univariate Generalised Additive Model (GAM) analysis to quantify the effects of simulated mean annual temperature and precipitation (MAT and MAP) on fire between 21-0kya, using separate models for either predictor. The analysis showed a positive fire-MAT relationship in which MAT explained two thirds of the overall fire variance. This is consistent with modern independent relationships found between temperature variables and fire [18]. Daniau et al. [87] further showed a unimodal response of fire to MAP in which MAP explained 14% of the fire variance. This is consistent with the modern observation of a unimodal emergent relationship between precipitation and burned area, and agrees with the intermediate fire-productivity hypothesis corroborated in the satellite era [18, 36, 37]. Considering that the simulated dataset used in the GAM analysis reproduces several major features of climate evolution since the last glacial period [88, 89], these results point to atmospheric temperature and moisture variables as robust indicators of fundamental fuel moisture and load controls on fire, and also suggest that they are robust at measuring these controls across interannual to palaeo timescales.

The evidence of increased global fire activity over the Holocene corresponds to evidence of fire use by humans for landscape modification and deforestation in various regions of the world (e.g. [90–92]). In light of this, Carcaillet et al. [93] hypothesised that human activities were the cause of the continental-scale increases in Holocene palaeofire activity revealed in their charcoal-based reconstructions. This hypothesis is contradicted by the absence of evidence supporting it in later charcoal syntheses investigating anthropogenic effects on palaeofires at continental and global scales [30, 94, 95].

This implies that human effects on fire at these spatial scales are exclusively a feature of the modern period. Importantly, this does not preclude human palaeofire effects at sub-continental scales.

The northern extratropics as a palaeofire study system

The boreal systems of the northern extratropics (NET) are estimated to contain 22% of the carbon sinks contained in established forests globally [96], highlighting the potential magnitude of carbon these systems could release to the atmosphere as wildfire emissions. Recent findings suggest that northern boreal carbon emissions have been increasing in recent decades, and wildfires have accelerated this carbon loss [97, 98]. Various NET regions are predicted to undergo the highest magnitude increase in fire activity relative to other regions of the globe in future decades [10], with general increases in severity of fire weather and head fire intensity predicted for Eurasian and North American boreal forests by the end of the 21st century [99]. These findings imply that the boreal region will undergo extreme ecological and biogeochemical changes under enhanced fire activity in future, potentially acting as a major carbon source to the atmosphere. The global relevance of the NET boreal region with respect to fire effects on global carbon cycling highlights why it is important to study fire in this region.

There are advantages to studying palaeofires in the NET because of the major environmental reorganisations it has experienced over millennia [64, 72, 100, 101]. For example, the last glacial-interglacial transition was largely driven by the deglaciation of the NET continental ice masses [64, 67, 102]. Over the Holocene, climate changes across the NET have varied widely over space, with different sub-continental-scale climates fluctuating by multiple degrees and with different temporal patterns [103–106]. This is expected given the different glacial histories of different NET regions. For example, in the early Holocene, the Laurentide Ice Sheet (LIS) retreated over North America towards the east of the continent, terminating over Quebec around ∼7kya [102]. Conversely, in Eurasia, the Fennoscandian Ice Sheet retreated to a final position over central Scandinavia where it terminated ∼9.9kya [107].

In addition to the heterogenous environmental history of the NET, the region is characterised by geographic and topographic variation, which adds further complexity to its climate space. For example, Europe's maritime location makes it characterised by an oceanic climate primarily influenced by the North Atlantic Oscillation (NAO) [108]. The NAO is characterised by fluctuations in north Atlantic meridional atmospheric pressure gradients that change the strength of westerly winds over Europe [108]. Eastern continental Europe is primarily influenced by the colder, continental Siberian High climate system [109, 110]. Added to this climatic complexity is the presence of various mountain ranges in the NET that can create spatial discontinuities in regional climate, such as the Scandinavian and Swiss Alps, the Romanian Carpathians, and the Altai Mountains in central Asia.

Fire-relevant land cover changes have occurred widely across the Holocene NET in response to environmental changes [46, 72, 101]. For example, an early-Holocene expansion of mixed-deciduous broadleaf tree cover across Europe and a reduction in coniferous needleleaf tree cover in central Europe is observed in multiple pollen record syntheses [72, 101, 111]. This occurred in response to the Fennoscandian Ice Sheet melt in Scandinavia, which exposed new land for plant colonisation, as well as the accompanying large climate shifts. For example, multiple-degree increases in summer and winter temperatures are observed in the early Holocene across large regions of Europe [105]. In central

boreal North America, a large expansion of coniferous needleleaf trees is observed between ∼7.6-5.6kya following exposure of this land by the retreating LIS in the early Holocene [46].

Palaeo environmental and archaeological evidence suggests that humans have been important agents of pasture and cropland expansion as well as deforestation from at least the mid-Holocene in Europe and Asia, and for centuries in North America, and probably commonly used fire as a landscape modification tool [90–92, 101, 112–115]. Estimates of cropland expansion show that Europe saw a greater rise in agriculture from the mid- to the late-Holocene relative to North America [32]. Additionally, observed European forest cover declines result in estimates of forest cover that fall outside the range of prior background variability from ∼4kya [101]. This implies that human land use had an important influence on European vegetation from the mid-Holocene, to much greater effect than in North America. The combination of spatially variable Holocene climate, land cover, and human histories across the NET is likely to have resulted in a diversity of Holocene fire regime dynamics at sub-continental scales, making the NET an apt palaeofire study system.

Existing evidence for palaeofires in the northern extratropics

Existing palaeofire studies that have focused on the NET have corroborated the increase in global fire activity observed with the shift from glacial to interglacial conditions, as well as the global positive fire-temperature relationship at sub-continental, continental and circum-NET scales [77, 87, 94, 116]. One study used a GAM to quantify the relationships between fire and simulated summer temperature data (which had been corrected for systematic simulation biases using observational data) for 12-8kya and 8-0kya respectively in three sub-regions of Europe [116]. In line with previous findings, temperature showed a positive fire relationship in all three sub-regions for the 12-8kya period. However, it showed a negative fire relationship over most of the 8-0kya period. The contrasting effect of temperature on fire between these two periods can be explained by the Holocene vegetation compositional changes that occurred across Europe. The authors used pollen-based reconstructions of vegetation and land use changes in relation to fire in their GAM analysis, showing that biomass burning was affected by tree cover, but that its relationship depended on forest type: broadleaf tree cover had a negative effect on fire, while needleleaf cover increased fire [116]. The general decline in summer temperatures over the mid-to-late Holocene corresponded to a long-term decline in broadleaf cover and a corresponding increase in fire. These contrasting effects of broadleaf and needleleaf cover on fire activity, which in this study led to an exception to the widely reported positive fire-temperature relationship, agrees with interpretations of fire relationships to vegetation in other sub-continental NET palaeofire analyses (Northeast Europe: [117]; Alaska: [118]) as well as modern findings [41, 48]. This points to the importance of accounting for broadleaf and needleleaf tree cover change when identifying controls on palaeofire variation.

Feurdean et al. [116] show that for the 8-0kya GAM analysis, fire generally responded positively to three indices of human landscape modification, deforestation, and agricultural activity, namely arable and disturbed land cover, grassland and pasture cover, and heath and scrubland cover. Increases in arable and disturbed and grassland and pasture cover above ∼16% showed strong monotonic positive relationships with fire, whereas these relationships were attenuated below this level. These land cover types increased above ∼16% in continental Europe in the late Holocene, especially in the last 1.5kya [101], suggesting that human effects on land cover would have led to increases in burning during this

time. Additionally, reductions in total tree cover occurring within the ∼40-57% range were shown to increase burning in this study. This is explained by reduced tree cover leading to a more open landscape that increases radiative energy reaching the forest floor, creating a drier and more wind-exposed sub-canopy layer that increases fire probability [119]. Additionally, tree cover affects ground-layer fuel characteristics of forests, with less dense forest facilitating a continuous ground layer of fine grassy and shrubby fuels that ultimately increases the probability of burning and fire spread [120].

Forest cover reductions in Europe over the Holocene are evidenced to have been human-induced [90–92, 101, 112–115]. It is difficult to identify to what extent the changes in fire with the late-Holocene landscape changes in Europe are due to human-set fires for forest clearance, agricultural expansion, and land management, or are a consequence of changes in fuel load and structure that these activities would have induced. Additionally, it can be difficult to disentangle human and climate effects on fire as they are often confounded [121, 122]. Indeed, climate changes in mid- to late-Holocene in Europe can explain forest cover losses in many regions [113].

Identifying palaeofire environments

Previous charcoal studies have derived much novel information about wildfire and its controls by reconstructing fire histories for specific regions. This has been done by synthesising multiple charcoal records into regionally aggregated fire histories (composites). For this type of analysis to be informative, reliable methods to spatially delineate geographic regions in which to generate composites are required. This is important for identifying well-constrained patterns in fire and its controls, as delineating regions that span wide ranges in fire-controlling environmental variance will result in high composite noise. The term 'palaeofire environment' is defined here as an idealised spatial unit within which fire-controlling variables vary coherently over palaeo timescales. For example, assuming summer temperature controls fire, the summer temperature responses at any two locations within a given palaeofire environment will be similar, and will differ from summer temperature responses at any point outside of the palaeofire environment. This concept is useful to illustrate the attempt to define spatial units that maximise the similarity of fire-relevant environmental change within them while minimising it among them. This is done ultimately to optimise the robustness of the resultant fire and environmental composites and hence the ability to constrain robust fire-environment relationships.

In previous charcoal syntheses, a typical method used to delineate spatial regions has been to separate the globe into latitudinal zones, for example, the NET, tropics, and southern extratropics [30, 87]. This approach is motivated by the expectation that fire responses will vary among these zones due to their different respective environmental histories [52]. Alternatively, regions have been defined based directly on the variation contained within individual charcoal records. For example, Vannière et al. [123] used a Principle Components Analysis applied to time series analysis of charcoal accumulation rate and fire frequency from 18 sites in southern Europe. The sites disassociated into three distinct elevational categories. Since elevational change represents an environmental gradient, this suggests that this method is effective at approximating palaeofire environments. Another approach is the use of a modern environmental stratification based on vegetation or climate, under the assumption that climate / vegetation patterns in modern times approximate palaeofire environments. Feurdean et al. [116] successfully use this approach based on the Environmental Stratification of Europe classification from Metzger et al. [124].

The latitudinal zonation approach of Daniau et al. [87] assumes a longitudinally uniform change in environmental space with latitude, and does not account for other sources of environmental variation like elevational gradients. It is therefore only useful for continental or hemisphere-scale fire syntheses. The Vannière et al. [123] approach of directly clustering individual charcoal-record variation may be inappropriate for defining borders among palaeofire environments at larger spatial scales than the scale of that study, as charcoal accumulation in sediments is shown to best record fires within tens of kilometres from a given coring site [51, 85], and the key patterns of fire variation at larger scales are revealed only when aggregating multiple records [78]. Additionally, robustly clustering individual charcoal records would require imposing filtering criteria on the records based on temporal length and time series continuity, and charcoal records vary widely in these criteria [125]. Lastly, the modern environmental stratification approach of Feurdean et al. [116] does not integrate palaeo environmental change and thus assumes static environmental space over time, which may preclude the detection of regions with different environmental trajectories in the palaeo record.

Research gaps in northern-extratropical palaeofire study

Most of the palaeofire syntheses focusing on the NET have explored continental-scale or circum-NET trends [30, 78, 87], and a small number of studies have focused on isolated sub-continental regions [51, 116, 123, 126]. The global charcoal synthesis of Marlon et al. [94] represents the most comprehensive sub-continental-scale synthesis of NET palaeofire evolution to date. They reconstruct Holocene fire composites for the British Isles, northeastern and central Europe, the Mediterranean, northwestern America, the western US, central North America, and the St. Lawrence region. Despite this, their fire reconstructions are limited by spatial biases in site coverage, which limit the geographic scope of the study. Spatial regions over which charcoal records are aggregated in Marlon et al. [94] have been defined as spatially discontinuous boxes covering regions of relatively high charcoal-record presence. Furthermore, many of the composites are composed of a low number of records, thereby limiting their robustness: the composites for central Europe, northeastern Europe, the British Isles and central North America are composed of less than 20 sites over most of the Holocene. Important spatial gaps still remain in the NET palaeofire literature, including central Asia, central Europe, Alaska and boreal North America [78, 87, 94].

Since the Marlon et al. [94] study, the number of charcoal records available across the NET has been vastly increased and centralised within a recently published global charcoal dataset, the Reading Palaeofire Database (RPD) [125]. The RPD contains improved site coverage for previously data-sparse NET regions, and improved charcoal-record chronological control and data accuracy relative to the datasets used in previous syntheses [78, 87, 94, 125]. The RPD therefore facilitates a novel opportunity to update outdated composites for various NET regions as well as expand the spatial scope of palaeofire analysis to regions not previously explored in the palaeofire literature.

The Feurdean et al. [116] synthesis for central and eastern Europe is the most comprehensive charcoal synthesis exploring spatial patterns in Holocene fire evolution across Europe. Like the Marlon et al. [94] study, their spatial delineation based on modern environmental space is spatially discontinuous and boxy. It is clear that there is a need for a comprehensive, quantitative attempt at delineating realistic palaeofire environments for the NET, for the purpose of constraining robust regional fire composites. Therefore, the first aim of this work is to quantitatively delineate sub-continental-scale

palaeofire environments for the Holocene NET and constrain their composite Holocene fire responses using charcoal records from the RPD.

There is limited application of quantitative statistical approaches towards understanding environmental controls on the temporal variability in fire in the NET. The modelling analyses by Daniau et al. [87] and Feurdean et al. [116] are exceptions, which are limited to the semi-hemispheric scale and isolated sub-regions of Europe respectively. Most other syntheses employ qualitative time series comparison [30, 77, 78, 86, 94]. There is a need for a comprehensive, quantitative investigation of Holocene fire-environment relationships for the NET at the sub-continental scale. Therefore, the second aim of this thesis is to employ quantitative methods towards identifying the climate and land cover controls on the fire responses defined under the first aim.

Addressing the study aims is facilitated by the availability of comprehensive palaeo environmental datasets that span the NET [88, 89, 101, 127]. At the circum-NET scale, spatially continuous climate and NPP model outputs are available that span the last glacial-interglacial transition [88, 89]. Spatially continuous Holocene climate and land cover reconstructions based on observational data are only available for Europe [101, 127]. Hence, a well-resolved investigation of Holocene wildfire controls that can evaluate effects of multiple land cover variables is only possible for Europe. This work is therefore composed of two distinct analyses, both of which respectively address the study aims: a circum-NET-scale charcoal synthesis that focuses on investigating the effects of broad-scale changes to climate and productivity on fire; and a more spatially resolved analysis at the European scale that uses climate and land cover reconstructions to understand controls on fire over the Holocene.

Methods

The first step in addressing the study aims was to generate a spatially continuous stratification that approximates coherent palaeofire environments for the respective NET and European study regions. The approach taken to achieve this was to cluster the grid cells of the abovementioned environmental datasets based on their similarity in temporal variation of fuel moisture and load indices. The decision to select fuel moisture and load variables to define the stratifications was motivated by the various sources of evidence from modern and palaeofire study that consistently point to these variables measuring fundamental wildfire controls [18, 87, 116].

At the NET scale, the TraCE-21ka model simulation [88, 89] was used for defining the stratification. At the European scale, two gridded palaeo environmental reconstructions covering the Holocene were used, a climate dataset [105] and a dataset of tree cover percentages [127]. The next step in addressing the first aim was to reconstruct the Holocene composite charcoal curves for the respective palaeofire environments using the RPD. To address the second aim, the temporal trends in the reconstructed fire composite curves were compared with the temporal trends in environmental variables that are considered important palaeofire controls in a correlation analysis. This included the variables used to define the stratifications, in addition to various land cover indices from the Fyfe et al. [101] dataset.

Datasets

The TraCE-21ka dataset

The TraCE-21ka dataset is a transient simulation from a synchronously coupled ocean–atmosphere–sea ice–land surface general circulation model (GCM), the National Center for Atmospheric Research Community Climate System Model 3 (CCSM3) that contains a dynamic global vegetation module [88, 89]. Each grid box of the land model accounts for different land units (including glaciers, lakes, and wetlands) and contains multiple soil-column levels and plant-type categories [89]. The model does not account for anthropogenic influences on the simulated variables over palaeo timescales. The data is gridded at ∼3.71-degree latitudinal and 3.75-degree longitudinal resolution in the NET and spans the time interval 21kya to 1989 CE. This dataset is considered adequate for use in defining general spatial patterns of palaeofire environments across the NET because it reproduces several major features of climate evolution since the last glacial period, and shows good agreement with northern-hemisphere observational climate reconstructions [88, 89, 100]. While the TraCE-21ka dataset has a non-uniform latitudinal resolution, in the NET above 30 latitudinal degrees north (30N), the latitudinal values approximate uniformity when rounded to two decimal places: all successive differences between latitude values above 30N are 3.71 degrees except for the difference between the lowest and second-

lowest latitude value which is 3.72. Only the TraCE-21ka data between 30-75N was used in this analysis.

The fuel moisture and load variables derived from the TraCE-21ka dataset were NPP, annual moisture index (MI), and maximum monthly vapour pressure deficit (VPD). NPP measures the amount of carbon fixed in plant tissues by photosynthesis per unit space and time after accounting for carbon lost through respiration. It is expressed as grams of carbon per square-metre per second, and is used here as a measure of fuel load. MI is defined as the ratio of annual precipitation to potential evapotranspiration and measures the amount of surface moisture availability and hence annually integrated fuel moisture. VPD is a measure of air dryness during the driest month in a given year, and is regarded as the main environmental control on the drying rate of dead fuel [18]. It is used here as an indication of maximal instantaneous fuel dryness during the year and hence captures seasonal effects on instantaneous fire probability.

The NPP data was obtained from the decadal-resolution TraCE-21ka dataset where it has been aggregated at a decadal time step. The VPD and MI variables were derived from default TraCE-21ka variables by a collaborator, Patrick Bartlein. The derivation of the VPD variable involved the use of functions native to the CCSM3 model (NCL: the "NCAR Command Language") [128, 129]. Hence, the VPD variable is technically a default feature of the core TraCE-21ka dataset. The MI variable was generated using a modified version of the SPLASH 1.0 model [130] in which the TraCE-21ka 2-metre air temperature, precipitation rate, net radiation, evaporation rate, and elevation variables were used as inputs (thereby bypassing the SPLASH 1.0 internal calculations of net radiation and evaporation). Unlike the NPP data which is provided as real values, both the VPD and MI variables are provided as anomalies relative to a 1975 CE mean value. These means were generated using a tricube-weight function with a 30-year window half-width. Both variables are supplied at decadal resolution, but they were generated by aggregation from monthly resolution. VPD is supplied as decadal climatologies i.e. each time step contains 12 data points representing monthly values averaged over a decade. Prior to decadal aggregation, both variables had their monthly values adjusted for the "paleo-calendar effect" [131] as this was shown to have an important influence on the decadal values (personal communication, Patrick Bartlein).

In addition to the MI, VPD, and NPP variables used to generate the stratification, decadally averaged growing degree days above 0°C (GDD) was obtained from the TraCE-21ka dataset, providing a measure of temperature change relevant for fuel load variation. This was used for the correlation analysis that followed the reconstruction of regional fire composites.

European climate and land cover datasets

The climate dataset used for the European-scale analysis is a gridded Holocene reconstruction based on pollen data [105]. The reconstruction incorporates the effects of palaeo geographic changes that occurred in Europe over the Holocene such as isostatic rebound and sea level changes. It is based on a rigorous modern pollen dataset of over 4700 samples, as well as a fossil pollen dataset comprising 879 pollen sites. It is currently the most up-to-date Holocene gridded climate reconstruction spanning Europe. The palaeo climatic values were reconstructed for each pollen sample using the Plant Functional Type Modern Analogue Technique [132, 133]. This assigns palaeo climate values to fossil pollen samples by assigning a given fossil sample the average climate value of its closest modern analogues. Prior

to matching fossil pollen samples with their modern analogues, the technique converts pollen taxa into plant functional types. This reduces the failure rate of the technique as a consequence of no-analogue fossil samples [132, 133]. The uniform spatiotemporal dataset was generated using a four-dimensional Thin Plate Spline interpolation through the pollen samples. The dataset is considered adequate for use in defining a palaeofire environment stratification because when it was evaluated against multiple independent climate reconstructions on a site-by-site basis, 78% of the independent reconstructions were qualitatively classified as a good or very good match. Furthermore, the 22% classified as a poor match nonetheless showed agreement that fell well within the combined confidence limits of the two records, and over half of these poorly matched independent reconstructions were based on methods that were found to be inconsistent for use in reconstructing climate [105].

The Mauri et al. [105] dataset provides nine climate variables, namely; mean summer (June-July-August), winter (December-January-February), annual temperature and precipitation, mean annual growing degree days, mean annual precipitation minus evaporation, and a moisture index variable. The dataset has a 1-arc-degree spatial resolution and a 1000-year time step spanning the interval 12-0kya, although it does not have a 0-years-before-present (BP) value. This is because the data are expressed as anomalies relative to a 100BP time point. The variables selected to represent seasonal fuel dryness and fuel moisture were mean summer temperature and precipitation. These variables were chosen because they showed better performance than other suitable variables (annual precipitation and precipitation minus evaporation) in a cross-validation exercise conducted by the authors [105]. Additionally, the moisture index variable is not described in the article, and the growing degree days variable has missing data in regions of high charcoal-record density such as the Swiss Alps [125].

The European forest cover reconstruction by Zanon et al. [127] is used as a measure of fuel load. It was generated using the same Plant Functional Type Modern Analogue Technique employed by Mauri et al. [105]. The dataset has a spatial resolution of 5 arc-minutes and spans the interval 12-0kya at a 250-year time step, with forest cover values expressed as percentages. The dataset also performs adequately in a cross-validation exercise, showing high agreement ($r = 0.75$) with the general trends of a separate forest cover reconstruction generated using an independent method [127]. The reconstruction also shows agreement with land cover change narratives for Europe (e.g. [101, 113]), and is further able to reproduce modern forest cover patterns.

In addition to the datasets used for defining the stratifications, land cover variables from the Fyfe et al. [101] European reconstruction, specifically; needleleaf and broadleaf tree cover, heath and scrubland, arable and disturbed land, and pasture and natural grassland cover reconstructions were used in the correlation analyses. The Fyfe et al. [101] dataset is an ungridded dataset of 982 pollen records where the percent cover of the various land cover classes have been reconstructed for each record at a 200-year time step spanning ∼11-0kya. The study generated the land cover values using a pseudo biomization method, which transforms pollen proportions from a given site into one of eight land cover classes. This method has been validated as effective at capturing pan-European patterns in land cover classes, as a comparison of its modern land cover values with remotely-sensed land cover maps showed that the two methods provided broadly similar estimates of percent cover [134].

The Reading Palaeofire Database

The RPD contains a more comprehensive coverage of charcoal records across the NET than any previous palaeofire database [78, 125]. Additionally, many of the records have new chronologies based on the appropriate IntCal20 radiocarbon age calibration curves [135], with the less recent, original chronologies also being preserved in the database. In the RPD, there are many cases where a single site (e.g. one lake basin) has had multiple records taken at different locations within the site, or has had different charcoal measurements (e.g. macro- vs micro- charcoal) or measurement methods (e.g. pollen slide vs sieved charcoal) applied to the same samples of a single record. These methodological site duplicates are treated as distinct entities in the RPD, such that there is a one-to-many relationship between the site metadata and the entity data of a given site. The ability to select from a range of entities within a site facilitates the customisation of the charcoal subset to better suit the study aims based on desirable methodological criteria of the records.

Analytical methods

Environmental data processing

In order to generate the NET stratification, it was necessary to apply various prior data filtering and processing steps to the NPP, VPD, and MI TraCE-21ka variables. These were needed in order to transform and standardise the variables into the appropriate form for clustering in line with the study aims, as well as to account for various sources of extraneous variation. The NPP variable is distributed across ten netCDF data layers, representing ten plant functional types. These were summed to produce a single NPP value per time point per grid cell. To identify and remove data values in the three variables that are present for periods of land ice coverage, the Ice-5G ice mask model (provided with the same coordinates and structure as the TraCE-21ka data by Patrick Bartlein) [136] was used. This ice mask is considered a reasonable approximation of ice cover change over palaeo timescales because it shows high agreement with time-dependent gravity field observations [137]. Lastly, to ensure that only grid cells with data presence in all three variables were used in the clustering, the three datasets were filtered to remove grid cells with no data across all time points in any one dataset. This may occur in cases where a grid cell contains a water body for the full time interval and hence has no NPP values but nonetheless has climate values present.

The VPD and MI data were converted from anomalies to actual values. This was done because clustering anomalies may obscure the detection of differences in baseline environmental space by the clustering algorithm. This effect can have consequences for the ability to detect distinct palaeofire environments with different respective fire-environment relationships. For example, consider the intermediate fire-productivity hypothesis [37], where the relationship of productivity to fire depends on the background level of moisture, and the effect of this interaction is most pronounced when comparing the humid tropics to arid regions. In a hypothetical case of arid and tropical regions experiencing similar moisture variability over a given time period, clustering anomalised data would group these regions into the same spatial unit, thereby confounding two distinct palaeofire environments. Given the broad geographic scope and environmental heterogeneity of the NET, the probability of any two TraCE-21ka grid cells that are from different background environments having similar environmental variability is likely to be non-negligible, especially considering that the dataset is effective at capturing

continental-scale palaeo climate changes in the NET which covary across different climate and biome space within continents [46, 88, 89, 100, 103, 104, 106].

To achieve the conversion of VPD and MI to actual values, the CRU TS 4.0.5 dataset [138], a modern climatology dataset with a 0.5-degree uniform grid, was used. This dataset is derived by the interpolation of monthly climate anomalies from broad networks of weather station observations from across the globe using an angular-distance weighting interpolation method. The interpolated temperature and precipitation data are considered an accurate representation of modern climate values because these variables are shown in a cross-validation exercise to be highly correlated to validation data and other global climate datasets [138]. The CRU TS dataset was used to generate respective 1975 CE mean VPD and MI gridded data layers to add to the VPD and MI anomalies. The means were generated in accordance with the method originally used to anomalise the MI and VPD data, i.e. using a tricube-weight function with a 30-year half-width. The CRU TS dataset supplies potential evapotranspiration and precipitation at monthly resolution, which was used to derive annual MI (ratio of annual precipitation to potential evapotranspiration). For the derivation of VPD, the CRU TS 2-metre temperature variable and the (actual) vapour pressure (AVP) variable were used. Temperature was used to derive saturation vapour pressure (SVP) in kilopascals using:

$$SVP = 0.6108.e^{\left(17.27(T)/(T+237.3)\right)} \quad (1)$$

where T is temperature in °C. AVP was converted to kilopascals from hectopascals and VPD was calculated as $VPD = SVP - AVP$, in agreement with how the TraCE-21ka VPD data was derived (personal communication, Patrick Bartlein).

To spatially align the TraCE-21ka and CRU TS datasets, the CRU TS dataset was downsampled from a 0.5-degree grid to an idealised version of the TraCE-21ka grid using a bilinear interpolation function from the 'raster' R package [139]. The idealised grid has identical coordinates to the TraCE-21ka grid except the latitudes increase uniformly (the only effective change was that the lowest latitude value was increased by 0.01 relative to the TraCE-21ka grid, creating a grid with latitudes increasing at exactly 3.71-degree increments). The irregular TraCE-21ka grid was then bilinearly interpolated to the idealised grid using the 'akima' R package [140]. Once the datasets were spatially aligned, the corresponding tricube-weighted means were added to the MI and VPD anomalies. Subsequently, the maximum monthly VPD value was selected within each decadal climatology of the VPD dataset.

At the European scale, the forest cover and climate datasets were spatially aligned for clustering, by projecting the forest cover dataset to the extent and resolution of the climate dataset using bilinear interpolation [139]. The forest cover dataset was then temporally binned to match the 1000-year resolution of the climate data, using a 500-year binning half-width. This was done by aggregating all time points present within each 1000-year time window into a mean value representing the given bin. The 0BP bin for a given forest cover grid cell was assigned the time value of 100BP to match the binning of the climate data, since the bin value centred on 0BP was identical to the hypothetical value if the bin were centred on 100BP at the same binning half-width. The forest cover time series of each grid cell was then anomalised relative to its 100BP value. In contrast to the NET analysis, anomalised data was used for clustering at the European scale. This is because the potential effect of anomalised data obscuring differences in baseline environmental space is expected to be unimportant at the European scale because of its relatively small geographic scope and the fact that European

climate is largely influenced by a single climate system [109, 110], as well as the fact that the Mauri et al. [105] and Zanon et al. [127] datasets capture spatial differences in environmental changes at a resolution well within the geographic scope of the different climate systems affecting the continent [108–110].

Charcoal data processing

The fire reconstructions were limited to the region >45N for this analysis. This limit was imposed in order to focus on the regions of the NET that experienced the latter stages of the most recent continental ice sheet declines [102, 107, 136, 141] and that contain the boreal carbon sinks [96, 142]. Additionally, since this work is the first attempt to delineate NET palaeofire environments, it was considered sensible to take a precautionary approach to minimise complexity of the analysis as far as possible. Limiting the latitudinal range over which charcoal records are aggregated reduces the environmental heterogeneity of the fire study region. This reduces the chance of producing fire histories for regions with similar fuel moisture and load history that may be divergent in other potentially fire-relevant processes not included in the stratification definition (e.g. species composition or temperature), thereby increasing the chances of producing robust fire composites. After limiting the RPD to >45N, there was a total number of 673 remaining charcoal sites.

To avoid pseudoreplication, a single charcoal entity was chosen from the sites that contain multiple entities. Primarily, cores extracted in a central location within a basin were prioritised over marginal cores because central cores provide a depositional environment that is typically more stable to geomorphological processes and where sediment accumulates more uniformly and completely relative to marginal locations. Secondarily, because charcoal sampling across the NET is typically biased in favour of the mid- and late-Holocene periods [78, 94, 138], cores with a larger depth interval (difference between the largest and smallest sample depth of a given core) were prioritised, to maximise the number of samples from the earlier periods of the Holocene. The third filtering criterion was to prioritise a smaller charcoal size fraction because microscopic charcoal fragments are regarded as more responsive to regionally integrated fire signals at the catchment scale and beyond compared to macroscopic particles, as their size facilitates long-distance aeolian transport [78, 81, 143]. The final filtering criterion was to select entities for which charcoal was measured on pollen slides rather than by sieving. The sieving method is used to identify macro charcoal fragments while pollen slide measurement enables identification of microscopic fragments, hence this criterion is included to account for cases where the size fraction was not evident from the unit of measurement. This tiered filtering structure is designed to favour records containing a more robust, long-term, regional charcoal signal over a less robust, temporally limited, and more localised signal. To avoid pseudoreplication at the sample level, reduce gaps in the charcoal time series, and maximise data consistency, data filters were applied to the charcoal samples comprising the entities. Namely, samples with missing charcoal or depth values were removed. Duplicate samples within an entity (identified as duplicates of charcoal measurement, depth, and age) were also removed.

The RPD records cannot be compared in raw form due to a wide array of measurement units used across records. It is thus necessary to standardise the units prior to compositing. A reliable approach in palaeofire literature and which is applied in this study is the charcoal standardisation and transformation procedure described in Power et al. [86]. This method converts charcoal sample

concentrations to influx by calculating sedimentation rates down core using the sample depths and core chronology. The influx values are then transformed to ensure all records are on a common scale and have normal variances, being expressed as Z-score anomalies relative to a common base period. In the data subset used here, the vast majority of records are available for this standardisation and transformation method. This is because most records are provided as the required concentration data, or are 'concentration-like', for example, being expressed as pollen concentrations (typically ratios of charcoal fragments to pollen, which are categorised as concentration in Power et al. [86]). Alternatively, they are expressed as fragments per unit weight rather than volume and therefore are synonymous with concentration. A few records are provided as raw counts with the sample volumes supplied enabling a simple conversion to concentration, which was done to these records in the >45N subset. Some records are provided in influx and can be directly transformed into Z-scores. A number of records are not provided with a clear unit, or are provided as raw counts without corresponding sample volumes and therefore cannot be expressed as concentration. These were filtered out of the analysis. Additionally, records with charcoal values in concentration that did not have a chronology supplied or that had depths of zero throughout the core were removed, because it is not possible to calculate their sedimentation rates for the required influx conversion.

To attempt to maximise the chronological accuracy of the charcoal records, the available IntCal20 chronologies for some charcoal records were used to derive influx. For entities in concentration, this was done by multiplying the charcoal concentrations by sedimentation rates calculated using the median values of the IntCal20 chronology. Concentration entities without IntCal20 chronologies were converted to influx using their original chronologies. For entities provided in influx, using the IntCal20 chronology required back-transforming the charcoal values to concentration using sedimentation rates derived from the original chronology, before converting these concentrations to influx using sedimentation rates derived from the median IntCal20 chronology. In total, IntCal20 chronologies were used to generate charcoal influx for 238 entities. Once all entities were expressed as influx, Z-scores were derived via the Power et al. [86] transformation and standardisation method. The base period used was 0.2-12kya, which excludes the effect of the industrial revolution and post-industrial period on fire activity.

Each charcoal record was temporally binned into a 500-year-resolution Z-score time series. The bin sequence used had the first bin centered on 100BP and the last on 11600BP with a half-width of 250 years. This sequence was chosen to preserve the highest amount of data per bin, reduce the number of missing bins in the dataset, and reduce the influence of age model uncertainty on the chronologies. At the relatively low number of charcoal records covering sub-continental regions in the NET (typically a few tens of records), it is reasonable to expect the prevalence of a low sample size per bin in the final composites, which can have important effects on the robustness of the reconstructed fire histories. Chronological uncertainty also becomes greater at higher bin resolution [144], as well as at lower sample sizes because uncertainties are not smoothed out to the same degree as when aggregating across a large number of records. Finally, a 500-year bin resolution is appropriate given the focus of the study being to capture general temporal fire patterns over the Holocene.

Palaeofire environment stratification definition

In order to define a palaeofire-environment stratification from the gridded environmental datasets, a biclustering algorithm was used. This simultaneously clusters grid cells as well as individual time points into a pre-specified number of spatial and temporal clusters, assessing the optimal cluster assignments as those that minimise the sum of squared errors across all clusters [145]. Clustering in time allows similarity among records that may exist for a subset of the time domain to influence the cluster assignments independently, which results in higher clustering precision than clustering in space only. This algorithm is also preferable to other clustering methods such as k-means because it is designed to handle missing values and therefore facilitates the preservation of a large amount of information [145]. It was implemented in this analysis with 500 repetitions to avoid convergence to local optima with the most parsimonious iteration being automatically selected using the R package 'biclustermd' [146].

The algorithm requires manual specification of the number of spatial and temporal clusters before implementation. To assist the selection of the appropriate number of clusters, a separate algorithm was formulated based on the Aikaike Information Criterion. This algorithm selects an optimal combination of space and time clusters from a pre-specified range, optimising for parsimony by penalising for a high number of parameters estimated and rewarding for the amount of variation explained. It is calculated as:

$$k = n.ln\left(\frac{sse}{n}\right) + 2(r.c) \tag{2}$$

Where n is the number of grid cells, r and c are the number of spatial and temporal clusters respectively, and sse is the final sum of squared errors across all biclusters within a given $r.c$ combination. The $r.c$ combination that results in the lowest value of k is selected as the optimal combination.

At the NET scale, the full dataset (with a latitudinal extent of 31.55-72.36N) was used in the biclustering algorithm, and at the European scale, all grid cells spanning Europe (with a latitudinal and longitudinal extent of 29.5-70.5N and -9.5-42.5 degrees east respectively) were included. The decision not to confine the biclustering to the >45N region of the charcoal analysis was done to allow fuel moisture and load processes spanning the 45N boundary (e.g. climate circulations) to inform the cluster assignments. This facilitates the respective fuel moisture and load stratifications being representative of fire-relevant environmental variation of the full NET/European regions. To ensure that the clusters represent spatiotemporal partitions that are temporally relevant to the fire responses, the three variables at the NET scale were binned in accordance with the charcoal binning specification. This was also done for the GDD variable to be used for later compositing and correlation with the fire responses.

After binning and at both respective scales, grid cells with more than half of their record missing were filtered out of the analysis. This was done to ensure that long-term palaeo environmental variation is used to determine the clusters. At the NET scale, an interval longer than the Holocene was used in the clustering, in order to obtain clusters that capture the long-term environmental transition from the last glacial period. It was found that using the full 21ky period would result in too many grid cells in regions with charcoal coverage being filtered out due to a large number of grid cells being ice-covered in the early part of the TraCE-21ka simulation (hence having more than half of their NPP record missing). An interval of 0-14.1kya was found to preserve all grid cells with high charcoal coverage

after applying the temporal filter, hence the three NET variables were subsetted to this interval prior to applying this filter.

In order to cluster the grid cells using the temporal variation in all three environmental variables simultaneously, the three variables were concatenated into a single dataframe to be biclustered, such that each grid cell contained all three environmental time series combined into a single effective time series. This approach creates two potential sources of erroneous cluster-assignment bias: 1) differences in bin missingness and hence data availability among variables within a grid cell. This can result in variables with more data than others contributing disproportionately to the assignment of the grid cell into a cluster; 2) since variances of the three variables at both respective scales span orders of magnitude, the variation of one variable may be flattened in the presence of a variable with much larger variance in the same grid cell, making it less visible to the algorithm.

To address these issues, the respective bin missingness patterns of the three variables within a given grid cell were homogenised. This was done within a given grid cell by deleting data across all three variables in a given bin, if the bin contained no data in any one variable. To address the second source of bias, the variances of the three variables were homogenised. This was done by scaling two of the three variables by a factor that resulted in them having an identical interquartile range to the third, unscaled variable. At the NET and European scales, the unscaled variable was MI and summer temperature respectively.

To avoid potentially defining the stratifications based on spurious variation, the three variables were examined for collinearity by correlating the three variables with each other at both respective scales. The three variables were judged to be independent at both scales (figure A.1).

The optimal combination of time and site clusters was selected at both scales using the AIC-based optimisation algorithm (equation 2). The optimal combination was chosen from a set of biclustering implementations containing all combinations of 2 to 18 site and 2 to 22 time clusters at the NET scale, and 2 to 13 site and 2 to 18 time clusters at the European scale. At the NET scale, 18 was chosen as the maximum number of possible site clusters as it provides adequate spatial separation to describe broad sub-continental patterns, and 22 time clusters provides enough resolution to detect important localised variation in the time axis of 29 time points (providing scope for <2 time points per time cluster). At the European scale, the choice of 13 as an upper site-cluster limit was guided by the number of zones in the modern environmental stratification for Europe of Metzger et al. [124]. Judging from the typical size of the clusters in the modern stratification, 13 sets an appropriate upper limit that prevents isolating very small clusters that are too specific and poorly sampled to be informative for a palaeo charcoal synthesis. The maximum time cluster allowance of 18 is appropriate given the 33 effective time points of the clustered dataset (three of the 36 time points, at 100BP, have values of zero for all grid cells as all values are anomalised relative to this time point). The optimal $r.c$ combination was found to be 13 site and 11 time clusters at the European scale by more than two k values (figure A.2), and at the NET scale the optimal combination was found to be 17 site and 8 time clusters by more than two k values as well (figure A.3).

Composite curve generation

Charcoal records were assigned to stratification clusters based on the site cluster value of the stratification grid cell that was in closest proximity to a given charcoal record. Closest proximity was

determined by finding the grid cell with the smallest summed latitude and longitude distance to a given charcoal record. Where a charcoal record was equidistant between two grid cells on the same line of latitude but which fell on longitudes on either side of the charcoal record or vice versa, the charcoal record was assigned to the grid cell with the smaller value in the axis that varied (this occurred for a single charcoal record). To ensure that charcoal records were spatially representative of the clusters to which they were assigned, if no stratification grid cell fell within a uniform 2-degree cell containing a given charcoal record at its centre, the charcoal record was filtered out of the analysis (this can occur in cases where a charcoal record was taken from a marine depositional environment, hundreds of kilometres from a land mass).

Composite charcoal curves were generated for each cluster by fitting a loess curve to the pooled records using the R package 'locfit' [147]. The curves were fitted with a window width of 1500 years and were estimated at the same time positions as the charcoal binning sequence. The fitted curves were bootstrap-resampled 500 times to derive 95% confidence intervals. Charcoal composites were generated only for clusters that had 10 or more charcoal records in each bin for a continuous 4ky interval, guided by previous literature [94].

As some NET clusters span both North America and Europe, this provides an opportunity to investigate whether the fire histories of a single palaeofire environment differ between two regions with different species composition and human land use histories. For this reason, all clusters with charcoal records located on both continents had composite curves generated separately for either continent.

Composites of the environmental variables were created in the same way as was done for the charcoal data. This was done only for clusters that had charcoal composites successfully generated. To ensure that the environmental composites represent the environmental variation that produced the fire variation of a given cluster, only the grid cells containing charcoal records within a cluster were used to generate the environmental composites. All environmental variables were composited in their original values (the actual values in the cases of VPD and MI at the NET scale), as opposed to using data that was transformed and filtered for clustering. Bootstrap-resampled confidence intervals were generated for the NET-scale composites on condition that there were 10 or more grid cells comprising the mean composite curve. At the European scale, the forest cover composites were generated after binning the data to the bin specification of the charcoal records. The European climate composites were generated at their native 1000-year time resolution for the 12-0kya period. The European-scale forest cover and climate data standard errors were used to obtain uncertainty estimates around the fitted composite curves. The forest cover standard error dataset was resampled to the spatial resolution of the climate dataset using bilinear interpolation [139], and composite curves were then generated for this and the climate standard error variables in the same manner as described for the mean datasets. The upper and lower uncertainty time series around a given mean composite were obtained by subtracting and adding the fitted standard error composite from and to the corresponding mean composite.

Composites of the five Fyfe et al. [101] land cover classes were also generated for the European-scale clusters as well as the NET clusters spanning the geographic range of the Fyfe et al. [101] dataset. The land cover data was filtered to contain a single entity per site by choosing the longer entity where this existed. There were eight sites where multiple entities were equivalent in length, and in these cases one entity from each site was selected arbitrarily. The Fyfe et al. [101] entities were assigned

to clusters in the same way as was done for the charcoal records except that only stratification grid cells containing charcoal records were used for this (figures A.4, A.5). These land cover entities were then binned to the charcoal-record bin specification and subsequently composited with estimation of bootstrap-resampled confidence intervals using the same approach as for the NET-scale environmental composites.

Fire-environment correlations

Quantitative relationships between the composite curves of the environmental variables and the charcoal were investigated using correlation analyses. For a given charcoal composite, this was done using only the time points that contained at least 10 charcoal records within the 1500-year smoothing window. Correlations were calculated for the intervals 4-0kya, 8-4kya, and 12-8kya respectively, provided there were at least three time points available in a given interval. These 4ky time intervals were motivated by previous palaeofire literature that used a similar temporal breakpoint structure to successfully analyse Holocene fire evolution [116]. They were also selected to ensure fair comparison of correlations among time intervals (given their equal number of time points), and in order to isolate potentially different fire-environment relationships during Holocene sub-periods expected to have generally different environmental states. Correlations between the charcoal and the Fyfe et al. [101] land cover composites were not interpreted for the 12-8kya interval because the method used by Fyfe et al. [101] to generate the land cover classes is unsuitable for quantifying early-Holocene vegetation change. This is because it is optimised to reconstruct anthropogenic as well as natural land cover classes, and anthropogenic land cover change is known to have become important from the mid-Holocene [101, 148]. To generate the European-scale fire-climate correlations, the charcoal composites were binned to the 1000-year resolution of the climate composites. For the clusters that spanned both continents at the NET scale, the two continental fire responses were correlated using the same approach as for the fire-environment correlations. All analyses were done in R [149]. A list of all software packages used in the analysis is provided in table A.1 in Appendix A. Supplementary analyses were conducted to provide additional validation of some of the methodological approaches employed, which are described in Appendix B.

Results and Discussion: Northern-extratropical scale

Results

A total of 593 grid cells from the TraCE-21ka climate model were clustered into the 17 spatial clusters to produce a continuous NET stratification between 30-75N (figures 1, 2, A.6-A.8). There was sufficient charcoal coverage to generate composites for 10 of the spatial clusters, hence the analysis was limited to these clusters. The 10 clusters show general latitudinal patterns in moisture availability, growing days and productivity (figures A.9-A.12). Clusters 1 and 4 are high-latitude clusters located in the general region of Beringia. They generally show the lowest NPP, GDD, and MI of all clusters, seen by the combined interquartile ranges (IQR) of their boxplots (12-0kya combined IQR: NPP: ∼0-200; GDD: ∼0-40; MI: ∼ −1-0.4). Clusters 5 and 6, located in Fennoscandia, far-southeast Russia, south west Canada, central Canada, and northeast Quebec, have low-to-intermediate NPP, GDD, MI, and VPD (12-0kya combined IQR: NPP: ∼150-600; GDD: ∼30-200; MI: ∼0.25-1.1; VPD: ∼0.3-1.1). Cluster 10 spans the Altai Mountain region of north west Mongolia and the West Siberian Plain, while cluster 11 is distributed in the regions of Lake Baikal in southern Siberia and Lake Hovsgol in north central Mongolia. Clusters 10 and 11 have similar NPP, MI, and VPD to clusters 5 and 6, but have slightly higher GDD values over 12-0kya (12-0kya combined IQR: GDD: ∼120-300).

Clusters 12 and 16 have higher NPP and GDD compared with clusters 10 and 11 (12-0kya combined IQR: NPP: ∼900-1700; GDD: ∼170-750; figures A.11, A.12). In Eurasia, cluster 12 spans the hemiboreal region between Fennoscandia and continental Europe, and northeast China (figures 1, 2). In America it is located south of James Bay and in the interior Pacific northwest region of the United States. Cluster 16 is located in the region of the Pacific northwest coast of North America, as well as the Atlantic northeast coast of the United States and southern Quebec. In Eurasia it covers the central British Isles and south/central Europe in the general region of the Swiss Alps. It has high MI relative to other clusters (12-0kya IQR: ∼1.4-2.4; figure A.9).

Cluster 13 has the highest NPP of any cluster and consistently high GDD relative to other clusters (12-0kya IQR: NPP: ∼1500-2000; GDD: ∼450-650; figures A.11, A.12). It is located directly south of the American clusters 5, 12, and 16 in the northern regions of the United States. In Eurasia it is also located in regions directly south of cluster 12, covering central and southern Europe and some spatially discontinuous grid cells in central eastern China (figures 1, 2). Cluster 17, mainly located in boreal eastern North America, exhibits generally very high MI and very low VPD relative to other clusters (12-0kya IQR: MI: ∼1.2-1.7; VPD: ∼0.1-0.4; figures A.9, A.10). It is thus an exception to the general latitudinal pattern in moisture availability seen across the clusters.

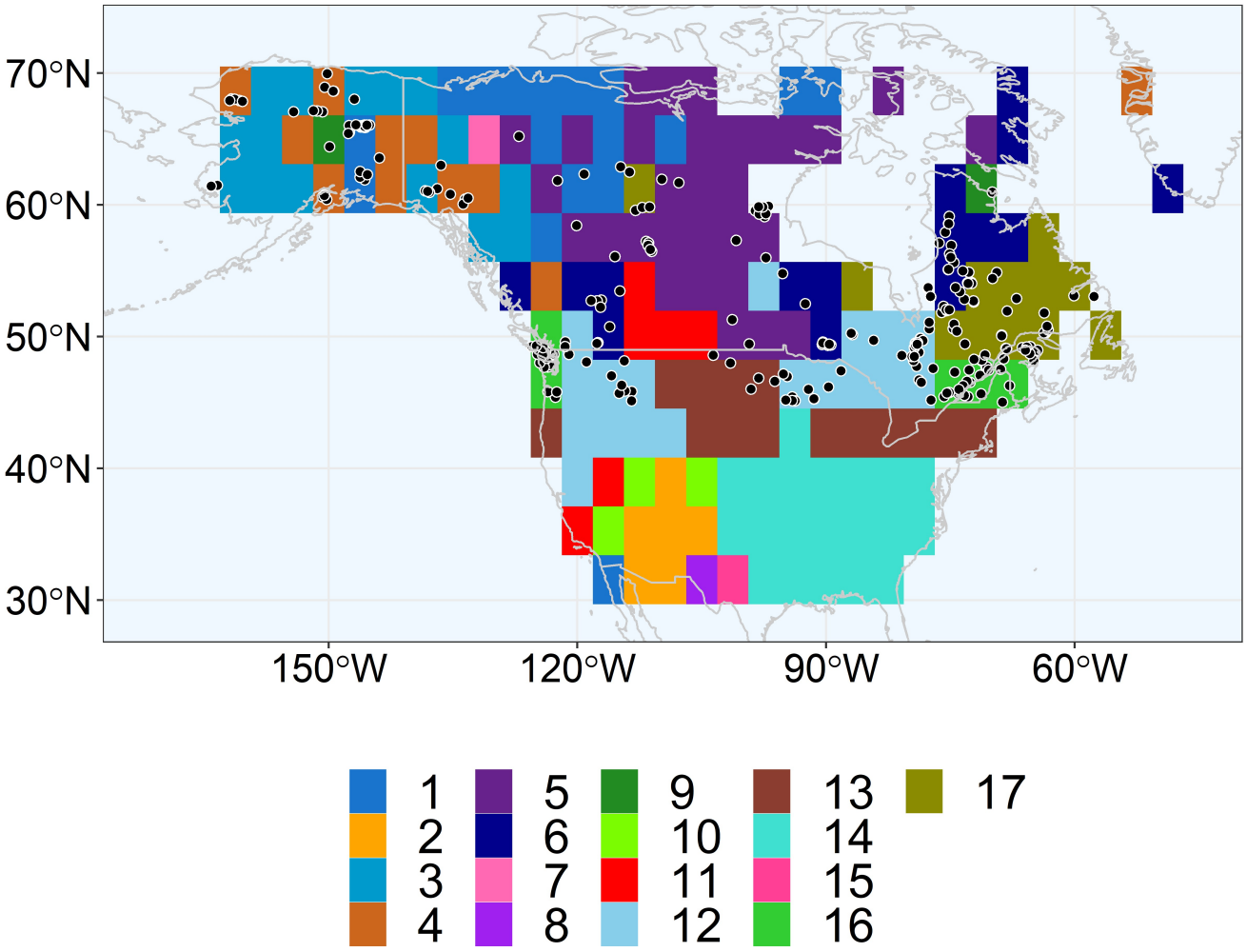

Figure 1: NET stratification of palaeo environmental space generated by biclustering grid cells of the TraCE-21ka dataset based on temporal variation in moisture index, vapour pressure deficit, and net primary productivity variables over the period 14.1-0kya, shown for North America. Black points are locations of charcoal records. Spatial clusters are colour-coded and numbered in the legend.

Of the 578 charcoal records that remained after pre-clustering filters were applied, 558 were used to generate composite curves for the 10 clusters (figures 1, 2). Clusters 5, 12, and 16 contain enough charcoal records to enable composite generation separately for either continent. This resulted in a total of seven composites being generated for America (clusters 1, 4, 5, 6, 12, 16, and 17), and six for Eurasia (clusters 5, 10, 11, 12, 13, and 16). All Eurasian clusters except 10 and 11 have at least 39 charcoal records comprising their composite curves and span the full time period investigated (figures A.13-A.18). Of the American clusters, 6, 12, 16, and 17 contain at least 41 charcoal records and their composites span at least the last 10.1ky (figures A.13, A.14, A.16, A.18-A.20). All clusters except most with lower sample sizes, namely the American clusters 1, 4, 5 and Eurasian cluster 10, show well-constrained charcoal composites with tight confidence intervals (figures 3-10, A.21-A.25). It is noteworthy that this is the case for cluster 11 considering its low sample size of 16 charcoal records and its broad geographic distribution (figure 2).

The fire responses of all clusters show correlations of $>= |0.5|$ with at least one TraCE-21ka environmental variable for the 12-0kya interval, except clusters 4, 6, 10, and the Eurasian cluster 5 (tables A.2, A.3). All clusters but one exhibit correlations of $>= |0.75|$ with at least one variable for

at least one 4ky interval (figure 11; tables A.2, A.3). The exception is cluster 1, which is nonetheless correlated with NPP during the 8-4kya interval with an r value of -0.72. In both American and Eurasian clusters, the direction of many of the fire-environment relationships change among the 4ky intervals. In the NET clusters spanning Europe, there is a systematic pattern in which the direction of the relationships change between the 12-8kya and 8-4kya intervals, namely for the clusters 5, 12, 13, and 16, at least one of the following changes in the sign of the correlation occurs: GDD, VPD, and NPP change from positive to negative; MI changes from negative to positive (table A.3). Additionally, between the 8-4kya and 4-0kya intervals in the NET clusters 13 and 16 in Europe, the dominant fire control changes from needleleaf cover and NPP respectively to open/human land classes (figure 11).

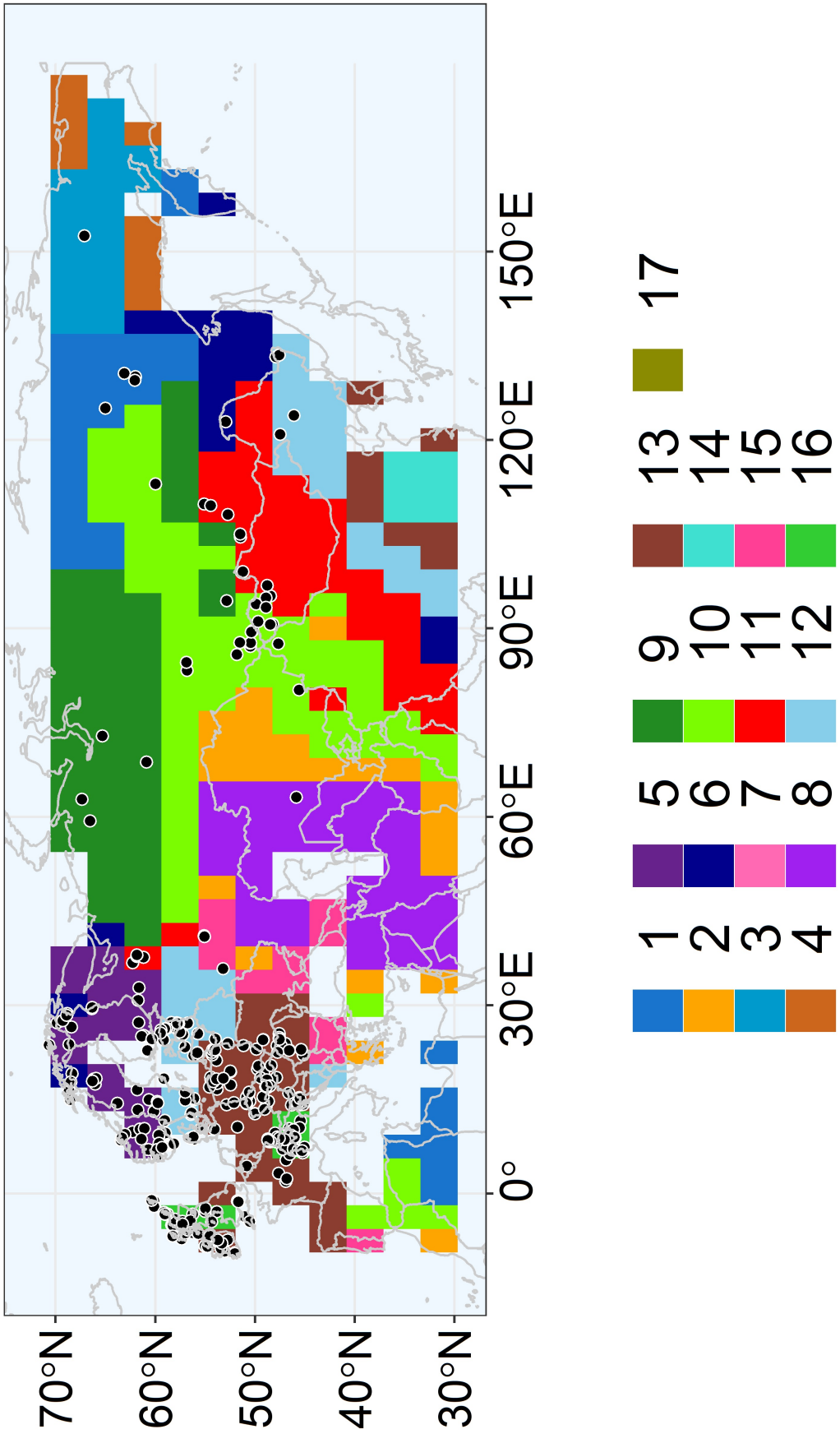

Figure 2: NET Stratification of palaeo environmental space generated by biclustering grid cells of the TraCE-21ka dataset based on temporal variation in moisture index, vapour pressure deficit, and net primary productivity variables over the period 14.1-0kya, shown for Eurasia. Black points are locations of charcoal records. Spatial clusters are colour-coded and numbered in the legend.

Individual cluster results

Clusters 1, 4, and 5: Boreal Northwestern America

Clusters 1, 4, and 5, which span boreal northwestern America, all experience long-term, generally linear declines in GDD, NPP, and VPD and a corresponding increase in MI from the early/mid-Holocene to the present (figures 3, A.21, A.22), however, the fire responses differ among these three clusters. In cluster 1, there is an abrupt fire increase between 7.1-6.1kya after which it remains relatively stable until 0.6kya, then moderately decreases. In cluster 4, the fire response gradually increases between 7.6-3.1kya and subsequently declines until the present. In cluster 5, the fire response generally declines over the full 5.6ky period, although this decline is poorly constrained. The cluster 5 fire decline is positively correlated with declining GDD, NPP, and VPD and negatively correlated with increasing MI (12-0kya correlations: GDD: $r = 0.74$; NPP: $r = 0.77$; VPD: $r = 0.83$; MI: $r = -0.71$). For clusters 1 and 4 in the 8-4kya interval, the fire increases are negatively correlated with declining NPP and GDD and increasing moisture levels (cluster 1: NPP: $r = -0.72$; VPD: $r = -0.67$; GDD: $r = -0.68$; cluster 4: NPP: $r = -0.75$; GDD: $r = -0.77$; VPD: $r = -0.72$; MI: $r = 0.66$), while in the 4-0kya interval in cluster 4, the same environmental patterns show the opposite relationship to the now-declining fire response (NPP: $r = 0.56$; GDD: $r = 0.58$; VPD: $r = 0.74$; MI: $r = -0.77$). The late-Holocene fire decline in this cluster occurs along with NPP and GDD reaching a value of $\sim$0 by $\sim$2.1kya. Similarly, the decrease in fire from 0.6kya in cluster 1 occurs as GDD, NPP, and VPD reach long term minima and MI is at a general high-point. The moisture variables are the strongest predictors of fire in the late-Holocene interval across boreal northwestern America (figure 11).

Clusters 6 and 12: mid-latitude boreal/temperate North America

The American cluster 12 experiences a large increase in fire between $\sim$11.1-9.6kya corresponding to large increases in GDD and NPP (figure 5). As a result, GDD and NPP are strongly positively correlated with fire in the 12-8kya interval (NPP: $r = 0.91$; GDD: $r = 0.79$). In clusters 6 and 12, fire declines between 10.1-7.1kya and 9.6-4.1kya respectively (figures 4, 5). In cluster 12, the gradual mid-Holocene fire decline follows a relatively stable pattern in NPP and GDD compared to the early Holocene, and fire is more strongly correlated to the increasing moisture levels than GDD and NPP during the 8-4kya interval (MI: $r = -0.58$; VPD: $r = 0.71$; GDD: $r = 0.46$; NPP: $r = -0.44$). Similarly, in cluster 6, the declining fire response until 7.1kya corresponds to generally increasing MI (figure 4). The oscillatory features of the fire curve within this declining trend appear related to similar features in the VPD curve that are large relative to the VPD variation across the Holocene (the change in VPD until 7.1kya spans $\sim$0.5 kilopascals, a similar range to the long-term declining VPD trend from the mid-Holocene onwards). This is supported by the 12-8kya correlations showing that fire has a relatively high positive correlation with VPD ($r = 0.6$), comparable to its highest 12-8kya correlation with NPP ($r = 0.62$). Additionally, the NPP correlation appears to be spuriously inflated due to it being generated from minimal variation in the NPP curve relative to the fire curve pre-8kya (figure 4).

From 7.6kya, the number of charcoal records in cluster 6 more-than doubles as the records in north Quebec begin recording charcoal (figure A.14). Between 7.1-5.1kya, there is a large increase in NPP corresponding to a large increase in fire (figure 4). This is reflected in the 8-4kya fire correlation

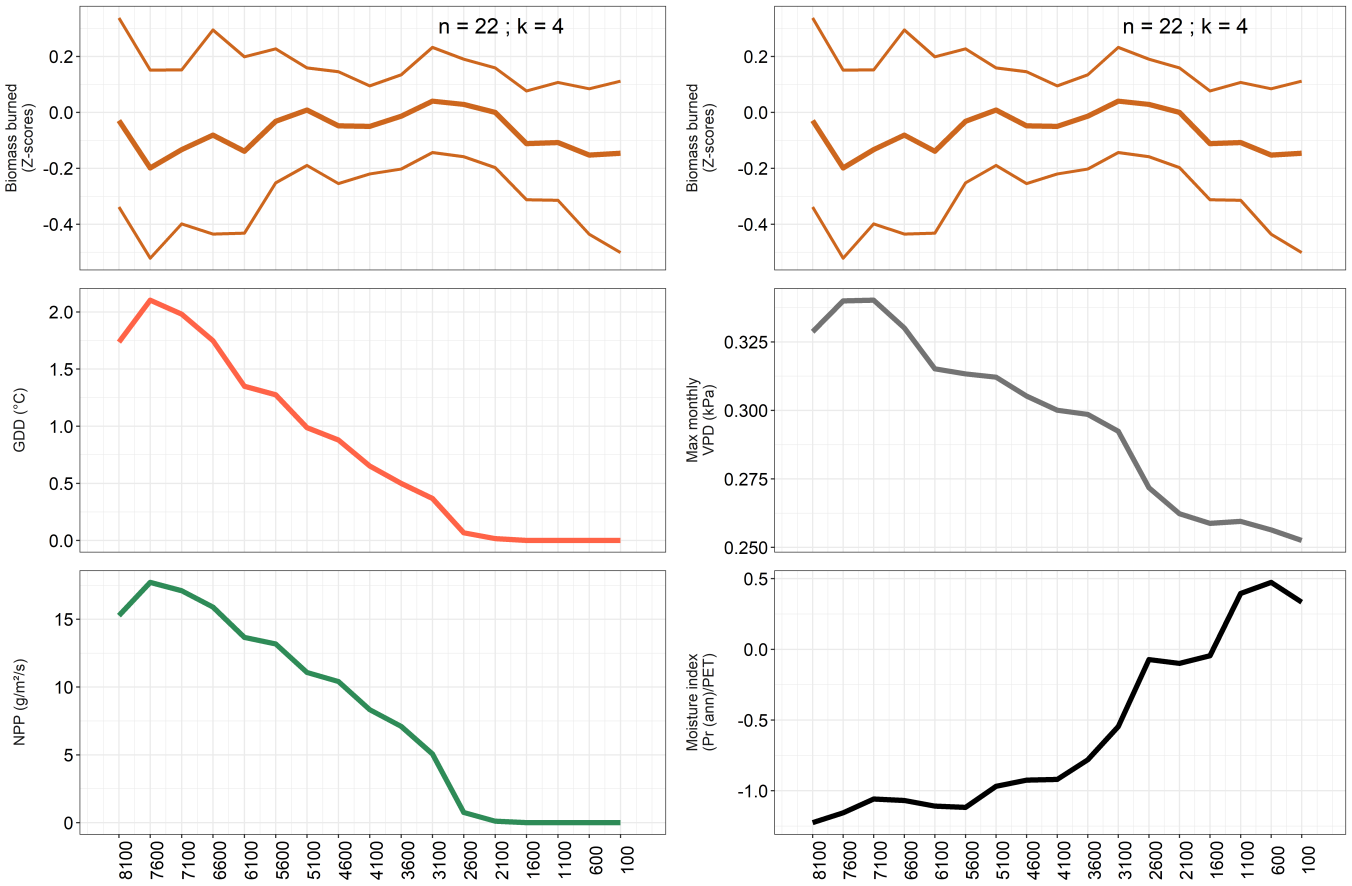

Figure 3: Holocene biomass burning and environmental composite curves for the NET cluster 4, North America, all smoothed using a 1500-year window width. The time interval (shown on the x-axis in years before 1950 CE) is limited to the period within the 11.6-0kya interval in which all time points contain at least 10 charcoal records in the smoothing window. The composite curves are shown with 95% bootstrap confidence intervals, except for composites comprised of less than 10 individual time series. The number of charcoal records comprising the biomass burning response (n) and the cluster identity value (k) are shown on the top panel.

with NPP (r = 0.77). Both NPP and fire stay at high levels until 2.1kya in cluster 6. In cluster 12, fire increases substantially between ∼4-1.6kya to its highest Holocene value, however, this occurs despite no proportional change to the environmental variables, which maintain their general long-term trends from the mid-Holocene (figure 5).

From 2.1kya, cluster 6 experiences a large, progressive fire decline to the present, reaching its lowest overall value throughout the 10.1kya period (figure 4). In accordance with this, between ∼3.1-0kya VPD and MI progressively decrease and increase respectively, reaching their lowest and highest overall values. This is reflected by the 4-0kya correlations for cluster 6, with VPD being the most important predictor of fire and exhibiting a strong positive fire relationship, while MI has the second-highest explanatory power and is negatively related (VPD: r = 0.7; MI: r = −0.44; figure 11; table A.2). Similarly, cluster 12 also experiences a decline in fire between 1.6-0kya from its overall maximum centred on 1.6kya, however the consistent environmental trends from preceding millennia persist into the 1.6-0kya interval and appear unable to account for the fire decline (figure 5).

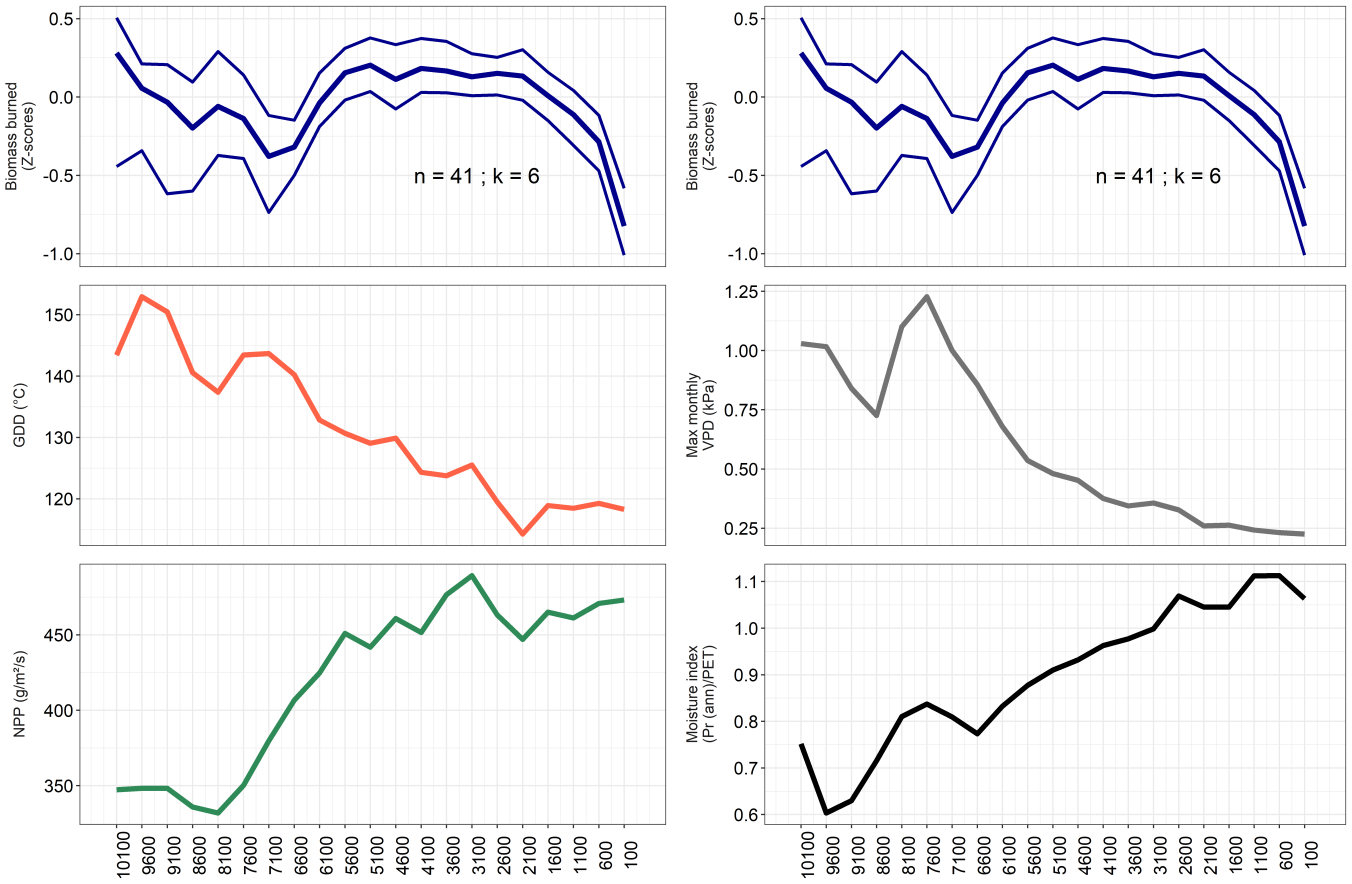

Figure 4: Holocene biomass burning and environmental composite curves for the NET cluster 6, North America, all smoothed using a 1500-year window width. The time interval (shown on the x-axis in years before 1950 CE) is limited to the period within the 11.6-0kya interval in which all time points contain at least 10 charcoal records in the smoothing window. The composite curves are shown with 95% bootstrap confidence intervals, except for composites comprised of less than 10 individual time series. The number of charcoal records comprising the biomass burning response (n) and the cluster identity value (k) are shown on the top panel.

Cluster 16: Maritime temperate North America

The American cluster 16 has a variable Holocene fire response that is most strongly explained by its inverse relationship with annual moisture variability (12-0kya correlation: MI: r = −0.51; table A.2; figure 6). As in the adjacent cluster 12, fire increases from the early Holocene to a high-point between 9.6-8.1kya. This increase corresponds to generally increasing GDD, a steep NPP increase, and lowered levels of MI. The 12-8kya correlations reflect these patterns, as fire is positively correlated with NPP (r = 0.67) and GDD (r = 0.87). Between 7.6-4.1kya, fire generally declines as NPP and MI increase and VPD decreases. In the 8-4kya interval, the fire decline is strongly negatively related to the increasing NPP (r = −0.77) and MI (r = −0.93) and positively related to the declining VPD (r = 0.96).

At 2.6kya, VPD and MI reach general long-term minimum and maximum values respectively (figure 6), similar to the moisture patterns seen in clusters 1, 4, 6, and 12. MI has a turning point at this time where it begins to gradually decline until the present, while the long-term VPD decline is similarly attenuated between 2.6-0kya. In addition to these moisture changes, from 2.6kya, GDD starts increasing at a slightly higher rate relative to the preceding three millennia. These environmental

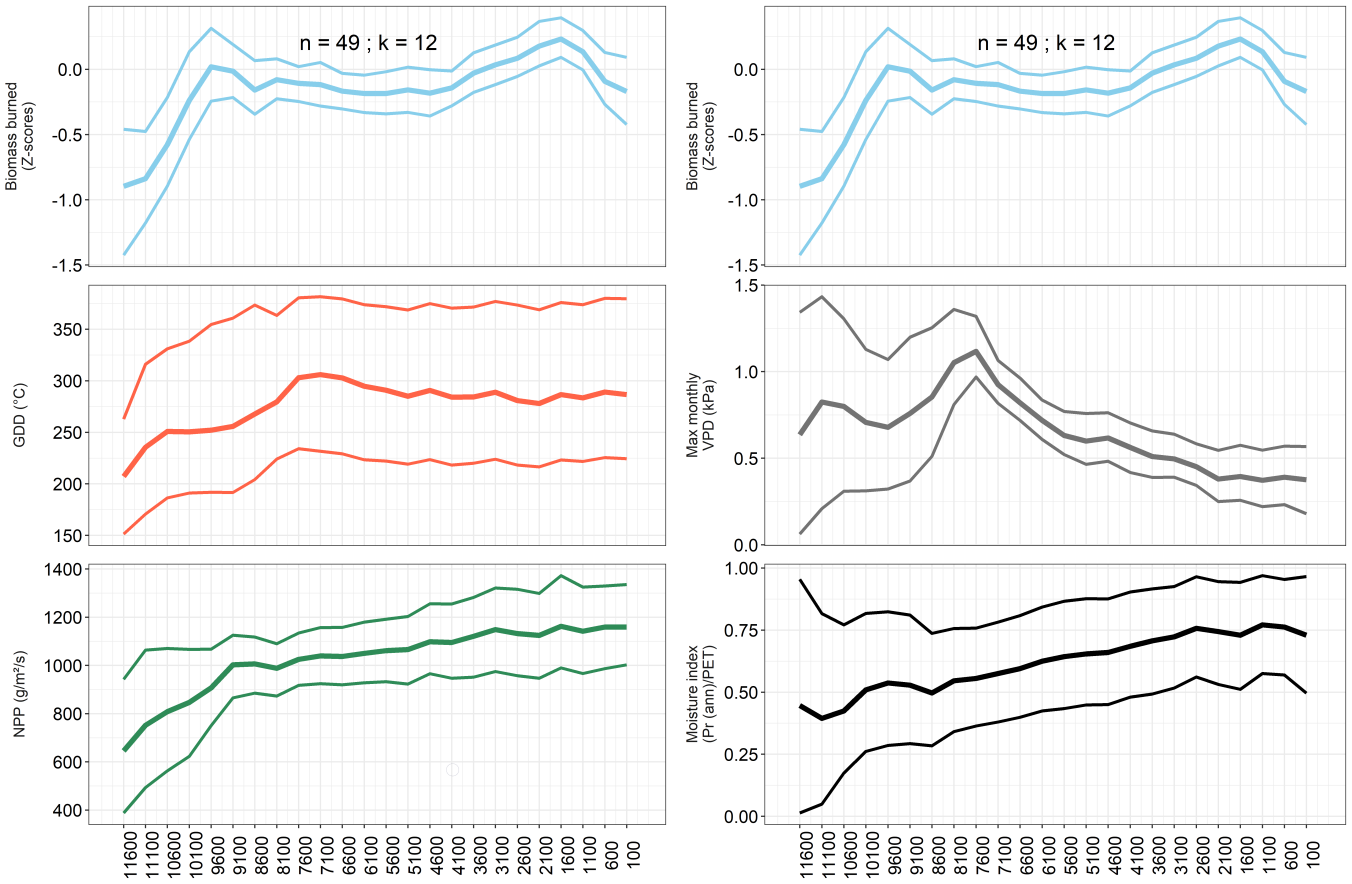

Figure 5: Holocene biomass burning and environmental composite curves for the NET cluster 12, North America, all smoothed using a 1500-year window width. The time interval (shown on the x-axis in years before 1950 CE) is limited to the period within the 11.6-0kya interval in which all time points contain at least 10 charcoal records in the smoothing window. The composite curves are shown with 95% bootstrap confidence intervals. The number of charcoal records comprising the biomass burning response (n) and the cluster identity value (k) are shown on the top panel.

changes correspond to a turning point in fire at 2.6kya where it starts increasing to the present. Moreover, fire is positively related to GDD between 4-0kya (r = 0.94), although the large increase in fire between 2.6-0kya appears out of proportion relative to the corresponding changes in the GDD, MI, and VPD patterns.

Cluster 17: Northeastern boreal America

Before ~8kya, cluster 17 shows extremely high levels of MI and very low levels of VPD (figure 7), and the predominant time of year in which VPD is at a maximum in the grid cells containing charcoal records is during the winter/spring months (figures A.26-A.29). After ~8kya, this changes to summer/autumn (figures A.30-A.37). This change occurs along with a near-tripling of VPD levels and a large decline in MI between 8.6-7.6kya. GDD and NPP increase substantially from the start of the record until ~7.6kya, after which they begin a more gradual decrease to the late Holocene, while MI shows the inverse Holocene trajectory. VPD declines from ~7.6kya, reaching its early-Holocene levels by 2.1kya.

The fire response increases from ~10kya (figure 7) to a peak between 9.6-9.1kya. Fire then

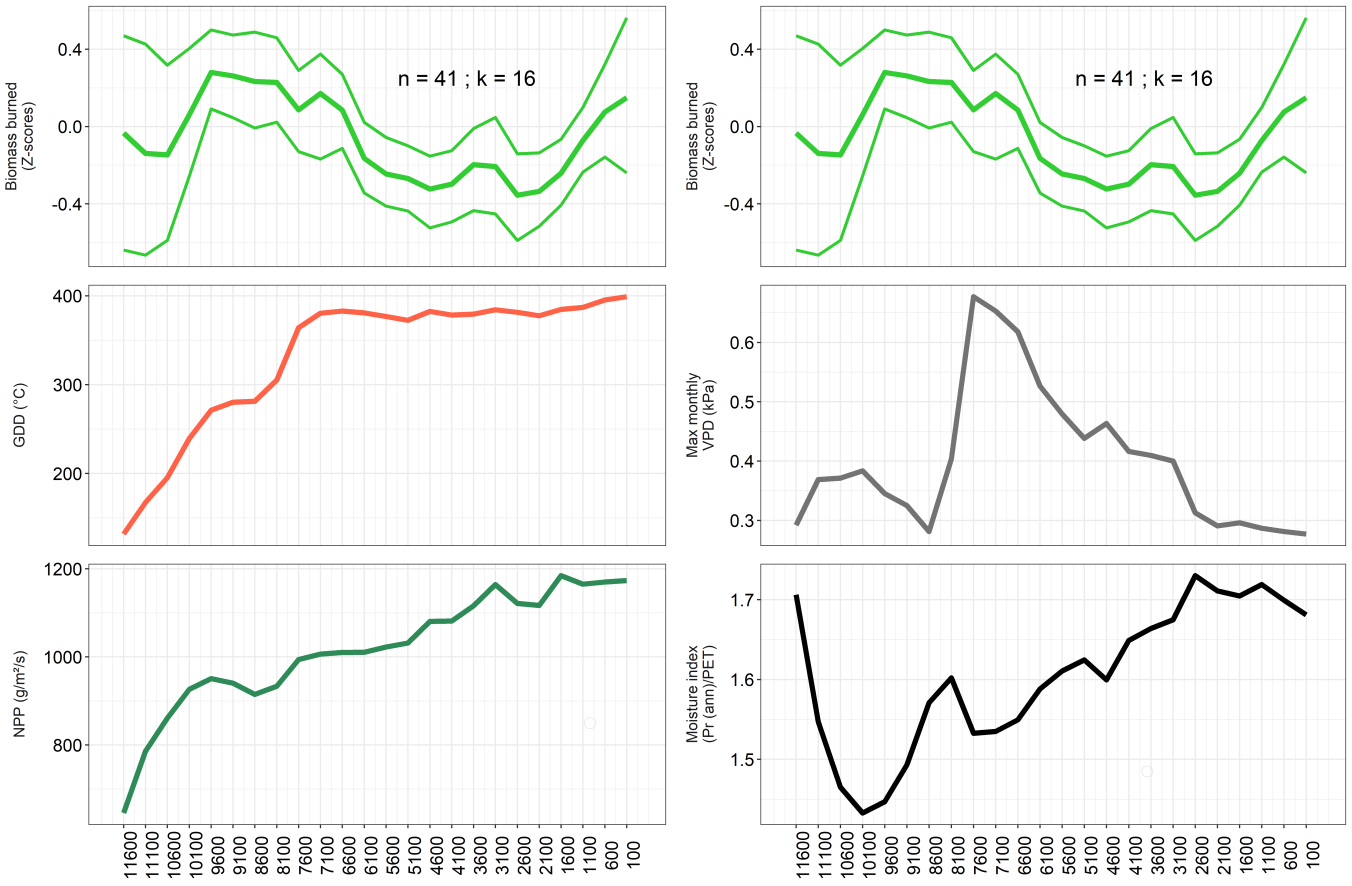

Figure 6: Holocene biomass burning and environmental composite curves for the NET clusters 16, North America, all smoothed using a 1500-year window width. The time interval (shown on the x-axis in years before 1950 CE) is limited to the period within the 11.6-0kya interval in which all time points contain at least 10 charcoal records in the smoothing window. The composite curves are shown with 95% bootstrap confidence intervals, except for composites comprised of less than 10 individual time series. The number of charcoal records comprising the biomass burning response (n) and the cluster identity value (k) are shown on the top panel.

declines to its lowest Holocene levels between ∼8-6.6kya, at a time when the cluster was its driest with maximal fuel loads, seen by GDD, NPP, and VPD being at their maximum Holocene values and MI at its minimum during this time. In agreement with these patterns, the 8-4kya correlations show that fire has high negative correlations with GDD, NPP, and VPD (GDD: $r = -0.79$; NPP: $r = -0.62$; VPD: $r = -0.84$) and a positive correlation with MI ($r = 0.76$). From ∼6.6kya, the number of charcoal records from central Quebec contributing to the fire composite substantially increased (figure A.20). Fire gradually increases between ∼6.6-0kya along with the increasing moisture and declining NPP trends. The correlation patterns seen in the 8-4kya interval are generally maintained in the 4-0kya interval (GDD: $r = -0.53$; NPP: $r = -0.48$; VPD: $r = -0.61$; MI: $r = 0.71$).

Clusters 5, 12, 13, and 16: Europe

Clusters 5, 12, 13, and 16 all show generally similar patterns of variability in their environmental variables, and all exhibit a general increase in fire over the Holocene (figures 8, A.23-A.25). Cluster 12 deviates from its long-term increasing trend between 8.1-6.1kya where it declines, culminating in a mid-Holocene minimum. Additionally, cluster 13 has a variable and weakly decreasing fire response

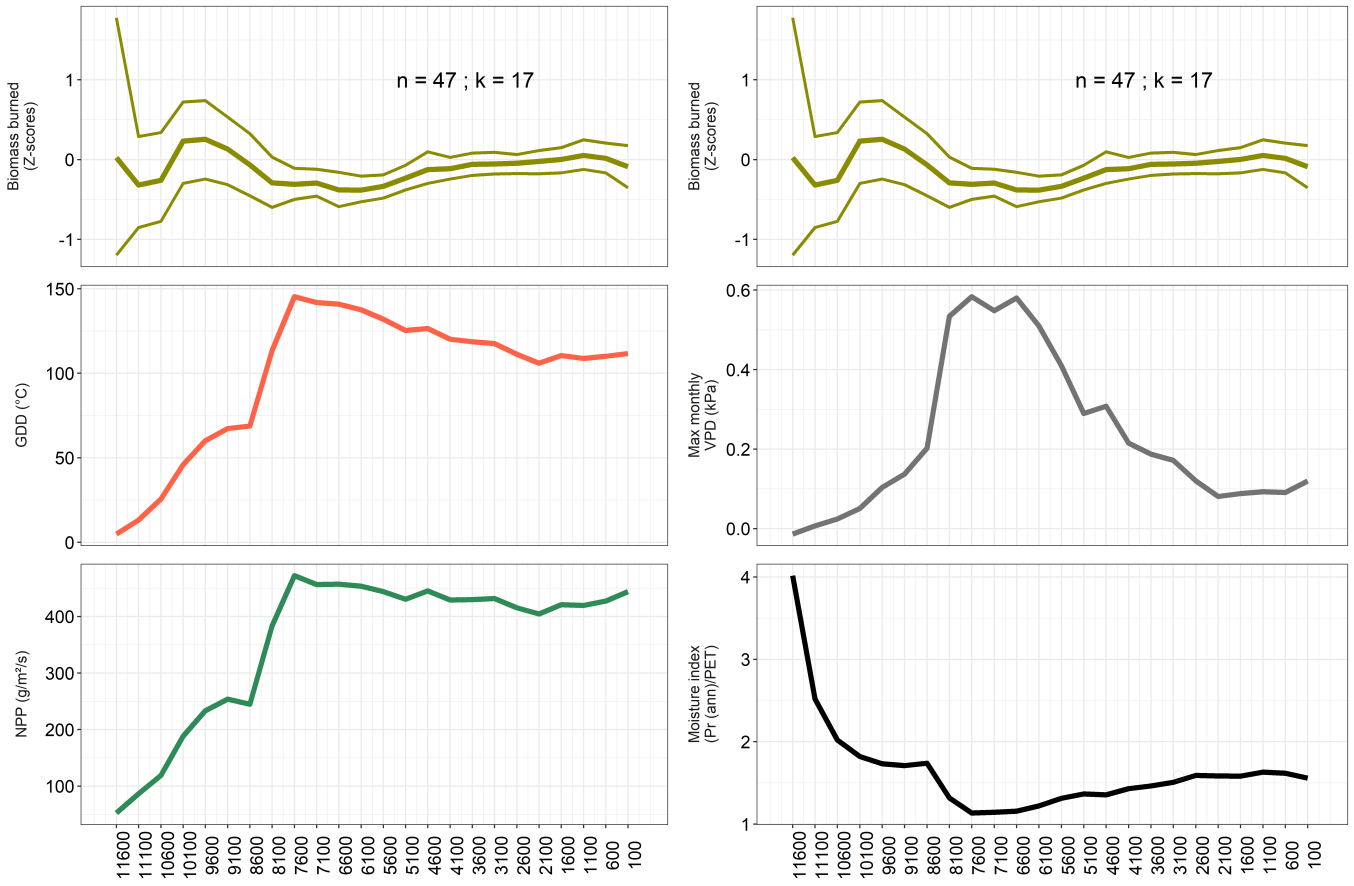

Figure 7: Holocene biomass burning and environmental composite curves for the NET clusters 17, North America, all smoothed using a 1500-year window width. The time interval (shown on the x-axis in years before 1950 CE) is limited to the period within the 11.6-0kya interval in which all time points contain at least 10 charcoal records in the smoothing window. The composite curves are shown with 95% bootstrap confidence intervals, except for composites comprised of less than 10 individual time series. The number of charcoal records comprising the biomass burning response (n) and the cluster identity value (k) are shown on the top panel.

between 9.6-3.6kya.

These four clusters experience a similar environmental shift towards more seasonally dry conditions in the early Holocene seen by large VPD increases, which correspond to their fire increases (figures 8, A.23-A.25). In the northern European clusters 5 and 12, this shift is accompanied by a large decline in year-round moisture as shown by their large MI declines. However, the early-Holocene decline in MI in cluster 12 reaches a minimum 0.5ky earlier than the minimum in cluster 5. This moisture shift occurs with a progressive shift in the predominant season in which VPD is at a maximum in northern and north-central Europe from winter/spring to summer, and a summer/autumn dry season prevails after ∼8kya until the present (figures A.26-A.37). The generally drying early-Holocene climate pattern also occurs along with a general climate warming and increase in productivity, with all four clusters showing substantial increases in GDD and NPP. The increased early-Holocene fire levels in accordance with these changes are generally reflected in the 12-8kya correlations (cluster 5: MI: $r = -0.93$; GDD: $r = 0.41$; VPD: $r = 0.75$; cluster 13: GDD: $r = 0.66$; VPD: $r = 0.62$; NPP: $r = 0.66$; cluster 16: GDD: $r = 0.79$; VPD: $r = 0.78$; NPP: $r = 0.76$).

The four clusters show different relationships between fire and environmental changes in the ∼8-4kya interval compared to the early Holocene. Contrary to the early-Holocene patterns, the NPP,

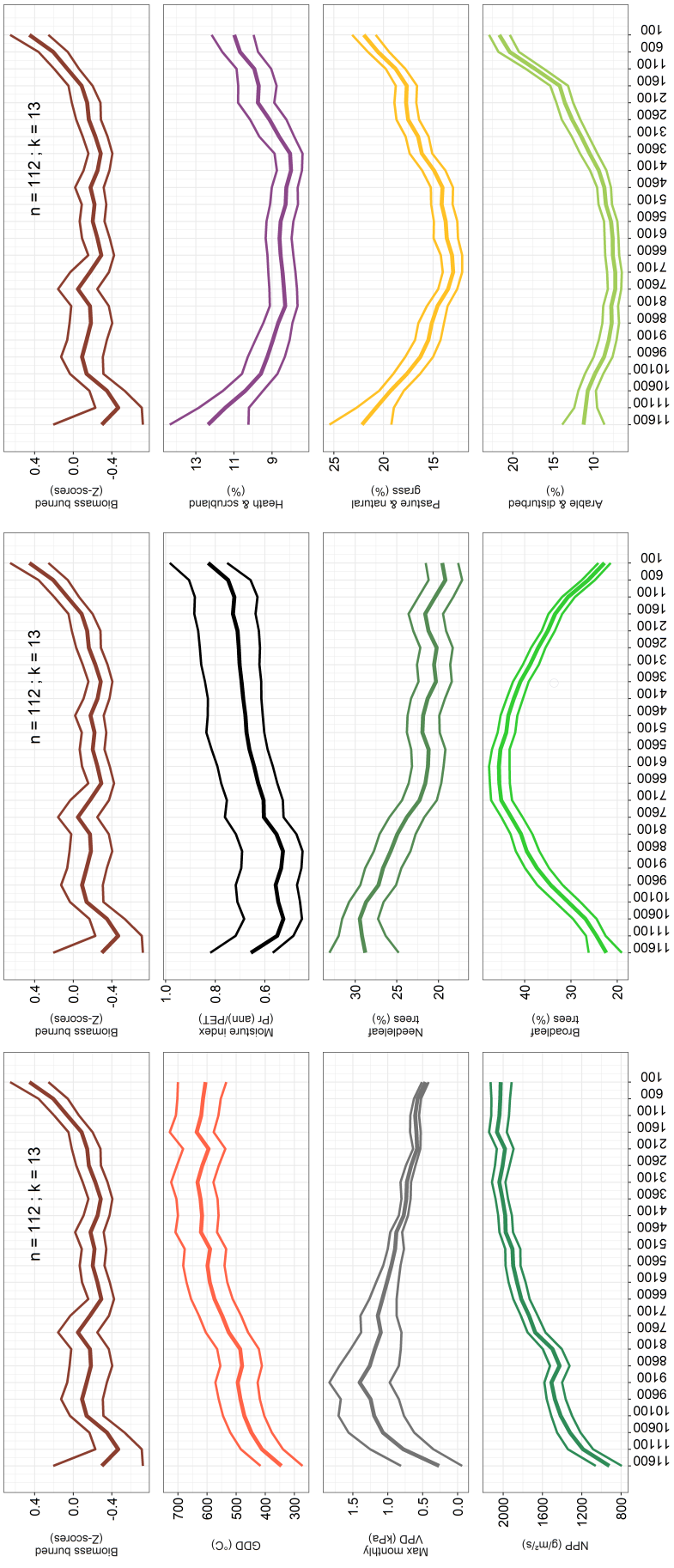

Figure 8: Holocene biomass burning and environmental composite curves for the NET cluster 13, Eurasia, all smoothed using a 1500-year window width. The time interval (shown on the x-axis in years before 1950 CE) is limited to the period within the 11.6-0kya interval in which all time points contain at least 10 charcoal records in the smoothing window. The composite curves are shown with 95% bootstrap confidence intervals. The number of charcoal records comprising the biomass burning response (n) and the cluster identity value (k) are shown on the top panel.

GDD, and moisture correlation patterns for clusters 5, 12, and 13 show that fire relates positively to increased moisture availability and negatively to increased temperature and productivity (8-4kya correlations: cluster 5: MI: r = 0.82; cluster 12: VPD: r = −0.5; cluster 13: NPP: r = −0.57; GDD: r = −0.61). This occurs while clusters 5, 12, and 13 all experience a Holocene maximum in broadleaf cover (figures 8, A.23, A.24). Cluster 16 is an exception to this pattern as its broadleaf cover declines consistently between 8-0kya (figure A.25). In all four clusters, fire is negatively related to broadleaf cover and positively related to needleleaf cover (8-4kya correlations: cluster 5: needleleaf: r = 0.67; broadleaf: r = −0.75; cluster 12: needleleaf: r = 0.75; broadleaf: r = −0.88; cluster 13: needleleaf: r = 0.88; broadleaf: r = −0.42; cluster 16: needleleaf: r = 0.61; broadleaf: r = −0.96).

In all four clusters there are large, long-term declines in broadleaf and tree cover from the mid-Holocene to the present (figures 8, A.23-A.25). In clusters 5, 12, and 13, the broadleaf cover composites decline from their mid-Holocene maxima of ∼40%, ∼50%, and ∼45% to modern values of under 22.5%, 30%, and 25% respectively. In cluster 16, broadleaf cover declines to a 6kya value of ∼30% and reaches a modern value below 20%. Unlike the other clusters, cluster 16 experiences a large reduction in needleleaf cover over the mid-to-late Holocene, of similar magnitude to its broadleaf decline. High levels of simulated NPP in these clusters in the late Holocene suggest that the high values of GDD, increasing MI, and declining VPD created favourable climatic conditions for high levels of productivity. This may contradict with the observed pattern of a substantial mid-to-late-Holocene broadleaf decline across Europe.

Clusters 5, 12, and 13 all experience large, progressive increases in fire over the mid-to-late Holocene, culminating in their highest overall Holocene values in the most recent bin (figures 8, A.23, A.24). Cluster 16 is an exception, which experiences its highest fire value at ∼2.6kya after which fire gradually declines to the present (figure A.25). For all clusters, the fire increases are accompanied by consistently increasing seasonal and annual moisture and open/human land cover classes. The open/human land class increases are particularly large in clusters 13 and 16, where both pasture and natural grassland and arable and disturbed land begin long-term, accelerating increases relatively early, from ∼6.6kya in cluster 13 and 7.1kya in cluster 16. Pasture and natural grassland cover reaches levels above 20% by 0.6kya in cluster 13 and 2.1kya in cluster 16, from 6.6kya levels of ∼13% and ∼16% respectively. Arable and disturbed land cover reaches levels above 20% in cluster 13 and 16% in cluster 16 by 0.6kya, representing a more-than doubling for both clusters relative to their mid-Holocene values. Comparing with cluster 12, arable and disturbed land had been increasing since 5.1kya, from ∼5% to ∼13% at 0.1kya. Pasture cover also moderately increases from 5.1kya levels of ∼8% to modern values of ∼13%. In this cluster, the open/human land classes and MI increase at an accelerated rate from ∼1.1kya, in tandem with a 1.1kya turning point in the increasing needleleaf composite after which it declines to the present.

The 4-0kya correlation patterns for clusters 12 and 13 reflect their fire increases occurring in tandem with increasing moisture and landscape opening (cluster 12: GDD: r = −0.79; VPD: r = −0.88; broadleaf: r = −0.99; heath: r = 0.91; pasture: r = 0.92; arable: r = 0.98; cluster 13: MI: r = 0.95; VPD: r = −0.89; needleleaf: r = −0.61; broadleaf: r = −0.98; heath: r = 0.92; pasture: r = 0.99; arable: r = 0.98). For cluster 16, the declining fire in the most recent 3kya in tandem with the accelerating increases in open/human land cover and maximum Holocene moisture levels is seen by the inverse patterns between fire and landscape openness and moisture increases in the 4-0kya correlations

(MI: r = −0.65; VPD: r = 0.66; heath: r = −0.76; pasture: r = −0.64; arable: r = −0.73; needleleaf: r = 0.67; broadleaf: r = 0.73). In cluster 5, the 4-0kya correlation patterns are consistent with the 8-4kya patterns (needleleaf: r = 0.13; MI: r = 0.94; arable: r = 0.92; heath: r = 0.94; pasture: r = 0.79; VPD: r = −0.91; broadleaf: r = −0.97). However, the needleleaf correlation drops to a low value as there is a turning point and subsequent decline from its long-term increase at 1.6kya (figure A.23). This is 0.5kya earlier than the similar pattern seen in the adjacent cluster 12 (figure A.24).

Cluster 10: Altai region

The fire response of cluster 10 shows an increase between 5.1-3.1kya which corresponds to increasing NPP (figure 9). Between 3.1-0kya, fire generally decreases, which corresponds to generally increasing annual and seasonal moisture and NPP, reflected in the 4-0kya correlations with NPP, MI, and VPD (NPP: r = −0.78; MI: r = −0.51; VPD: r = 0.64). The fire decline in the most recent 1ky corresponds to a general maximum in MI and minimum in VPD.

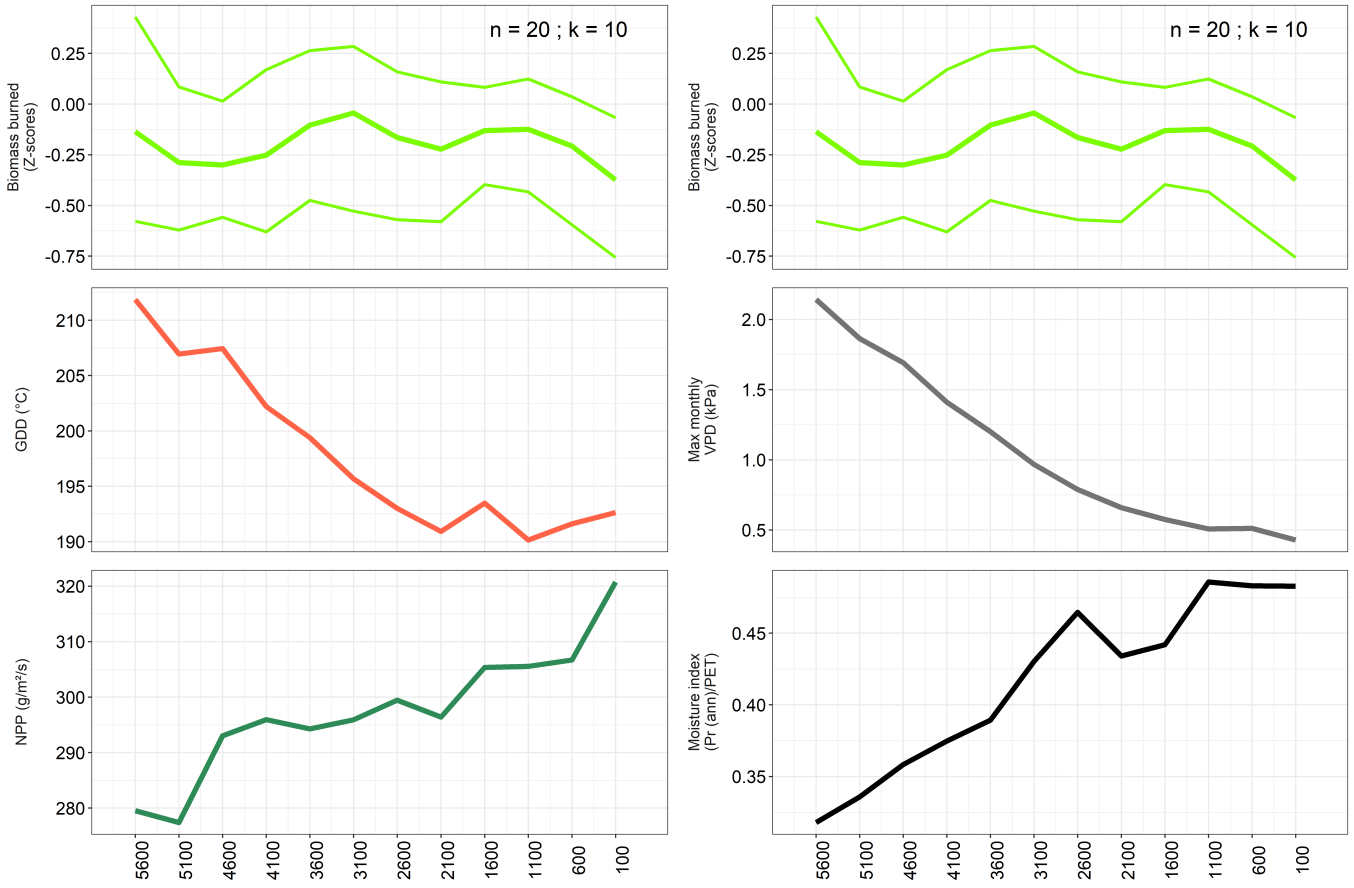

Figure 9: Holocene biomass burning and environmental composite curves for the NET cluster 10, Eurasia, all smoothed using a 1500-year window width. The time interval (shown on the x-axis in years before 1950 CE) is limited to the period within the 11.6-0kya interval in which all time points contain at least 10 charcoal records in the smoothing window. The composite curves are shown with 95% bootstrap confidence intervals, except for composites comprised of less than 10 individual time series. The number of charcoal records comprising the biomass burning response (n) and the cluster identity value (k) are shown on the top panel.

Cluster 11: Southern Siberia and north-central Mongolia

In cluster 11, fire generally declines from a high early-Holocene value to low levels in the late Holocene (figure 10). This follows a general long-term increase in summer and annual moisture with declining temperatures, reflected in the 12-0kya correlations with VPD, MI, and GDD (VPD: r = 0.69; MI: r = −0.62; GDD: r = 0.67). The fire response varies around the long-term trend, namely it increases between 9.1-7.1kya and 3.6-1.1kya respectively.

The late-Holocene period of elevated fire corresponds to elevated levels of heath cover, lowered broadleaf cover, and generally declining NPP (figure 10), while needleleaf cover is at a general high-point in the late Holocene. However, the land cover reconstructions for this cluster are based on only three records (figure A.5).

Cross-continental cluster comparisons

The correlations between the continental fire responses of the three clusters that had composites generated for both America and Eurasia suggest that the fire responses of the same clusters on separate continents were initially similar in the early Holocene, but became increasingly dissimilar from the mid- to the late Holocene (table A.4). High dissimilarity between fire responses is most consistent among clusters in the 4-0kya interval (cluster 5: r = −0.72; cluster 12: r = −0.36; cluster 16: r = −0.82). For the 8-4kya interval, only the continental responses of cluster 16 are highly negatively correlated (r = −0.87), while the other two clusters show correlation values of $< |0.3|$. For the two clusters that cover the early Holocene (12 and 16), their 12-8kya correlations indicate general similarity between the two continents (cluster 12: r = 0.4; cluster 16: r = 0.65).

Discussion

The definition of a spatial stratification representing millennial-scale fuel moisture and load variability has allowed this study to isolate coherent and largely distinct sub-continental patterns in palaeofire evolution across the NET. The results show that Holocene fire evolution is spatially variable across the NET, with no clear systematic trends besides a general Holocene fire increase across Europe. In general, divergent sub-continental-scale climate and land cover histories can account for distinct regional fire histories, where the effects of a given environmental variable on fire change over time as environmental thresholds are crossed and fire controls interact. This agrees with Feurdean et al. [116] who showed that fire relationships to fuel moisture, load, and composition variables are non-monotonic over much of the Holocene and that different sub-continental-scale regions have different fire relationships to these controls. This is probably a consequence of different background environmental characteristics leading to spatially variable interaction effects.

The spatial coverage and sampling level of the charcoal composites generated in this work represents a substantial improvement to the previous NET charcoal synthesis of Marlon et al. [94]. Within the >45N region, that study reconstructed four composites for America, and three for Eurasia which were all concentrated in Europe. This study provides composites for more spatially resolved divisions of the regions in Marlon et al. [94], as well as two novel central Asian composites. The Marlon et al. [94] reconstructions have relatively wide confidence intervals in proportion to the variance of their mean curves. In comparison, the charcoal composites shown here have mean curve features that are

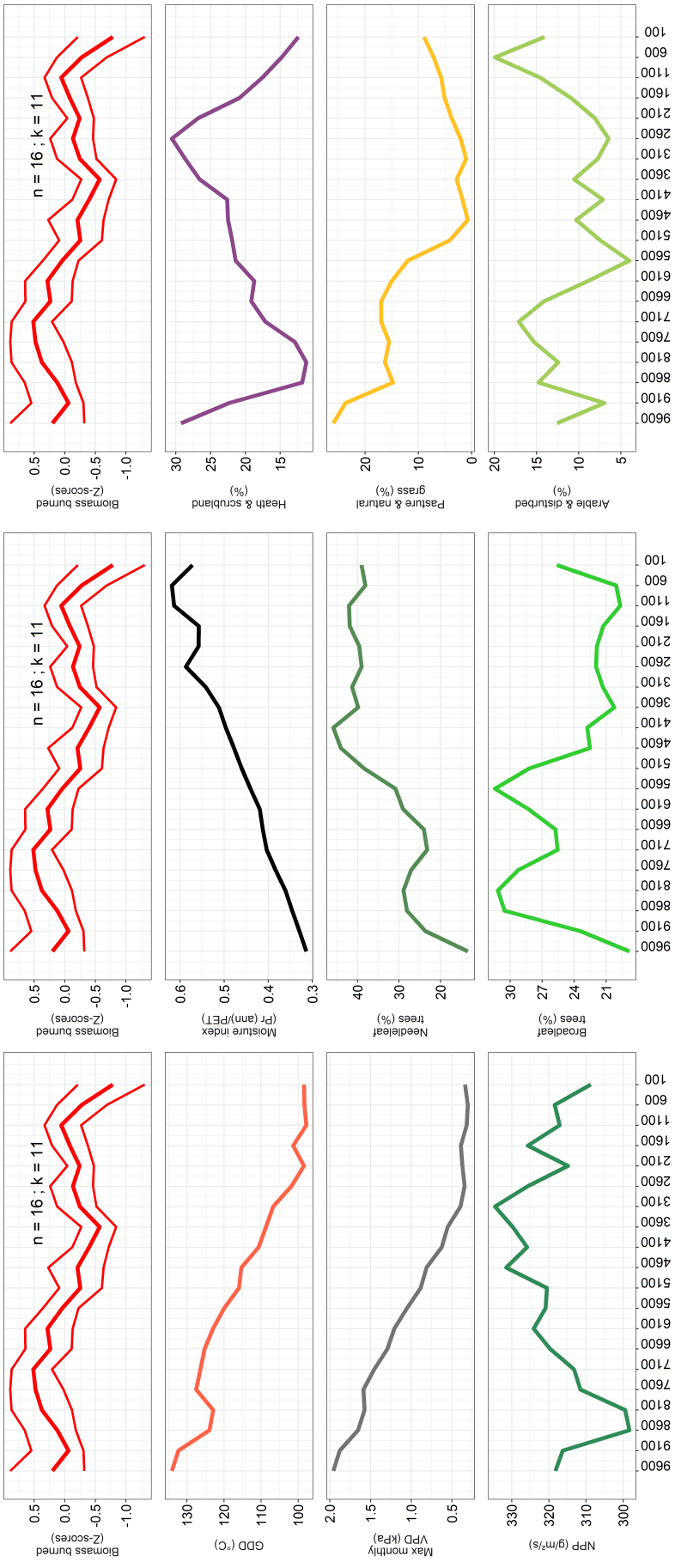

Figure 10: Holocene biomass burning and environmental composite curves for the NET cluster 11, Eurasia, all smoothed using a 1500-year window width. The time interval (shown on the x-axis in years before 1950 CE) is limited to the period within the 11.6-0kya interval in which all time points contain at least 10 charcoal records in the smoothing window. The composite curves are shown with 95% bootstrap confidence intervals, except for composites comprised of less than 10 individual time series. The number of charcoal records comprising the biomass burning response (n) and the cluster identity value (k) are shown on the top panel.

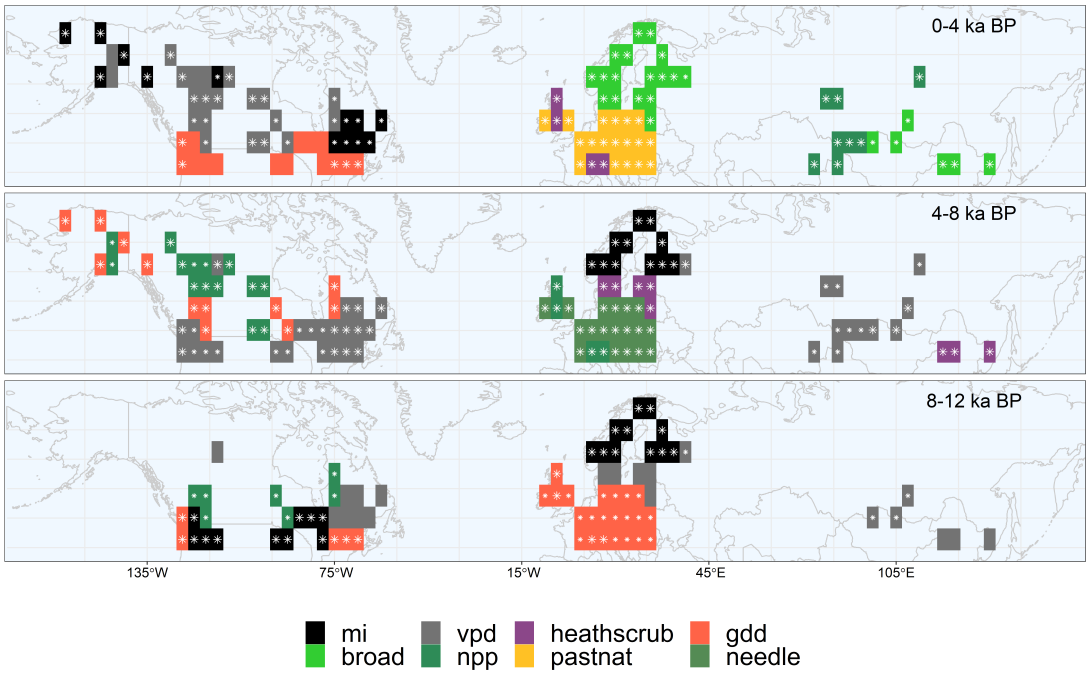

Figure 11: Map showing the environmental variable with the highest explanatory power for the fire response of each cluster at the NET scale within 4ky time intervals. Only grid cells that contain charcoal records are shown. Grid cells are colour-coded by the environmental variable whose composite mean exhibits the highest absolute correlation with the fire response of its cluster within a given 4ky interval. Small white asterisks indicate correlation values >= |0.5| and < |0.75|, large white asterisks indicate correlation values >= |0.75|, grid cells with no shape fill indicate correlation values < |0.5|. Legend: mi = moisture index; broad = broadleaf tree cover; vpd = maximum monthly vapour pressure deficit; npp = net primary productivity; heathscrub = heath and scrubland cover; pastnat = pasture and natural grassland cover; gdd = growing degree days; needle = needleleaf tree cover.

generally tightly constrained, with the exception of clusters 1, 4, 5, and 10. This implies coherent fire responses to similar environmental changes within clusters, including across large geographic and elevational ranges. Ultimately, this points to the efficacy of the stratification at approximating palaeofire environments.

The NET stratification is broadly congruent with the spatial patterns of a modern environmental stratification of biome distributions that was defined based on climate varation by Hengl et al. [150]. The high-latitude clusters 1 and 4 fall within cold biome types such as cold forests and tundra regions in the Hengl et al. [150] stratification. Clusters 5 and 6 fall almost exclusively within regions of cold evergreen needleleaf forest and overlap with the modern boreal regions on both continents. Clusters 12 and 16 represent transitional environmental space between boreal and temperate systems on both continents, and they largely overlap with cool forest biomes in Hengl et al. [150]. Cluster 13 follows areas of temperate broadleaf and cool mixed forest in Europe, America, and Asia, with the exception of its central American zone which is steppe. The grid cells containing charcoal records for clusters 10 and 11 mostly lie within central Asian steppe or the transition between steppe and boreal forest. The congruence with the Hengl et al. [150] stratification supports the notion that the NET stratification captures real differences in environmental space across the NET.

The NET stratification also agrees with the spatial patterns of environmental changes that occurred over palaeo timescales. For example, cluster 17 falls within the boreal cold needleleaf forest region in Hengl et al. [150], but is distinct from the other cold needleleaf clusters 5 and 6. This is

likely due to its unique climate history, which was directly influenced by the LIS decline and final termination [102, 151]. It experienced much larger moisture changes, as suggested by the MI and VPD variables, than the other cold needleleaf clusters, particularly during and probably as a consequence of the early-Holocene LIS recession [151].

Another example is the Holocene moisture variability of the NET clusters in Europe, which can be explained by the collapse of the Fennoscandian Ice Sheet. In general agreement with the patterns of summer and winter precipitation in Mauri et al. [105], the magnitude of the early-Holocene moisture decline increases with latitude across clusters 5, 12, and 13, as does the timing of the moisture minima following the declines, which occur at ∼10.6kya for cluster 13, ∼9.1kya for cluster 12, and ∼8.6kya for cluster 5. These patterns are consistent with the relative proximity of the clusters to the ice sheet during its pattern of recession that occurred in a general latitudinal direction, namely a progressive contraction to the north west of the continent. At 10.5kya, the ice sheet had a south-eastern margin at southern Sweden and crossing the southern region of the gulf of Bothnia, while at 9.9kya it had terminated in north/central Scandinavia at ∼67N [107]. In addition to its congruence with modern environmental space, the agreement of the NET stratification with known patterns of palaeo environmental change implies that it provides a more accurate representation of NET palaeofire environments than the previous arbitrary attempt at delineating paleofire regions of Marlon et al. [94]).

Controls on palaeofire evolution across the northern extratropics

Clusters 1, 4, and 5: Boreal Northwestern America

The fire increase in the early/mid Holocene in the Beringian clusters 1 and 4 is counterintuitive given the corresponding climate wettening and decline in productivity. It is evident that the *Picea* genus expanded across Alaska and northern boreal America ∼7-6kya [46]. The dominant *Picea* species in the American boreal region is *P. mariana*, a strongly fire-promoting species [41, 46]. This plant-compositional change may have overrode the probable negative effects of the climate and productivity changes on fire. A mid-Holocene rise in *P. mariana* and its modulation of fire-climate linkages in this manner was also found to be important in a palaeolimnological study of charcoal and fossil pollen records in the south-central Brooks Range of Alaska [118].

Cluster 4 shows a more sustained, gradual, though relatively poorly constrained increase in fire over the mid-Holocene compared to the rapid increase between ∼7.1-6.1kya in cluster 1. This may be due to the more geographically disparate distribution of cluster 4. It may be expected to experience different timing of land cover changes across its various zones, especially considering the geographic and topographic complexity of the northwestern American region that can create barriers to species movement. This is supported by more localised studies from the south-central Brooks Range and the Kenai peninsula [118, 152], which show that the expansion of *P. mariana* and concominant fire rise in the south-central Brooks Range occurred ∼5.5kya [118] while in the Kenai peninsula, expanded coniferous biomass along with elevated fire activity is evident between ∼8.5-4.6kya [152].

The climate wettening from the mid- to the late Holocene in clusters 1 and 4 corresponds to a southward expansion of the tundra biome in Alaska that replaces boreal forest [46]. Concominant with this tundra rise is an expansion of sedges and grasses that reach highest coverage in the most recent 1ky [46]. The decline in fire in the last 1ky and 3.1ky in clusters 1 and 4 respectively can thus be put down to a declining amount and flammability of fuel, as mesic tundra vegetation became more

abundant relative to the preceding forested state with fire-promoting trees. In support of this notion of a wettening climate inducing vegetation shifts to more mesic plant communities, a decline in fire frequency is recorded in the Kenai peninsula from 4.6kya and is attributed to wetland development [152]. Additionally, in cluster 4 in the last 2.6kya, the GDD and NPP composites suggest that their long-term declines resulted in a virtual absence of growing days and productivity, which alone can be expected to reduce fire activity.

Cluster 5 does not experience any major vegetation shift after 5.6kya [46], hence it is apparent that climate and productivity were the main causes of its gradual decline in fire between 5.6-0kya. Declining summer insolation from the mid- to the late Holocene [53] would have resulted in progressively lower GDD and hence NPP. The lower fuel loads, along with the gradual year-round wettening of the region would have created progressively less favourable fire conditions. In contrast to this, the boreal northwestern American fire reconstruction of Marlon et al. [94], which spatially overlaps clusters 1, 4, and 5, shows a generally increasing fire response over the mid-to-late Holocene, which also contradicts the patterns of clusters 1 and 4. Marlon et al. [94] interpret the increasing fire response as a consequence of a warmer and wetter boreal region during the mid-to-late Holocene, stating further that it is difficult to explain the generally high biomass burning in the late Holocene given the high moisture and temperature levels. However, the GDD signals of clusters 1, 4, and 5 suggest the boreal American region got progressively colder from the mid-Holocene onwards. In agreement with this, the Viau and Gajewski [153] pollen-based reconstruction of the Holocene climate of boreal Canada shows that summer temperatures declined in central Canada from ∼5.5kya to the present. Evidently, the fire reconstruction for cluster 5 and the interpretation of its controls are in better agreement with available evidence than the Marlon et al. [94] reconstruction. Nonetheless, it is difficult to infer an explicit decrease in fire in this cluster due to the relatively high uncertainty of the fire response.

Clusters 6 and 12: mid-latitude boreal/temperate North America

The large fire increase between 11.6-9.6kya in cluster 12 is evidently brought about by the substantial increase in fuel as a consequence of vegetation colonisation of newly-opened land following the LIS recession [46]. The general decline in fire in both clusters 6 and 12 between 10.1-7.6kya and 9.6-4.6kya respectively can be explained by generally increasing annual moisture, which would have reduced fire probability. In cluster 12, increasing moisture indicated by both VPD and MI is likely to have been the predominant fire control over this time given their high explanatory power. Additionally, independent pollen-based evidence of Holocene land cover change in these regions shows that the levels of broadleaf and needleleaf cover generally maintained stable, high levels between 9.6-0kya, making it less likely that vegetation changes induced the fire changes from 9.6kya [46]. In cluster 6, the 10.1-7.6kya moisture increase occurred along with large variations in seasonal dryness seen in the VPD composite, which can explain the similar pattern of variability in fire around its declining trend. Following the LIS collapse in Quebec ∼8.1kya, cluster 6 experienced a large increase in boreal forest cover [46]. This increase in fuel loads explains the large increase in fire between 7.1-5.1kya. Between 5.1-2.1kya, the elevated and stable fire levels of cluster 6 can be explained by relatively stable and high levels of productivity, as well as stability in seasonal dryness as seen in the VPD composite.

In both clusters 6 and 12, the relative stability of climate, productivity, and needleleaf and broadleaf cover between 2.1-0kya and 4.6-0kya respectively [46], appear unable to account for the

rise in fire in cluster 12 between 4.6-1.6kya and its subsequent decline, and the disproportionately large decline in fire from 2.1kya in cluster 6. Moreover, the fact that these fire patterns are tightly constrained implies that the disparate zones of these clusters experienced synchronous changes to their respective fire controls. These patterns may suggest that a continental-scale process drove the fire changes (e.g. insolation changes). Two independent studies of fire history in the Quebec region to the south east of James Bay by Oris et al. [81] and Ali et al. [154] show a decline in fire season length (which was defined using temperature, moisture, and summer insolation patterns) accompanied by attenuated fire levels between 3-1kya and 2-0kya respectively. Additionally, Oris et al. [155] also observed a fire increase between ∼4-3kya as is observed for cluster 12, explaining this as a result of an anomalous increase in fire season length at ∼3kya. It appears that changes to fire season length had an important influence on the fire responses of these clusters in the late Holocene. The pronounced fire decline in cluster 6 is suggestive of a system crossing a critical environmental threshold and transitioning to a novel fire regime. This may be related to the progressively increasing seasonal and annual moisture to their maximum levels and contributing to the decline in fire season length in the regions of cluster 6.

Cluster 16: Maritime temperate North America

The fire response of the American cluster 16 appears to be primarily controlled by moisture changes in which periods of relative dryness resulted in elevated fire. The moisture changes occurred in tandem with vegetation composition shifts in this region [46, 156], which probably contributed to the fire variability. Between 11-9kya when temperatures, NPP, and fire increased while annual moisture levels were relatively low, there was a large expansion of needleleaf trees into cluster 16 on the east coast of North America, synchronous with the northward contraction of the LIS [46]. In the mid-Holocene, increasing temperatures and moisture likely resulted in an observed needleleaf decline when broadleaf cover was at a maximum [46]. This probably contributed to the declining mid-Holocene fire response and can also explain the inversion of the NPP relationship to fire between the 12-8kya and 8-4kya intervals from positive to negative as NPP increased. In support of this, there is evidence that the climate became wetter in the region of the eastern zone of cluster 16 between 8-7kya [151]. Accompanying this change was a vegetation shift from *Picea-Pinus*-dominated needleleaf forest to *Fagus-Quercus-Tsuga* hardwood-hemlock, which are considered to be more mesophillic taxa than needleleaf pines [151]. This pattern is also corroborated by the *Fagus* increases in the eastern zone of the cluster and *Tsuga* increases in both zones observed between 8-6kya in an independent pollen-based vegetation reconstruction [46].

From 2.6kya, the attenuation of the seasonal and annual moisture increases shown by the VPD and MI curves suggest a slight drying of the cluster in the most recent two millennia, despite the cluster being at a general Holocene moisture maximum. These moisture changes are unlikely to be the predominant control on fire given the disproportionately large fire increase observed. In the western zone of the cluster, broadleaf trees declined while needleleaf tree cover remained high between 2-0kya [46], which may have contributed to the fire increase. Additionally, humans are implicated in increased fire activity in the western zone in the late Holocene, specifically in the south of Vancouver Island where most charcoal records in the western zone are concentrated [90]. It is argued that fire increases were likely human-caused since there is evidence of human settlement in the region from ∼2kya and

the region was dominated by mesic forest at the time [90]. Additionally, in the eastern zone of the cluster, there is localised evidence for human influences on fire regimes that suggests humans may have increased fire sizes from ∼1.5kya [157]. It is also worth noting that all American clusters experience a long-term moisture maximum in the late Holocene, but only this cluster experiences a pronounced fire increase within the last 2kya, which points towards a non-climatic influence such as anthropogenic activities shaping its fire regime. It seems plausible that a combination of an attenuated wettening of the cluster, tree composition changes, and human activities all contributed to the fire increase in the last 2.6ky.

Cluster 17: Northeastern boreal America

Similar to the fire trajectory of cluster 17, a fire reconstruction from a synthesis of 30 charcoal records from lakes in Quebec by Carcaillet and Richard [158] identified a period of elevated fire activity between ∼10-8kya, a decrease in fire between ∼8-6kya, and higher fire values in the late Holocene. The study interpreted the elevated fire activity between ∼10-8kya as a consequence of dry adiabatic winds and air-mass instability associated with the LIS that promoted frequent lightning [158]. In agreement with this interpretation, the elevated fire in the early Holocene in cluster 17 can be explained by the drying climate given by the MI and VPD curves. Additionally, there are important increases in productivity and needleleaf tree cover in this region as the LIS contracted northward between ∼10-8kya [46], which would have contributed to the increased fire. In agreement with this, Marlon et al. [94] interpret the elevated burning observed between 10-8kya in their fire reconstruction for the St Lawrence region as the result of the expansion of needleleaf forests. In contrast, the role of vegetation transitions in affecting the fire response of this region is downplayed by Carcaillet and Richard [158] who claim that the region is unlikely to have experienced a synchronous change to forest composition given its large latitudinal range. However, most of the charcoal records of this cluster fall within a latitudinal range of 1.3 degrees before 7kya, which is a smaller range than regions that have experienced largely synchronous changes to vegetation. For example, forest cover changes on the order of 10^1% are observed within ∼1ky Holocene intervals in various European regions such as the British Isles and Atlantic western Europe [127]. Therefore, vegetation changes cannot be ignored in terms of their likely effects on increasing the amount and flammability of fuel in this region.

The mid-Holocene fire minimum of cluster 17 is interpreted by Carcaillet and Richard [158] as the result of the Atlantic Maritime Tropical humid air mass that could flow over southern Quebec in summer following the LIS collapse. In contrast to this, the VPD and MI curves suggest that summers got drier at ∼8.6kya with the onset of the pronounced summer/autumn dry season following the LIS recession. Furthermore, annual moisture reached its lowest and productivity its highest values at 7.6kya, suggesting that environmental conditions favoured more fire at this time. In general agreement with the MI curve, a pollen-based reconstruction of the Holocene annual precipitation of northern Quebec shows that precipitation generally declined between ∼8.5-6kya [153], supporting the notion that fire conditions became more favourable in the northern and central regions of this cluster during the mid-Holocene fire minimum. The counterintuitive pattern between these climate patterns and fire activity at this time is understood by considering that most of the charcoal records contributing to the fire composite are concentrated near the southern border of the cluster below 50N until ∼7ky. In the region of the adjacent eastern zone of cluster 16, the evidence of moistening climate and a shift from

needleleaf to hardwood-hemlock forest [151] probably also affected the southern margin of cluster 17 and hence the fire record, but not the central and northern parts of the cluster where the VPD and MI composites detect the observed drier conditions [153]. This is evident from the Williams et al. [46] vegetation reconstruction, which shows that there was a substantial northward hemlock rise into the southernmost part of cluster 17 between 8-6kya but not into higher latitudes [46]. Therefore, in agreement with the Carcaillet and Richard [158] hypothesis of a shift to a more humid climate, the low-point in fire in the mid-Holocene can be explained by an increase in moisture in the southern regions of cluster 17, as well as an associated forest compositional change from needleleaf forests to less fire-tolerant taxa [151]. Since this moisture shift does not occur uniformly across the cluster, it is not evident in the VPD and MI composites.

From the mid- to the late Holocene, central Quebec experienced a general needleleaf cover increase and broadleaf cover decrease as the climate cooled in summer and generally wettened [46, 153]. These vegetation changes can explain the gradually increasing fire response over this time. Overall, it is evident that the fire response of this cluster is strongly regulated by the vegetation changes that have characterised the region over the Holocene.

Clusters 5, 12, 13, and 16: Europe

The early-Holocene increases in fire across Europe are understood by considering the Fennoscandian Ice Sheet collapse over Scandinavia at ∼9.9kya [107], the associated climate warming and drying [105] and accentuation of moisture seasonality, and the accompanying forestation across the continent [127]. These changes would have increased fire probability through increasing fuel loads and dryness in the fire season. In support of this, the GAM analysis by Feurdean et al. [116] shows that in the 12-8kya interval, summer temperature and moisture both exhibit a generally positive relationship with fire in all three regions of their analysis, and the elevated fire seen in the three ecoregions is interpreted by Feurdean et al. [116] as being driven primarily by increasing temperatures and corresponding fuel load increases.

The pattern of reversed fire-environment correlation values between the 12-8kya and 8-4kya intervals for these European clusters, with positive needleleaf and negative broadleaf 8-4kya correlations, suggests that moisture and biomass changes were less important for fire variability in the mid-Holocene and that forest composition changes became the dominant influence. In agreement with this, the Feurdean et al. [116] GAM analysis shows that the positive summer temperature and moisture relationships with fire in the 12-8kya interval become generally negative in the 8-0kya interval, explained by Feurdean et al. [116] as the increasing importance of land cover variations on fire regimes. This transition from a greater importance of fuel load for fire to fuel composition is probably a consequence of forests covering a large enough proportion of European landscapes to become the primary determinant of ignition probability and fire spread. Under such extended forest cover levels, the role of open landscapes in controlling fire ignition and spread is attenuated as they are increasingly fragmented and reduced. Differences in fire-relevant forest compositional characteristics then become important for determining changes to a given fire regime.

In all four of the NET clusters spanning Europe, the general fire increases in the late Holocene can be explained by the continent-wide decline in broadleaf cover and increase in open and agricultural land cover. The broadleaf declines in the temperate clusters 13 and 16 do not appear to be predicted

by climate because the simulated NPP and GDD responses show increases in the late Holocene but both needleleaf and broadleaf cover decline. Considering also the large increases in open and human landscapes in these two clusters from the mid-Holocene onwards, it is evident that human land use intensification and human-driven broadleaf deforestation played a major role in these fire increases. Humans are evidenced to have started farming in the British Isles around 6kya, but potentially much earlier, around 7.5kya, in southern Germany and eastern France [159]. This agrees with the early onset of arable and pasture land expansion in the Eurasian cluster 16 at ∼7.1kya. In continental Europe, it is apparent that these human activities were under way from as early as 6.6kya [113, 159], supporting a human role in altering land cover in cluster 13. The cluster 13 composites suggest that human landscape expansion and broadleaf deforestation greatly intensified between 3.6-0kya, leading to the large late-Holocene fire increase observed. In agreement with this, the same increase in fire is observed from ∼3.6kya in the continental European composite in Feurdean et al. [116], which they interpret as deforestation-related fires that started at the Bronze or Iron Age that reached a maximum during the early modern period.

In contrast to other European clusters, the increasing land use intensification and forest decline in cluster 16 between 3.1-0kya corresponds to a gradual decline in fire. This may be related to the relatively low levels of forest cover in this cluster, especially by the time fire starts decreasing. A threshold of landscape fragmentation may have been crossed at this point, where the fuel load was too discontinuous and depleted to sustain high fire levels. This is supported by the Marlon et al. [94] interpretation of the fire response of the British Isles over the mid-to-late Holocene. They suggest that human use of fire to open woodlands and improve grazing contributed to the increase in fire between 5-1kya while the decline in their reconstruction after 1kya is put down to increased cultivation. Alternatively, the decline in fire from 3.1kya may be due to the high moisture levels at the time, which are progressively higher than at any previous Holocene period and are additionally generally higher than any other cluster in the NET analysis. This may have acted in concert with landscape fragmentation to reduce fire in the last three millennia.

The late-Holocene land cover changes in the hemiboreal and boreal clusters 12 and 5, namely broadleaf declines concominant with generally increasing needleleaf cover, are in agreement with the declining temperatures in northern Europe at the time [105, 132] and can explain the fire increases observed. However, it is also evident that agriculture and hence probable human deforestation practices began almost synchronously across southern Scandinavia and hemiboreal northeastern Europe ∼6kya [159, 160]. Additionally, there is evidence of human settlement and anthropogenic effects on local vegetation assemblages corresponding to increased fire activity from as early as 8.7kya at as high a latitude as 70N in Scandinavia [161], supporting that land cover changes in these clusters were influenced by anthropogenic processes. However, the open/human land classes for these clusters show more modest increases in the late Holocene relative to the temperate European regions, and generally show higher rates of increase only within the most recent 2ky, implying that the predominant cause of deforestation from the mid-Holocene onwards in these clusters was climate change.

Consistent with these patterns, it is suggested by Roberts et al. [113] that the needleleaf cover of boreal Europe started declining due to human activity from ∼2kya. This is further consistent with Feurdean et al. [116], who interpret the relatively late (from ∼2kya) signal of agricultural expansion in their boreo-nemoral reconstruction as a consequence of this region exhibiting a very high needleleaf

component, making it edaphically and climatically less favourable for agricultural conversion relative to broadleaf forests [113]. The relatively depleted broadleaf forest cover observed for clusters 12 and 5 within the last 2ky may have led humans to begin clearing needleleaf forests for agriculture, seen by the needleleaf declines in both clusters starting within the most recent 2ky. The earlier turning point in needleleaf cover in cluster 5 at 1.6kya, as opposed to 1.1kya in cluster 12, is congruent with this hypothesis. This is because cluster 5 has lower broadleaf cover than cluster 12, and therefore reached the equivalent level of broadleaf depletion ∼0.5ky earlier. Finally, the continued fire increases in both clusters after 2ky further points towards anthropogenic activities shaping these fire regimes because the fire increases contrast with the wettening climate and declining needleleaf and broadleaf cover in these clusters, which according to the fire relationships shown by Feurdean et al. [116] should lead to weak and generally negative fire responses.

Cross-continental cluster comparisons

The correlations between the Eurasian and American fire responses of the three clusters that span both continents suggest that fire activity of the same clusters on the two continents was driven by broadly similar environmental processes in the early Holocene, which diverged from the mid-Holocene. This can be understood by considering the early-Holocene ice sheet collapses on both continents, the subsequent role of land cover processes, and the unique European legacy of human agricultural intensification. In the 12-8kya interval, the main control on fire across the NET clusters was evidently the climate changes associated with the ice sheet collapses on both continents [102, 107]. On both continents, the magnitude of the climate and productivity changes were high in this interval compared to subsequent intervals. This would have muted the role of land cover compositional effects on fire, making changes to biomass and fuel dryness the primary fire controls and thereby homogenising the fire responses between the continents. It is apparent in the results that the NPP, MI, and VPD variables are adequate at capturing these similar environmental signals.

The divergence of the continental fire responses of cluster 16 in the mid-Holocene appears a consequence of different timing of broadleaf cover declines that predict fire increases, which started in the early Holocene in Eurasia and the late Holocene in America. This difference may reflect substantially different Holocene moisture levels between the two continents (the median MI of the charcoal-covered grid cells of cluster 16 in Eurasia is >2 while in America it is <1.5). Under the same rate of climate change, moisture thresholds that may affect distributions of broadleaf species with identical climate tolerances would be achieved at different times on the respective continents. Additionally, the species composition of broadleaf taxa differs between the continents [46, 111], which may result in different species climate tolerances.

The dissimilarity of the continental fire responses is most evident in the 4-0kya interval when human influences on European land cover are most pronounced. This suggests that the increasing role of humans in shaping European fire regimes from the mid-Holocene onwards is an important factor leading to the divergence of fire histories of similar palaeo environmental space on the two continents.

Cluster 10: Altai region

Palynological investigation of climate and vegetation patterns in the Altai region suggests that after ∼6.8kya, decreasing temperatures resulted in cold winter air masses penetrating into this region which

led to permafrost growth [162]. Because Eurasian species of the *Larix* genus have a greater ability to grow on continuous permafrost soils and withstand extreme continental winter climates relative to other Eurasian trees in the genii *Picea* and *Pinus* [163], this environmental change may have been responsible for the mid-Holocene transition from *Picea*/*Pinus sibrica*-type forests to *P. sibrica*/*Larix* forests observed in this region [162]. Eurasian *Larix* trees are classed as "fire resisters", which are fire adapted with forests that exhibit frequent fire occurrence [41], while *P. sibrica* and *Picea* species are classed as "fire avoiders" with no fire strategy traits [41]. Thus, the *Larix* rise would have promoted a more fire-prone landscape relative to the previous forest state. The general fire rise from the mid-Holocene until ∼3.1kya may be related to this and to the generally increasing productivity over this period.

From 3.1-0kya, the general fire decline can be explained by this cluster experiencing high levels of annual and seasonal moisture, which are at general long-term maxima in the last 3ky. This long-term moisture increase from the mid-Holocene culminating in elevated late-Holocene values is supported by a proxy-based reconstruction of moisture changes in central Asia [164]. However, the poorly constrained trends of the fire response and its low sample size make these interpretations uncertain.

Cluster 11: Southern Siberia and north-central Mongolia

The long-term decline in fire in cluster 11 can be explained by the general Holocene wettening trend observed in the MI and VPD curves. This wettening trend is corroborated by palaeo climate reconstructions in the charcoal-covered regions of this cluster, which show that they shifted to a wetter state from the early to the late Holocene [164]. The increased fire activity observed between ∼9-7kya may have been the result of an increase in the fuel load brought about by landscape forestation. This is evidenced by a synthesis of pollen records from Lake Baikal, Lake Hovsgol, and north-central Mongolia [165]. This study shows that from 9kya, the proportion of needleleaf trees greatly expanded in the Lake Hovsgol region and the system transitioned from a state characterised by high shrub and steppe-type vegetation cover to a more coniferous-tree vegetation state dominated by *Pinus sylvestris*, a fire-adapted species [41], and *P. sibrica* trees [165]. Additionally, the records from Lake Baikal indicate that in the north-east and south of the lake catchment there was a rise in needleleaf tree dominance [166].

The increase in fire between 3.6-1.1kya corresponds to a moderate forest expansion from a previous forest-steppe type vegetation in the Lake Hovsgol region [165]. This contrasts with the evidence from three different pollen cores from across Lake Baikal, which shows increased open vegetation and *Larix* forest development from a previous taiga state dominated by *P. sylvestris* and *Larix* trees [166]. These contrasting patterns of landscape closure and opening respectively also correspond to a cluster-wide general decline in productivity, low levels of broadleaf cover, and greatly increased heath cover during a time of high needleleaf cover. However, the low sample size composing the land cover composites of this cluster makes them uncertain. Nonetheless, these patterns suggest that the cluster transitioned to a relatively more open landscape populated with fire-adapted trees, while Lake Hovsgol experienced a contrary increase in tree cover. The elevated fire activity during the 3.6-1.1kya interval may be a consequence of the forest expansion in the Lake Hovsgol region overshadowing any fire declines that may have been caused by reduced fuel load in the Lake Baikal region. However, an alternative explanation is that the transition to relatively more open *Larix* forests in the Lake Baikal region created

a more ignitable ground layer of fuel that promoted forest fire spread, while the forest expansion in the Lake Hovsgol region may have increased the fuel load below levels of forest density that would reduce ground-layer fire probability.

Results and Discussion: European scale

Results

A total of 1126 grid cells were clustered into 13 spatial clusters to produce a continuous European stratification (figures 12, A.38, A.39). There is a general latitudinal gradient among the clusters, shown by generally distinct high (9, 11, 12, 13), mid- (3, 4, 7, 8) and low (1, 2, 5, 6, 10) latitude cluster partitions. There is also a longitudinal partition bisecting central Europe, namely cluster 3 is to the continental east and cluster 8 to the west in a more oceanic position. The high-latitude clusters 9, 11, and 12 generally have higher needleleaf and lower pasture and natural grassland cover than the mid-latitude clusters 3, 4, 7, and 8 (figures A.40, A.41).

There are spatial discontinuities for some clusters, including the clusters in the Mediterranean region (10, 6, and 2; figure 12). Additionally, the central Scandinavian and Swiss Alpine regions have been separated into a single distinct cluster 9. Furthermore, an association between the British Isles and north and central/western continental Europe is evident, seen by clusters 4, 7, and 8. Cluster 11 is located in northern Scandinavia with a separate zone in the alpine region of southern Norway, and its two zones are separated by cluster 9. Finally, cluster 5 has multiple separate zones spread across mainland Europe in a north-east direction from Iberia to northeastern Europe.

For the overlapping European region, the NET stratification is spatially simplified relative to the European stratification. Nonetheless, there are similar features between the two stratifications, including a general latitudinal pattern in the cluster partitions of both stratifications (figures 2, 12). Additionally, two European clusters stand out as close analogues of two NET clusters: 1) the hemiboreal northeastern European region is separated into a distinct cluster at both scales; 2) The European cluster 7, which registers to the north/west of the Swiss Alpine region as well as in the British Isles, is analogous to cluster 16 at the NET scale that registers in the central British Isles and the general north western and central Swiss Alpine region.

A total of 268 charcoal records were used to generate eight European-scale composite curves for clusters 3, 4, 5, 7, 8, 9, 11, and 12 (figures 12-20). The charcoal records comprising clusters 12 and 8 have relatively small respective geographic distributions and make up composite curves composed of >30 records with relatively small confidence intervals. Clusters 3 and 11 are composed of <20 charcoal records and span relatively large geographic ranges yet they have composite confidence intervals that are comparable to clusters 12 and 8. The geographically discontinuous clusters 7 and 9 also have well-constrained mean fire responses over most of the Holocene. This contrasts with cluster 4, for which its 25 charcoal records are concentrated mostly in the northern British Isles, but its composite has relatively wide confidence intervals. Despite this, its confidence interval trajectories are in good agreement with its mean curve and isolate clear patterns of fire variability. Cluster 5 has 15 charcoal

records spread across its discontinuous range and has a poorly constrained mean fire response.

All European fire responses are generally well correlated to at least one of the environmental variables investigated (figure 21). With the exception of clusters 7 and 8, all fire responses show correlations >= |0.5| with at least one of forest cover, temperature, and precipitation across their full time domain (table A.5). At the 4ky resolution, all clusters exhibit correlations >= |0.75| with at least one variable for at least one 4ky interval. In agreement with the NET-scale results, there is a clear pattern in these correlations where they invert between the 12-8kya and 8-4kya intervals; all except cluster 5 experience this inversion for at least one of the fire correlations with forest cover, precipitation, and temperature where the correlation is > |0.5| for at least one of the two time intervals. In further agreement with the NET results, between the 8-4kya and 4-0kya intervals, the variable with the highest explanatory power changes from forest cover, forest composition, and climate variables to open/human land cover variables across much of continental Europe and the British Isles (figure 21). Additionally, two of the three clusters that are most strongly predicted by climate variables in the 4-0kya interval (3 and 5) nonetheless have high correlations with land cover variables in this interval: cluster 5 has correlations >= |0.75| with all land cover variables, as is the case for cluster 3 with the exception of the fire-heath cover correlation.

The environmental composites of the European clusters show some important similarities in summer temperature and land cover trajectories (figures 13-20). Summer temperature generally increases from the early to the mid-Holocene in all clusters except in the eastern continental cluster 3 where the increase stops at 8kya and temperatures then decline until ∼5kya. Despite this similarity, the temperature responses change by different magnitudes and there are differences in the timing of temperature variations among clusters. Subsequent mid-to-late Holocene temperature changes are also variable among the clusters, but there is a general decline from their mid-Holocene high-points among all except cluster 3, which shows a slight increasing trend from 5kya onwards. Additionally, all clusters generally show the same Holocene pattern in forest and broadleaf cover, namely mid-Holocene maxima followed by declining trends to the modern period. Exceptions to this pattern are, again, cluster 3, which shows a more delayed peak in broadleaf cover at 3.6kya, cluster 9, which has an earlier peak in broadleaf cover at 8.6kya, and cluster 11, which has a broadleaf cover response that linearly declines over most of the Holocene. The open/human land classes for all clusters generally show a long-term accelerating increase from the mid-Holocene onwards.

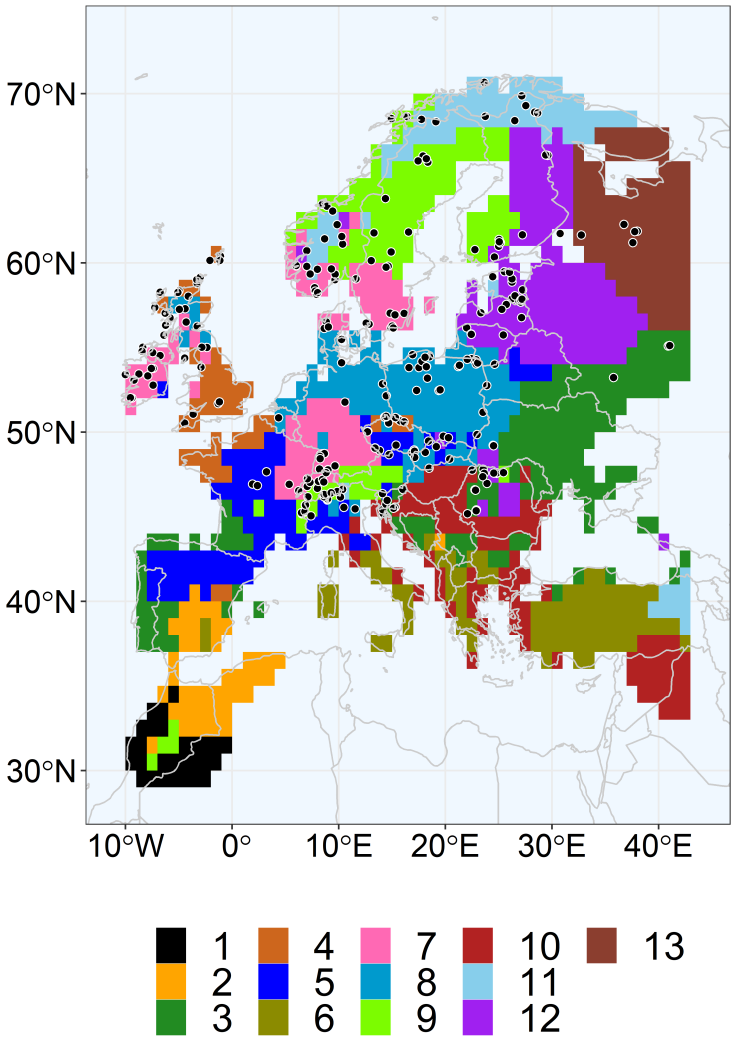

Figure 12: European stratification of palaeo environmental space generated by biclustering grid cells based on temporal variation in summer temperature, summer precipitation, and forest cover over the period 12-0kya. Black points are locations of charcoal records. Spatial clusters are colour-coded and numbered in the legend.

Individual cluster results

Clusters 7, 8, 9, and 11: Central/Northern Europe and western British Isles

Clusters 7, 8, 9, and 11 have similar Holocene environmental histories, including early-Holocene forest cover increases to early/mid Holocene maxima (figures 13-16). Additionally, from the mid- to the late Holocene, broadleaf and forest cover decline and open/human landscape classes increase as temperatures decline. Clusters 11, 9, and 7 show a general increase in fire over the Holocene, with cluster 11 showing a faster rate of increase from 4.6-0kya. Cluster 8 shows a large fire increase until 9.6kya, then a subsequent gradual decline to a mid-Holocene local minimum, followed by a gradual increase until 1.1kya where it begins increasing at an accelerated rate to its highest Holocene value by modern times.

The early-Holocene fire increases in clusters 7, 8, and 9 correspond to summer temperature increases that are large relative to their overall Holocene temperature variability, namely increases of ∼2.5°C between 11-7kya in cluster 7, ∼1°C during the fire increase in cluster 8, and ∼1°C between

11.6-8.6kya in cluster 9 (figures 13-15). These occur without similar proportionally large increases in summer precipitation, implying substantially increased summer dryness in these clusters. In all four clusters, the temperature increases occur along with large forest cover increases, from under 40% to well over 70% at ∼8kya in cluster 7, from under 60% at 11.6kya to up to ∼80% by 8.6kya in cluster 8, from ∼30% to ∼70% by 8.6kya in cluster 9, and from under ∼30% to ∼60% by 8.1kya in cluster 11. The 12-8kya correlations show that landscape forestation and temperature increases strongly predict the fire increases in these clusters (cluster 7: temperature: r = 0.98; forest: r = 0.92; cluster 8: temperature: r = 0.84; forest: r = 0.92; cluster 9: temperature: r = 0.98; forest: r = 0.97; cluster 11: temperature: r = 0.98; forest: r = 0.87).

The nature of the inversion in fire-environment correlations between the early and mid-Holocene intervals is similar among clusters 7, 8, 9, and 11, with temperature being inversely related to fire in all four clusters and forest cover in clusters 7, 9, and 11 in the 8-4kya interval (cluster 7: temperature: r = −0.74; forest: r = −0.61; cluster 8: temperature: r = −0.97; cluster 9: temperature: r = −0.86; forest: r = −0.85; cluster 11: temperature: r = −0.63; forest: r = −0.85; figures 13-16). As seen in the mid-Holocene NET results for these regions, it is generally evident that fire negatively responds to broadleaf cover variations and positively to needleleaf variations, with the exception of cluster 11 (8-4kya correlations: cluster 7: needleleaf: r = 0.94; broadleaf: r = −0.88; cluster 8: needleleaf: r = 0.91; cluster 9: needleleaf: r = 0.88; broadleaf: r = −0.93; cluster 11: needleleaf: r = −0.75; broadleaf: r = −0.57).

All four clusters experience a general temperature decline from the mid-Holocene, with the cluster 11 temperature composite declining to its lowest Holocene levels by modern times (figures 13-16). Along with the temperature decreases, broadleaf cover declines to low modern levels in all four clusters. In clusters 11 and 9, it reaches ∼15% and ∼17% respectively, declining from respective ∼4ky levels of ∼22% and ∼30%. In clusters 7 and 8, the mid-Holocene broadleaf maxima, which are at ∼55% and ∼43% respectively, reach respective values of ∼26% and ∼23% in the most recent time bin. For cluster 8, this broadleaf decline is disproportionate relative to its early-Holocene increase under more extreme climate change, and for cluster 7, the decline is not matched by proportional changes to the climate variables. Additionally, all clusters experience increases in open/human land classes in the 4-0kya interval that are disproportionate relative to their variability in previous Holocene periods. Between 4.1-0kya, cluster 11 experiences arable and pasture land increases from ∼6% to ∼14% and from ∼15% to ∼22% respectively. Over the same interval, cluster 9 experiences arable, pasture, and heath increases from ∼7%, ∼14%, and ∼11% to ∼18%, ∼23%, and ∼16% respectively. In cluster 8 from ∼7.1kya, arable and pasture cover increase to levels of 10% and 15% by ∼4kya respectively, and by the modern period they reach levels of ∼19% and ∼21% respectively. In cluster 7, arable, pasture, and heath cover increase from 5ky levels of ∼5%, ∼12%, and ∼8% to modern values of ∼17.5%, ∼20%, and 13% respectively.

In clusters 7, 8, and 11, the decline in broadleaf cover and increase in open/human land classes all predict the fire increases experienced by these clusters in the late Holocene (4-0kya correlations: cluster 7: broadleaf: r = −0.98; arable: r = 0.97; pasture: r = 0.96; heath: r = 0.99; cluster 8: broadleaf: r = −0.89; heath: r = 0.96; pasture: r = 0.92; arable: r = 0.86; cluster 11: broadleaf: r = −0.86; heath: r = 0.6; arable: r = 0.91; pasture: r = 0.83; figures 13-16). For cluster 11, the fire increase also corresponds to a needleleaf cover decline (4-0kya correlation: needleleaf: r = −0.88). In

cluster 9, the fire response begins to decline from ∼1.6kya, which corresponds to summer precipitation increasing to its highest Holocene value by modern times, as well as a summer temperature decline. The cluster 9 fire response is strongly positively related to the temperature decline in the 4-0kya interval ($r = 0.93$) and weakly negatively related to the increasing summer precipitation ($r = -0.48$).

There are analogous patterns between clusters 11 and 9 and the spatially overlapping clusters 5 and 16 at the NET scale, which span northern Europe and the Swiss Alpine region (figures 2, 12). Clusters 11 and 9 both share the NET cluster 5 pattern of a long-term fire increase corresponding to the early-Holocene increases in forest cover/productivity and summer dryness (except for the precipitation increase until 8kya in cluster 11), and the mid-to-late Holocene pattern of landscape opening given by broadleaf declines and increased open/human land classes (figures 15, 16, A.23). Additionally, cluster 9 and the NET cluster 16 show not only a similar environmental history, but the fire responses closely resemble each other, namely a long-term Holocene fire increase culminating in a fire decline in the most recent two millennia (figures 15, A.25). For both cluster 9 and the NET cluster 16, the late-Holocene fire decline corresponds to the clusters reaching their maximal moisture/precipitation levels by modern times.

Cluster 8 shows a similar environmental response to the spatially overlapping NET cluster 13 spanning temperate Europe (figures 8, 14). At both scales, between 2.6-1.6kya there is a decline in the rate of increase of arable and pasture cover as well as a small recovery of needleleaf cover. In the NET cluster 13, there is a small dip in GDD at 2.6ky and similarly there is a local summer temperature minimum at 2kya in cluster 8. From 1.1kya, the more pronounced increase in the cluster 8 fire response relative to preceding millennia corresponds to an increase in the summer temperature composite, while at both scales there are large declines in broadleaf cover and the largest Holocene increases in the open/human land classes.

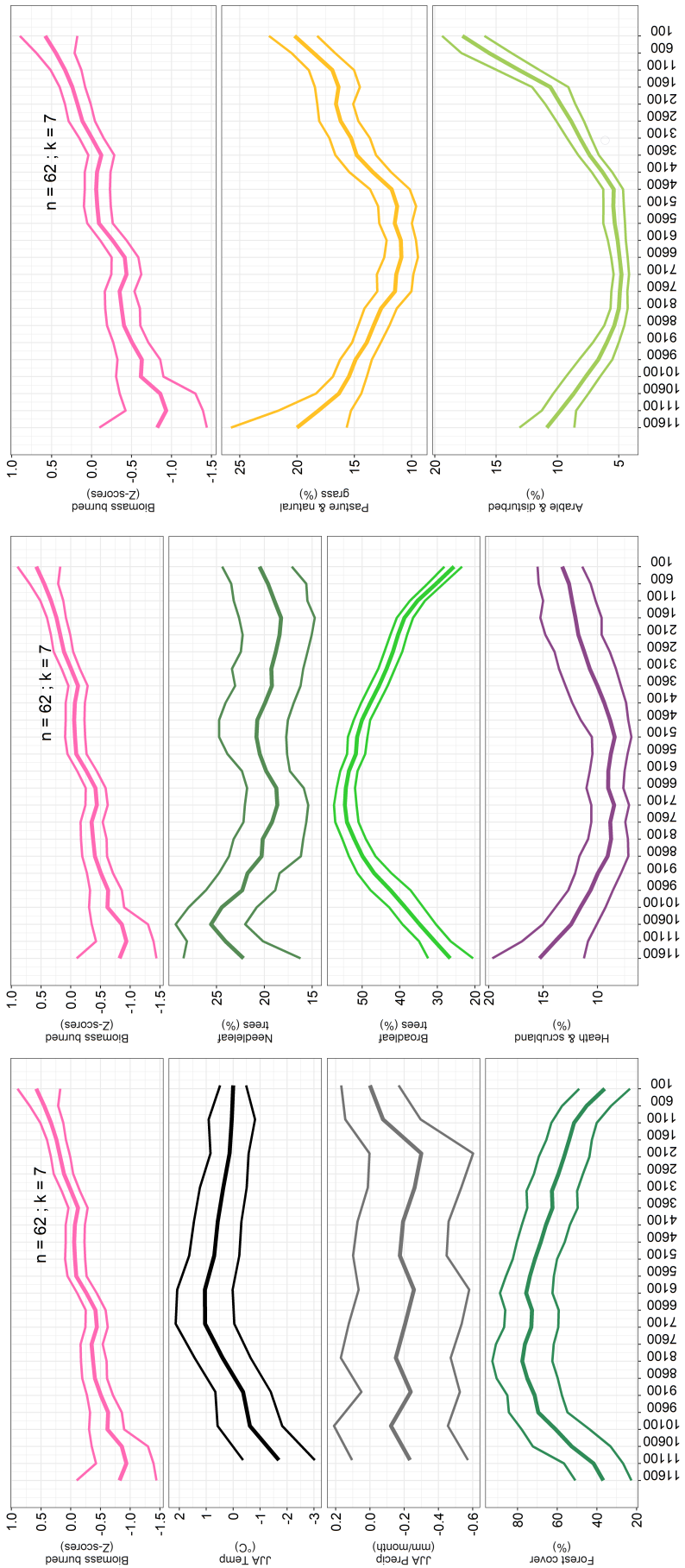

Figure 13: Holocene biomass burning and environmental composite curves for the European cluster 7, all smoothed using a 1500-year window width. The time interval (shown on the x-axis in years before 1950 CE) is limited to the period within the 11.6-0kya interval in which all time points contain at least 10 charcoal records in the smoothing window. The composite curves are shown with 95% bootstrap confidence intervals, except for the temperature, precipitation, and forest cover composite means which are shown with upper and lower standard error composites. The number of charcoal records comprising the biomass burning response (n) and the cluster identity value (k) are shown on the top panel.

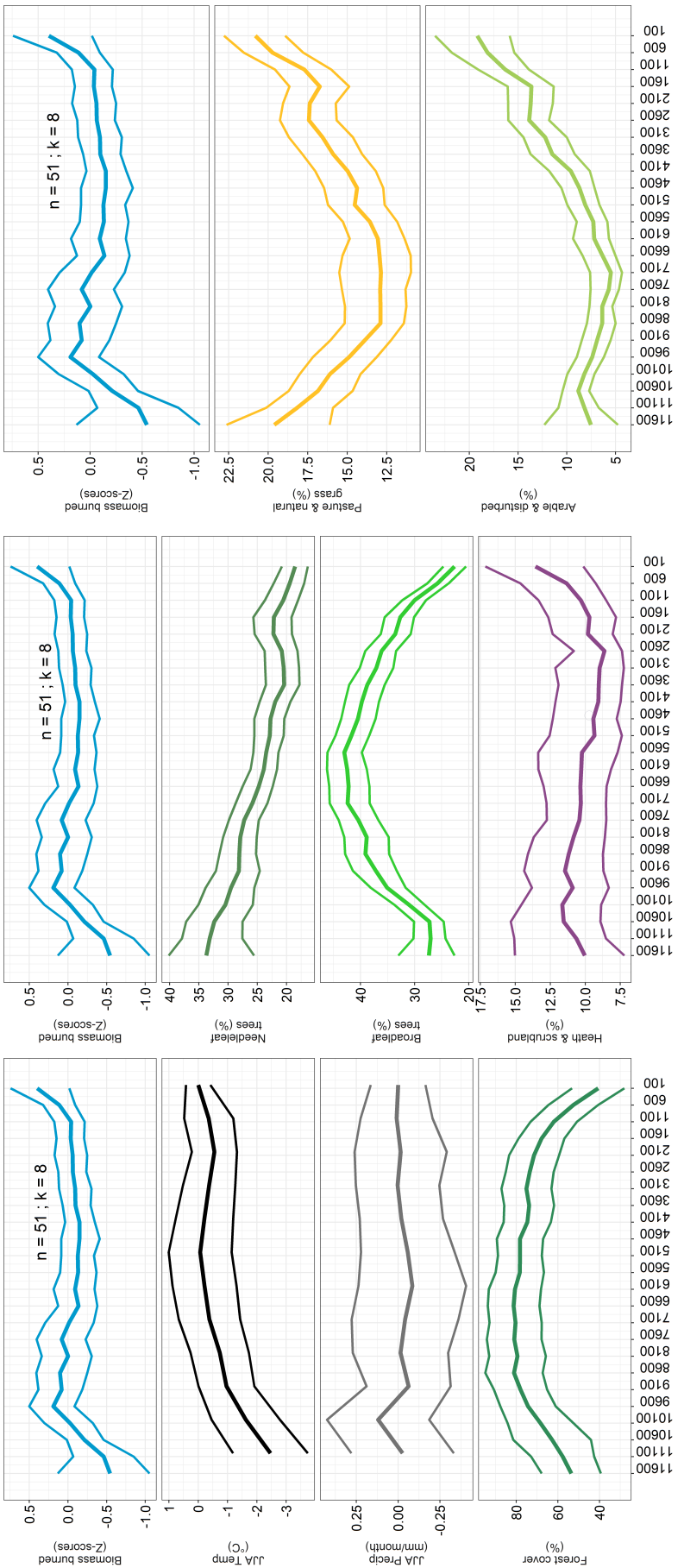

Figure 14: Holocene biomass burning and environmental composite curves for the European cluster 8, all smoothed using a 1500-year window width. The time interval (shown on the x-axis in years before 1950 CE) is limited to the period within the 11.6-0kya interval in which all time points contain at least 10 charcoal records in the smoothing window. The composite curves are shown with 95% bootstrap confidence intervals, except for the temperature, precipitation, and forest cover composite means which are shown with upper and lower standard error composites. The number of charcoal records comprising the biomass burning response (n) and the cluster identity value (k) are shown on the top panel.

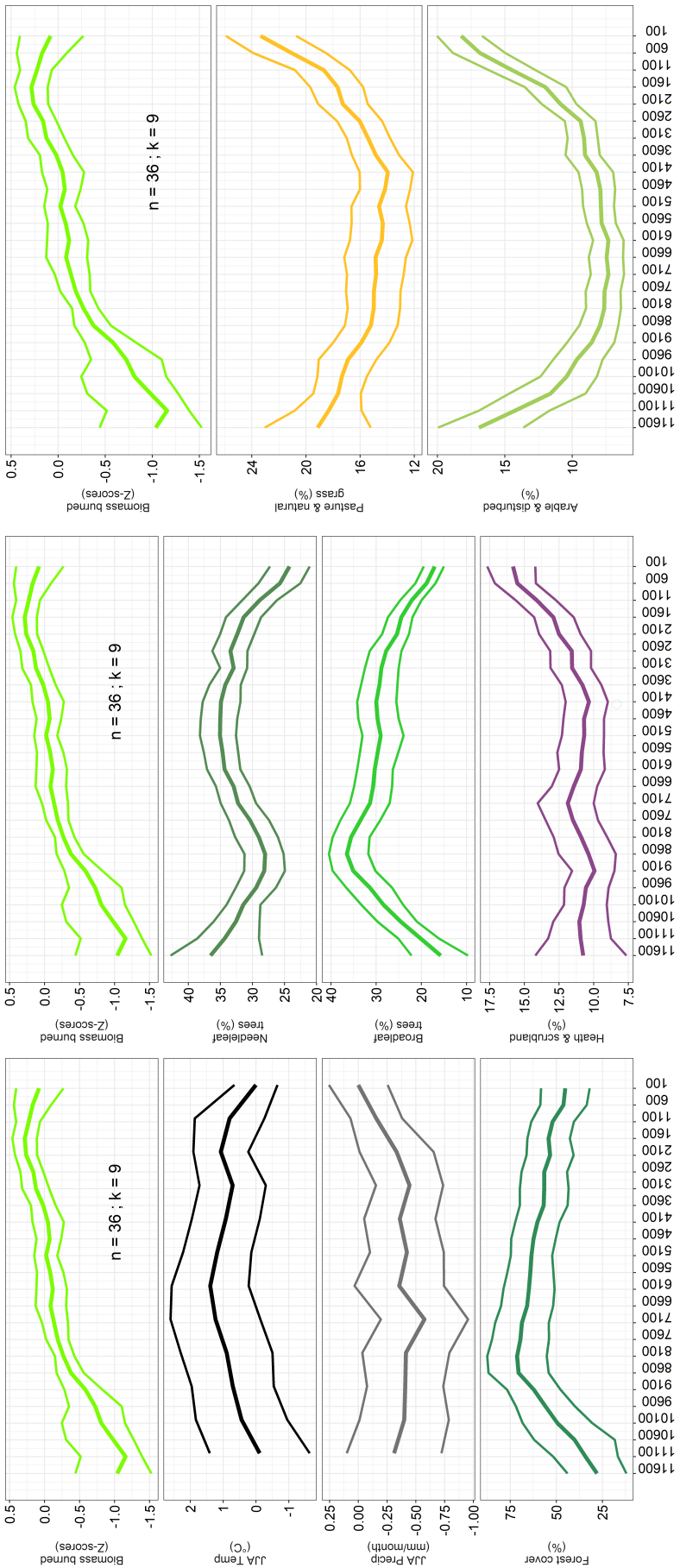

Figure 15: Holocene biomass burning and environmental composite curves for the European cluster 9, all smoothed using a 1500-year window width. The time interval (shown on the x-axis in years before 1950 CE) is limited to the period within the 11.6-0kya interval in which all time points contain at least 10 charcoal records in the smoothing window. The composite curves are shown with 95% bootstrap confidence intervals, except for the temperature, precipitation, and forest cover composite means which are shown with upper and lower standard error composites. The number of charcoal records comprising the biomass burning response (n) and the cluster identity value (k) are shown on the top panel.

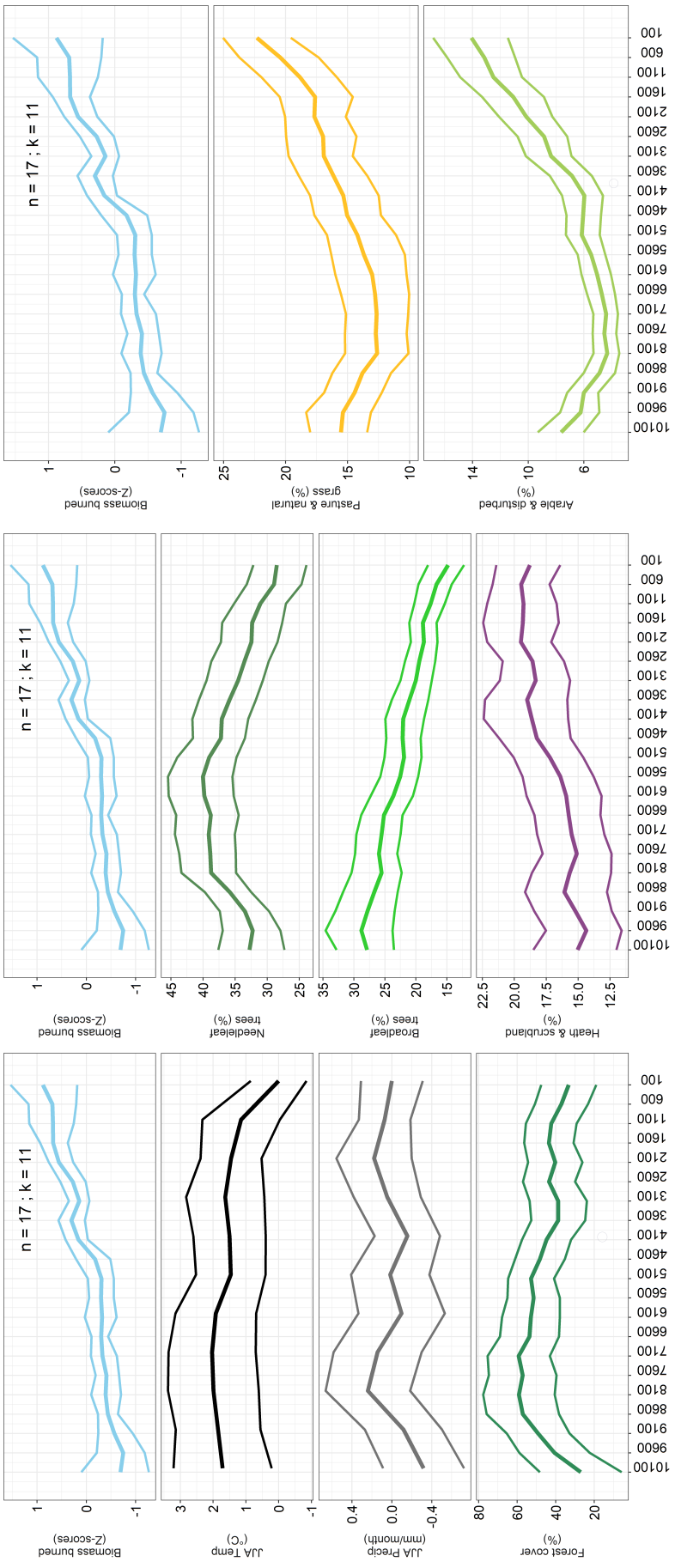

Figure 16: Holocene biomass burning and environmental composite curves for the European cluster 11, all smoothed using a 1500-year window width. The time interval (shown on the x-axis in years before 1950 CE) is limited to the period within the 11.6-0kya interval in which all time points contain at least 10 charcoal records in the smoothing window. The composite curves are shown with 95% bootstrap confidence intervals, except for the temperature, precipitation, and forest cover composite means which are shown with upper and lower standard error composites. The number of charcoal records comprising the biomass burning response (n) and the cluster identity value (k) are shown on the top panel.

Cluster 12: Hemiboreal northeastern Europe

Cluster 12 has high forest and needleleaf cover levels compared to other European clusters (figures A.40, A.42). Unlike clusters 7, 8, 9, and 11, the large increases in temperature and forest cover in the early Holocene do not correspond to a fire increase, rather this cluster experiences a general fire decline from the onset of the Holocene until 3.6kya (figure 17). At the onset of the 9-7kya temperature and forest cover increases, forest cover was already at high levels of ∼70%, substantially higher than forest cover levels of other European clusters at the time of their early-Holocene temperature increases (under 50% for clusters 7, 9, and 11 and ∼60% for cluster 8).

In the 8-4kya period, temperature reaches a 7kya high-point and subsequently declines, while forest cover remains high at ∼80% and precipitation steadily increases (figure 17). In this interval, the declining fire response is most strongly related to the decline in temperature (r = 0.98). From 3.6kya, there is a turning point in the fire curve where it starts increasing at a high rate to its modern value, which is its highest value across the Holocene record. The 3.6kya turning point occurs soon after the turning point in arable land cover at 4.1kya. The large late-Holocene fire increase also corresponds to declining temperatures, forest and broadleaf cover, and generally increasing precipitation. Pasture and heath cover increase only in the last 1.6kya. The correlations in the 4-0kya interval generally reflect these patterns (temperature: r = −0.88; forest: r = −0.98; broadleaf: r = −0.99; arable: r = 0.97; pasture: r = 0.84; heath: r = 0.9).

Cluster 12 has a few important differences to the overlapping cluster 12 at the NET scale. Unlike the NET cluster 12, this cluster includes many of the records in Finland and does not include any records from Jutland (figures 2, 12). The NET cluster has a higher broadleaf maximum and a lower needleleaf maximum than this cluster, namely the NET and European clusters reach mid-Holocene broadleaf maxima of ∼50% and ∼46% respectively, and late-Holocene needleleaf maxima of ∼35% and ∼42% respectively (figures 17, A.24). A key difference between the two clusters is that the NET cluster has the onset of the needleleaf decline at 1.1kya, while at the European scale it occurs at 1.6kya, which is congruent with the boreal European cluster 5 at the NET scale (figure A.23).

Cluster 3: Eastern continental Europe

Over its full Holocene interval, the cluster 3 fire response positively covaries with summer temperature (12-0kya correlation: temperature: r = 0.73). In the early Holocene, the environmental patterns of this cluster are similar to most other European clusters, with fire generally increasing in accordance with temperature and forest cover increases (figure 18). This is reflected in the 12-8kya correlations (temperature: r = 0.99; forest: r = 0.4). In the mid-Holocene interval, the temperature response is relatively stable, and the fire response is inversely related to precipitation variability (8-4kya interval: precipitation: r = −0.61). In the late Holocene, the temperature and precipitation responses show a pronounced oscillatory pattern, with lower summer temperatures being associated with higher summer precipitation. The late-Holocene fire response exhibits a slight increasing trend in accordance with the slightly increasing temperature trend. Pasture and arable land cover also show increasing trends which begin at 5.6kya, while broadleaf, needleleaf, and forest cover decline. These patterns are reflected in the 4-0kya correlations: (temperature: r = 0.92; forest: r = −0.82; needleleaf: r = −0.76; broadleaf: r = −0.91; pasture: r = 0.88; arable: r = 0.81).

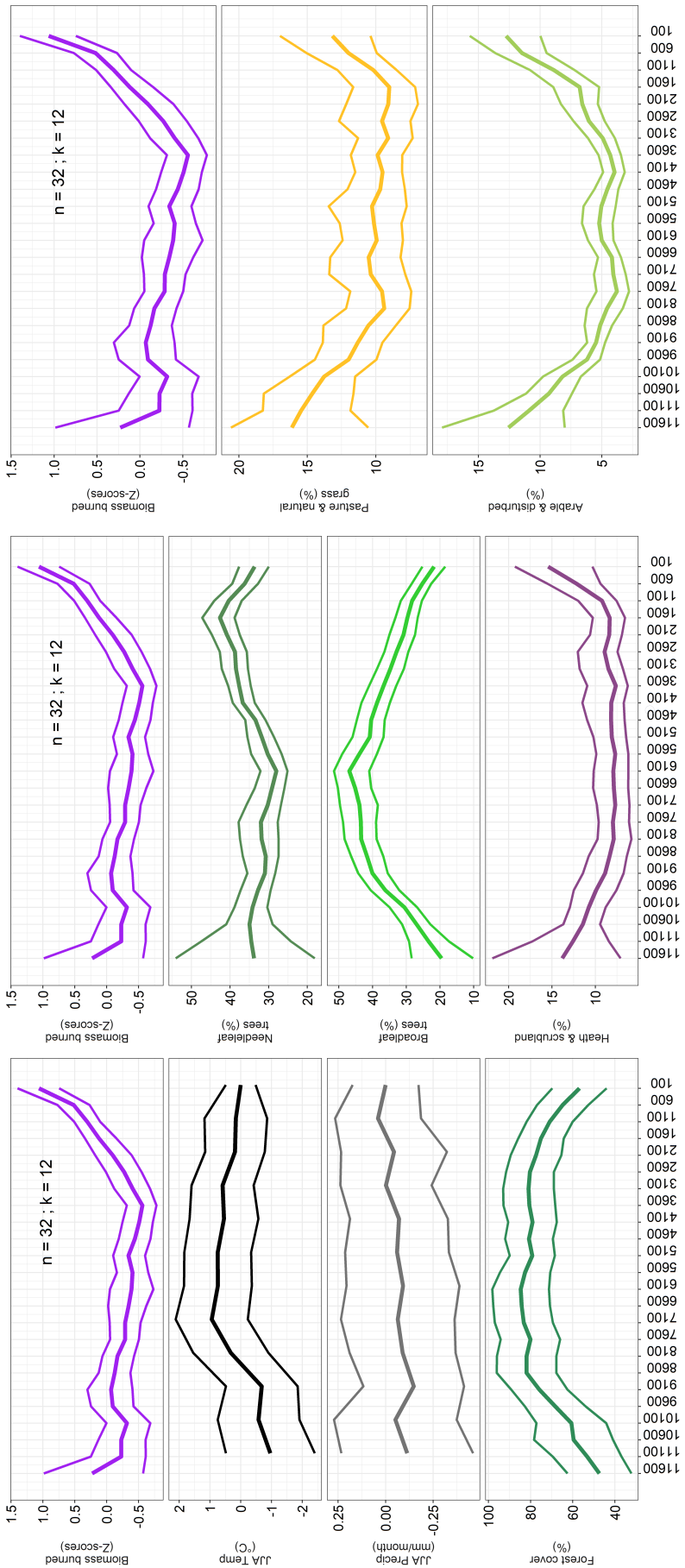

Figure 17: Holocene biomass burning and environmental composite curves for the European cluster 12, all smoothed using a 1500-year window width. The time interval (shown on the x-axis in years before 1950 CE) is limited to the period within the 11.6-0kya interval in which all time points contain at least 10 charcoal records in the smoothing window. The composite curves are shown with 95% bootstrap confidence intervals, except for the temperature, precipitation, and forest cover composite means which are shown with upper and lower standard error composites. The number of charcoal records comprising the biomass burning response (n) and the cluster identity value (k) are shown on the top panel.

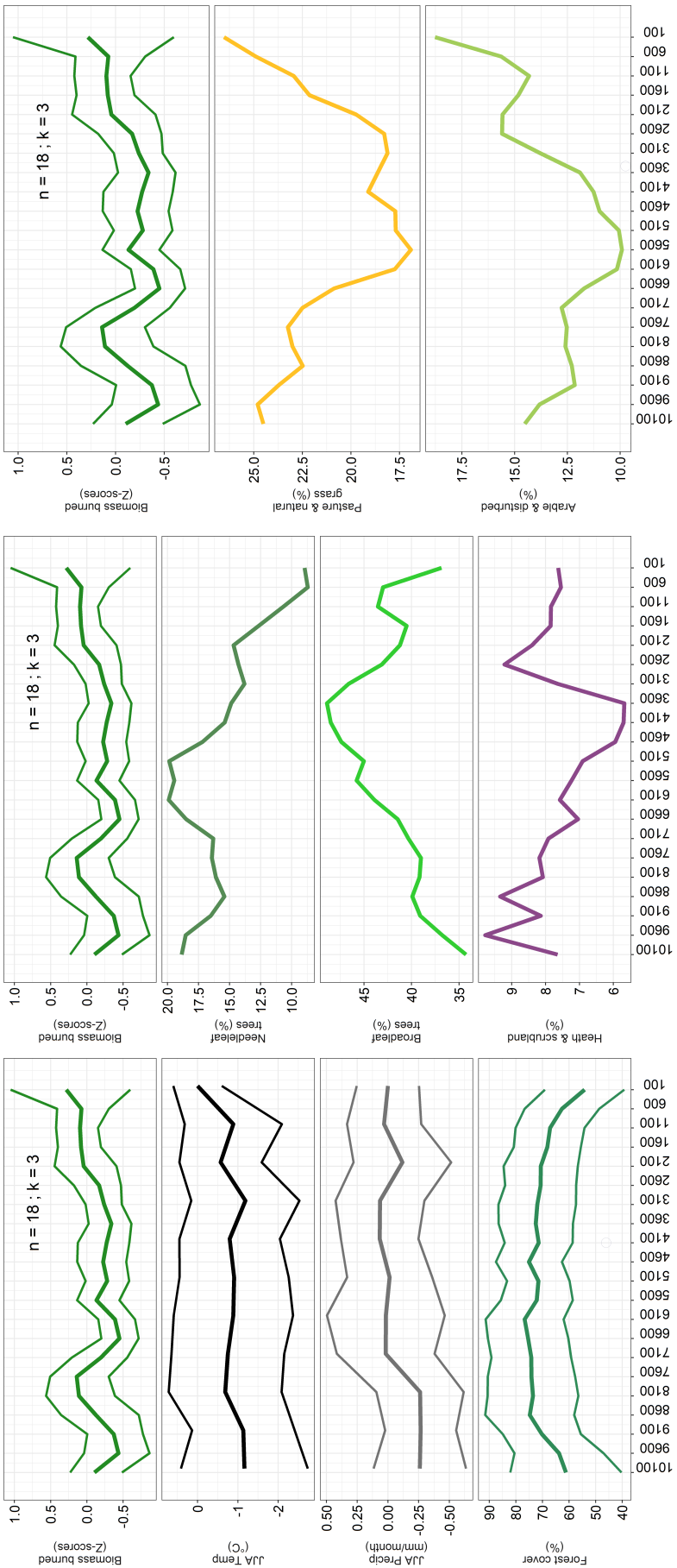

Figure 18: Holocene biomass burning and environmental composite curves for the European cluster 3, all smoothed using a 1500-year window width. The time interval (shown on the x-axis in years before 1950 CE) is limited to the period within the 11.6-0kya interval in which all time points contain at least 10 charcoal records in the smoothing window. The temperature, precipitation, and forest cover composite means are shown with upper and lower standard error composites. The number of charcoal records comprising the biomass burning response (n) and the cluster identity value (k) are shown on the top panel.

Cluster 5: Central Europe and France

Like cluster 3, the overall Holocene fire response of cluster 5 shows similarity with summer temperature variations (12-0kya correlation: temperature: r = 0.6; figure 19). From 10.6kya, the fire response generally increases to a mid-Holocene maximum along with general temperature and forest cover increases. Summer temperature remains important for fire variability in the 8-4kya interval (temperature: r = 0.76). In the 4-0kya interval, the same fire-temperature pattern is evident, but precipitation variability and increasing agricultural land cover also positively relate to fire, while needleleaf and forest cover are negatively related (temperature: r = 0.93; precipitation: r = 0.63; forest: r = −0.86; needleleaf: r = −0.92; heath: r = 0.85; pasture: r = 0.87; arable: r = 0.8). These patterns are particularly apparent in the composites during the fire increase in the last 2ky.

Cluster 4: British Isles

Cluster 4 is characterised by a high heath and grassland coverage relative to other clusters (figures A.41, A.43), which have mean composite values that remain above 15% and 17.5% respectively over the 8-0kya interval (figures 20). The fire response of cluster 4 is characterised by a mid-Holocene low-point and subsequent increase to its highest Holocene level between 3.1-0kya. Throughout the Holocene, forest cover variations are negatively related to fire (12-0kya correlation: forest: r = −0.82). In the early Holocene, unlike other clusters there is an absence of a large fire increase corresponding to the large temperature increase observed. In keeping with the overall Holocene pattern, the variations in fire are inversely related to forest cover variability (12-8kya correlation: forest: r = −0.58).

In the mid-Holocene, the inverse relationship between forest cover and fire persists (8-4kya correlation: forest: r = −0.52), with the mid-Holocene fire low-point corresponding to both elevated broadleaf and forest cover levels (figure 20). In the late Holocene, the large increase in fire between 4.6-3.1kya and subsequent general plateau in the last 3ky occur in tandem with progressively diminishing forest and broadleaf cover, both of which had started decreasing from 6.1kya. In the most recent bin, forest cover reaches an exceptionally low level of under 30%, which is a level of depletion not seen in any other cluster. The late-Holocene fire patterns also correspond to very high levels of pasture and arable land cover that had been increasing from at least 5.1kya, achieving levels of ∼30% and ∼15% respectively by modern times.

Some features of the cluster 4 fire response are shared with the spatially overlapping NET-scale cluster 16, namely, the fire increase between 4.6-3.1kya and subsequent general plateau associated with very low and declining forest cover, the high and increasing levels of open/human land cover, and the exceptionally high moisture levels (figures 20, A.25). On another note, as is also evident in cluster 8, there is a slowdown in pasture land expansion between 2.6-1.6kya that corresponds to a small reduction in fire and a local maximum in precipitation at 2kya. These patterns also correspond to a GDD decline between ∼3.1-2.1kya in the NET cluster 16.

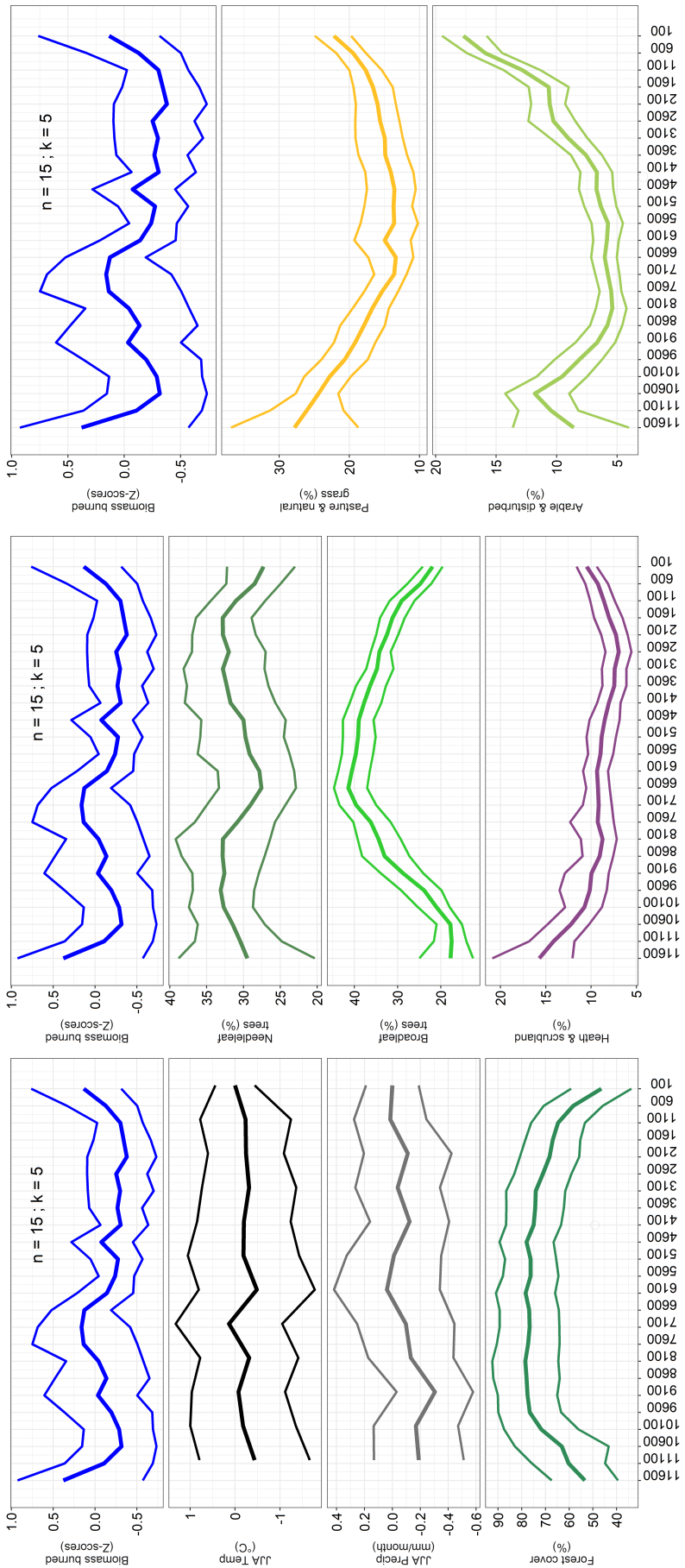

Figure 19: Holocene biomass burning and environmental composite curves for the European cluster 5, all smoothed using a 1500-year window width. The time interval (shown on the x-axis in years before 1950 CE) is limited to the period within the 11.6-0kya interval in which all time points contain at least 10 charcoal records in the smoothing window. The composite curves are shown with 95% bootstrap confidence intervals, except for the temperature, precipitation, and forest cover composite means which are shown with upper and lower standard error composites. The number of charcoal records comprising the biomass burning response (n) and the cluster identity value (k) are shown on the top panel.

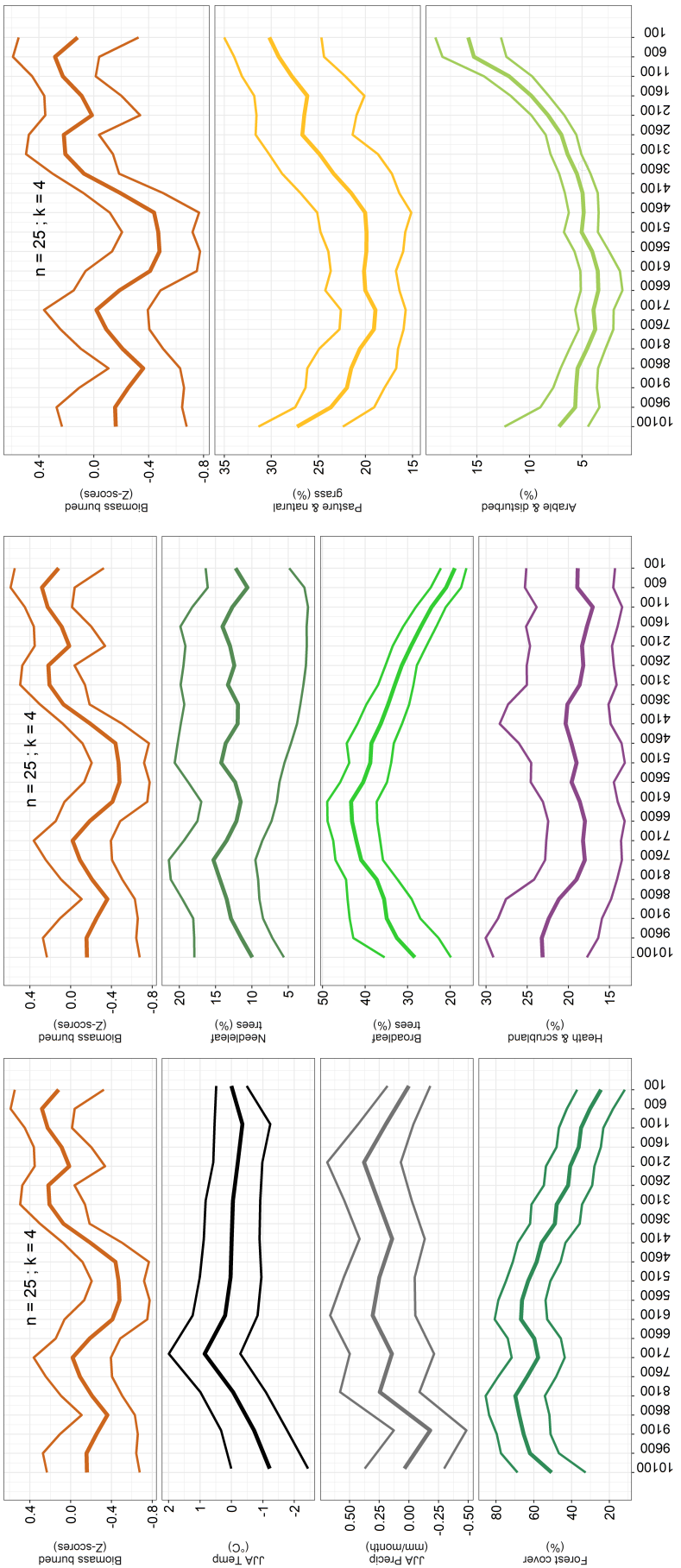

Figure 20: Holocene biomass burning and environmental composite curves for the European cluster 4, all smoothed using a 1500-year window width. The time interval (shown on the x-axis in years before 1950 CE) is limited to the period within the 11.6-0kya interval in which all time points contain at least 10 charcoal records in the smoothing window. The composite curves are shown with 95% bootstrap confidence intervals, except for the temperature, precipitation, and forest cover composite means which are shown with upper and lower standard error composites. The number of charcoal records comprising the biomass burning response (n) and the cluster identity value (k) are shown on the top panel.

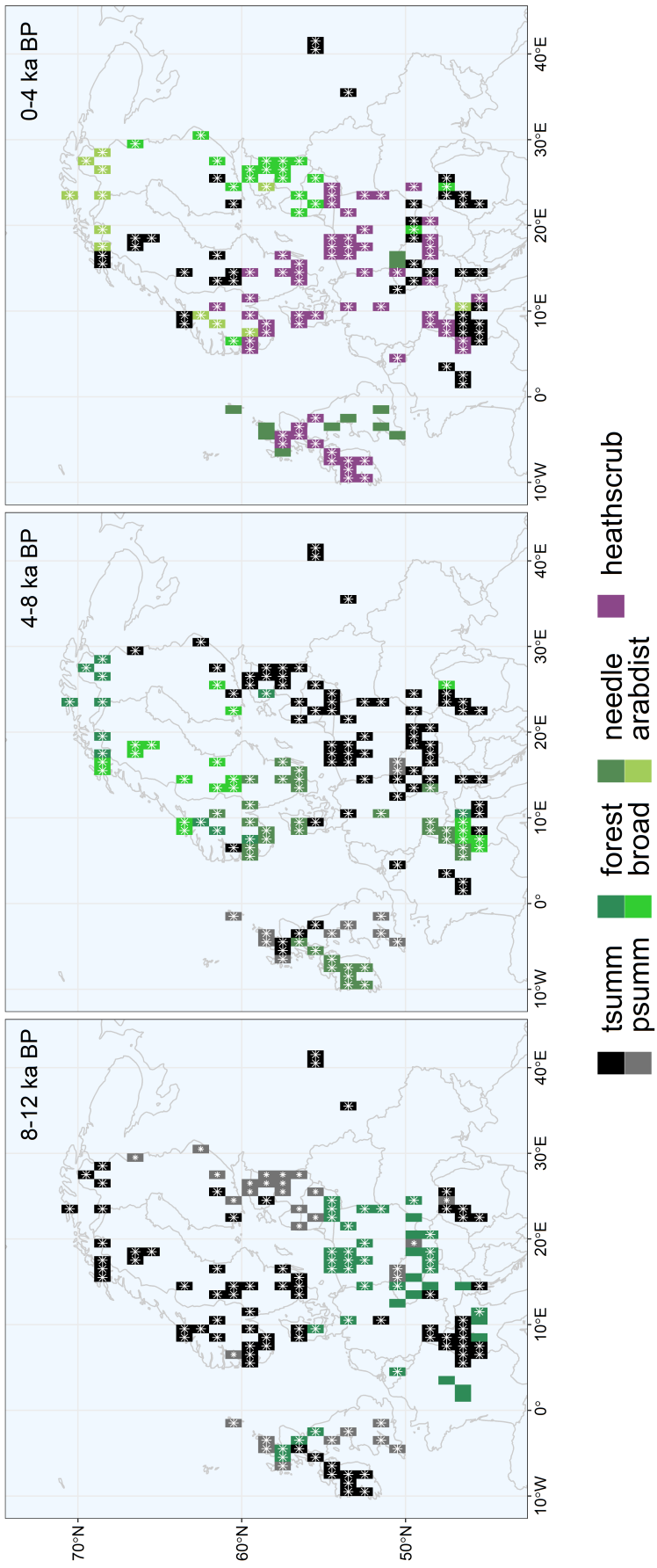

Figure 21: Map showing the environmental variables with the highest explanatory power for the fire response of each cluster at the European scale within 4ky time intervals. Only grid cells that contain charcoal records are shown. Grid cells are colour-coded by the environmental variable whose composite mean exhibits the highest absolute correlation with the fire response of its cluster within a given 4ky interval. Small white asterisks indicate correlation values >= |0.5| and < |0.75|, large white asterisks indicate correlation values >= |0.75|, grid cells with no shape fill indicate correlation values < |0.5|. Legend: tsumm = summer (June-July-August) temperature anomalies; psumm = summer (June-July-August) precipitation anomalies; forest = forest cover; broad = broadleaf tree cover; needle = needleleaf tree cover; arabdist = arable and disturbed land cover; heathscrub = heath and scrubland cover.

Discussion

This chapter expands on the NET-scale findings by showing that it is possible to produce a spatial stratification that captures coherent sub-continental patterns in palaeofire evolution across Europe by grouping the variation in environmental variables considered indicators of Holocene fuel moisture and load variability. In agreement with the NET results, the European findings show general fire increases associated with similar environmental changes across most of the western, central, and northern parts of the continent. Exceptions to this pattern are evident in the southern and eastern European clusters as well as the British Isles, which show different environmental histories and patterns of importance of fire controls through time. The generally well-constrained composite curves across the European analysis, including for composites with low sample sizes (e.g. clusters 3, 4, and 11) imply that fire responded coherently to similar environmental changes within the respective clusters, supporting that the stratification reasonably approximates palaeofire environments.

The European stratification broadly captures the spatial patterns shown in the modern environmental stratification for Europe of Metzger et al. [124]. The patterns shared between the two stratifications include the general latitudinal gradient seen between the high and mid-latitude clusters, the spatial complexity of the Mediterranean clusters, the association between the Scandinavian and Swiss Alpine regions, the association between the British Isles and north and central/western continental Europe, and the isolation of a distinct hemiboreal northeastern region. This spatial congruence suggests that the palaeo stratification captures general environmental gradients native to Europe.

There are differences between the Metzger et al. [124] stratification and this palaeo stratification that can be interpreted with reference to the Holocene environmental evolution of the various European sub-regions. For example, the Scandinavian cluster 11 is separated into its northern and southern zones by cluster 9. Cluster 9 is comparable to the "Alpine" clusters in the Metzger et al. [124] stratification, as these register along the coast of Norway and the Swiss Alps in that study. In the palaeo stratification, cluster 9 is extended further inland relative to the modern stratification, covering most of Scandinavia. This difference can be explained by the history of deglaciation of the region, which may have homogenised the environmental space of central Scandinavia where the Fennoscandinan Ice Sheet terminated in the early Holocene [107]. This may have extended the modern alpine environment further inland, thereby zonally splitting the other Scandinavian cluster 11 into two zones.

Another difference between the Metzger et al. [124] modern stratification and the palaeo stratification is the location of the "Continental" cluster in the modern stratification, which has a western border around the longitudinal position of Jutland and the Swiss Alps. The analogous cluster in the palaeo stratification appears to be cluster 3, which is located further east in a more continental position. Speleothem evidence from central Europe indicates that the boundary between the continental Siberian High and the warmer maritime NAO experienced repeated shifts over at least the last 4kya and suggests that the modern NAO is weakened compared to its values over the mid-to-late Holocene [110]. The palaeo stratification may be capturing a generally stronger influence of NAO westerlies over the Holocene that penetrated deeper into the continental interior, pushing the boundary between the continental cluster 3 and the Atlantic cluster 8 further to the east. In support of this, Holocene hydroclimatic variability in eastern Europe is linked to major NAO shifts, with warmer and drier phases being associated with a dominant NAO mode [110, 167]. The oscillatory behaviour in the

late-Holocene temperature and precipitation curves of cluster 3 are in agreement with this. Moreover, the similar Holocene environmental history of the central, northern, and western European regions is congruent with a predominant role of the maritime climate mode over Europe. Overall, the general similarities between the modern Metzger et al. [124] and palaeo stratifications, as well as the ability to explain key differences in terms of the palaeo environmental processes that Europe experienced, suggest that the European palaeo stratification provides a more accurate representation of palaeofire environments than previous attempts at delineating palaeofire-relevant sub-continental regions in Europe which are based on arbitrary judgement and/or do not incorporate any palaeo environmental information (e.g. [94, 116]).

The charcoal records comprising the central and hemiboreal northeastern clusters 8 and 12 are mostly the same records used to generate the continental and boreo-nemoral fire curves in Feurdean et al. [116] and, unsurprisingly, the fire responses are similar. In keeping with the Feurdean et al. [116] study, the fire responses of all European clusters can be explained by changes to fuel loads and summer dryness, land cover, and landscape openness. The congruence of the fire responses with Feurdean et al. [116] for the overlapping clusters, as well as the ability to explain the fire responses of all European clusters in terms of their environmental histories in keeping with that study and the NET findings, supports the robustness of these results.

Controls on palaeofire evolution across Europe

The early Holocene: 12-8kya

In general agreement with Feurdean et al. [116] and the NET results, the large increase in temperatures and fuel loads in the early Holocene interval, associated with and in the millennia following the Fennoscandinan Ice Sheet collapse, are shown to be the dominant influence increasing fire in most regions of Europe (clusters 3, 5, 7, 8, 9, and 11). This is not the case for the British Isles cluster 4 where forest cover is negatively correlated with fire in the early Holocene. This may be a consequence of this region having a high representation of open landscape classes relative to other regions, such that the early-Holocene forest cover increases created less favourable fire conditions through reducing high levels of fine and shrubby fuel cover and continuity. The Fyfe et al. [101] dataset cannot be used to corroborate that this cluster contained high levels of pasture and heath-type landscapes pre-8kya which declined as forests increased in extent, but a pollen-based reconstruction of European vegetation change by Giesecke et al. [111] shows that the Ericaceae plant family associated with heath and scrubland land class generally declined during the early Holocene pre-8kya in the northern British Isles. This provides some indication that the exceptionally high heath cover and open landscape representation from 8kya in this cluster is at least conserved (if not greater) in the early Holocene. This supports the notion that high amounts of shrubby and fine vegetation cover were reduced and fragmented as forests expanded in the early Holocene, which is likely to have had a negative effect on fire activity.

The hemiboreal northeastern European cluster 12 does not experience a fire increase in response to its much-increased temperatures and fuel loads in the early Holocene. Its exceptionally high forest cover levels from the early Holocene may have attenuated the positive effects of even large increases to summer dryness and fuel loads on fire, such that fire was more responsive to variations in landscape openness as a result of the forest changes. This is supported by Feurdean et al. [116] who demonstrate

that the influence of tree cover change is different in the boreo-nemoral region of their study, which has higher needleleaf and forest cover compared to continental and western Atlantic Europe. Increased tree cover above 65% in this region has a strong negative effect on fire, while this is not the case in the other regions of their study. The decline in fire in cluster 12 in the early Holocene can thus be attributed to tree cover percentages increasing above 65% at ∼9.6kya and remaining high into the late Holocene.

It is evident that the large early-Holocene increases in temperatures and fuel loads in clusters 4 and 12 were not sufficient to cause pronounced fire increases due to the modulating effects of land cover changes. These results therefore extend the Feurdean et al. [116] findings that climate effects on fire can be modulated by land cover changes, demonstrating this for the early Holocene in the context of larger climate variation than was included in their 8-0kya GAM analysis.

The mid-Holocene: 8-4kya

The European-scale results generally corroborate findings from the NET chapter and the Feurdean et al. [116] study that suggest a less important role of climate and fuel increases for European fire variability from 8kya and a greater importance of forest compositional changes. This is seen in the negative correlations between fire and temperature and forest cover for clusters 7, 8, 9, and 11, and their respective positive and negative relationships with needleleaf and broadleaf cover. The pattern of broadleaf decline and agricultural land class increases across Europe also agrees with the timeline of human-caused broadleaf deforestation and agricultural expansion outlined in the NET-scale chapter. During the mid-Holocene interval, the boreal clusters 9, 11, and 12 generally experience more modest increases in arable land cover compared to the lower-latitude clusters, supporting the notion that human-caused land cover change became important at an earlier time in temperate Europe compared to the boreal regions.

In the region of the continental cluster 3, there is evidence of herding-related vegetation changes from ∼6kya [168], and this is borne out by the cluster 3 increases in pasture and arable land cover from ∼5.6kya. However, a multi-proxy study of Holocene climate change and human impacts on the environment of the Romanian Carpathians, which fall within this cluster, suggests that human impacts were minimal before ∼4.5kya [167]. This is congruent with the mid-Holocene results of cluster 3, which show that summer wettening led to a reduction in fire and show no clear evidence of human influences on fire. Similarly, although cluster 5 shows an early onset of the increase in arable and pasture cover and decline in broadleaf cover around 8-6kya and humans are evidenced to have begun farming in the general regions of the zones of this cluster around 7kya [159], it experiences a general mid-Holocene decline in fire, with summer temperature remaining the most important fire control in the 8-4kya interval. These patterns suggest that mid-Holocene fire variability in clusters 3 and 5 were primarily climate-driven, with a less important role of land cover changes compared to other temperate European regions.

In the British Isles cluster 4, landscape openness remains important for fire in the mid-Holocene, seen by fire reaching a minimum at the maxima in broadleaf and forest cover and maintaining a negative relationship with forest cover. Increases in agricultural expansion from ∼6kya in this region [159] probably contributed to the onset of the broadleaf decline from ∼6kya that would have created a less forested landscape, reversing the early-Holocene decline in shrubby and fine fuels and leading to

an increase in fire between 4.6-3.1kya. This fire increase is disproportionate relative to the variability in the climate variables, increasing the certainty that human-caused landscape changes played a major role in this pattern.

Despite evidence that agriculture and hence probable human deforestation practices were underway in localised areas of hemiboreal northeastern Europe ∼6kya [160], effects of these activities on the fuel properties of cluster 12 were probably minimal throughout the mid-Holocene. This is evidenced by cluster 12 showing an absence of continuous mid-Holocene increases in human land classes, in contrast to many other European clusters. Like clusters 3 and 5 and contrary to most of Europe, the climate changes appear more important for fire than land cover changes in the 8-4kya period. The gradual mid-Holocene temperature decline and precipitation increase probably caused a gradual decline in fire through a reduction in fuel dryness. Increasing levels of forest cover had reduced fire in the early Holocene, and its subsequent stable high levels throughout the mid-Holocene probably maintained the general fire minimum in this cluster.

The late Holocene: 4-0kya

In keeping with the NET results, fire variability across Europe in the most recent 4kya is more clearly attributable to human-caused land cover changes than during the mid-Holocene. This is because firstly, the climate changes alone are unable to account for the fire changes as in theory they predict opposing fire changes to those observed. For example, in clusters 9, 11, and 12, increased fire between ∼4.1-1.6kya, 4-0kya, and from 3.6kya respectively occur while summers generally get colder and wetter in all three clusters. A similar pattern is again evident in cluster 7 for the 4-0kya period and in cluster 4 during its fire increase between 4-3kya. Secondly, it is unlikely that the late-Holocene land cover changes were climate driven, because they are generally disproportionate in magnitude relative to the climate changes seen during this interval, which is a pattern not evident in earlier periods. Thirdly, the broadleaf and forest cover declines, human land class increases, and fire variability of most clusters generally vary outside of their ranges of variability seen in previous Holocene intervals, indicative of the clusters transitioning to novel fire regime states. This set of observations is expected under widespread human deforestation practices in Europe that are known to have intensified in the late Holocene [113].

In the central European cluster 8, the signal of slowed agricultural expansion and associated needleleaf increases between ∼2.6-1.6kya may be related to a decline in human land management. It is unclear what may have caused this, but the minor reductions in GDD and temperatures observed in the NET cluster 13 and this cluster may indicate less favourable climatic conditions for agriculture during this time, which may have also favoured needleleaf expansion. Between 1.7-1.3kya, slowed forest decline in Europe has been associated with the post-Roman migration period when there were mass migrations of human populations across temperate Europe, which may have led to declines in rural settlement and re-growth of forests in various regions [113]. The renewed increase in fire in the most recent millennium is consistent with the declining tree cover and increases in agricultural land cover and their relationships to fire shown in Feurdean et al. [116]. This is in accordance with historical documentation indicating renewed forest clearance to make way for farms and villages soon before 1kya in north-central mid-latitude Europe [113]. Unlike many other European clusters, this increase occurs along with increasing temperatures, hence was probably caused by a combination of human activities and enhanced summer drying.

In the Scandinavian and Swiss Alpine cluster 9, fire declines in the most recent 1.6kya when human landscape modification is evidently most pronounced. Cluster 9 has a very high general level of moisture, which is evidenced to have reached its maximum levels in the most recent millennia. At 1.6kya, the moisture levels may have become too high to sustain further fire increases. This is congruent with the explanation for the similar pattern observed for the spatially overlapping NET cluster 16. It appears less likely that the fire decline was caused by fuel depletion and landscape fragmentation because the adjacent cluster 11 has lower forest cover and comparable open/human landscape cover at 1.6kya, yet its fire response does not decline. A pre-industrial decline in fire in central Sweden, which overlaps with the northern zone of this cluster, has also been observed in a study combining fire scar and charcoal records and is linked with a cultural transition from traditional slash and burn agriculture to modern agriculture and forestry practices that did not entail substantial use of fire [169, 170]. The onset of this decline occurs ∼0.6-0.4kya, ∼0.3ky earlier than other parts of Fennoscandia and Denmark [170]. This agrees with the fire response of cluster 9, suggesting that the transition away from fire-intensive land management practices was an important influence on the latter stages of its late-Holocene decline.

In the British Isles cluster 4, it is apparent that the very low forest cover and high levels of agricultural and open landscape representation by 3kya probably resulted in a fuel load that was too low to sustain further fire increases in later millennia of the same magnitude seen between 4.6-3.1kya. This hypothesis is more plausible for this cluster as opposed to the climate wettening explanation given for cluster 9 because the cluster 4 precipitation decline from 2kya indicates that its climate became drier. Moreover, the degree to which forests are reduced and open landscapes are extended in the late Holocene is greater in this cluster than in other European clusters. At the centennial scale, cluster 4 shows a similar pattern to cluster 8 in that the attenuated increase in pasture cover between 2.6-2.1kya may have been caused by a regional reduction in summer dryness and temperature, observed in the precipitation curve as well as the GDD response of the overlapping NET cluster 16. This climate change may have caused the cluster 4 decline in fire between 2.6-2.1kya. The synchrony of these environmental patterns between the spatially disparate clusters 4 and 8 is consistent with the notion that this fire decline was caused by a regional climate change as opposed to more localised landscape effects.

While the turning point in fire at 3.6kya in the hemiboreal northeastern cluster 12 appears attributable to human activities, Feurdean et al. [116] show that increases in arable and grassland cover at levels that induce the strongest positive response in fire only occur within the past 2.1kya in the boreo-nemoral region of their study, consistent with the large fire and open/human land increases seen in the last two millennia in this cluster. Feurdean et al. [116] attribute the fire increase before this time to the rise in needleleaf cover. However, between 3.6-2.1kya, arable land cover increases between ∼4-6%, whereas in the Feurdean et al. [116] GAM analysis, the range of values of the arable and disturbed land cover variable does not include values under ∼6% in the boreo-nemoral region, and this variable is strongly positively related to fire from 6% cover and above. It is evident that agriculture and hence probable human deforestation practices were underway in hemiboreal northeastern Europe ∼6kya, hence it is plausible that the onset of the increase in fire at 3.6kya occurred as a result of a combination of climate-driven needleleaf increases and human landscape management.

Clusters 3 and 5 show a different pattern relative to other European clusters in that summer

dryness variations are consistently the most important fire control from the early to the late Holocene, despite these regions experiencing similar land cover variations to the rest of Europe. The climate history of cluster 3 is in keeping with the evidence for Holocene shifts in NAO dominance that probably played an important role in regulating the environment of this region [110, 167]. Despite the results suggesting temperature variations were the principal control on fire in cluster 3 in the late Holocene, effects of human activity are still evident, since the general fire increase between 3.6-0kya is concomitant with increasing human land use intensification. This is consistent with findings from the multi-proxy study of climate and human impacts on the environment of the Romanian Carpathians which suggest that human-induced deforestation and agriculture became important after ∼4.5kya [167]. In cluster 5, the disproportionate fire increase in the last 1ky corresponds with the pattern of declining broadleaf cover and increased agricultural land cover, suggesting that human activities became important for fire only in the most recent millennium.

The higher spatial detail of the European results relative to the NET results provide more details regarding the timing of human-induced deforestation practices in different regions of Europe. For example, the decline in needleleaf cover in cluster 12 that occurs at 1.6kya is more similar to the NET cluster 5 which experiences this decline at the same time, compared to the overlapping NET cluster 12 that contains the northern central Europe/Jutland region and which experiences the needleleaf decline at 1.1kya. This suggests that the human deforestation history of the hemiboreal northeastern region is more similar to Fennoscandia than to the northern central Europe/Jutland region. Given that the European cluster 12 experienced higher needleleaf and lower broadleaf maxima than the NET cluster 12, this pattern is consistent with the notion of a human preference for deforesting broadleaf forests prior to needleleaf forests, because broadleaf forests would have become depleted at an earlier stage in hemiboreal northeastern Europe relative to the Jutland region, hence its earlier onset of the needleleaf decline.

Limitations

Despite the improvements that this work makes to the spatial scope and sampling of charcoal composites presented in previous literature, some composites nonetheless have low sample sizes and are poorly constrained, and a few only cover part of the Holocene. There are also large uncertainties in many environmental composites. For example, many of the NET-scale GDD curves have large confidence intervals, as do the climate variables at the European scale. These environmental composite uncertainties are likely to be inflated by the low number of grid cells comprising them. Since the environmental composites are generated only for the grid cells with charcoal-record coverage, low cluster grid-cell sizes are a consequence of the low charcoal-record sample size and/or low geographic spread of charcoal records within some clusters, in addition to the large grid-cell size of the TraCE-21ka dataset. These factors also result in multiple clusters containing less than 10 grid cells, which are deemed unsuitable for generating environmental composite confidence intervals. These shortcomings reduce the certainty of the interpretations of the controls on the fire and environmental histories of some clusters.

Another consequence of low charcoal-record sample sizes and geographic spread within clusters is that the fire response of a given cluster is defined using a spatial subset of the fire variation of the cluster as a whole. This may result in fire composites that misrepresent the fire history of the palaeofire environment that the cluster represents. Additionally, when comparing fire evolution of the same clusters on different continents, this can increase the difference in environmental space that generated the two fire responses being compared, making them less likely to represent fire responses of similar palaeo environmental evolution on separate continents, thereby reducing the veracity of the comparisons. Despite the sampling limitations of this work, for most clusters investigated it was possible to derive well-constrained fire composites from charcoal records spanning wide geographic ranges, an observation that would not be expected if the charcoal records of a given cluster did not capture the aggregate fire history of a palaeofire environment. It was also possible to derive novel information from the fire composites and their comparisons across continents and with environmental changes, specifically the generation of multiple plausible hypotheses regarding controls on fire evolution that are consistent with independent sources of evidence.

Improvements in the spatial coverage of charcoal records would facilitate a more robust analysis of sub-continental fire and environmental histories in the NET. Some regions that would benefit greatly from this include central Asia, western Russia, and the Eurasian and North American high latitudes. An alternative way of improving charcoal sampling may be through alternative methods of transforming and standardising charcoal records, as many records were filtered out of the analysis due to having inadequate units for the charcoal transformation method used here.

The fact that the environmental composites were generated without taking into account differences

in charcoal-record coverage among the grid cells comprising them makes it possible for the environmental composites of a given cluster to spatially misrepresent the environmental changes that inform its fire response. This was evident in the VPD and MI curves of the NET cluster 17, which failed to capture the climate patterns attributed to driving the mid-Holocene fire response of this cluster. However, cluster 17 was the only case where there was an obvious contradiction between independent evidence and the environmental composites, and it was nonetheless possible to explain this in terms of the environmental history of the cluster. This suggests that the current method is largely resilient to such spatial biases, which is expected if the clusters reasonably approximate palaeofire environments. Employing higher precision in aligning the charcoal to the environmental data would preclude the ability to gain insight into the resilience of the method and would be more appropriate in later iterations of the analytical approach used in this work.

The uncertainties in some composite reconstructions may also reflect inaccuracies in the stratification, i.e. the limits of the ability of the clustering method to approximate true spatial boundaries separating palaeofire environments. Some degree of noise in the stratifications is expected due to the inherent uncertainties in the datasets used. It is expected that these uncertainties may inflate at sub-continental scales, especially for the TraCE-21ka dataset which was chosen in part due to it reliably capturing the main features of palaeo environmental variation across the NET, but not necessarily sub-continental-scale patterns. Despite this, the TraCE-21ka dataset shows agreement with independent, observation-based climate reconstructions for various sub-continental regions in this analysis. For example, the MI curve of the NET cluster 17 indicates the same decline in moisture availability between ∼8.5-6kya and increase from the mid- to the late Holocene seen in the annual precipitation reconstruction for northern Quebec in Viau and Gajewski [153], and the patterns of early-Holocene moisture variability of the NET clusters 5, 12, and 13 also agree with the moisture evolution of northern and central Europe shown in Mauri et al. [105]. Additionally, the evidence for the long-term Holocene wettening of central Asia shown by the MI and VPD curves of cluster 11 generally agrees with proxy-based moisture reconstructions showing that the regions represented by the MI and VPD composites trended towards a wetter state as the Holocene progressed [164]. These patterns suggest the TraCE-21ka dataset provides a reasonable description of sub-continental-scale moisture evolution across the NET, and therefore that the lower robustness of some NET composites is largely related to the spatial and sampling limitations of the charcoal data comprising them.

Another potential source of stratification inaccuracy is the fact that the variables chosen to define them were limited to three measures of fuel moisture and load. These were chosen as a minimum set of variables that capture processes considered to be fundamentally important for fire, which was informed by wildfire theory and constrained by the datasets available in the literature. However, these variables do not capture the full scope of fire-relevant environmental processes. For example, annual moisture is shown in previous work and in the NET-scale analysis to be an important fire control, but it was not included in the European stratification. Similarly, various land cover types, such as those from Fyfe et al. [101], are considered important wildfire controls (e.g. in Feurdean et al. [116]) but are not incorporated into either stratification definition. Moreover, there are climate variables not included in the stratifications that may be important for fire-relevant land cover change. For example, temperature is an important predictor of plant distributions [171] and hence land cover. Nonetheless, it was expected that grouping regions with similar climate and fuel load history would

translate into spatial groupings with similar fire-relevant land cover history. This is supported by the well-constrained land cover composites for most clusters. It is also useful to undertake the first instance of this clustering analysis with a minimum set of variables considered necessary to capture broad patterns in palaeofire environments in order to avoid overfitting the stratification models.

An example evidencing the limited ability of the TraCE-21ka simulation to precisely delineate palaeofire environments is that the simulated NPP variable used at the NET scale does not detect the influence of land cover changes that are independent of what climate alone would predict. For example, human-induced tree cover declines may be expected to result in detectable NPP declines, but NPP does not decline in the NET clusters with high forest loss in the late Holocene. Furthermore, the environmental composites of the NET American cluster 12 did not detect the changes to fire season length observed in independent literature [81, 154] that explained the fire response. Finally, the fact that the continental fire responses of the clusters spanning both continents were largely dissimilar points to the limited ability of the available variables to associate similar fire-relevant environmental space across continents. However, this was to some degree expected, given the substantially different tree species composition of the respective continents and their differential effects on fire regimes. Accounting for these differences would require incorporating tree composition data into the stratification definition with higher taxonomic resolution than the needleleaf and broadleaf categories used in this analysis. More generally, the finding of different continental fire responses within the same clusters nonetheless highlights the environmental differences between the two continents and the relevance of these differences for palaeofire evolution.

Further work seeking to improve on the accuracy of the stratifications may pursue incorporating more variables into the clustering method and weighting variables based on a priori knowledge of their relative importance for fire. Using dimension-reduction steps, e.g. with Principle Components Analysis, may be useful to this end. A future investigation might define an optimal protocol by testing the performance of various clustering methods and combinations of variables at maximising signal-to-noise ratios for fire-environment relationships in the resultant stratifications. This would only be possible with more rigorous and comprehensive environmental datasets. Specifically, more spatially resolved environmental data than the TraCE-21ka dataset that are ideally reconstructed from observational data would greatly improve on the ability to constrain fire-environment relationships across the NET. At present, it was not possible to correlate fire with land cover changes in North America and for one Asian cluster due to the lack of land cover reconstructions in these regions, highlighting the need for Holocene land cover reconstructions like the Fyfe et al. [101] dataset for these continents.

A limitation of the stratification at the European scale is the millennial resolution of the clustered dataset. This smooths over time series features that might isolate palaeofire-environment distinctions at the 500-year resolution of the charcoal composites. The European analysis would benefit from less noisy climate reconstructions with higher temporal resolution than the Mauri et al. [105] data.

The correlations taken as representative of fire-environment relationships are in some cases weakly informative. This is because the correlation metric does not account for differences in amplitude or magnitude of time series features being compared, and can be inflated when there is a general trend even if variability around the trend is substantially different between two curves. Here, correlation values are used as a general guide to quantitatively corroborate conclusions drawn from qualitative

comparisons, rather than a rigorous method to test similarity of two time series. Another limitation of the fire-environment comparisons is that in some cases, the correlations consist of a very low number of time points. For example, the 4ky correlations for the European climate variables are, at best, made up of only four data points. Finally, the correlation analyses do not have the ability to quantitatively isolate independent fire-environment relationships and interactions among environmental variables. Despite this, this type of correlation analysis still facilitates reasonable inferences of causative mechanisms driving fire evolution. For example, assigning causation to a single variable is more certain when there is disproportionate change in one environmental variable and fire but not the others, and/or other variables change in a manner that would otherwise predict a different fire response to the one observed. This is the case for late-Holocene fire increases in European clusters that occur along with anthropogenic land cover class increases and climate changes that predict fire declines. Nonetheless, the analysis would benefit from a GAM analysis that can isolate independent relationships and interactions among environmental variables. This would be most informative with more resolved and comprehensive datasets.

Conclusions

This thesis has provided insights into the environmental controls on sub-continental-scale spatial and temporal variation of Holocene fire regimes across the NET. It has done this through the novel application of a recently developed clustering method to palaeo environmental data, which has resulted in the generation of palaeofire-relevant spatial stratifications at respective circum-NET and European scales. The stratifications expand on previous attempts to spatially delineate regions with different Holocene fire histories, ultimately enhancing the ability to understand controls on palaeofires. These stratifications, and the generation of Holocene fire composites for 21 of 29 total clusters using records from the RPD, successfully addresses the first aim of quantitatively delineating sub-continental-scale palaeofire environments for the Holocene NET and constraining their composite Holocene fire responses. The generally high explanatory power afforded by the correlations between fire and the climate and land cover composites and the wide agreement of these results with the understanding of fire controls and Holocene climate and land cover evolution demonstrates that the second aim of using quantitative methods to identify the climate and land cover controls on the fire responses defined under the first aim has been successfully addressed.

Consistent with the notion that the stratifications at the two scales both approximate palaeofire environments, the spatial patterns of the two stratifications are broadly congruent with one another. Both stratifications show a general latitudinal gradient, consistent associations between the Swiss Alpine region and Scandinavia, the British Isles and the north/west Swiss Alpine region, and the isolation of an exclusively Scandinavian cluster. This is notable given the different variables and methods used to define either stratification. In further agreement with the stratifications being representative of palaeofire environments, it is possible to explain the differences between them in terms of the differences in environmental history that they measure. The spatial simplification of the NET stratification relative to the European stratification is predictable given the lower spatial precision of the NET analysis, as well as its larger spatial scope and hence broader range of environmental variation (making the same magnitude of environmental similarity less likely to be separated into different clusters at the NET scale relative to the European scale). Additionally, since the NET stratification was generated using a longer time interval, the effect of the transition from the last glacial period on the climate of the NET has a greater influence on the NET-scale cluster groupings than at the European scale. For example, the Fennoscandian Ice Sheet influences the NET-scale variables for a longer period than the European-scale variables, which may contribute to boreal Europe being grouped into a single cluster at the NET scale but not at the European scale.

In addition to the similarities in the spatial patterns between the two stratifications, there is broad agreement in the temporal patterns in fire and environmental changes when comparing various European clusters to their more spatially integrated, overlapping NET-scale clusters (e.g. comparing

the European clusters 4 and 9 to the NET-scale cluster 16, the European clusters 9 and 11 to the NET-scale cluster 5, and the European-scale cluster 8 to the NET-scale cluster 13). This points to the spatial robustness of the fire and environmental reconstructions in this analysis and ultimately further corroborates the accuracy of the stratifications at capturing palaeofire environments.

Besides this work demonstrating the first application of the biclustering algorithm in palaeofire research to cluster multiple environmental variables simultaneously, it makes other important methodological research contributions. It provides a novel, quantitative, automated cluster quantity selection protocol for the biclustering algorithm. It also provides quantitative comparisons between fire and environmental composites at 4ky resolution, improving on the qualitative approaches and coarser temporal resolution of time series comparisons in previous literature.

This work also makes several contributions that enhance the current knowledge of palaeofires in the NET. In addition to the development of palaeofire-environment stratifications, it: 1) provides updated composite curves for sub-continental regions of the NET, expanding on the spatial scope and resolution of the reconstructions in previous work, including by generating fire histories for regions not previously explored such as central Asia; 2) corroborates and expands on previous findings that changes to fuel moisture and load are important controls on palaeofires in the NET, and that their effects have been modulated by fuel structure and composition in various regions; 3) corroborates that human activities have been important for shaping fuel composition, landscape openness, and fire regimes since the mid-Holocene across Europe, and that their effects on Holocene fire regimes in North America were negligible with the exception of a few localised regions in the late Holocene.

While the sub-continental-scale fire histories of each cluster are unique, there are general patterns in palaeofire evolution at the continental scale. Across Europe in the early- to mid-Holocene, fire generally increased in response to the Fennoscandian Ice Sheet collapse and associated forestation and climate warming. It continued to increase from the mid- to late-Holocene to its highest Holocene level in response to land cover changes and widespread landscape deforestation, with human-caused forest clearance and landscape management playing a major role. In North America, the progressive decline of the LIS in the early Holocene led to early-to-mid Holocene forest expansion in various regions that resulted in fire increases across the mid-latitude regions of the continent. A subsequent long-term, continent-wide moisture increase drove late-Holocene fire declines across most of boreal and temperate North America. However, in central and southern Quebec as well as the Pacific Northwest of the United States, vegetation changes and human influences overrode this effect, leading to fire increases. In central Asia, a long-term climate wettening from the early Holocene to the modern period resulted in a generally declining fire response, with vegetation composition changes leading to millennial-scale variations around this trend.

The stratifications provide spatial units that can be seen as fire management boundaries wherein coherent long-term fire regime changes occur, which is useful for long-term conservation efforts. For example, it facilitates the management of the disturbance regime of a region in accordance with its natural background dynamics to facilitate persistence of vegetation adapted to such a disturbance regime. This may be particularly useful in clusters that show fire regimes reaching unprecedented states in response to late-Holocene human land use activities and where conservation efforts may seek to restore pre-modern land cover patterns (e.g. the European clusters 8, 11 and 12). Moreover, the environmental histories of the clusters shown here provide a basis for spatial prediction of fire regime

and vegetation changes that may occur in response to future climate changes or human land use processes.

Appendix A

Supplementary Information: Figures and Tables

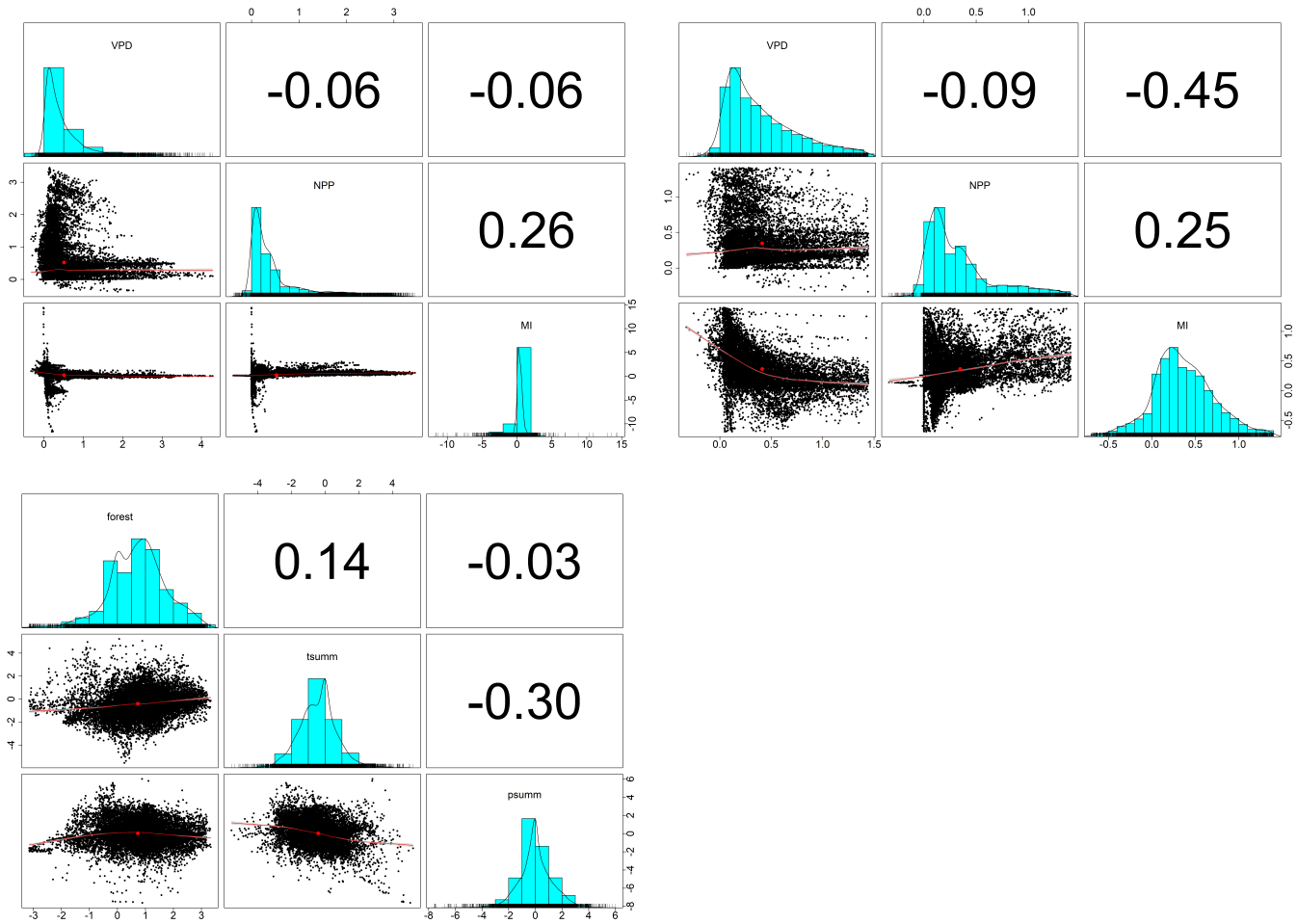

Figure A.1: Correlation multiplot for the three variables used in the biclustering algorithm after all pre-clustering data processing steps were applied. Correlation values are shown on the off-diagonals. Red curves are loess-smoothed lines of best fit, with red points representing the intersection of the maxima of the probability density functions of the two correlated variables. The distributions of the variables are shown by histograms, probability density functions, and rug plots on the diagonals. Top: correlations among the three variables used in the NET-scale clustering analysis. Top right: the three NET variables have had outliers removed prior to correlation, by calculating the lower (upper) quartile $-(+)$ 1.5 * the interquartile range for the three variables, then removing all data points from the three variables less than (greater than) the maximum (minimum) quantity among these values. Bottom: correlations among the three variables used in the European-scale clustering analysis (tsumm: summer temperature; psumm: summer precipitation; forest: forest cover).

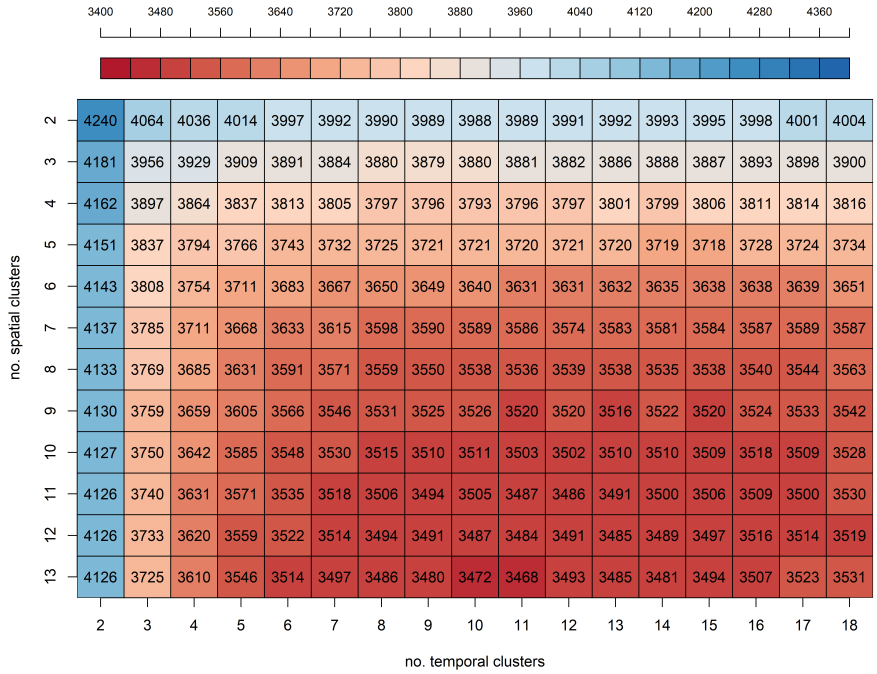

Figure A.2: Output of the cluster quantity selection optimisation protocol for the biclustering algorithm implemented at the European scale. The k values (see methods) for all combinations of site and time clusters investigated are shown as a 2D surface and are rounded to the nearest integer. The optimal site-time combination chosen is 13 site and 11 time clusters.

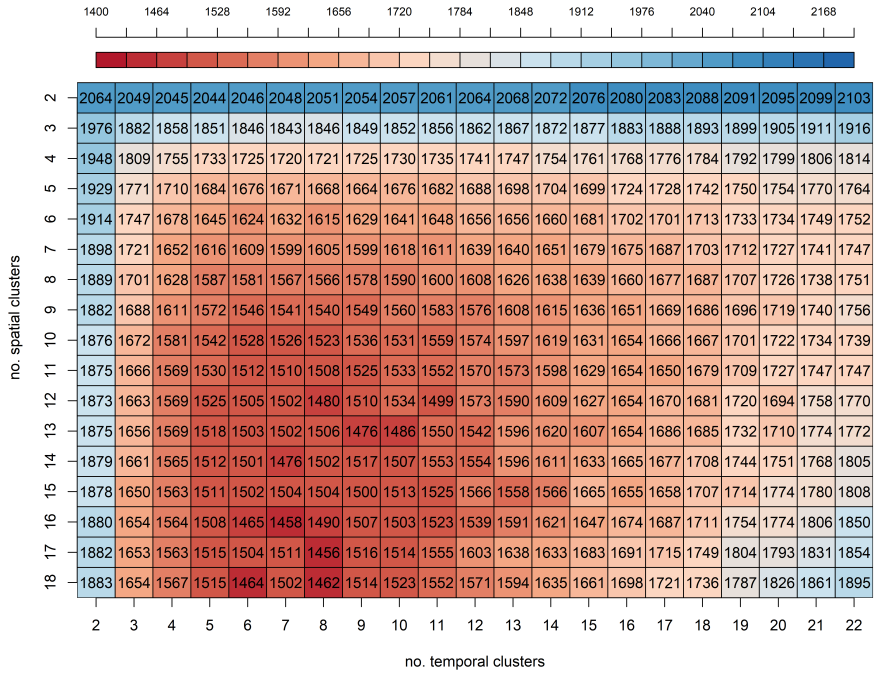

Figure A.3: Output of the cluster quantity selection optimisation protocol for the biclustering algorithm implemented at the NET scale. The k values (see methods) for all combinations of site and time clusters investigated are shown as a 2D surface and are rounded to the nearest integer. The optimal site-time combination chosen is 17 site and 8 time clusters.

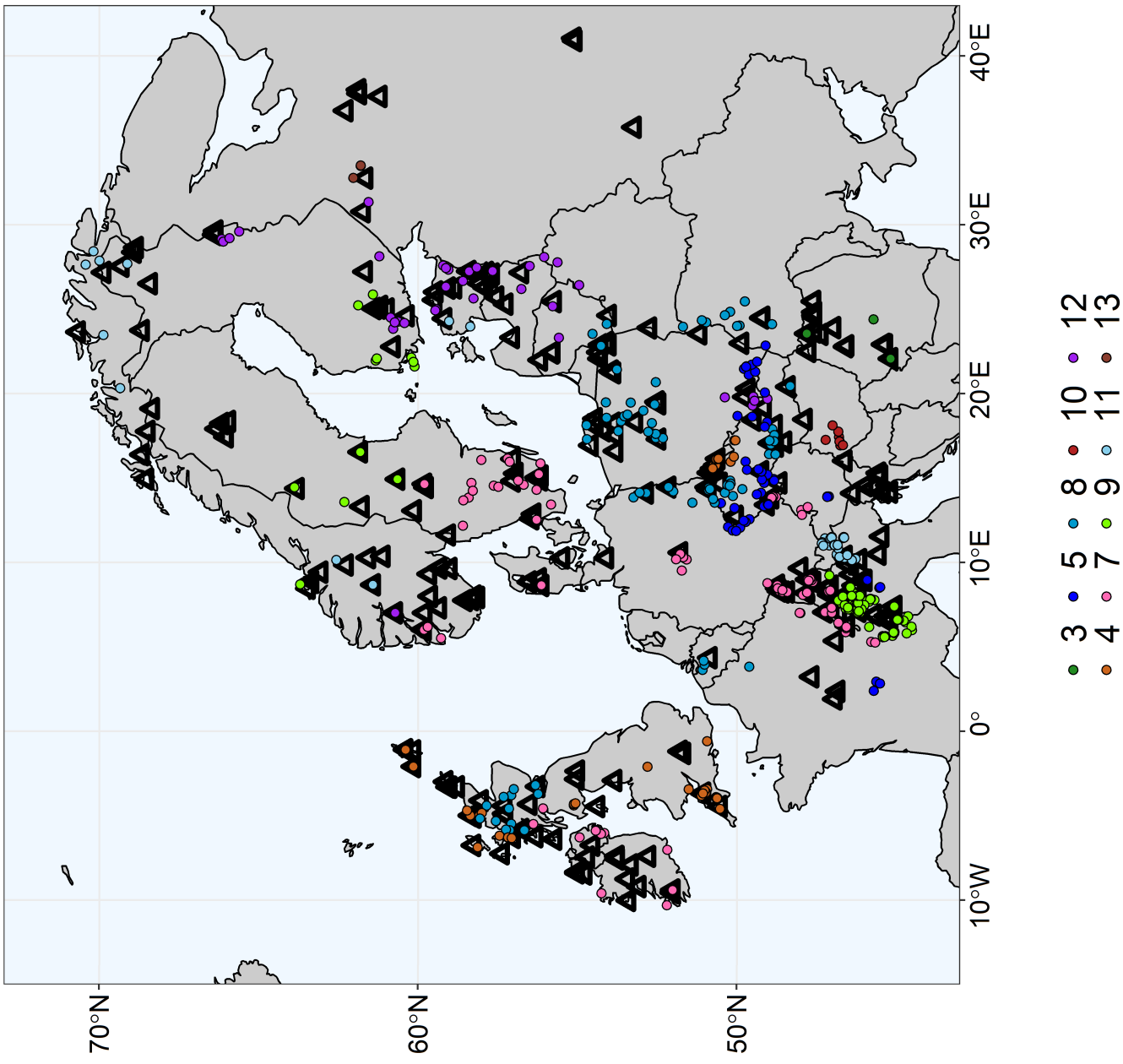

Figure A.4: Locations of pollen records from the Fyfe et al. [101] dataset that were used to generate land cover composites at the European scale, plotted in relation to the locations of charcoal records used to generate charcoal composites at the European scale. The land cover records are colour-coded by the European-scale spatial cluster (colour-coded and numbered in the legend) to which they were assigned. Black triangles are locations of charcoal records.

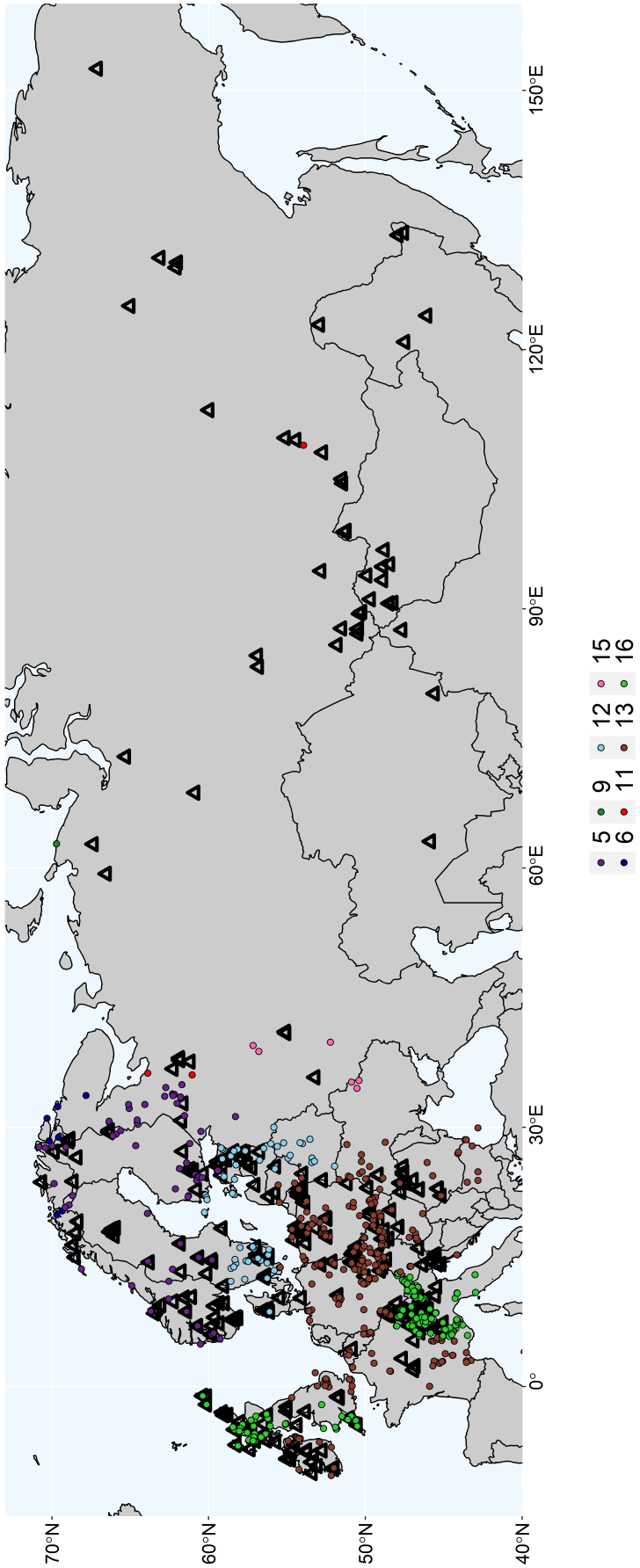

Figure A.5: Locations of pollen records from the Fyfe et al. [101] dataset that were used to generate land cover composites at the NET scale, plotted in relation to the locations of charcoal records used to generate charcoal composites at the NET scale. Land cover records are colour-coded by the NET spatial cluster (colour-coded and numbered in the legend) to which they were assigned. Black triangles are locations of charcoal records.

Table A.1: List of R packages not cited in the main text that were used in the analysis.

R package	**purpose**
dplyr[172]	data manipulation
tidyr[173]	data manipulation
reshape2[174]	data manipulation
stringr[175]	data processing
ncdf4[176]	netCDF data processing
rgdal[177]	spatial data analysis and visualisation
sf[178]	spatial data analysis and visualisation
maps[179]	spatial data visualisation
lattice[180]	spatial data visualisation
rnaturalearth[181]	spatial data visualisation
rnaturalearthdata[182]	spatial data visualisation
rgeos[183]	spatial data visualisation
maptools[184]	spatial data visualisation
RColorBrewer[185]	data visualisation
plot.matrix[186]	matrix visualisation
psych[187]	correlation multiplot generation
Metrics[188]	calculation of RMSE values
EGRET[189]	calculation of tricube-weighted means

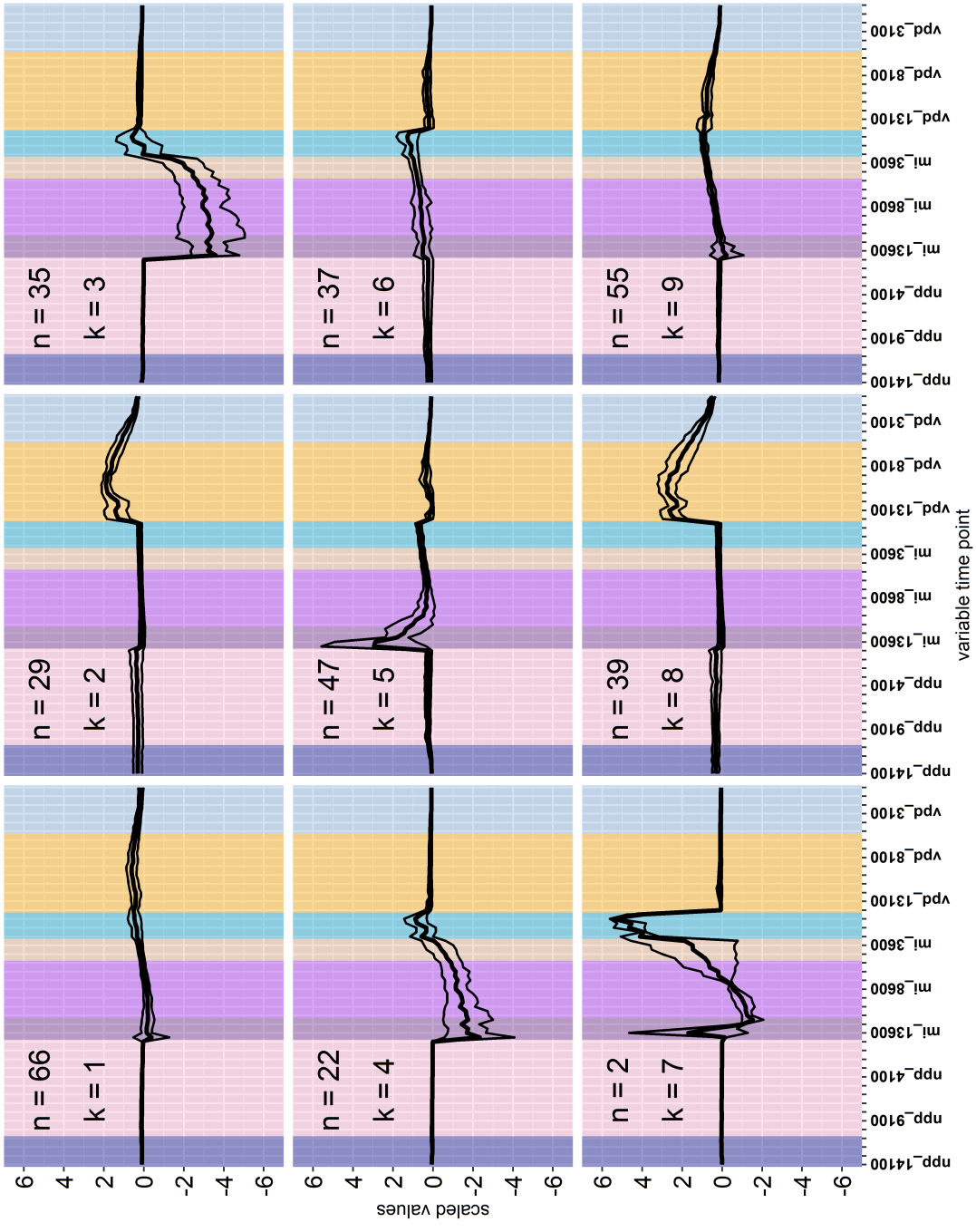

Figure A.6: Temporal patterns of spatial clusters 1-9 at the NET scale. Thick black lines represent the mean across all individual grid-cell time series comprising the cluster, where each time series is a concatenation of net primary productivity, moisture index, and vapour pressure deficit time series, each of which span the period 14.1-0kya. Thin black lines are the standard deviations around these means. The x-axis denotes the position and time order (in years before 1950 CE) of the respective variables within the concatenated time series (npp: net primary productivity; mi: moisture index; vpd: vapour pressure deficit). Coloured vertical bars represent temporal clusters defined by the biclustering algorithm. The number of grid cells comprising the clusters (n) and the cluster identity values (k) are shown.

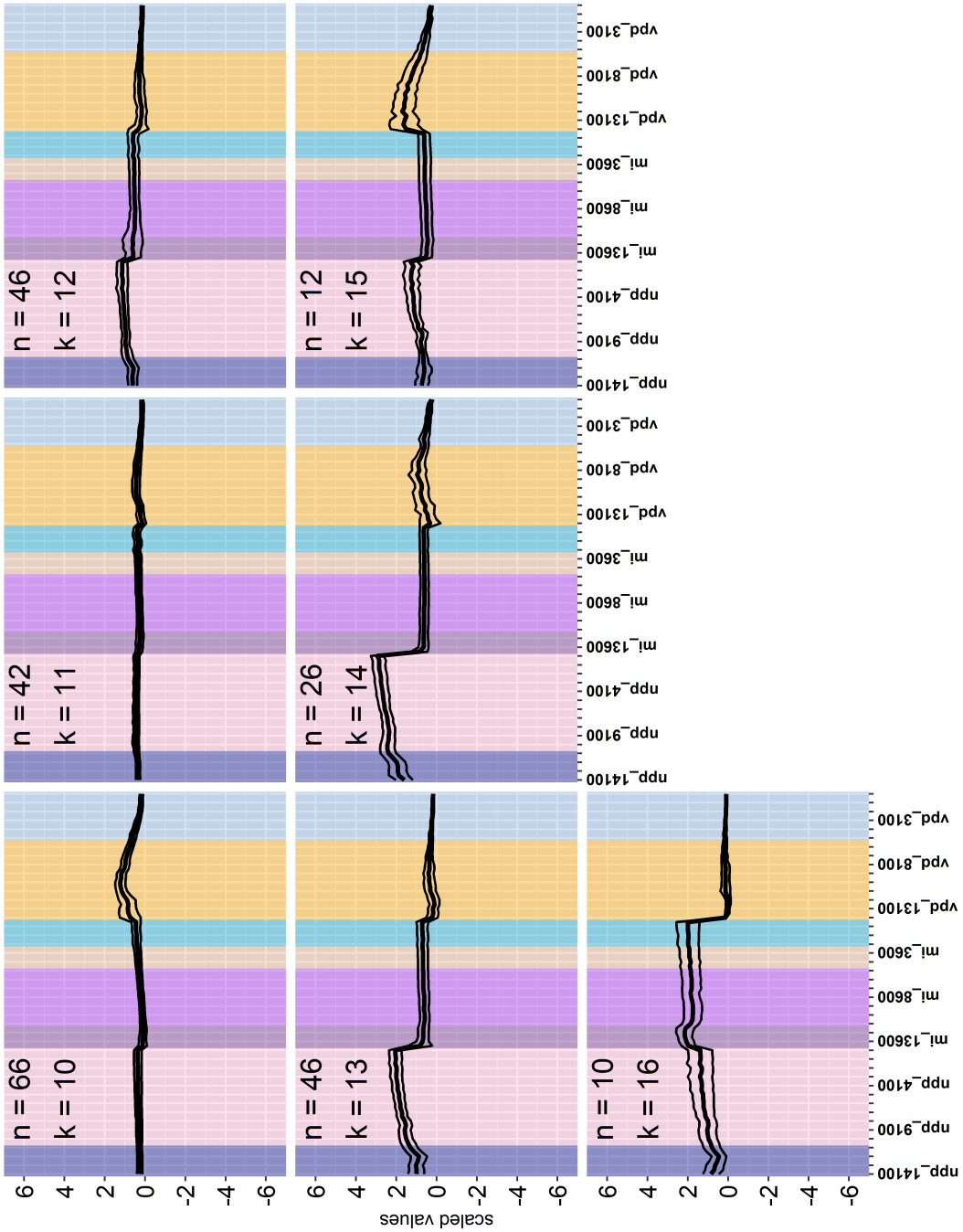

Figure A.7: Temporal patterns of spatial clusters 10-16 at the NET scale. Thick black lines represent the mean across all individual grid-cell time series comprising the cluster, where each time series is a concatenation of net primary productivity, moisture index, and vapour pressure deficit time series, each of which span the period 14.1-0kya. Thin black lines are the standard deviations around these means. The x-axis denotes the position and time order (in years before 1950 CE) of the respective variables within the concatenated time series (npp: net primary productivity; mi: moisture index; vpd: vapour pressure deficit). Coloured vertical bars represent temporal clusters defined by the biclustering algorithm. The number of grid cells comprising the clusters (n) and the cluster identity values (k) are shown.

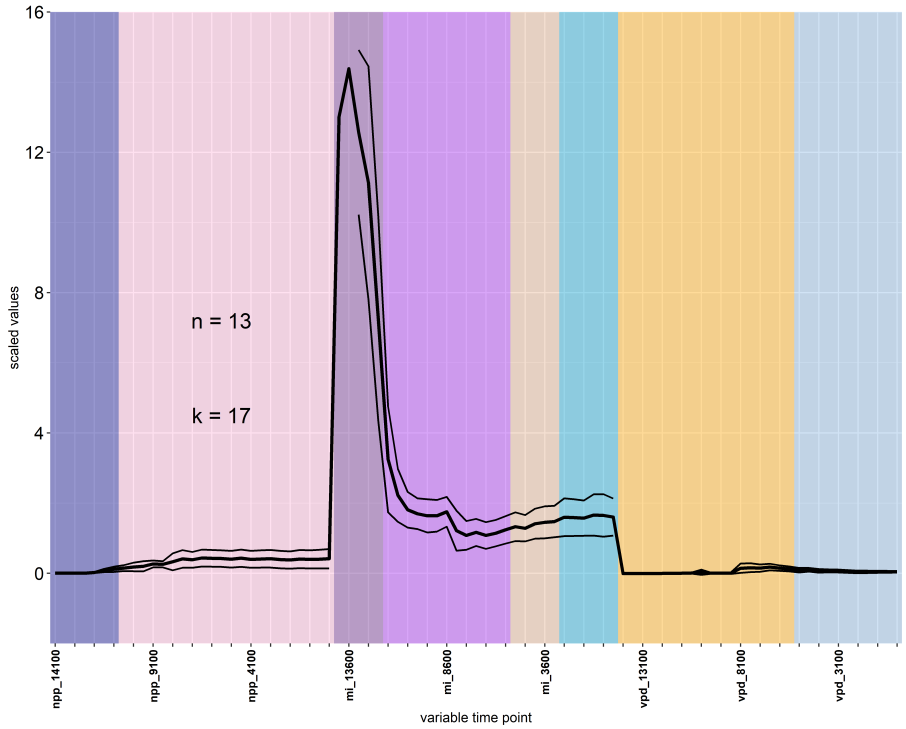

Figure A.8: Temporal patterns of spatial cluster 17 at the NET scale. The thick black line represents the mean across all individual grid-cell time series comprising the cluster, where each time series is a concatenation of net primary productivity, moisture index, and vapour pressure deficit time series, each of which span the period 14.1-0kya. Thin black lines are the standard deviations around this mean. The x-axis denotes the position and time order (in years before 1950 CE) of the respective variables within the concatenated time series (npp: net primary productivity; mi: moisture index; vpd: vapour pressure deficit). Coloured vertical bars represent temporal clusters defined by the biclustering algorithm. The number of grid cells comprising the cluster (n) and the cluster identity value (k) are shown.

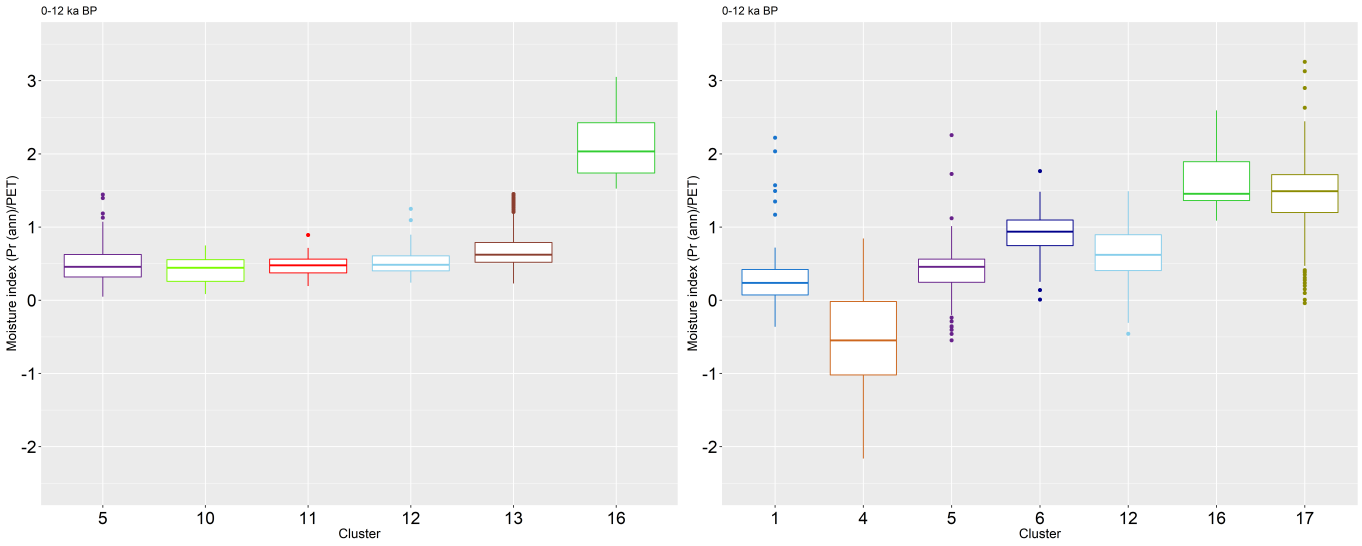

Figure A.9: Boxplots showing the distribution of moisture index values used to generate the composite curves of each spatial cluster at the NET scale for the 12-0kya interval. Left: Eurasia; Right: North America.

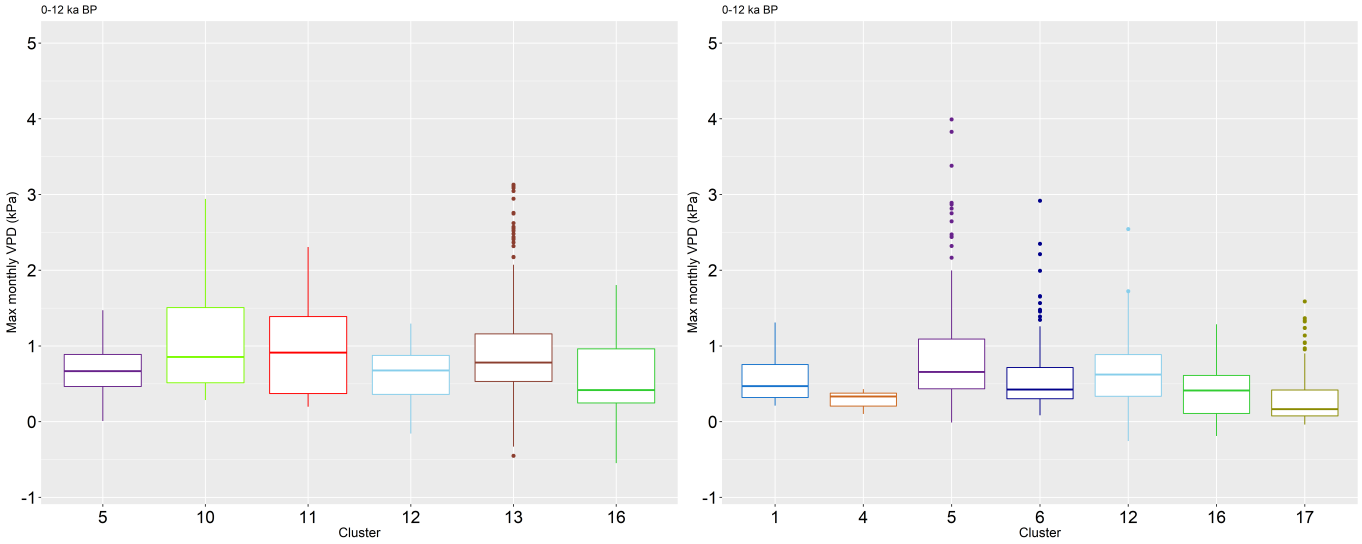

Figure A.10: Boxplots showing the distribution of vapour pressure deficit values used to generate the composite curves of each spatial cluster at the NET scale for the 12-0kya interval. Left: Eurasia; Right: North America.

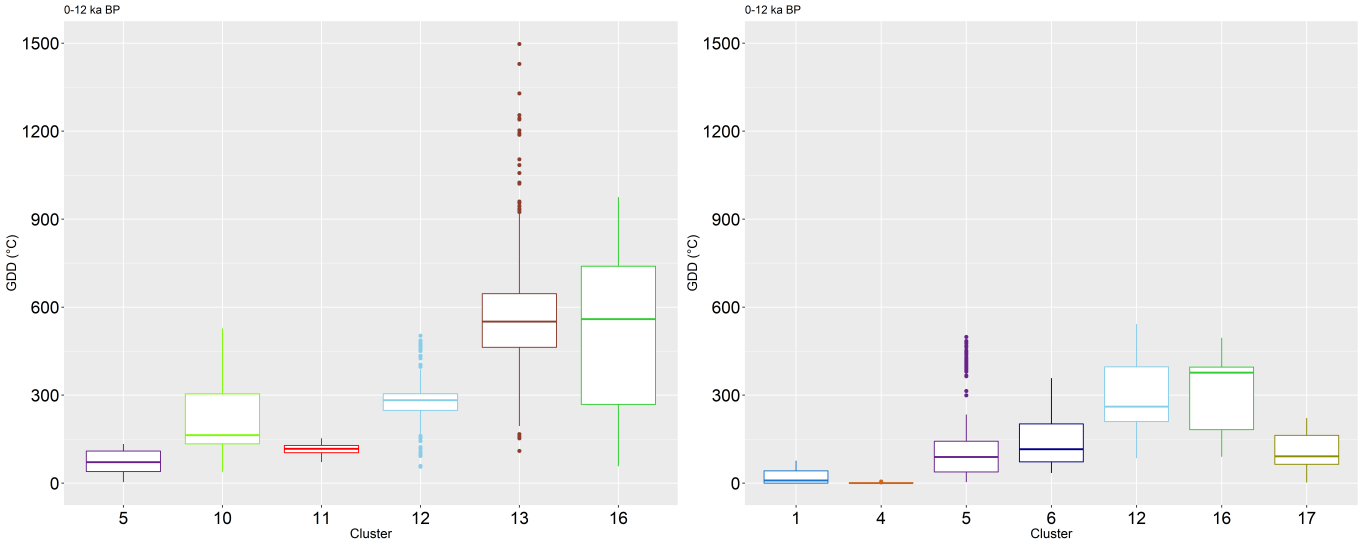

Figure A.11: Boxplots showing the distribution of values of growing degree days above 0°C used to generate the composite curves of each spatial cluster at the NET scale for the 12-0kya interval. Left: Eurasia; Right: North America.

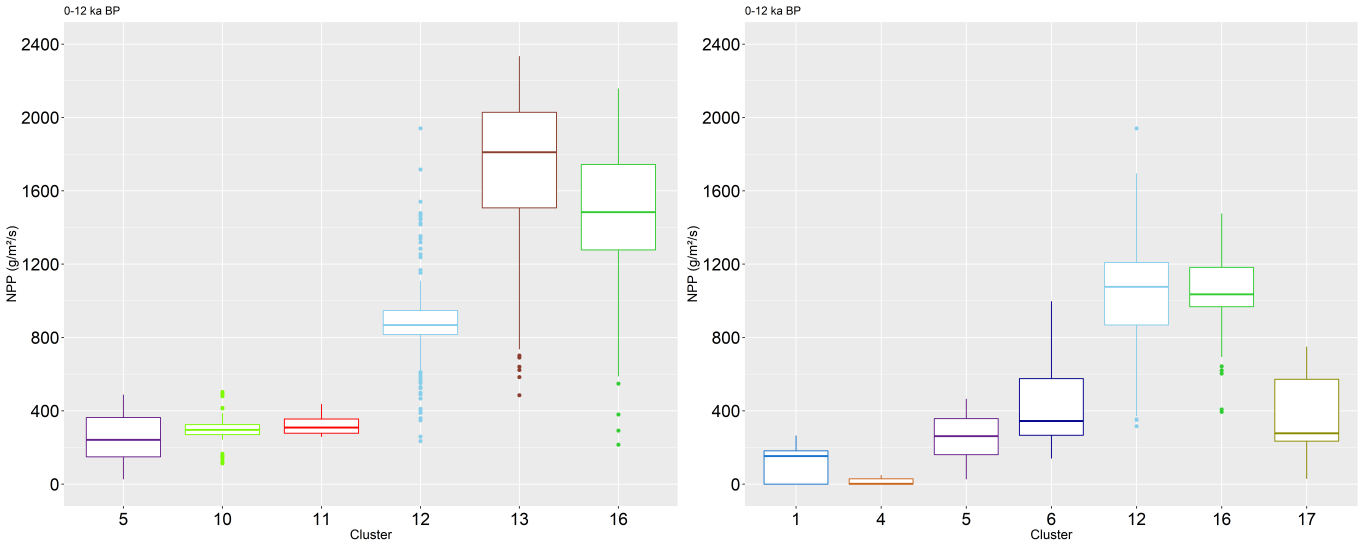

Figure A.12: Boxplots showing the distribution of net primary productivity values used to generate the composite curves of each spatial cluster at the NET scale for the 12-0kya interval. Left: Eurasia; Right: North America.

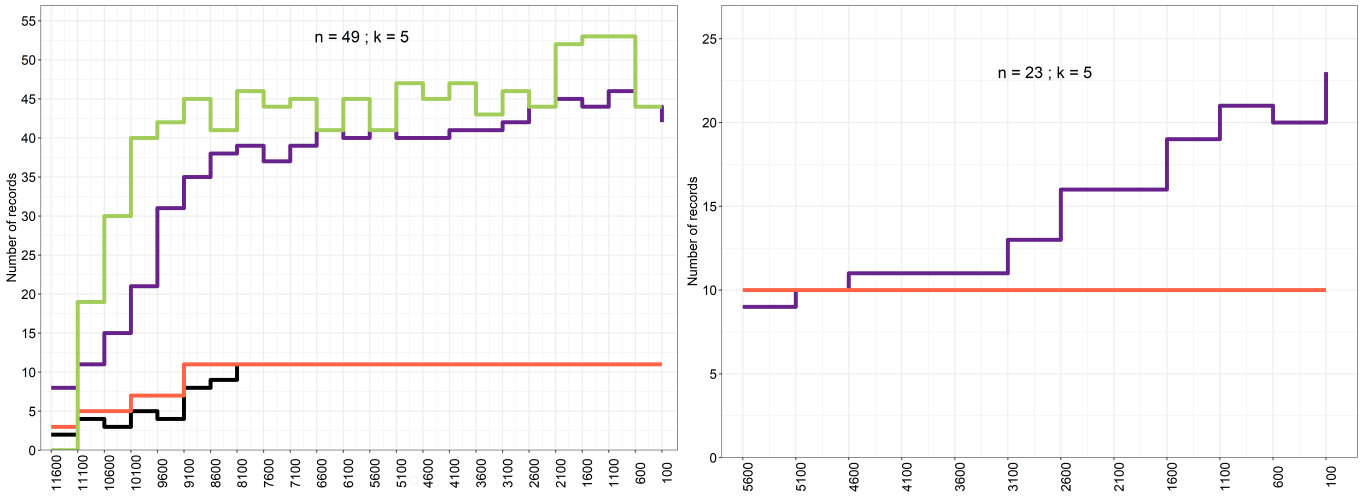

Figure A.13: Number of records comprising the fire and environmental composite curves for each time bin (shown on the x-axis in years before 1950 CE) for the NET cluster 5, Eurasia (left) and North America (right). The curves are coloured in accordance with the colours of the corresponding composite curves shown in the main text. Some environmental curves are not visible due to having identical sampling through time to other curves from the same dataset. The total number of charcoal records comprising the charcoal composite (n) and the cluster identity value (k) are shown.

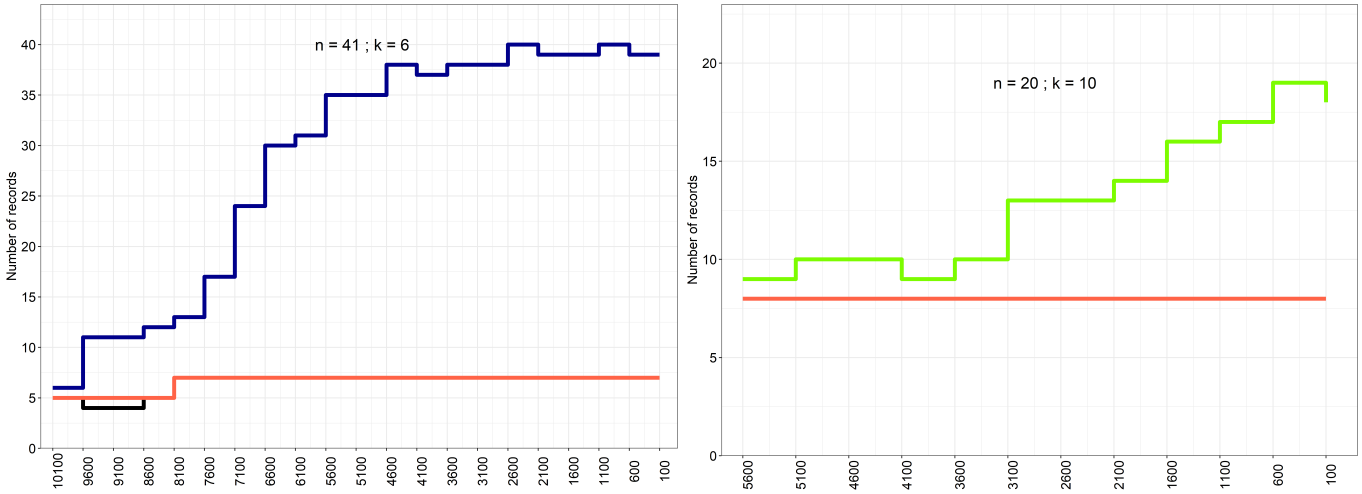

Figure A.14: Number of records comprising the fire and environmental composite curves for each time bin (shown on the x-axis in years before 1950 CE) for the NET clusters 6 (left) and 10 (right). The curves are coloured in accordance with the colours of the corresponding composite curves shown in the main text. Some environmental curves are not visible due to having identical sampling through time to other curves from the same dataset. The total number of charcoal records comprising the charcoal composite (n) and the cluster identity value (k) are shown.

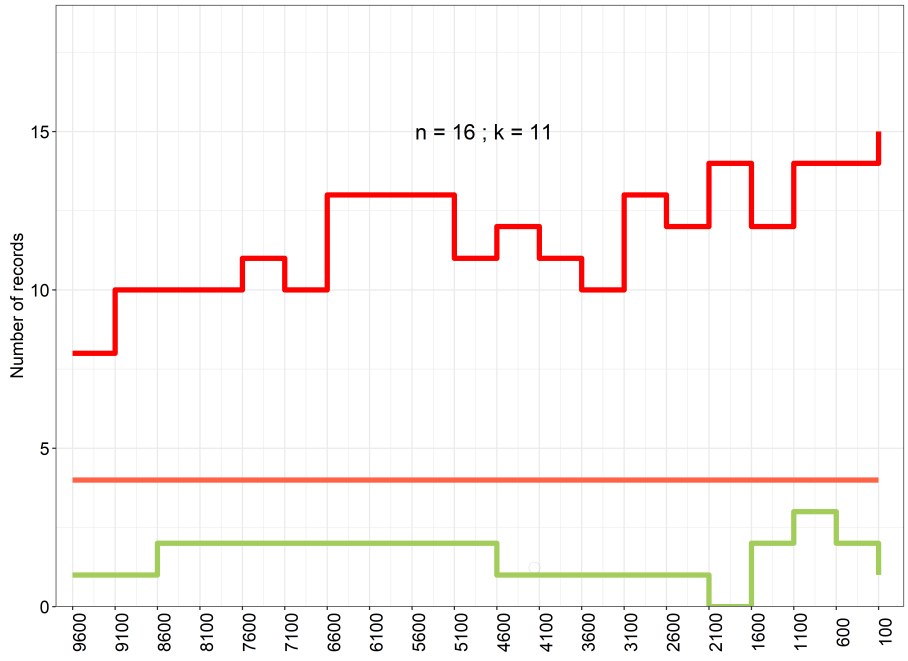

Figure A.15: Number of records comprising the fire and environmental composite curves for each time bin (shown on the x-axis in years before 1950 CE) for the NET cluster 11. The curves are coloured in accordance with the colours of the corresponding composite curves shown in the main text. Some environmental curves are not visible due to having identical sampling through time to other curves from the same dataset. The total number of charcoal records comprising the charcoal composite (n) and the cluster identity value (k) are shown.

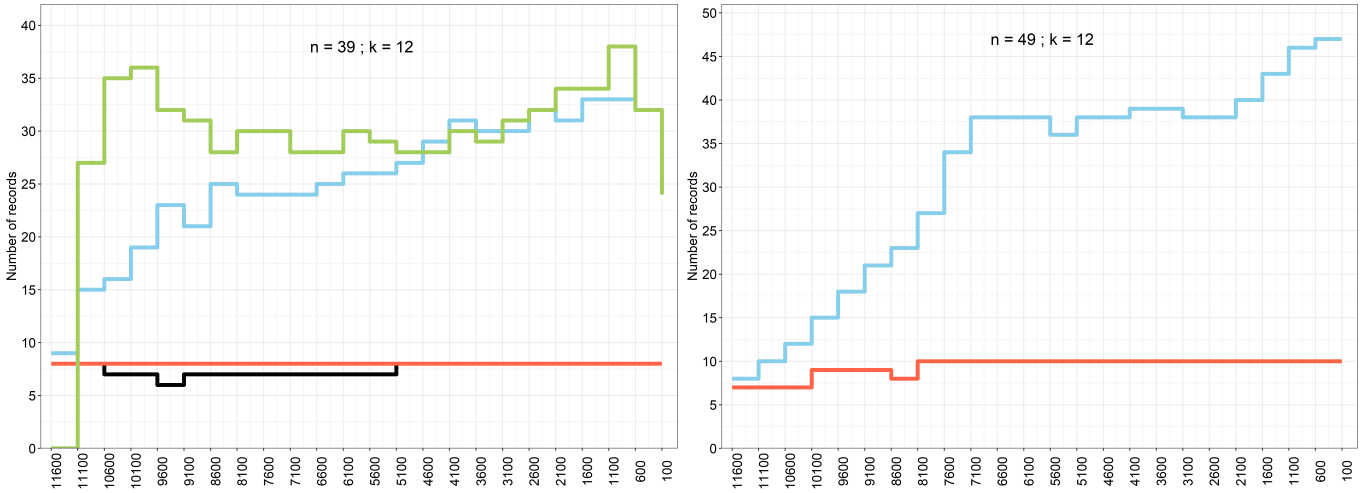

Figure A.16: Number of records comprising the fire and environmental composite curves for each time bin (shown on the x-axis in years before 1950 CE) for the NET cluster 12, Eurasia (left) and North America (right). The curves are coloured in accordance with the colours of the corresponding composite curves shown in the main text. Some environmental curves are not visible due to having identical sampling through time to other curves from the same dataset. The total number of charcoal records comprising the charcoal composite (n) and the cluster identity value (k) are shown.

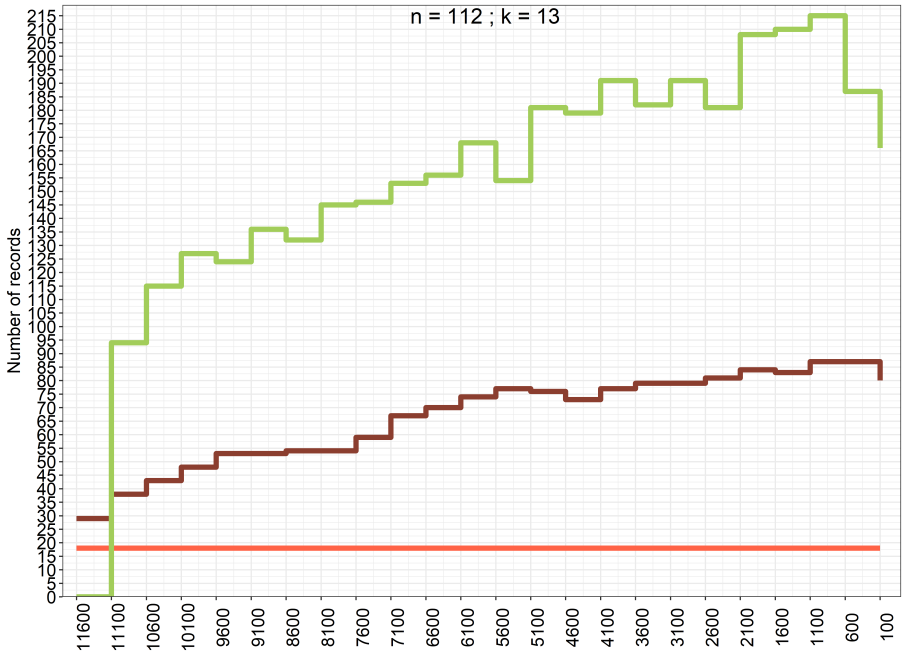

Figure A.17: Number of records comprising the fire and environmental composite curves for each time bin (shown on the x-axis in years before 1950 CE) for the NET cluster 13. The curves are coloured in accordance with the colours of the corresponding composite curves shown in the main text. Some environmental curves are not visible due to having identical sampling through time to other curves from the same dataset. The total number of charcoal records comprising the charcoal composite (n) and the cluster identity value (k) are shown.

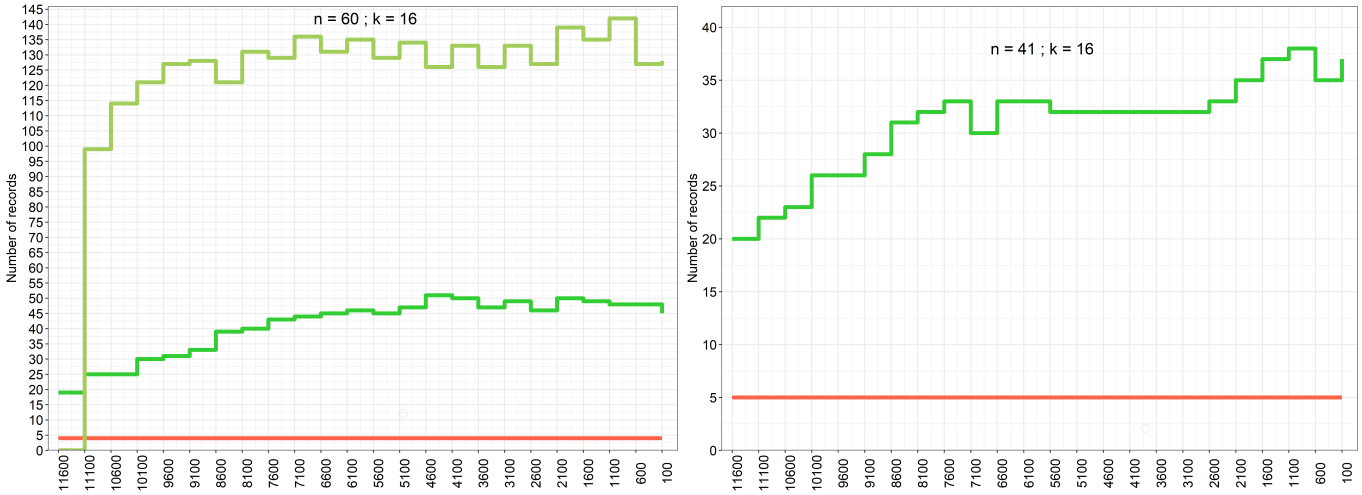

Figure A.18: Number of records comprising the fire and environmental composite curves for each time bin (shown on the x-axis in years before 1950 CE) for the NET cluster 16, Eurasia (left) and North America (right). The curves are coloured in accordance with the colours of the corresponding composite curves shown in the main text. Some environmental curves are not visible due to having identical sampling through time to other curves from the same dataset. The total number of charcoal records comprising the charcoal composite (n) and the cluster identity value (k) are shown.

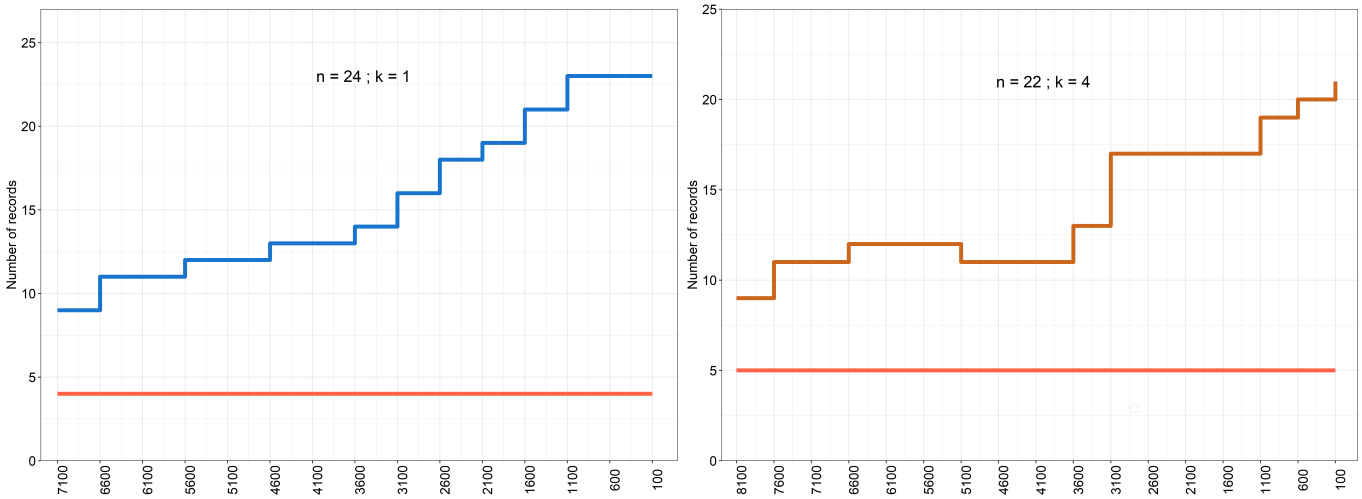

Figure A.19: Number of records comprising the fire and environmental composite curves for each time bin (shown on the x-axis in years before 1950 CE) for the NET clusters 1 (left) and 4 (right). The curves are coloured in accordance with the colours of the corresponding composite curves shown in the main text. Some environmental curves are not visible due to having identical sampling through time to other curves from the same dataset. The total number of charcoal records comprising the charcoal composite (n) and the cluster identity value (k) are shown.

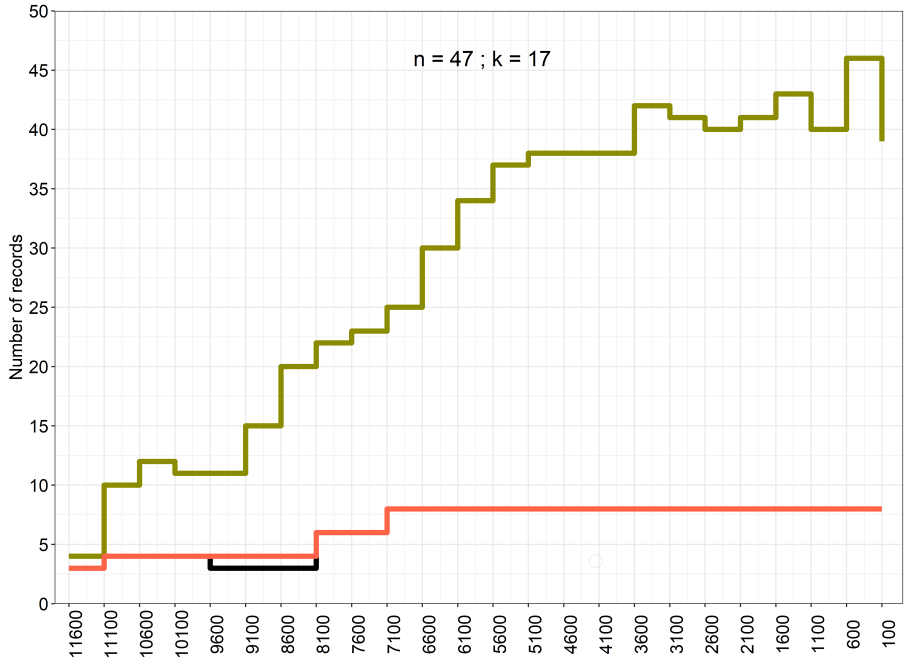

Figure A.20: Number of records comprising the fire and environmental composite curves for each time bin (shown on the x-axis in years before 1950 CE) for the NET cluster 17. The curves are coloured in accordance with the colours of the corresponding composite curves shown in the main text. Some environmental curves are not visible due to having identical sampling through time to other curves from the same dataset. The total number of charcoal records comprising the charcoal composite (n) and the cluster identity value (k) are shown.

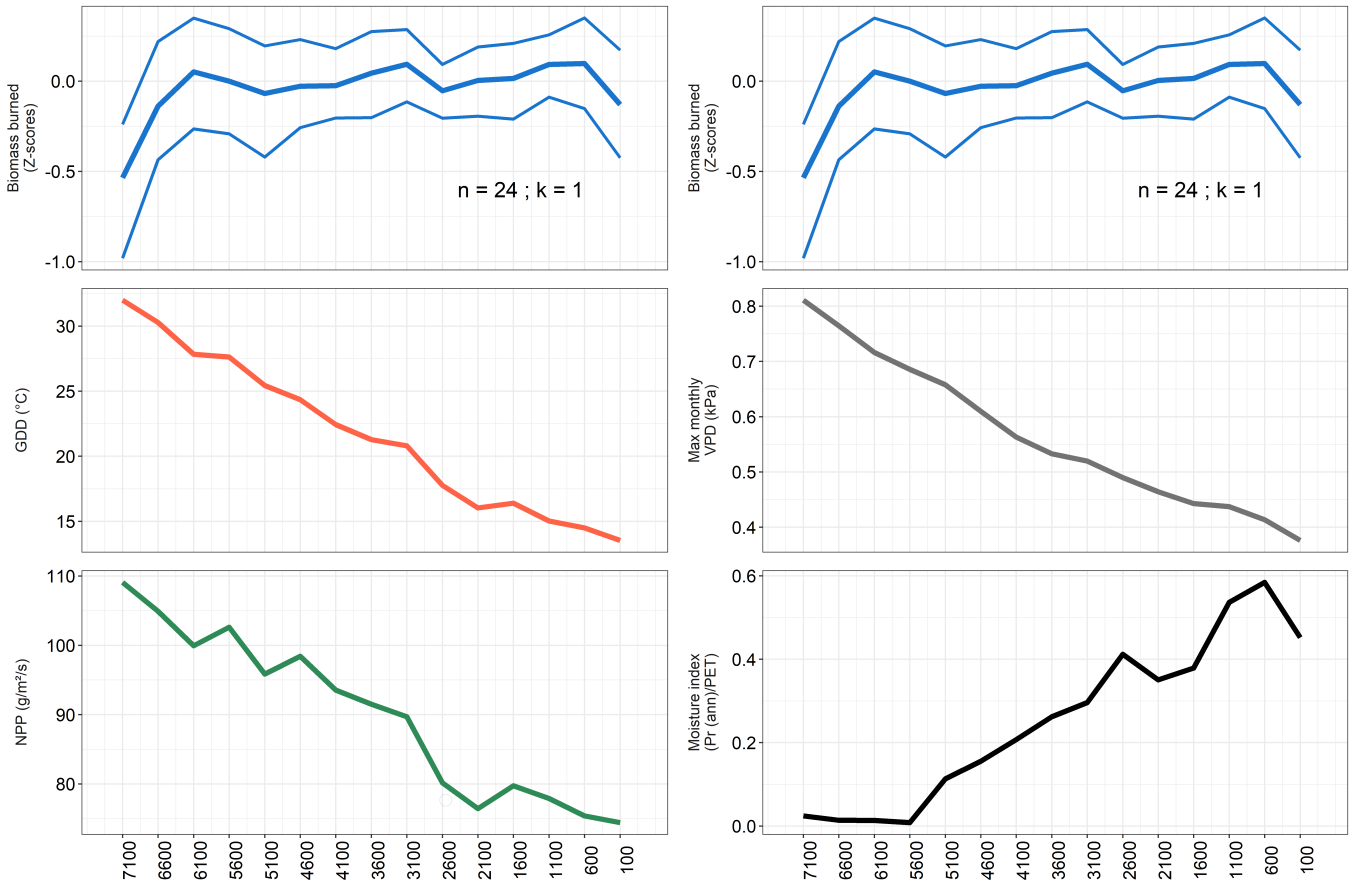

Figure A.21: Holocene biomass burning and environmental composite curves for the NET cluster 1, North America, all smoothed using a 1500-year window width. The time interval (shown on the x-axis in years before 1950 CE) is limited to the period within the 11.6-0kya interval in which all time points contains at least 10 charcoal records in the smoothing window. The composite curves are shown with 95% bootstrap confidence intervals, except for composites comprised of less than 10 individual time series. The number of charcoal records comprising the biomass burning response (n) and the cluster identity value (k) are shown on the top panel.

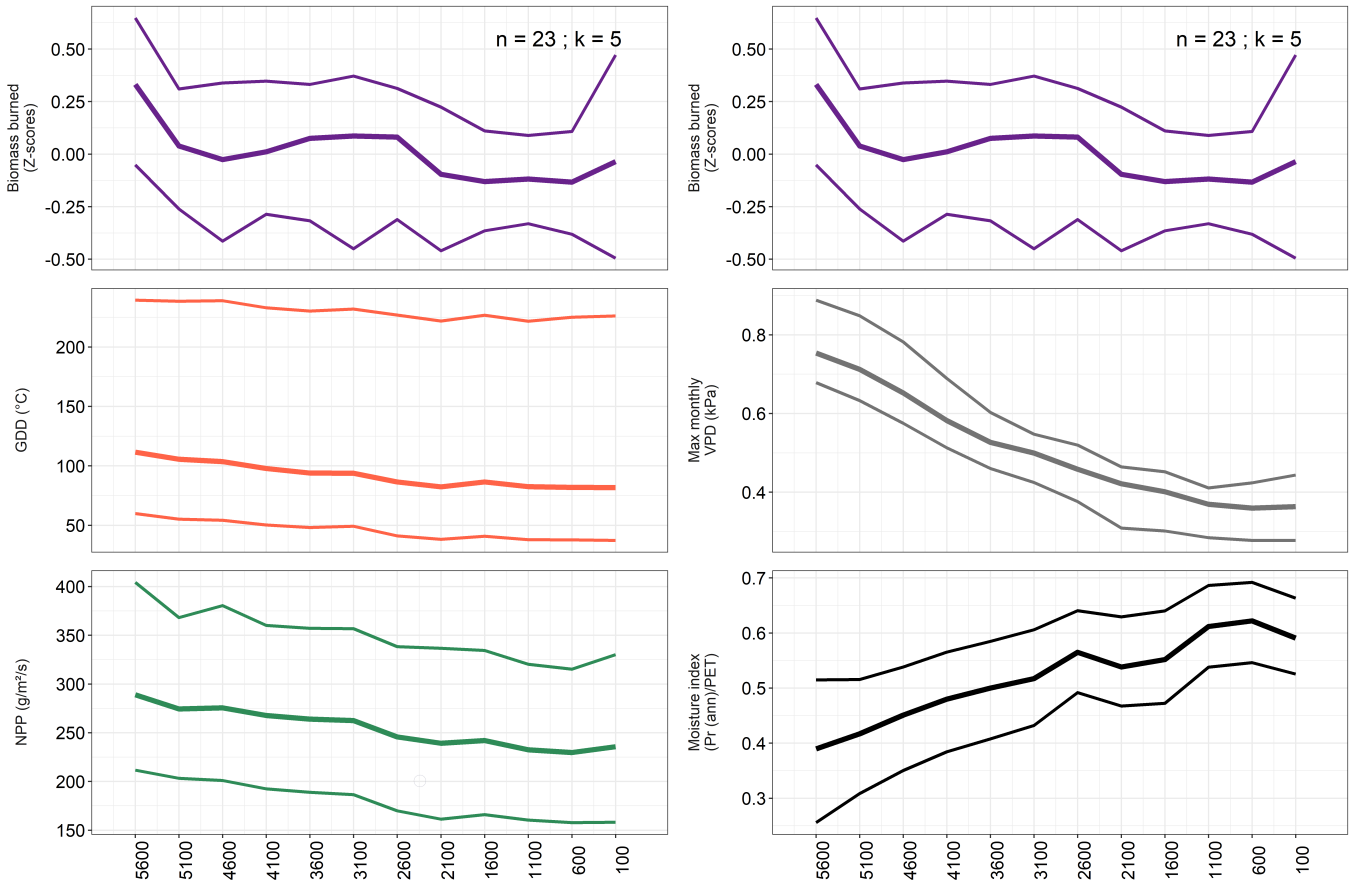

Figure A.22: Holocene biomass burning and environmental composite curves for the NET cluster 5, North America, all smoothed using a 1500-year window width. The time interval (shown on the x-axis in years before 1950 CE) is limited to the period within the 11.6-0kya interval in which all time points contain at least 10 charcoal records in the smoothing window. The composite curves are shown with 95% bootstrap confidence intervals. The number of charcoal records comprising the biomass burning response (n) and the cluster identity value (k) are shown on the top panel.

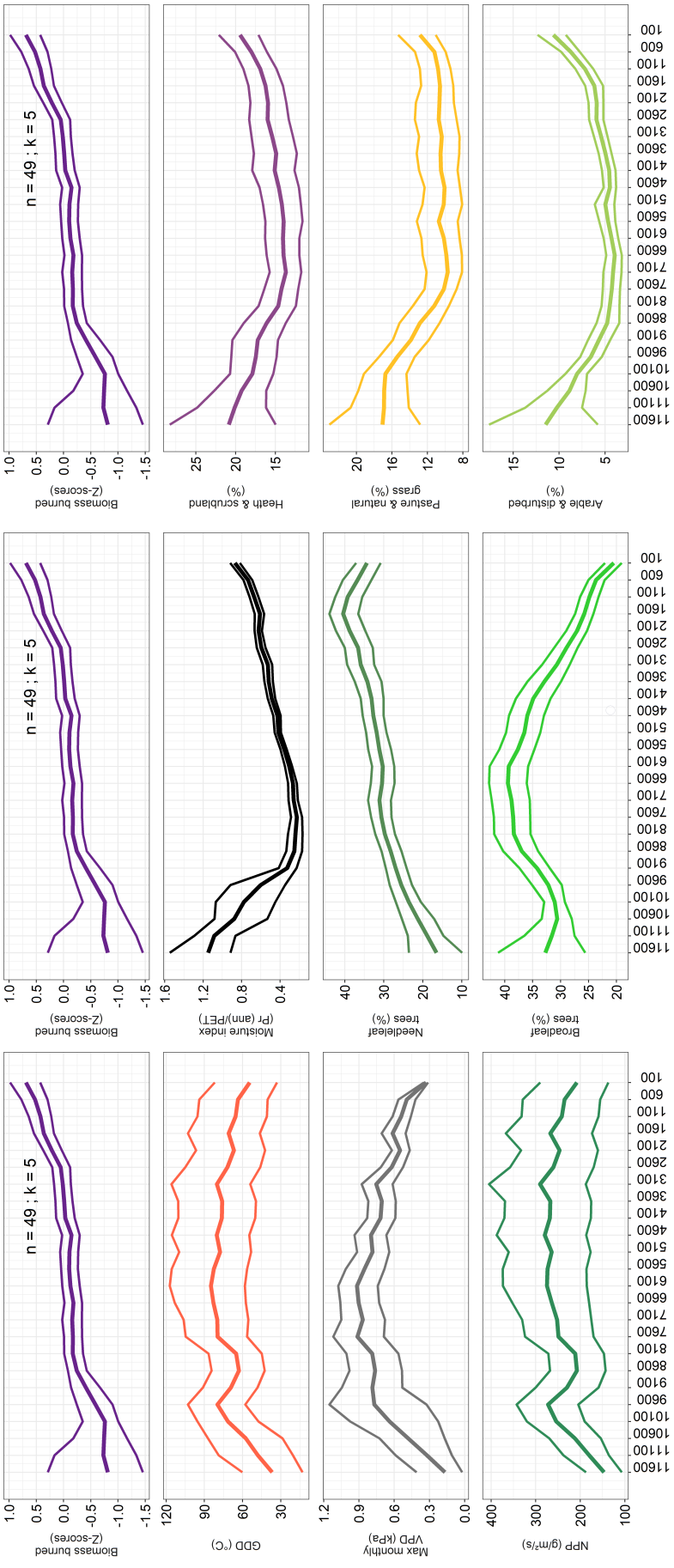

Figure A.23: Holocene biomass burning and environmental composite curves for the NET cluster 5, Eurasia, all smoothed using a 1500-year window width. The time interval (shown on the x-axis in years before 1950 CE) is limited to the period within the 11.6-0kya interval in which all time points contain at least 10 charcoal records in the smoothing window. The composite curves are shown with 95% bootstrap confidence intervals. The number of charcoal records comprising the biomass burning response (n) and the cluster identity value (k) are shown on the top panel.

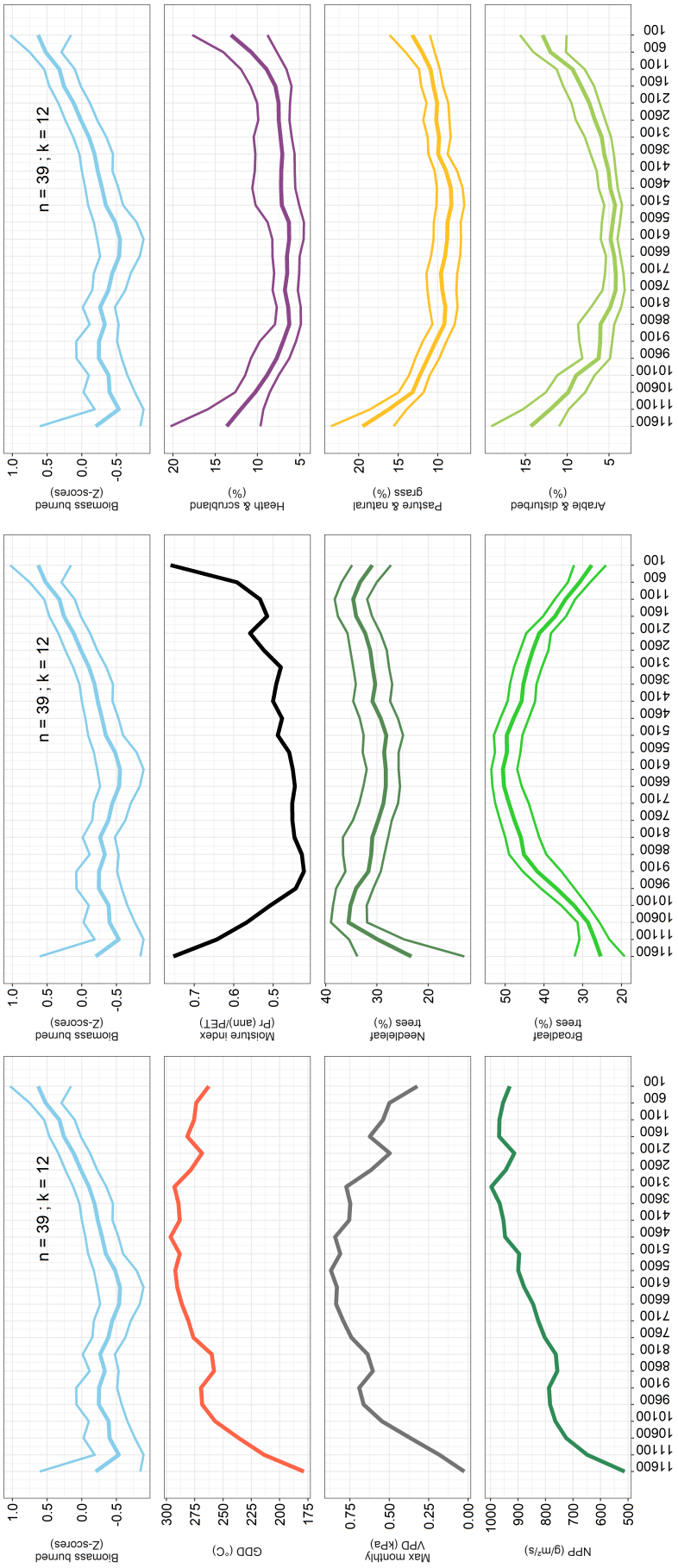

Figure A.24: Holocene biomass burning and environmental composite curves for the NET cluster 12, Eurasia, all smoothed using a 1500-year window width. The time interval (shown on the x-axis in years before 1950 CE) is limited to the period within the 11.6-0kya interval in which all time points contain at least 10 charcoal records in the smoothing window. The composite curves are shown with 95% bootstrap confidence intervals, except for composites comprised of less than 10 individual time series. The number of charcoal records comprising the biomass burning response (n) and the cluster identity value (k) are shown on the top panel.

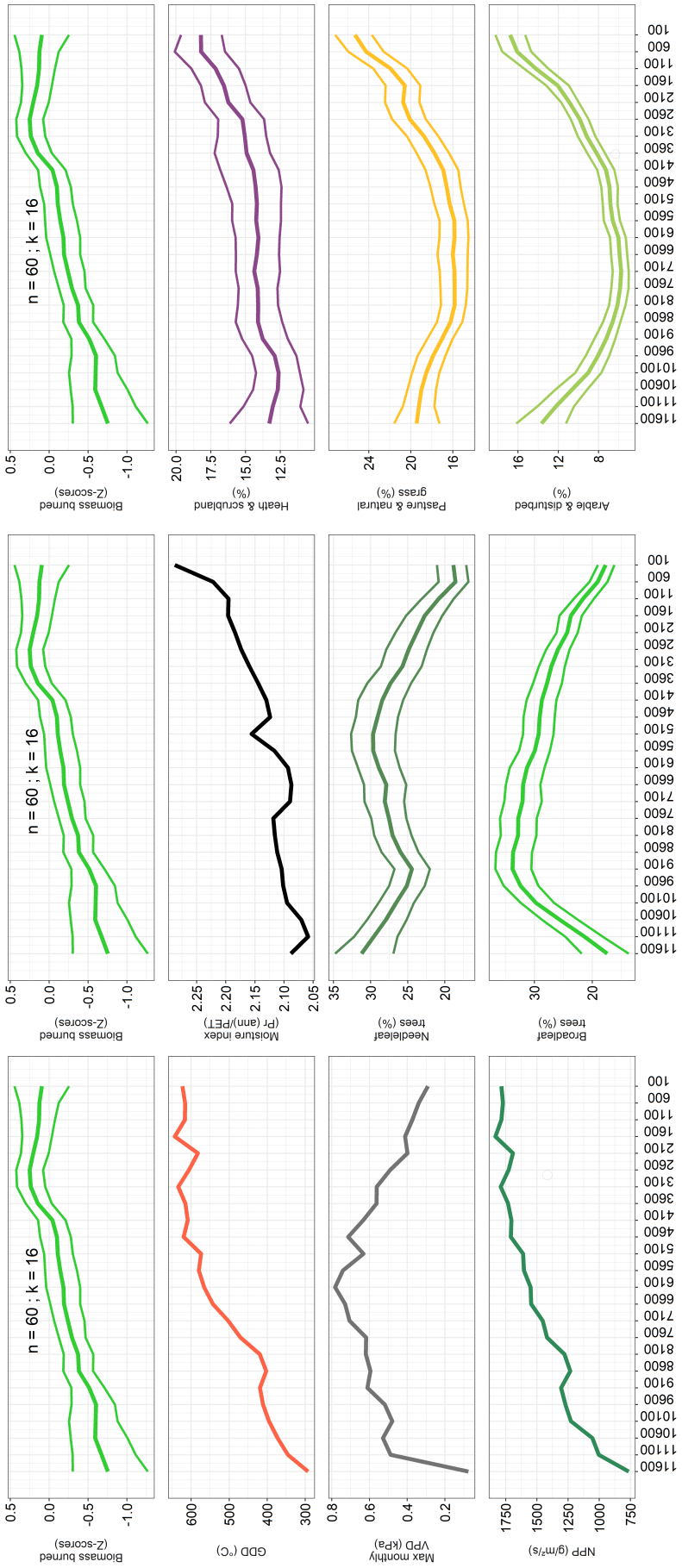

Figure A.25: Holocene biomass burning and environmental composite curves for the NET cluster 16, Eurasia, all smoothed using a 1500-year window width. The time interval (shown on the x-axis in years before 1950 CE) is limited to the period within the 11.6-0kya interval in which all time points contain at least 10 charcoal records in the smoothing window. The composite curves are shown with 95% bootstrap confidence intervals, except for composites comprised of less than 10 individual time series. The number of charcoal records comprising the biomass burning response (n) and the cluster identity value (k) are shown on the top panel.

Table A.2: Correlation values for the fire-environment comparisons for the North American clusters from the NET-scale analysis. Correlations are generated for 4ky-intervals as well as the full time interval that each cluster spans. Correlations are rounded to the nearest second decimal value. gdd: growing degree days; mi: moisture index; npp: net primary productivity; vpd: maximum monthly vapour pressure deficit.

cluster	variable correlated	time interval	correlation (r)
1	gdd	12-0kya	−0.53
1	gdd	8-4kya	−0.68
1	gdd	4-0kya	0.33
1	mi	12-0kya	0.44
1	mi	8-4kya	0.26
1	mi	4-0kya	0.08
1	npp	12-0kya	−0.49
1	npp	8-4kya	−0.72
1	npp	4-0kya	0.38
1	vpd	12-0kya	−0.56
1	vpd	8-4kya	−0.67
1	vpd	4-0kya	0.38
4	gdd	12-0kya	−0.25
4	gdd	8-4kya	−0.77
4	gdd	4-0kya	0.58
4	mi	12-0kya	−0.12
4	mi	8-4kya	0.66
4	mi	4-0kya	−0.77
4	npp	12-0kya	−0.16
4	npp	8-4kya	−0.75
4	npp	4-0kya	0.56
4	vpd	12-0kya	−0.06
4	vpd	8-4kya	−0.72
4	vpd	4-0kya	0.74
5	gdd	12-0kya	0.74
5	gdd	8-4kya	0.81
5	gdd	4-0kya	0.77
5	mi	12-0kya	−0.71
5	mi	8-4kya	−0.8
5	mi	4-0kya	−0.64
5	npp	12-0kya	0.77
5	npp	8-4kya	0.9
5	npp	4-0kya	0.83
5	vpd	12-0kya	0.73
5	vpd	8-4kya	0.74
5	vpd	4-0kya	0.84

Continued on next page.

Table A.2: Continued.

cluster	variable correlated	time interval	correlation (r)
6	gdd	12-0kya	0
6	gdd	12-8kya	0.25
6	gdd	8-4kya	−0.91
6	gdd	4-0kya	0.26
6	mi	12-0kya	−0.07
6	mi	12-8kya	0.03
6	mi	8-4kya	0.88
6	mi	4-0kya	−0.44
6	npp	12-0kya	0.05
6	npp	12-8kya	0.62
6	npp	8-4kya	0.77
6	npp	4-0kya	−0.12
6	vpd	12-0kya	−0.03
6	vpd	12-8kya	0.6
6	vpd	8-4kya	−0.81
6	vpd	4-0kya	0.7
12	gdd	12-0kya	0.66
12	gdd	12-8kya	0.79
12	gdd	8-4kya	0.46
12	gdd	4-0kya	−0.49
12	mi	12-0kya	0.74
12	mi	12-8kya	0.92
12	mi	8-4kya	−0.58
12	mi	4-0kya	0.19
12	npp	12-0kya	0.84
12	npp	12-8kya	0.91
12	npp	8-4kya	−0.44
12	npp	4-0kya	−0.22
12	vpd	12-0kya	−0.35
12	vpd	12-8kya	0.26
12	vpd	8-4kya	0.71
12	vpd	4-0kya	−0.13
16	gdd	12-0kya	−0.27
16	gdd	12-8kya	0.87
16	gdd	8-4kya	−0.15
16	gdd	4-0kya	0.94
16	mi	12-0kya	−0.51
16	mi	12-8kya	−0.12
16	mi	8-4kya	−0.93

Continued on next page.

Table A.2: Continued.

cluster	variable correlated	time interval	correlation (r)
16	mi	4-0kya	−0.33
16	npp	12-0kya	−0.32
16	npp	12-8kya	0.67
16	npp	8-4kya	−0.77
16	npp	4-0kya	0.61
16	vpd	12-0kya	0.05
16	vpd	12-8kya	−0.19
16	vpd	8-4kya	0.96
16	vpd	4-0kya	−0.34
17	gdd	12-0kya	−0.39
17	gdd	12-8kya	0.02
17	gdd	8-4kya	−0.79
17	gdd	4-0kya	−0.53
17	mi	12-0kya	0.3
17	mi	12-8kya	−0.02
17	mi	8-4kya	0.76
17	mi	4-0kya	0.71
17	npp	12-0kya	−0.3
17	npp	12-8kya	0.05
17	npp	8-4kya	−0.62
17	npp	4-0kya	−0.48
17	vpd	12-0kya	−0.69
17	vpd	12-8kya	−0.28
17	vpd	8-4kya	−0.84
17	vpd	4-0kya	−0.62

Table A.3: Correlation values for the fire-environment comparisons for the Eurasian clusters from the NET-scale analysis. Correlations are generated for 4ky-intervals as well as the full time interval that each cluster spans. Correlations are rounded to the nearest second decimal value. arable: arable and disturbed land cover; broadleaf: broadleaf tree cover; gdd: growing degree days; heath: heath and scrubland cover; mi: moisture index; needleleaf: needleleaf tree cover; npp: net primary productivity; pasture: pasture and natural grassland cover; vpd: maximum monthly vapour pressure deficit.

cluster	variable correlated	time interval	correlation (r)
5	arable	12-0kya	−0.15
5	arable	12-8kya	−0.91
5	arable	8-4kya	0.64
5	arable	4-0kya	0.92
5	broadleaf	12-0kya	−0.5
5	broadleaf	12-8kya	0.94
5	broadleaf	8-4kya	−0.75
5	broadleaf	4-0kya	−0.97
5	gdd	12-0kya	0.19
5	gdd	12-8kya	0.41
5	gdd	8-4kya	−0.49
5	gdd	4-0kya	−0.91
5	heath	12-0kya	−0.27
5	heath	12-8kya	−0.91
5	heath	8-4kya	0.67
5	heath	4-0kya	0.94
5	mi	12-0kya	−0.19
5	mi	12-8kya	−0.93
5	mi	8-4kya	0.82
5	mi	4-0kya	0.94
5	needleleaf	12-0kya	0.9
5	needleleaf	12-8kya	0.9
5	needleleaf	8-4kya	0.67
5	needleleaf	4-0kya	0.13
5	npp	12-0kya	0.32
5	npp	12-8kya	0.19
5	npp	8-4kya	0.4
5	npp	4-0kya	−0.85
5	pasture	12-0kya	−0.7
5	pasture	12-8kya	−0.99
5	pasture	8-4kya	0.7
5	pasture	4-0kya	0.79
5	vpd	12-0kya	0.03
5	vpd	12-8kya	0.75
5	vpd	8-4kya	−0.79

Continued on next page.

Table A.3: Continued.

cluster	variable correlated	time interval	correlation (r)
5	vpd	4-0kya	−0.91
10	gdd	12-0kya	−0.16
10	gdd	8-4kya	0.61
10	gdd	4-0kya	0.43
10	mi	12-0kya	0.07
10	mi	8-4kya	−0.62
10	mi	4-0kya	−0.51
10	npp	12-0kya	−0.18
10	npp	8-4kya	−0.37
10	npp	4-0kya	−0.78
10	vpd	12-0kya	−0.08
10	vpd	8-4kya	0.62
10	vpd	4-0kya	0.64
11	arable	12-0kya	0.26
11	arable	12-8kya	0.62
11	arable	8-4kya	0.72
11	arable	4-0kya	−0.12
11	broadleaf	12-0kya	0.42
11	broadleaf	12-8kya	0.38
11	broadleaf	8-4kya	0.41
11	broadleaf	4-0kya	−0.65
11	gdd	12-0kya	0.67
11	gdd	12-8kya	−0.53
11	gdd	8-4kya	0.98
11	gdd	4-0kya	−0.22
11	heath	12-0kya	−0.29
11	heath	12-8kya	−0.36
11	heath	8-4kya	−0.88
11	heath	4-0kya	0.27
11	mi	12-0kya	−0.62
11	mi	12-8kya	0.5
11	mi	8-4kya	−0.97
11	mi	4-0kya	0.43
11	needleleaf	12-0kya	−0.69
11	needleleaf	12-8kya	0.14
11	needleleaf	8-4kya	−0.93
11	needleleaf	4-0kya	0.53
11	npp	12-0kya	−0.37
11	npp	12-8kya	−0.5

Continued on next page.

Table A.3: Continued.

cluster	variable correlated	time interval	correlation (r)
11	npp	8-4kya	−0.76
11	npp	4-0kya	0.26
11	pasture	12-0kya	0.64
11	pasture	12-8kya	−0.39
11	pasture	8-4kya	0.93
11	pasture	4-0kya	−0.34
11	vpd	12-0kya	0.69
11	vpd	12-8kya	−0.55
11	vpd	8-4kya	0.98
11	vpd	4-0kya	−0.36
12	arable	12-0kya	0.52
12	arable	12-8kya	−0.27
12	arable	8-4kya	0.36
12	arable	4-0kya	0.98
12	broadleaf	12-0kya	−0.45
12	broadleaf	12-8kya	0.37
12	broadleaf	8-4kya	−0.88
12	broadleaf	4-0kya	−0.99
12	gdd	12-0kya	0.05
12	gdd	12-8kya	0.1
12	gdd	8-4kya	0.1
12	gdd	4-0kya	−0.79
12	heath	12-0kya	0.43
12	heath	12-8kya	−0.24
12	heath	8-4kya	0.92
12	heath	4-0kya	0.91
12	mi	12-0kya	0.5
12	mi	12-8kya	−0.18
12	mi	8-4kya	0.86
12	mi	4-0kya	0.81
12	needleleaf	12-0kya	0.37
12	needleleaf	12-8kya	−0.35
12	needleleaf	8-4kya	0.75
12	needleleaf	4-0kya	0.46
12	npp	12-0kya	0.47
12	npp	12-8kya	−0.03
12	npp	8-4kya	0.57
12	npp	4-0kya	−0.38
12	pasture	12-0kya	0.16

Continued on next page.

Table A.3: Continued.

cluster	variable correlated	time interval	correlation (r)
12	pasture	12-8kya	−0.13
12	pasture	8-4kya	−0.28
12	pasture	4-0kya	0.92
12	vpd	12-0kya	−0.32
12	vpd	12-8kya	0.25
12	vpd	8-4kya	−0.5
12	vpd	4-0kya	−0.88
13	arable	12-0kya	0.73
13	arable	12-8kya	−0.75
13	arable	8-4kya	−0.36
13	arable	4-0kya	0.98
13	broadleaf	12-0kya	−0.31
13	broadleaf	12-8kya	0.72
13	broadleaf	8-4kya	−0.42
13	broadleaf	4-0kya	−0.98
13	gdd	12-0kya	0.37
13	gdd	12-8kya	0.66
13	gdd	8-4kya	−0.61
13	gdd	4-0kya	−0.39
13	heath	12-0kya	0.19
13	heath	12-8kya	−0.73
13	heath	8-4kya	−0.08
13	heath	4-0kya	0.92
13	mi	12-0kya	0.57
13	mi	12-8kya	−0.15
13	mi	8-4kya	−0.45
13	mi	4-0kya	0.95
13	needleleaf	12-0kya	−0.45
13	needleleaf	12-8kya	−0.63
13	needleleaf	8-4kya	0.88
13	needleleaf	4-0kya	−0.61
13	npp	12-0kya	0.43
13	npp	12-8kya	0.66
13	npp	8-4kya	−0.57
13	npp	4-0kya	0.22
13	pasture	12-0kya	0.31
13	pasture	12-8kya	−0.75
13	pasture	8-4kya	−0.16
13	pasture	4-0kya	0.99

Continued on next page.

Table A.3: Continued.

cluster	variable correlated	time interval	correlation (r)
13	vpd	12-0kya	−0.26
13	vpd	12-8kya	0.62
13	vpd	8-4kya	0.34
13	vpd	4-0kya	−0.89
16	arable	12-0kya	0.2
16	arable	12-8kya	−0.91
16	arable	8-4kya	0.93
16	arable	4-0kya	−0.73
16	broadleaf	12-0kya	−0.23
16	broadleaf	12-8kya	0.83
16	broadleaf	8-4kya	−0.96
16	broadleaf	4-0kya	0.73
16	gdd	12-0kya	0.95
16	gdd	12-8kya	0.79
16	gdd	8-4kya	0.94
16	gdd	4-0kya	−0.24
16	heath	12-0kya	0.79
16	heath	12-8kya	0.72
16	heath	8-4kya	0.47
16	heath	4-0kya	−0.76
16	mi	12-0kya	0.77
16	mi	12-8kya	0.71
16	mi	8-4kya	0.55
16	mi	4-0kya	−0.65
16	needleleaf	12-0kya	−0.5
16	needleleaf	12-8kya	−0.63
16	needleleaf	8-4kya	0.61
16	needleleaf	4-0kya	0.67
16	npp	12-0kya	0.94
16	npp	12-8kya	0.76
16	npp	8-4kya	0.97
16	npp	4-0kya	−0.38
16	pasture	12-0kya	0.37
16	pasture	12-8kya	−0.95
16	pasture	8-4kya	0.85
16	pasture	4-0kya	−0.64
16	vpd	12-0kya	0.01
16	vpd	12-8kya	0.78
16	vpd	8-4kya	−0.07

Continued on next page.

Table A.3: Continued.

cluster	variable correlated	time interval	correlation (r)
16	vpd	4-0kya	0.66

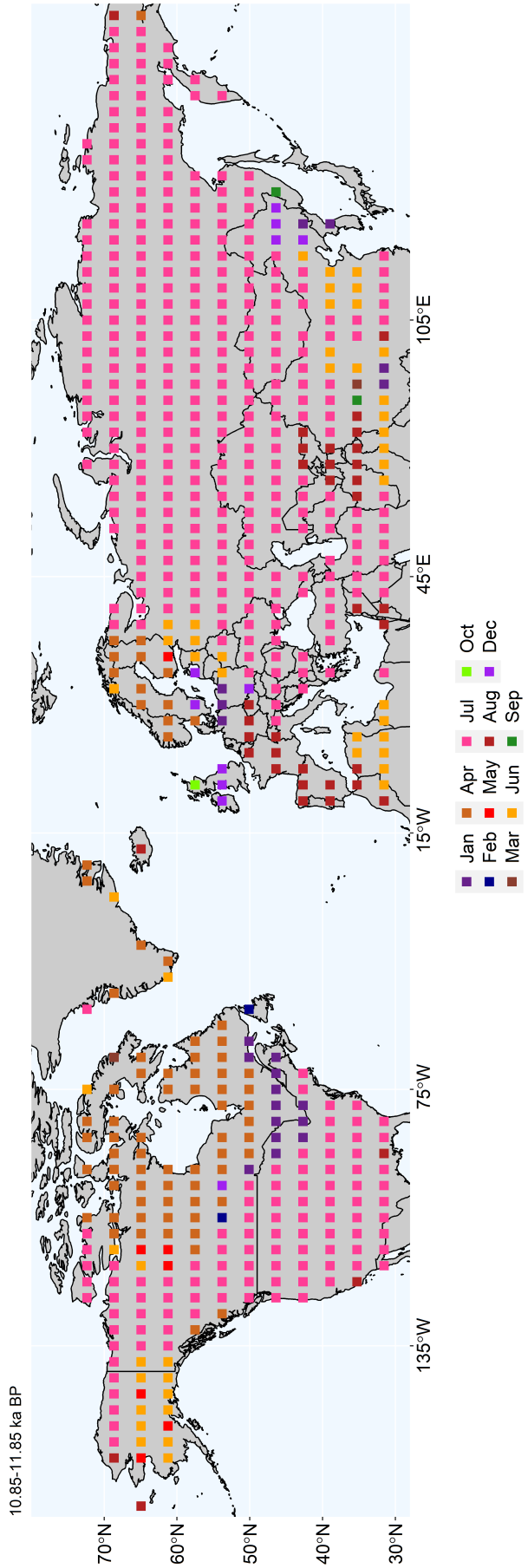

Figure A.26: Spatial distribution of the most commonly occurring months during the interval 11.85-10.85kya in which vapour pressure deficit is at a yearly maximum. The surface is generated using maximum monthly vapour pressure deficit data in which monthly values are aggregated at decadal resolution.

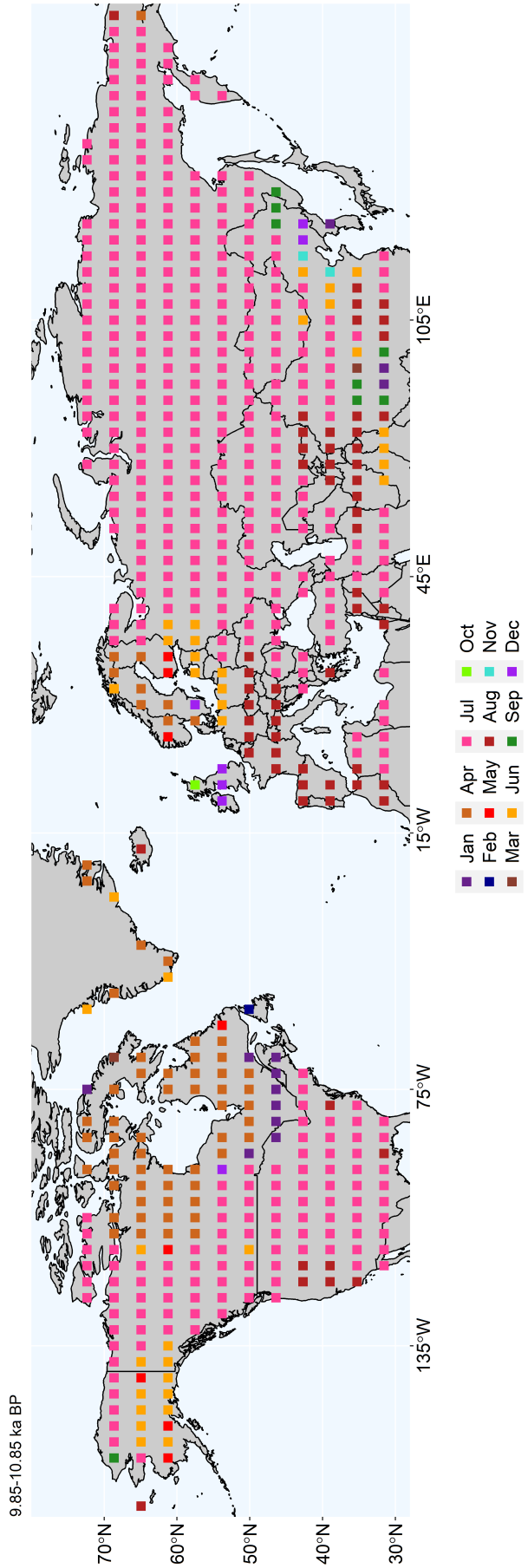

Figure A.27: Spatial distribution of the most commonly occurring months during the interval 10.85-9.85kya in which vapour pressure deficit is at a yearly maximum. The surface is generated using maximum monthly vapour pressure deficit data in which monthly values are aggregated at decadal resolution.

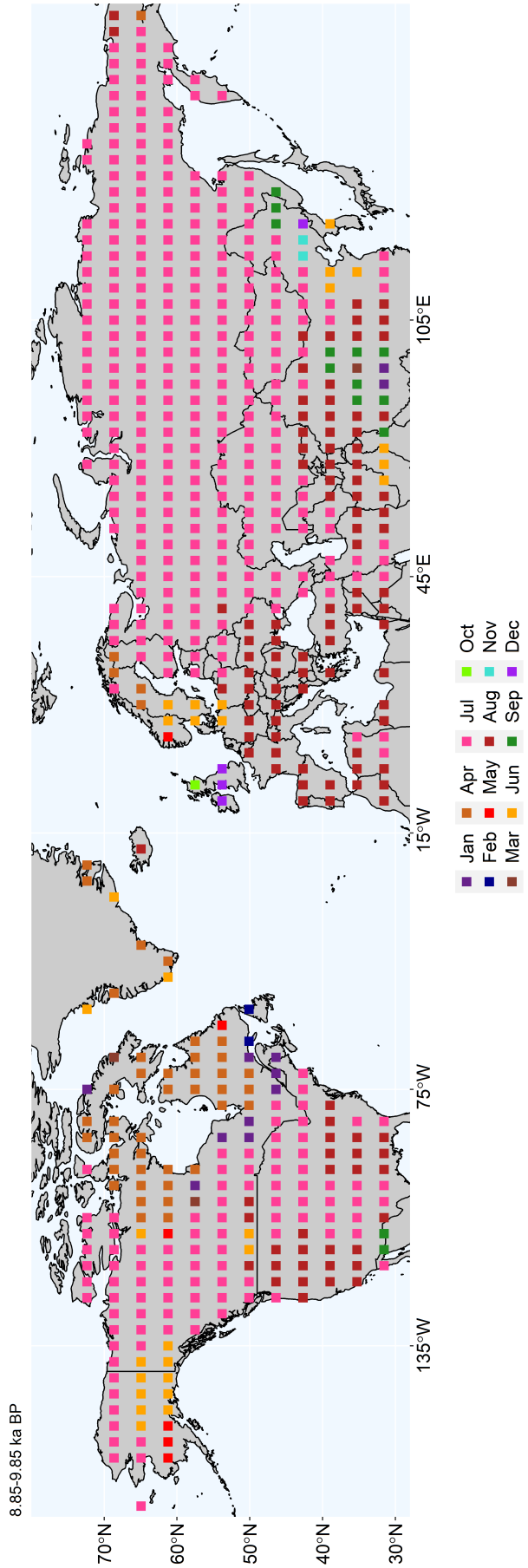

Figure A.28: Spatial distribution of the most commonly occurring months during the interval 9.85-8.85kya in which vapour pressure deficit is at a yearly maximum. The surface is generated using maximum monthly vapour pressure deficit data in which monthly values are aggregated at decadal resolution.

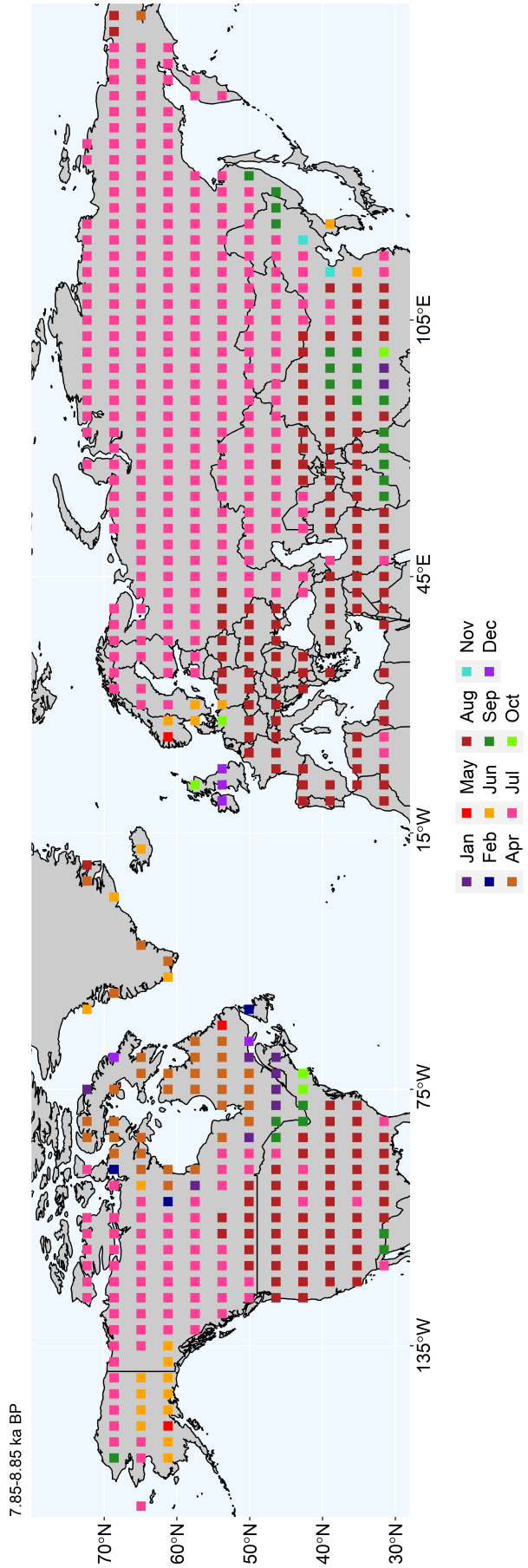

Figure A.29: Spatial distribution of the most commonly occurring months during the interval 8.85-7.85kya in which vapour pressure deficit is at a yearly maximum. The surface is generated using maximum monthly vapour pressure deficit data in which monthly values are aggregated at decadal resolution.

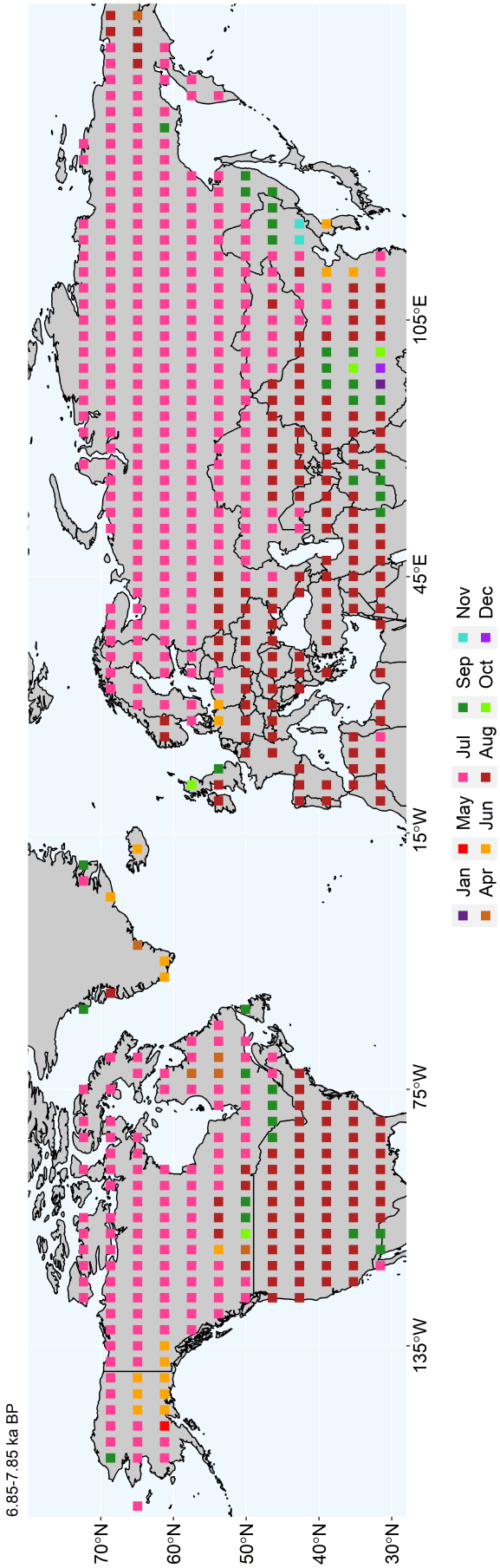

Figure A.30: Spatial distribution of the most commonly occurring months during the interval 7.85-6.85kya in which vapour pressure deficit is at a yearly maximum. The surface is generated using maximum monthly vapour pressure deficit data in which monthly values are aggregated at decadal resolution.

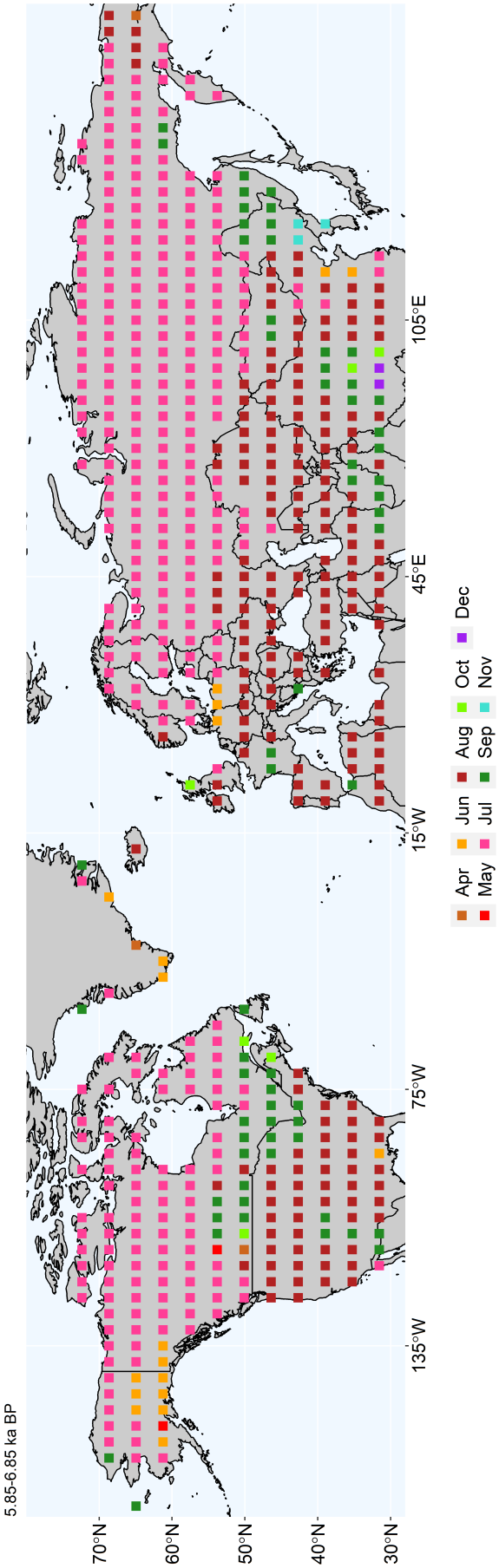

Figure A.31: Spatial distribution of the most commonly occurring months during the interval 6.85-5.85kya in which vapour pressure deficit is at a yearly maximum. The surface is generated using maximum monthly vapour pressure deficit data in which monthly values are aggregated at decadal resolution.

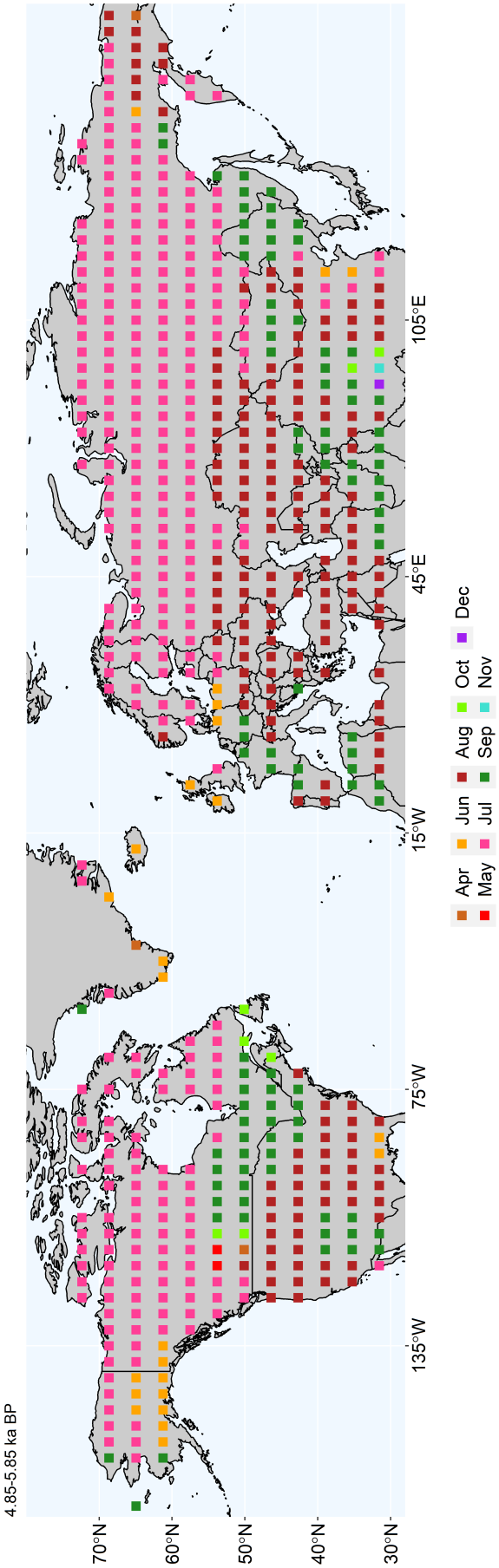

Figure A.32: Spatial distribution of the most commonly occurring months during the interval 5.85-4.85kya in which vapour pressure deficit is at a yearly maximum. The surface is generated using maximum monthly vapour pressure deficit data in which monthly values are aggregated at decadal resolution.

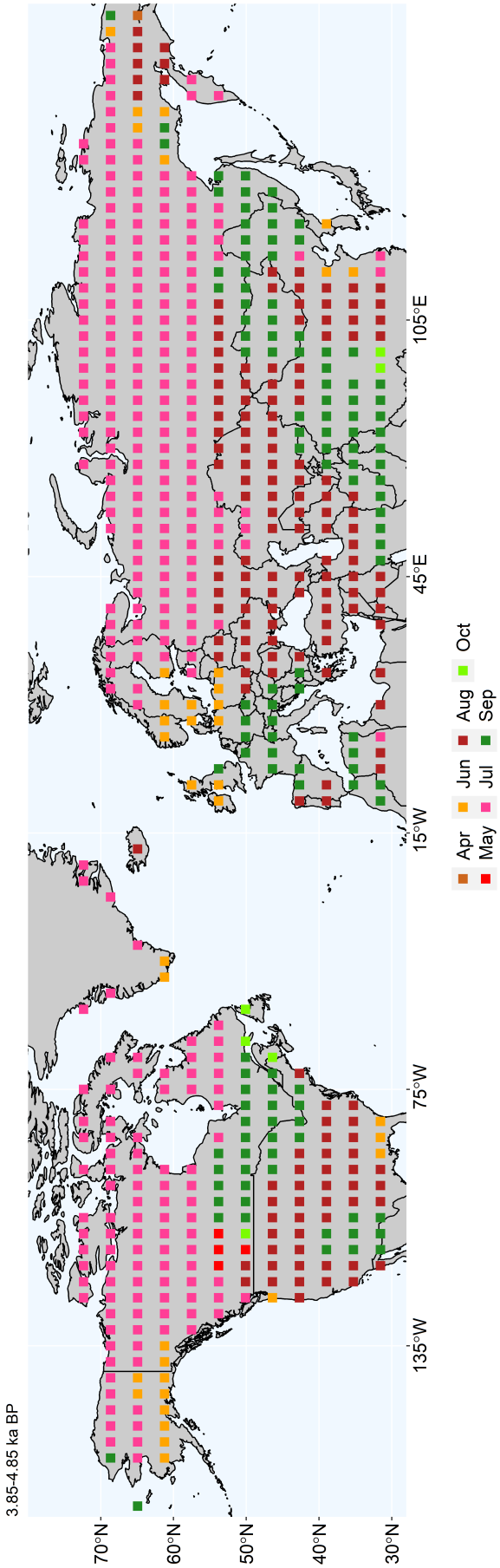

Figure A.33: Spatial distribution of the most commonly occurring months during the interval 4.85-3.85kya in which vapour pressure deficit is at a yearly maximum. The surface is generated using maximum monthly vapour pressure deficit data in which monthly values are aggregated at decadal resolution.

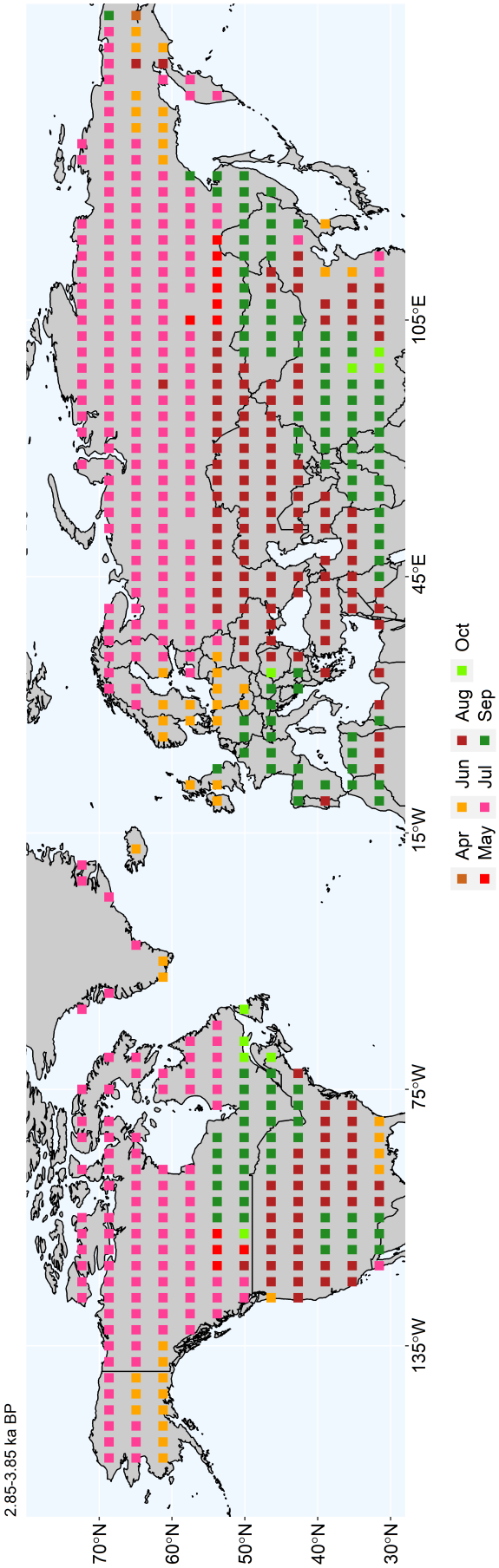

Figure A.34: Spatial distribution of the most commonly occurring months during the interval 3.85-2.85kya in which vapour pressure deficit is at a yearly maximum. The surface is generated using maximum monthly vapour pressure deficit data in which monthly values are aggregated at decadal resolution.

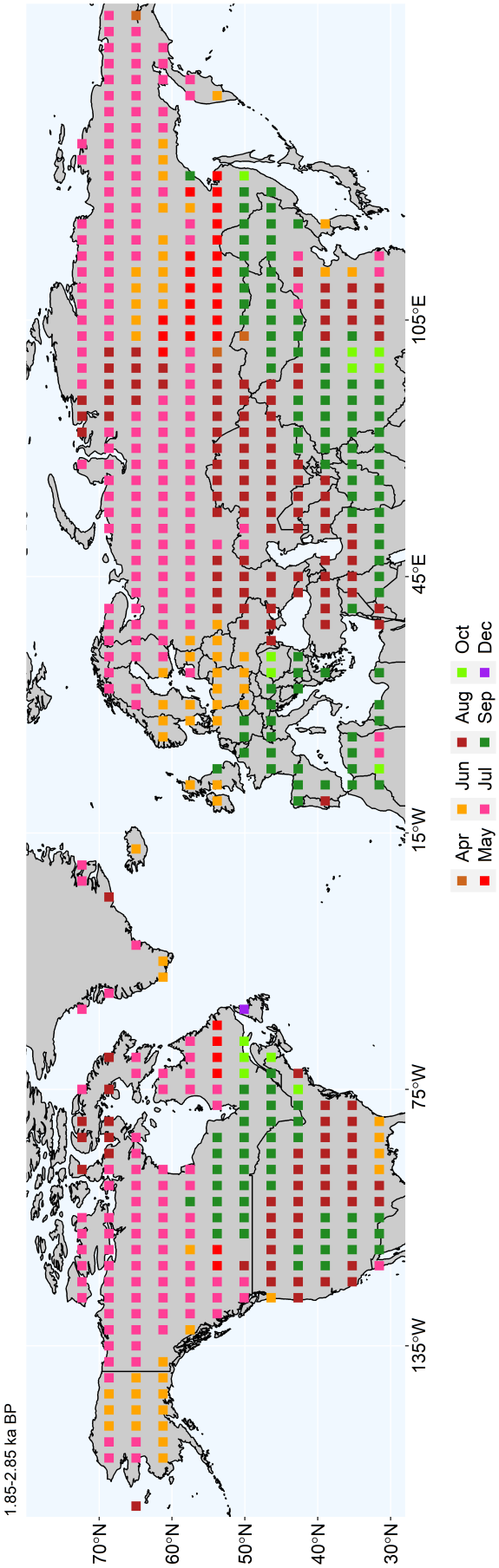

Figure A.35: Spatial distribution of the most commonly occurring months during the interval 2.85-1.85kya in which vapour pressure deficit is at a yearly maximum. The surface is generated using maximum monthly vapour pressure deficit data in which monthly values are aggregated at decadal resolution.

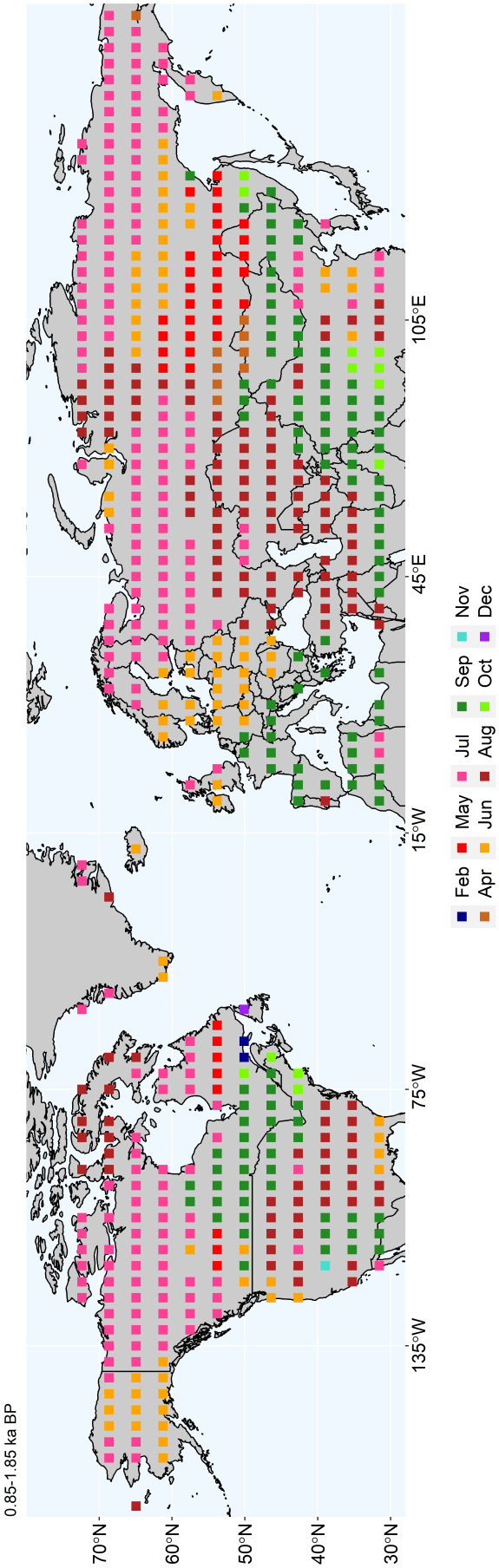

Figure A.36: Spatial distribution of the most commonly occurring months during the interval 1.85-0.85kya in which vapour pressure deficit is at a yearly maximum. The surface is generated using maximum monthly vapour pressure deficit data in which monthly values are aggregated at decadal resolution.

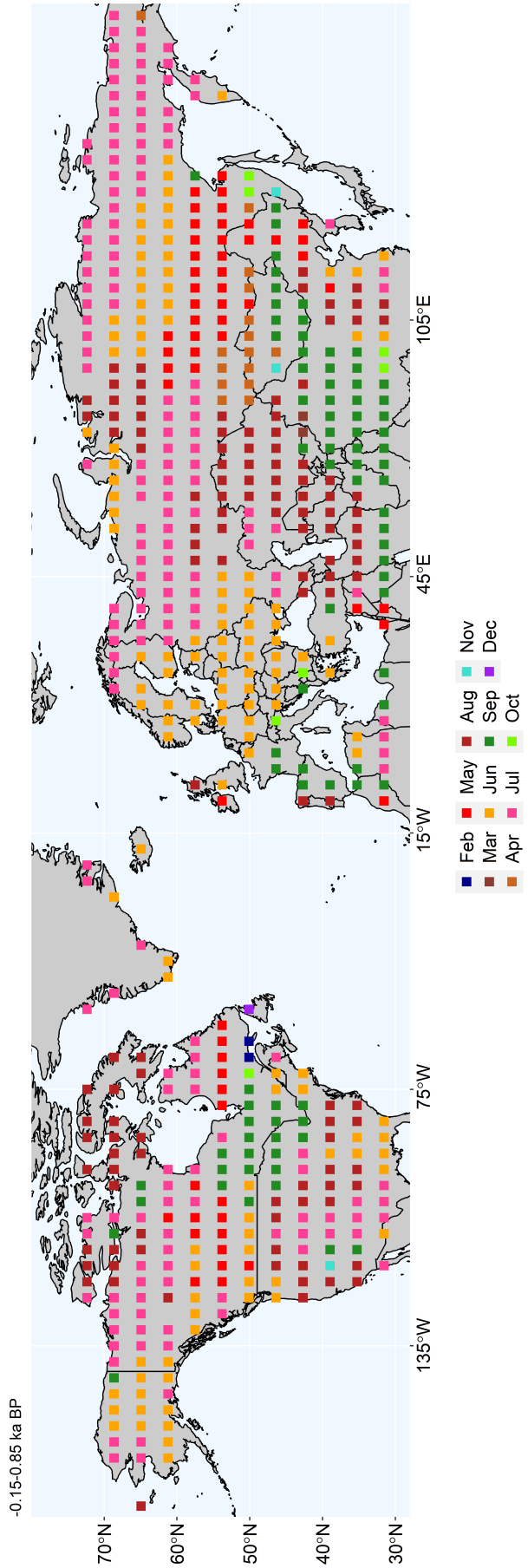

Figure A.37: Spatial distribution of the most commonly occurring months during the interval 0.85-0kya in which vapour pressure deficit is at a yearly maximum. The surface is generated using maximum monthly vapour pressure deficit data in which monthly values are aggregated at decadal resolution.

Table A.4: Correlation values for the comparisons between Eurasian and American fire responses of the same cluster from the NET-scale analysis. Correlations are rounded to the nearest second decimal value.

cluster	**time interval**	**correlation (r)**
5	12-0kya	−0.63
5	8-4kya	−0.01
5	4-0kya	−0.72
12	12-0kya	0.41
12	12-8kya	0.4
12	8-4kya	0.28
12	4-0kya	−0.36
16	12-0kya	−0.5
16	12-8kya	0.65
16	8-4kya	−0.87
16	4-0kya	−0.82

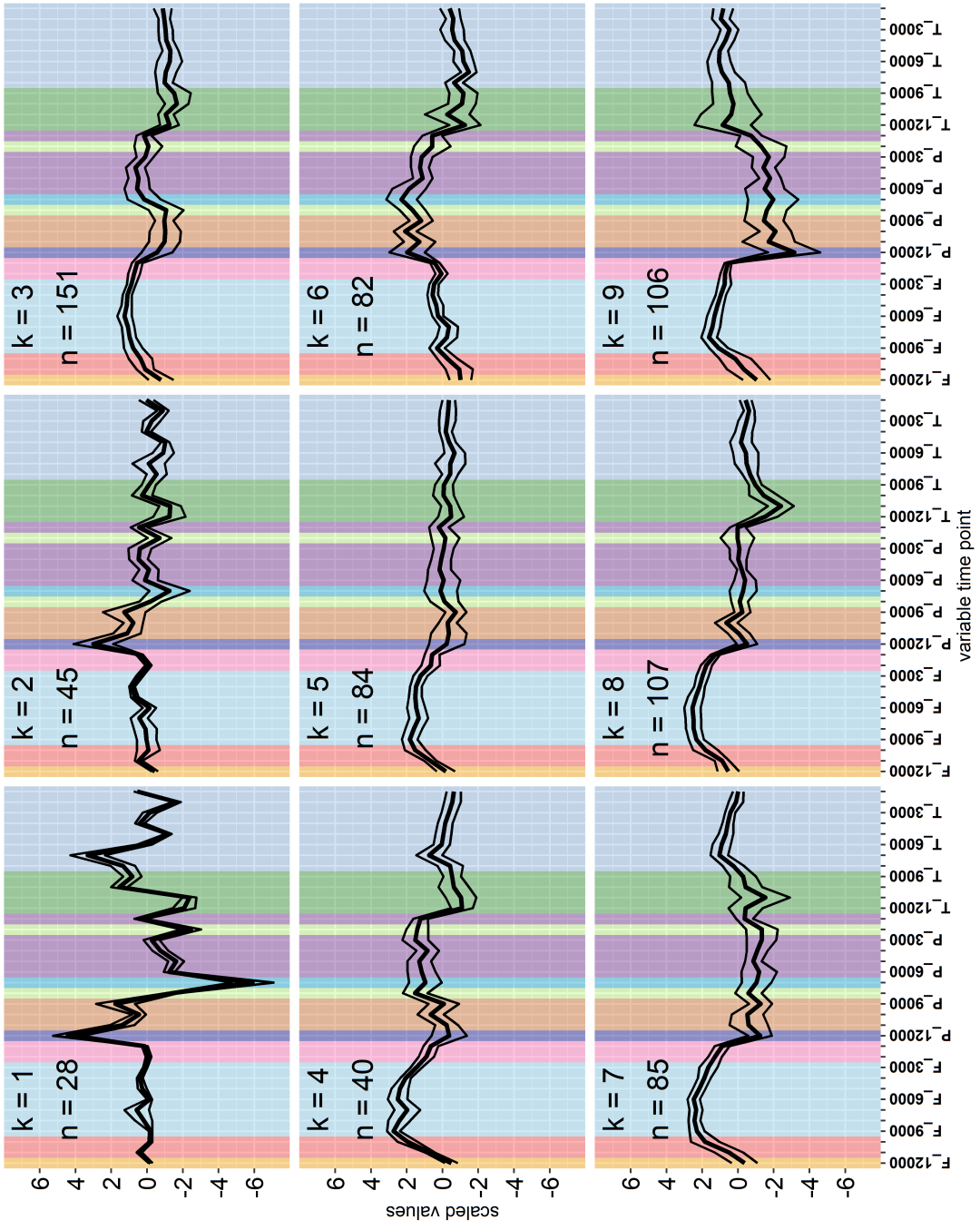

Figure A.38: Temporal patterns of the European spatial clusters 1-9. Thick black lines represent the mean across all individual grid-cell time series comprising the cluster, where each time series is a concatenation of forest cover, summer precipitation, and summer temperature time series, each of which span the period 12-0kya. Thin black lines are the standard deviations around these means. The x-axis denotes the position and time order (in years before 1950 CE) of the respective variables within the concatenated time series (F: forest cover; P: summer precipitation; T: summer temperature). Coloured vertical bars represent temporal clusters defined by the biclustering algorithm. The number of grid cells comprising the clusters (n) and the cluster identity values (k) are shown.

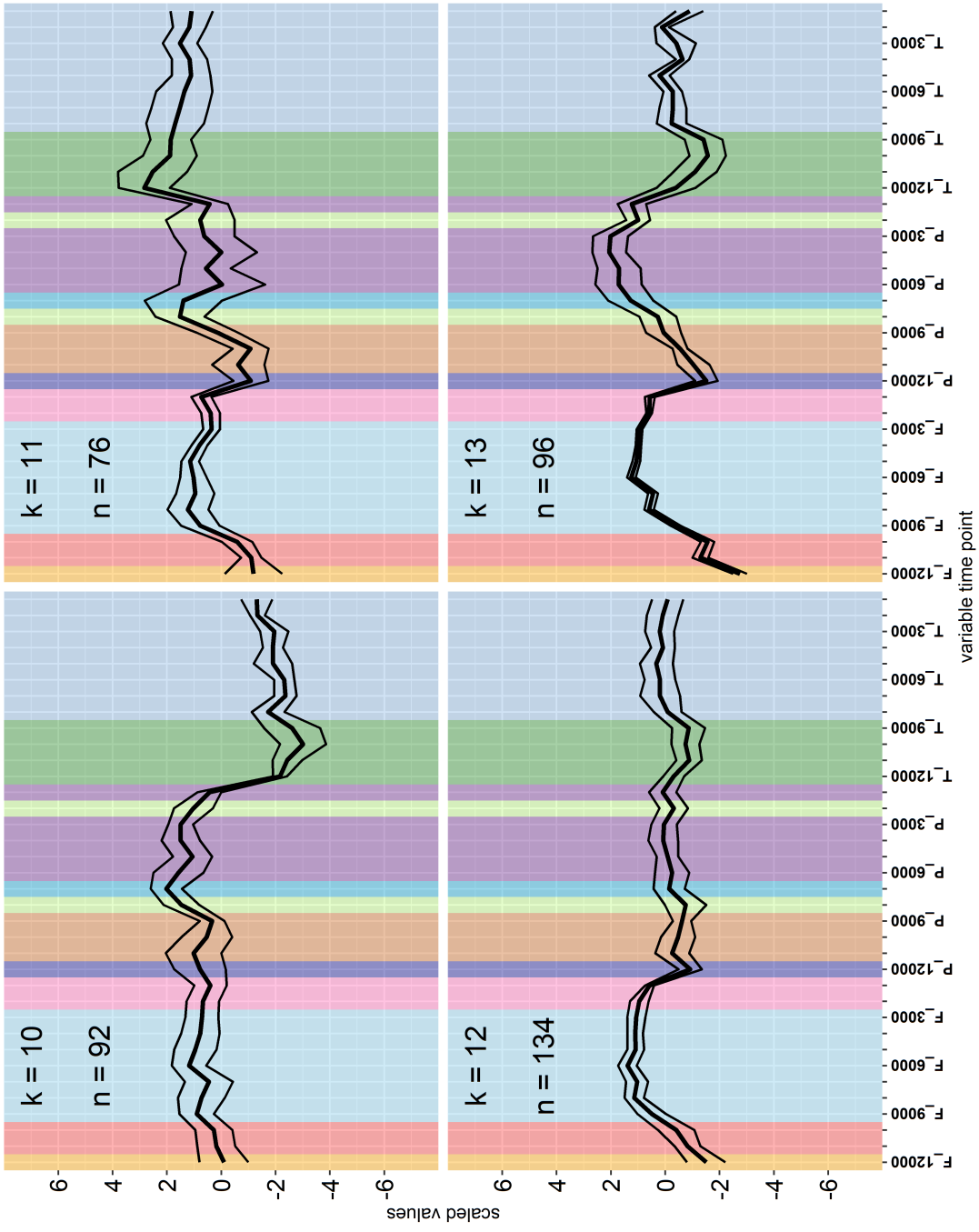

Figure A.39: Temporal patterns of the European spatial clusters 10-13. Thick black lines represent the mean across all individual grid-cell time series comprising the cluster, where each time series is a concatenation of forest cover, summer precipitation, and summer temperature time series, each of which span the period 12-0kya. Thin black lines are the standard deviations around these means. The x-axis denotes the position and time order (in years before 1950 CE) of the respective variables within the concatenated time series (F: forest cover; P: summer precipitation; T: summer temperature). Coloured vertical bars represent temporal clusters defined by the biclustering algorithm. The number of grid cells comprising the clusters (n) and the cluster identity values (k) are shown.

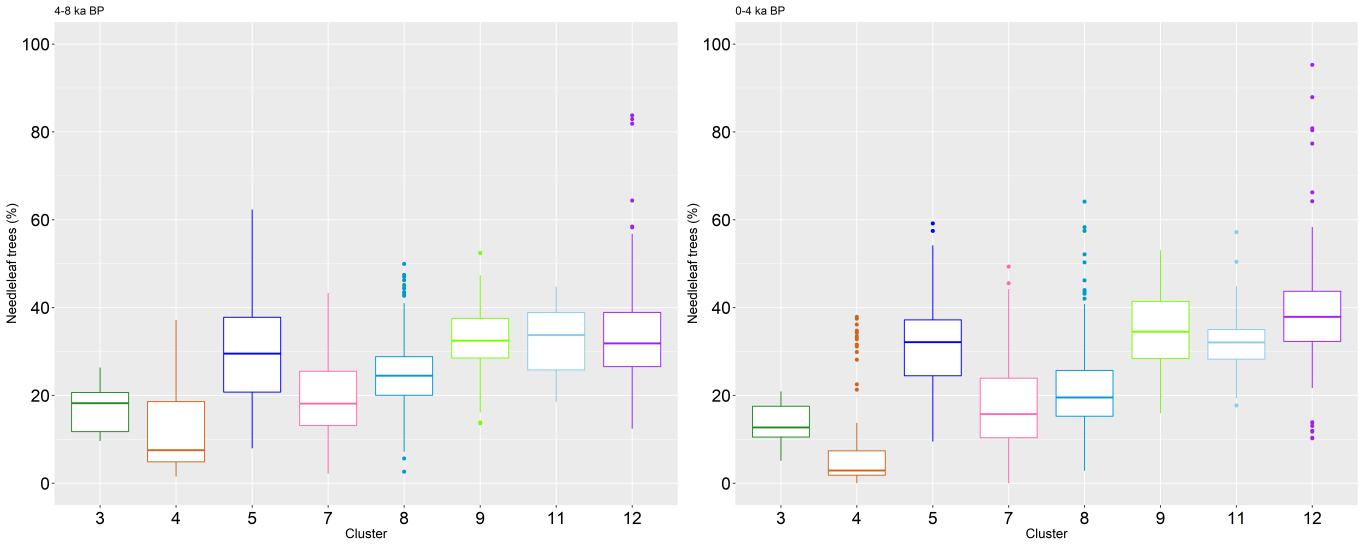

Figure A.40: Boxplots showing the distribution of needleleaf cover values used to generate the composite curves of each spatial cluster at the European scale. Left: 8-4kya interval; right: 4-0kya interval.

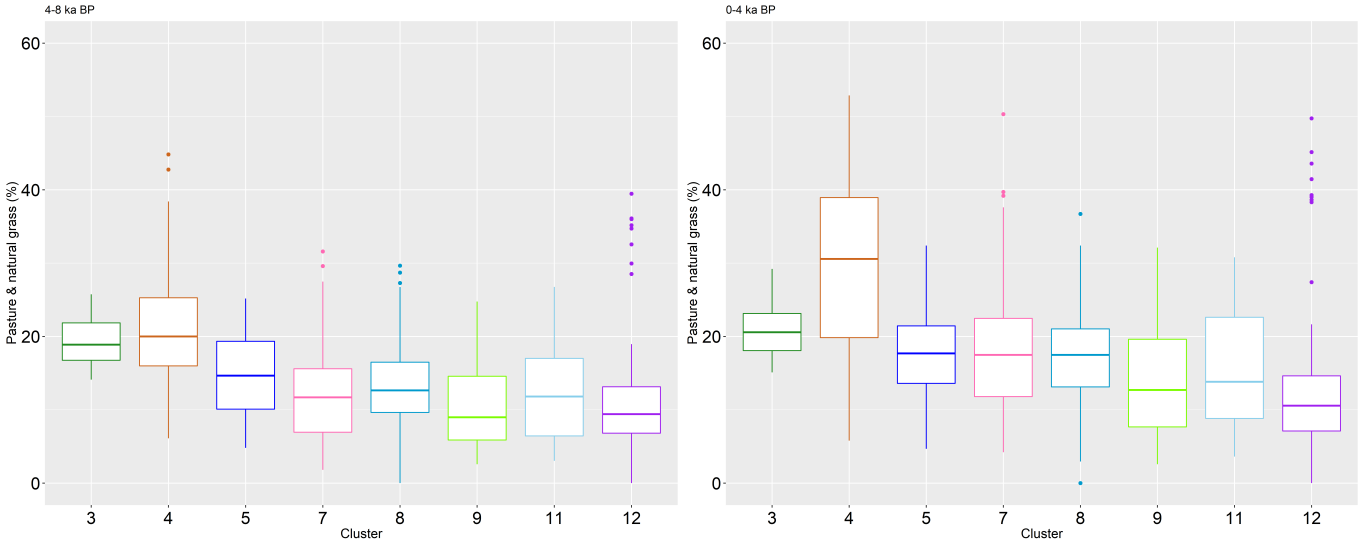

Figure A.41: Boxplots showing the distribution of pasture and natural grassland cover values used to generate the composite curves of each spatial cluster at the European scale. Left: 8-4kya interval; right: 4-0kya interval.

Table A.5: Correlation values for the fire-environment comparisons for the European-scale clusters. Correlations are generated for 4ky-intervals as well as the full time interval that each cluster spans. Correlations are rounded to the nearest second decimal value. arable: arable and disturbed land cover; broadleaf: broadleaf tree cover; forest: forest cover; heath: heath and scrubland cover; needleleaf: needleleaf tree cover; pasture: pasture and natural grassland cover; precipitation: mean summer (June-July-August) precipitation; temperature: mean summer (June-July-August) temperature.

cluster	variable correlated	time interval	correlation (r)
3	arable	12-0kya	0.62
3	arable	12-8kya	−0.09
3	arable	8-4kya	0.38
3	arable	4-0kya	0.81
3	broadleaf	12-0kya	−0.32
3	broadleaf	12-8kya	0.13
3	broadleaf	8-4kya	−0.34
3	broadleaf	4-0kya	−0.91
3	forest	12-0kya	−0.45
3	forest	12-8kya	0.4
3	forest	8-4kya	−0.25
3	forest	4-0kya	−0.82
3	heath	12-0kya	0.17
3	heath	12-8kya	−0.49
3	heath	8-4kya	0.4
3	heath	4-0kya	0.33
3	needleleaf	12-0kya	−0.66
3	needleleaf	12-8kya	−0.37
3	needleleaf	8-4kya	−0.4
3	needleleaf	4-0kya	−0.76
3	pasture	12-0kya	0.46
3	pasture	12-8kya	−0.57
3	pasture	8-4kya	0.43
3	pasture	4-0kya	0.88
3	precipitation	12-0kya	−0.09
3	precipitation	12-8kya	0.22
3	precipitation	8-4kya	−0.61
3	precipitation	4-0kya	−0.35
3	temperature	12-0kya	0.73
3	temperature	12-8kya	1
3	temperature	8-4kya	−1
3	temperature	4-0kya	0.92
4	arable	12-0kya	0.66
4	arable	12-8kya	0.36
4	arable	8-4kya	−0.36

Continued on next page.

Table A.5: Continued.

cluster	variable correlated	time interval	correlation (r)
4	arable	4-0kya	0.33
4	broadleaf	12-0kya	−0.69
4	broadleaf	12-8kya	−0.57
4	broadleaf	8-4kya	0.21
4	broadleaf	4-0kya	−0.27
4	forest	12-0kya	−0.82
4	forest	12-8kya	−0.58
4	forest	8-4kya	−0.52
4	forest	4-0kya	−0.2
4	heath	12-0kya	−0.37
4	heath	12-8kya	0.37
4	heath	8-4kya	−0.49
4	heath	4-0kya	−0.24
4	needleleaf	12-0kya	−0.16
4	needleleaf	12-8kya	−0.6
4	needleleaf	8-4kya	0.24
4	needleleaf	4-0kya	−0.46
4	pasture	12-0kya	0.75
4	pasture	12-8kya	0.58
4	pasture	8-4kya	−0.3
4	pasture	4-0kya	0.36
4	precipitation	12-0kya	0.08
4	precipitation	12-8kya	0.89
4	precipitation	8-4kya	−0.95
4	precipitation	4-0kya	−0.19
4	temperature	12-0kya	−0.02
4	temperature	12-8kya	0.13
4	temperature	8-4kya	0.38
4	temperature	4-0kya	−0.32
5	arable	12-0kya	−0.13
5	arable	12-8kya	−0.3
5	arable	8-4kya	−0.53
5	arable	4-0kya	0.8
5	broadleaf	12-0kya	−0.09
5	broadleaf	12-8kya	−0.04
5	broadleaf	8-4kya	0.04
5	broadleaf	4-0kya	−0.78
5	forest	12-0kya	−0.22
5	forest	12-8kya	−0.45

Continued on next page.

Table A.5: Continued.

cluster	variable correlated	time interval	correlation (r)
5	forest	8-4kya	0.41
5	forest	4-0kya	−0.86
5	heath	12-0kya	0.52
5	heath	12-8kya	0.52
5	heath	8-4kya	0.61
5	heath	4-0kya	0.85
5	needleleaf	12-0kya	−0.54
5	needleleaf	12-8kya	−0.62
5	needleleaf	8-4kya	−0.32
5	needleleaf	4-0kya	−0.92
5	pasture	12-0kya	0.24
5	pasture	12-8kya	0.31
5	pasture	8-4kya	0.1
5	pasture	4-0kya	0.87
5	precipitation	12-0kya	0.02
5	precipitation	12-8kya	0.1
5	precipitation	8-4kya	−0.2
5	precipitation	4-0kya	0.63
5	temperature	12-0kya	0.6
5	temperature	12-8kya	0.05
5	temperature	8-4kya	0.76
5	temperature	4-0kya	0.93
7	arable	12-0kya	0.51
7	arable	12-8kya	−0.92
7	arable	8-4kya	0.78
7	arable	4-0kya	0.97
7	broadleaf	12-0kya	−0.12
7	broadleaf	12-8kya	0.94
7	broadleaf	8-4kya	−0.88
7	broadleaf	4-0kya	−0.98
7	forest	12-0kya	−0.18
7	forest	12-8kya	0.92
7	forest	8-4kya	−0.61
7	forest	4-0kya	−0.96
7	heath	12-0kya	−0.01
7	heath	12-8kya	−0.91
7	heath	8-4kya	0.14
7	heath	4-0kya	0.99
7	needleleaf	12-0kya	−0.68

Continued on next page.

Table A.5: Continued.

cluster	variable correlated	time interval	correlation (r)
7	needleleaf	12-8kya	−0.79
7	needleleaf	8-4kya	0.94
7	needleleaf	4-0kya	0.5
7	pasture	12-0kya	0.17
7	pasture	12-8kya	−0.89
7	pasture	8-4kya	0.51
7	pasture	4-0kya	0.96
7	precipitation	12-0kya	0.4
7	precipitation	12-8kya	0.33
7	precipitation	8-4kya	0.26
7	precipitation	4-0kya	0.91
7	temperature	12-0kya	0.42
7	temperature	12-8kya	0.98
7	temperature	8-4kya	−0.74
7	temperature	4-0kya	−0.92
8	arable	12-0kya	0.33
8	arable	12-8kya	−0.49
8	arable	8-4kya	−0.74
8	arable	4-0kya	0.86
8	broadleaf	12-0kya	0
8	broadleaf	12-8kya	0.83
8	broadleaf	8-4kya	−0.09
8	broadleaf	4-0kya	−0.89
8	forest	12-0kya	0
8	forest	12-8kya	0.92
8	forest	8-4kya	0.55
8	forest	4-0kya	−0.95
8	heath	12-0kya	0.49
8	heath	12-8kya	0.61
8	heath	8-4kya	0.58
8	heath	4-0kya	0.96
8	needleleaf	12-0kya	−0.45
8	needleleaf	12-8kya	−0.9
8	needleleaf	8-4kya	0.91
8	needleleaf	4-0kya	−0.74
8	pasture	12-0kya	−0.08
8	pasture	12-8kya	−0.89
8	pasture	8-4kya	−0.62
8	pasture	4-0kya	0.92

Continued on next page.

Table A.5: Continued.

cluster	variable correlated	time interval	correlation (r)
8	precipitation	12-0kya	0.32
8	precipitation	12-8kya	0.26
8	precipitation	8-4kya	0.07
8	precipitation	4-0kya	0.16
8	temperature	12-0kya	0.38
8	temperature	12-8kya	0.84
8	temperature	8-4kya	−0.97
8	temperature	4-0kya	0.93
9	arable	12-0kya	−0.13
9	arable	12-8kya	−0.87
9	arable	8-4kya	0.64
9	arable	4-0kya	0.04
9	broadleaf	12-0kya	0.07
9	broadleaf	12-8kya	0.91
9	broadleaf	8-4kya	−0.93
9	broadleaf	4-0kya	−0.12
9	forest	12-0kya	0.46
9	forest	12-8kya	0.97
9	forest	8-4kya	−0.85
9	forest	4-0kya	0.01
9	heath	12-0kya	0.5
9	heath	12-8kya	−0.44
9	heath	8-4kya	−0.74
9	heath	4-0kya	0.14
9	needleleaf	12-0kya	−0.17
9	needleleaf	12-8kya	−0.86
9	needleleaf	8-4kya	0.88
9	needleleaf	4-0kya	0.02
9	pasture	12-0kya	−0.09
9	pasture	12-8kya	−0.96
9	pasture	8-4kya	−0.61
9	pasture	4-0kya	0.04
9	precipitation	12-0kya	0.2
9	precipitation	12-8kya	−0.86
9	precipitation	8-4kya	0.56
9	precipitation	4-0kya	−0.48
9	temperature	12-0kya	0.52
9	temperature	12-8kya	0.98
9	temperature	8-4kya	−0.86

Continued on next page.

Table A.5: Continued.

cluster	variable correlated	time interval	correlation (r)
9	temperature	4-0kya	0.93
11	arable	12-0kya	0.85
11	arable	12-8kya	−0.86
11	arable	8-4kya	0.58
11	arable	4-0kya	0.91
11	broadleaf	12-0kya	−0.95
11	broadleaf	12-8kya	−0.94
11	broadleaf	8-4kya	−0.57
11	broadleaf	4-0kya	−0.86
11	forest	12-0kya	−0.46
11	forest	12-8kya	0.87
11	forest	8-4kya	−0.85
11	forest	4-0kya	−0.33
11	heath	12-0kya	0.93
11	heath	12-8kya	0.91
11	heath	8-4kya	0.83
11	heath	4-0kya	0.6
11	needleleaf	12-0kya	−0.6
11	needleleaf	12-8kya	0.93
11	needleleaf	8-4kya	−0.75
11	needleleaf	4-0kya	−0.88
11	pasture	12-0kya	0.84
11	pasture	12-8kya	−0.95
11	pasture	8-4kya	0.81
11	pasture	4-0kya	0.83
11	precipitation	12-0kya	0.35
11	precipitation	12-8kya	0.94
11	precipitation	8-4kya	−0.67
11	precipitation	4-0kya	−0.13
11	temperature	12-0kya	−0.77
11	temperature	12-8kya	0.98
11	temperature	8-4kya	−0.63
11	temperature	4-0kya	−0.82
12	arable	12-0kya	0.77
12	arable	12-8kya	0.33
12	arable	8-4kya	−0.17
12	arable	4-0kya	0.97
12	broadleaf	12-0kya	−0.65
12	broadleaf	12-8kya	−0.26

Continued on next page.

Table A.5: Continued.

cluster	variable correlated	time interval	correlation (r)
12	broadleaf	8-4kya	0.54
12	broadleaf	4-0kya	−0.99
12	forest	12-0kya	−0.57
12	forest	12-8kya	−0.24
12	forest	8-4kya	0.28
12	forest	4-0kya	−0.98
12	heath	12-0kya	0.73
12	heath	12-8kya	0.34
12	heath	8-4kya	−0.52
12	heath	4-0kya	0.9
12	needleleaf	12-0kya	0.2
12	needleleaf	12-8kya	−0.2
12	needleleaf	8-4kya	−0.6
12	needleleaf	4-0kya	−0.49
12	pasture	12-0kya	0.35
12	pasture	12-8kya	0.2
12	pasture	8-4kya	0.5
12	pasture	4-0kya	0.84
12	precipitation	12-0kya	0.53
12	precipitation	12-8kya	−0.67
12	precipitation	8-4kya	0.13
12	precipitation	4-0kya	0.3
12	temperature	12-0kya	−0.26
12	temperature	12-8kya	−0.29
12	temperature	8-4kya	0.98
12	temperature	4-0kya	−0.88

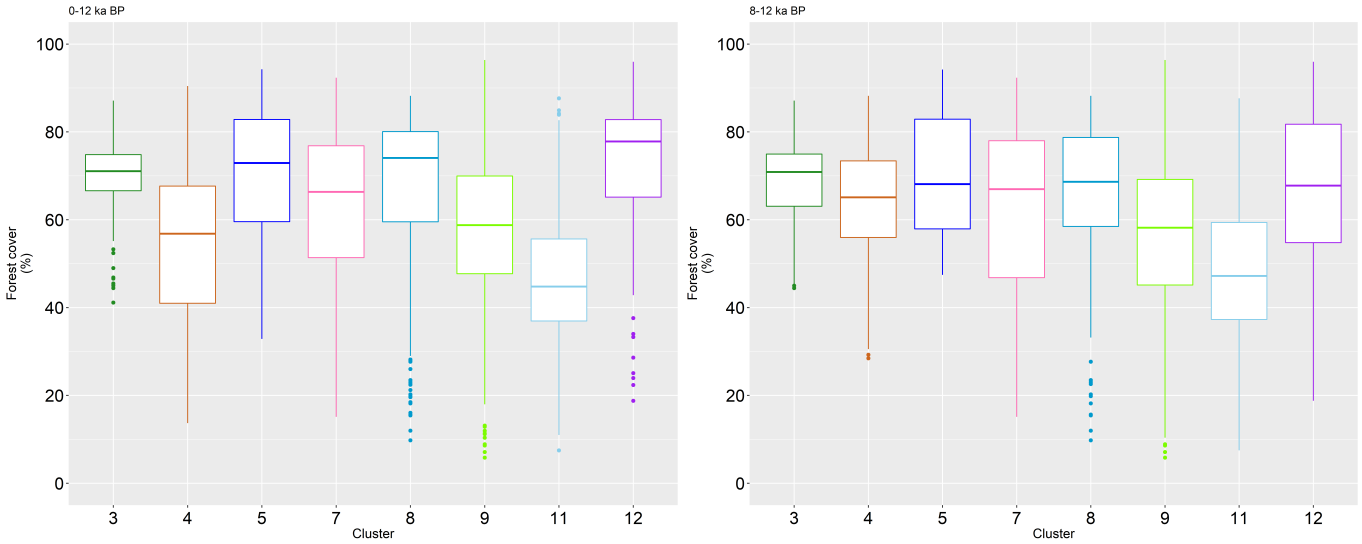

Figure A.42: Boxplots showing the distribution of forest cover values used to generate the composite curves of each spatial cluster at the European scale. Left: 12-0kya interval; right: 12-8kya interval.

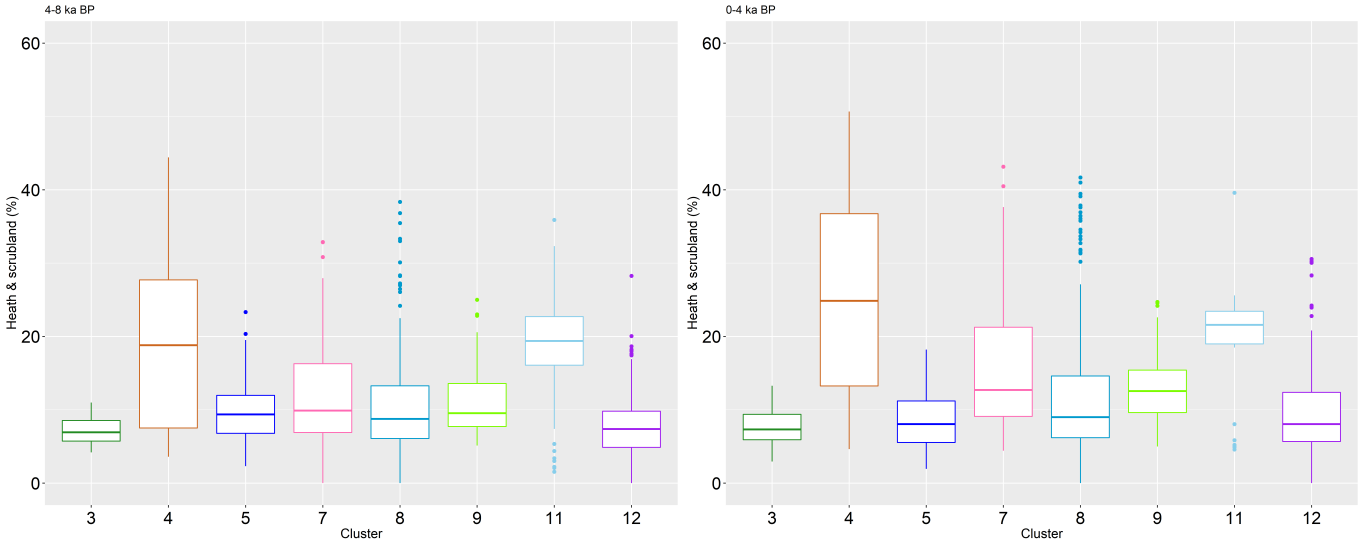

Figure A.43: Boxplots showing the distribution of heath and scrubland cover values used to generate the composite curves of each spatial cluster at the European scale. Left: 8-4kya interval; right: 4-0kya interval.

Appendix B

Supplementary Information: Methodological Validation

Since the NET-scale MI variable was derived from the TraCE-21ka dataset using unpublished methods, it was considered worthwhile to evaluate its accuracy. To do this, MI was compared to the CRU TS climatology data for an overlapping period. The CRU-adjusted TraCE-21ka MI values were averaged over the period 1960-1989 CE, and were then spatially correlated with CRU MI data that was temporally averaged over the same time interval. The RMSE between these two datasets was also measured. While these variables are expected to be correlated by design, this comparison is relevant as it provides a means of evaluating whether the method used to generate the MI data used in the biclustering is capable of reproducing observation-based MI patterns. The datasets showed strong agreement ($r = 0.998$, $p = <0.0001$; RMSE = 0.351; figures B.1, B.2).

Within the concatenated dataframe to be biclustered, the order and orientation (i.e. whether reversed or not) of the time axis of each variable may have influence on the cluster partitions. This is because the values of each variable at their most and least-recent bins differ in magnitude, creating a source of time series variation at the breakpoints among the three concatenated variables. To investigate this, an experiment was conducted where all (48) permutations of the time order and orientation of the three NET-scale variables were run through the biclustering algorithm. The resultant site-cluster partitioning of the grid cells for each permutation were compared to one permutation that was selected as a reference output. The reference clusters were matched to the 'treatment' clusters by assigning a given reference cluster the treatment cluster with the maximum proportion of grid cells in common with the reference cluster. The similarity between the matched clusters was then assessed. All clustering implementations for this experiment were run with 17 spatial and 8 temporal clusters (the number of site and time clusters are irrelevant to the experiment and only their consistency across all permutations matters).

Across all permutations, the median and mean overlap of a reference cluster with its corresponding treatment cluster was 92% and 85% respectively. These same comparisons for the overlap of a treatment cluster with its corresponding reference cluster yielded median and mean overlap percentages of 88% and 76% respectively. The minimum single reference-cluster overlap with its corresponding treatment cluster was 32% across all permutations, while this quantity for the treatment-cluster overlap with its reference cluster was 3%. Across all clusters within a given permutation, the median grid-cell reference-cluster overlap with its corresponding treatment cluster was measured. Across all

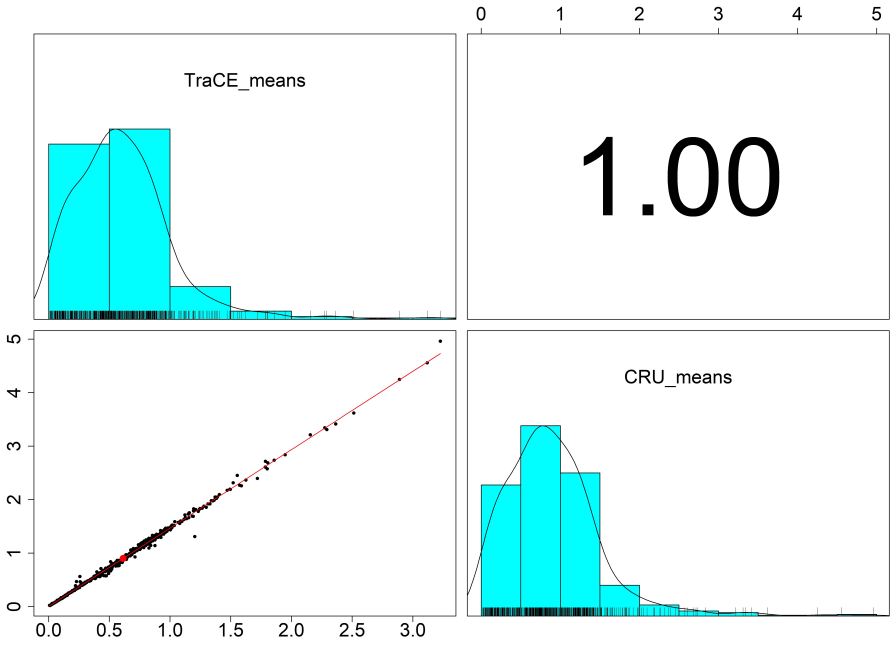

Figure B.1: Spatial correlation between mean moisture index values from the CRU TS 4.0.5 dataset [138] and CRU-adjusted TraCE-21ka data [88, 89] for the 30-75N region. Means are calculated over the period 1960-1989 CE. The correlation value is shown in the top right and is rounded to the nearest second decimal. The red curve is the line of best fit, with the red point representing the intersection of the maxima of the probability density functions of the two variables. The distributions of the CRU-adjusted TraCE-21ka and CRU TS 4.0.5 MI data are shown in the top left and bottom right respectively by histograms, probability density functions, and rug plots.

permutations, the minimum median value was 79% and the median was 92%. This same measurement of the treatment-cluster overlap with its corresponding reference cluster yielded minimum and median values of 57% and 87% respectively.

The results of this experiment suggest that there may be some degree of bias introduced by the order and orientation of the variables in the concatenated dataframe to be clustered. Nonetheless, the very high general similarity of the outputs across the different permutations suggests that regardless of this potential effect, the current biclustering method is highly likely to capture general environmental patterns relevant for palaeofires across a given spatial domain, which is the main goal of applying this clustering method in this analysis. Additionally, since there is no guarantee that 500 iterations will ensure that the biclustering algorithm converges in every case, some variance among different runs of the same permutation would be expected, hence this effect may be contributing to the dissimilarities observed between treatment and reference clusters. There is also no obvious alternative clustering method that has the advantages of the biclustering algorithm and that allows clustering of multiple variables simultaneously without concatenating the datasets.

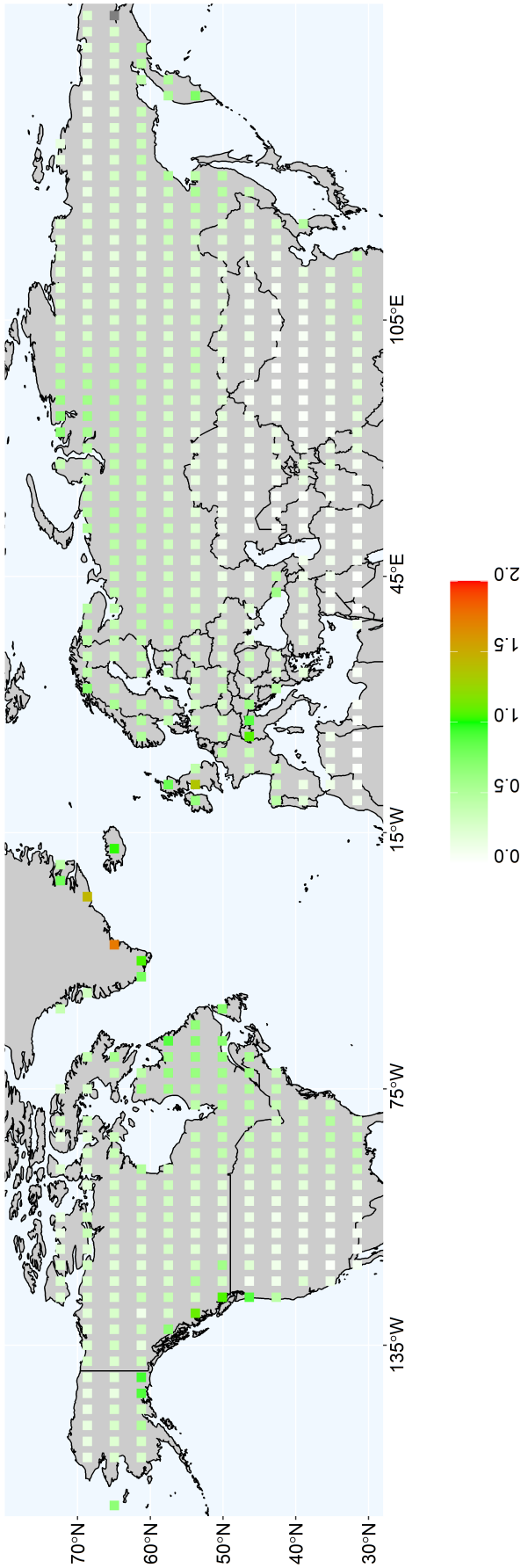

Figure B.2: Absolute differences between mean moisture index values from the CRU TS 4.0.5 dataset [138] and CRU-adjusted TraCE-21ka dataset [88, 89] for the 30-75N region. Means are calculated for the period 1960-1989 CE.

Glossary

albedo the fraction of incident electromagnetic radiation reflected by a surface

composite an aggregated time series composed of many individual time series, each of which are measured independently

fire regime the repeated patterns of fire at a particular location, characterised by a particular combination of fire characteristics such as frequency, intensity, size, seasonality, extent, spread rate, and severity of ecological destruction caused [4, 6, 190]

fire return interval the time interval between fires at any one site [6, 191]

fire weather the use of meteorological parameters such as relative humidity, wind speed and direction, mixing heights, and soil moisture to determine whether conditions are favourable for fire growth and smoke dispersion [192]

head fire intensity an indicator of fire suppression resource requirements and control difficulty [99]

insolation the amount of solar power (watts) striking the earth's surface, measured per unit area

last glacial period the period roughly 21 thousand years ago when the ice sheet extent over the northern continents was expanded relative to the present day

palaeofire wildfire that occurred prior to the modern period

paleo-calendar effect an expression for the impact that changes in the length of months or seasons over millennia, related to changes in the eccentricity of earth's orbit and precession, have on the analysis or summarisation of climate model outputs [131]

transient simulation a climate model simulation in which input variables are continuously varying over the simulated time interval in order to attempt to realistically simulate climate change

Bibliography

[1] Luke T Kelly, Katherine M Giljohann, Andrea Duane, Núria Aquilué, Sally Archibald, Enric Batllori, Andrew F Bennett, Stephen T Buckland, Quim Canelles, Michael F Clarke, et al. Fire and biodiversity in the anthropocene. *Science*, 370(6519), 2020.

[2] Guido R Van Der Werf, James T Randerson, Louis Giglio, Thijs T Van Leeuwen, Yang Chen, Brendan M Rogers, Mingquan Mu, Margreet JE Van Marle, Douglas C Morton, G James Collatz, et al. Global fire emissions estimates during 1997–2016. *Earth System Science Data*, 9(2):697–720, 2017.

[3] Gongbo Chen, Yuming Guo, Xu Yue, Shilu Tong, Antonio Gasparrini, Michelle L Bell, Ben Armstrong, Joel Schwartz, Jouni JK Jaakkola, Antonella Zanobetti, et al. Mortality risk attributable to wildfire-related pm2·5 pollution: a global time series study in 749 locations. *The Lancet Planetary Health*, 5(9):e579–e587, 2021.

[4] Sally Archibald, Caroline ER Lehmann, Claire M Belcher, William J Bond, Ross A Bradstock, Anne-Laure Daniau, Kyle G Dexter, Elisabeth J Forrestel, Michelle Greve, Tianhua He, et al. Biological and geophysical feedbacks with fire in the earth system. *Environmental Research Letters*, 13(3):033003, 2018.

[5] Juli G Pausas, Jon E Keeley, and Dylan W Schwilk. Flammability as an ecological and evolutionary driver. *Journal of Ecology*, 105(2):289–297, 2017.

[6] William J Bond and Jon E Keeley. Fire as a global 'herbivore': the ecology and evolution of flammable ecosystems. *Trends in ecology & evolution*, 20(7):387–394, 2005.

[7] Gitta Lasslop, Stijn Hantson, Sandy P Harrison, Dominique Bachelet, Chantelle Burton, Matthias Forkel, Matthew Forrest, Fang Li, Joe R Melton, Chao Yue, et al. Global ecosystems and fire: Multi-model assessment of fire-induced tree-cover and carbon storage reduction. *Global change biology*, 26(9):5027–5041, 2020.

[8] William J Bond, F Ian Woodward, and Guy F Midgley. The global distribution of ecosystems in a world without fire. *New phytologist*, 165(2):525–538, 2005.

[9] Peter S Coates, Mark A Ricca, Brian G Prochazka, Matthew L Brooks, Kevin E Doherty, Travis Kroger, Erik J Blomberg, Christian A Hagen, and Michael L Casazza. Wildfire, climate, and invasive grass interactions negatively impact an indicator species by reshaping sagebrush ecosystems. *Proceedings of the National Academy of Sciences*, 113(45):12745–12750, 2016.

[10] Max A Moritz, Marc-André Parisien, Enric Batllori, Meg A Krawchuk, Jeff Van Dorn, David J Ganz, and Katharine Hayhoe. Climate change and disruptions to global fire activity. *Ecosphere*, 3(6):1–22, 2012.

[11] Silvia Kloster and Gitta Lasslop. Historical and future fire occurrence (1850 to 2100) simulated in cmip5 earth system models. *Global and Planetary Change*, 150:58–69, 2017.

[12] Andreas Veira, Gitta Lasslop, and Silvia Kloster. Wildfires in a warmer climate: Emission fluxes, emission heights, and black carbon concentrations in 2090–2099. *Journal of Geophysical Research: Atmospheres*, 121(7):3195–3223, 2016.

[13] Douglas W Bird, Rebecca Bliege Bird, and Christopher H Parker. Aboriginal burning regimes and hunting strategies in australia's western desert. *Human ecology*, 33(4):443–464, 2005.

[14] Paul Laris. Burning the seasonal mosaic: preventative burning strategies in the wooded savanna of southern mali. *Human Ecology*, 30(2):155–186, 2002.

[15] Jia C Liu, Gavin Pereira, Sarah A Uhl, Mercedes A Bravo, and Michelle L Bell. A systematic review of the physical health impacts from non-occupational exposure to wildfire smoke. *Environmental research*, 136:120–132, 2015.

[16] Jerry Williams, Dorothy Albright, Anja A Hoffmann, Andrey Eritsov, Peter F Moore, JC Mendes De Morais, Michael Leonard, Jesus San Miguel-Ayanz, Gavriil Xanthopoulos, and P Van Lierop. Findings and implications from a coarse-scale global assessment of recent selected mega-fires. In *FAO at the Vth International Wildland Fire Conference. Sun City, South Africa*, pages 27–40, 2011.

[17] Insurance Bureau of Canada. Northern alberta wildfire costliest insured natural disaster in canadian history - estimate of insured losses: $3.58 billion. http://www.ibc.ca/bc/resources/media-centre/media-releases/northern-alberta-wildfire-costliest-insured-natural-disaster-in-canadian-history. [Online; accessed 6-February-2023].

[18] Ioannis Bistinas, Sandy P Harrison, I Colin Prentice, and Jose MC Pereira. Causal relationships versus emergent patterns in the global controls of fire frequency. *Biogeosciences*, 11(18):5087–5101, 2014.

[19] Wolfgang Knorr, Thomas Kaminski, Almut Arneth, and Ulrich Weber. Impact of human population density on fire frequency at the global scale. *Biogeosciences*, 11(4):1085–1102, 2014.

[20] Matthias Forkel, Wouter Dorigo, Gitta Lasslop, Emilio Chuvieco, Stijn Hantson, Angelika Heil, Irene Teubner, Kirsten Thonicke, and Sandy P Harrison. Recent global and regional trends in burned area and their compensating environmental controls. *Environmental Research Communications*, 1(5):051005, 2019.

[21] David MJS Bowman, Jennifer K Balch, Paulo Artaxo, William J Bond, Jean M Carlson, Mark A Cochrane, Carla M D'Antonio, Ruth S DeFries, John C Doyle, Sandy P Harrison, et al. Fire in the earth system. *Science*, 324(5926):481–484, 2009.

[22] N Phillip Cheney, James S Gould, and Wendy R Catchpole. The influence of fuel, weather and fire shape variables on fire-spread in grasslands. *International Journal of Wildland Fire*, 3(1): 31–44, 1993.

[23] Michael D Flannigan, B Mike Wotton, Ginny A Marshall, William J De Groot, Joshua M Johnston, Natasha Jurko, and Alan S Cantin. Fuel moisture sensitivity to temperature and precipitation: climate change implications. *Climatic Change*, 134(1):59–71, 2016.

[24] Anne Ganteaume, Andrea Camia, Marielle Jappiot, Jesus San-Miguel-Ayanz, Marlène Long-Fournel, and Corinne Lampin. A review of the main driving factors of forest fire ignition over europe. *Environmental management*, 51(3):651–662, 2013.

[25] Miguel G Cruz and Martin E Alexander. The 10% wind speed rule of thumb for estimating a wildfire's forward rate of spread in forests and shrublands. *Annals of Forest Science*, 76(2):1–11, 2019.

[26] Letícia Gomes, Heloisa S Miranda, Divino V Silvério, and Mercedes MC Bustamante. Effects and behaviour of experimental fires in grasslands, savannas, and forests of the brazilian cerrado. *Forest Ecology and Management*, 458:117804, 2020.

[27] Jon E Keeley and Alexandra D Syphard. Historical patterns of wildfire ignition sources in california ecosystems. *International journal of wildland fire*, 27(12):781–799, 2018.

[28] Jennifer K Balch, Bethany A Bradley, John T Abatzoglou, R Chelsea Nagy, Emily J Fusco, and Adam L Mahood. Human-started wildfires expand the fire niche across the united states. *Proceedings of the National Academy of Sciences*, 114(11):2946–2951, 2017.

[29] Niels Andela, Douglas C Morton, Louis Giglio, Yang Chen, Guido R van der Werf, Prasad S Kasibhatla, Rurth S DeFries, GJ Collatz, S Hantson, Silvia Kloster, et al. A human-driven decline in global burned area. *Science*, 356(6345):1356–1362, 2017.

[30] Jennifer R Marlon, Patrick J Bartlein, Christopher Carcaillet, Daniel G Gavin, Sandy P Harrison, Philip E Higuera, Fortunat Joos, Mitchell J Power, and I Colin Prentice. Climate and human influences on global biomass burning over the past two millennia. *Nature Geoscience*, 1 (10):697–702, 2008.

[31] Alex F Bouwman, Tom Kram, and Kees Klein Goldewijk. Integrated modelling of global environmental change. *An overview of IMAGE*, 2(4):225–228, 2006.

[32] Kees Klein Goldewijk, Arthur Beusen, Jonathan Doelman, and Elke Stehfest. Anthropogenic land use estimates for the holocene–hyde 3.2. *Earth System Science Data*, 9(2):927–953, 2017.

[33] Moinuddin Ahmed, Kevin J Anchukaitis, Asfawossen Asrat, Hemant P Borgaonkar, Martina Braida, Brendan M Buckley, Ulf Büntgen, Brian M Chase, Duncan A Christie, Edward R Cook, et al. Continental-scale temperature variability during the past two millennia. *Nature geoscience*, 6(5):339–346, 2013.

[34] Michael E Mann, Zhihua Zhang, Scott Rutherford, Raymond S Bradley, Malcolm K Hughes, Drew Shindell, Caspar Ammann, Greg Faluvegi, and Fenbiao Ni. Global signatures and dynamical origins of the little ice age and medieval climate anomaly. *Science*, 326(5957):1256–1260, 2009.

[35] Matthias Forkel, Niels Andela, Sandy P Harrison, Gitta Lasslop, Margreet van Marle, Emilio Chuvieco, Wouter Dorigo, Matthew Forrest, Stijn Hantson, Angelika Heil, et al. Emergent relationships with respect to burned area in global satellite observations and fire-enabled vegetation models. *Biogeosciences*, 16(1):57–76, 2019.

[36] Guido R Van Der Werf, James T Randerson, Louis Giglio, Nadine Gobron, and AJ Dolman. Climate controls on the variability of fires in the tropics and subtropics. *Global Biogeochemical Cycles*, 22(3), 2008.

[37] Juli G Pausas and Eloi Ribeiro. The global fire–productivity relationship. *Global Ecology and Biogeography*, 22(6):728–736, 2013.

[38] Steven G Cumming. Forest type and wildfire in the alberta boreal mixedwood: what do fires burn? *Ecological applications*, 11(1):97–110, 2001.

[39] Juli G Pausas. Evolutionary fire ecology: lessons learned from pines. *Trends in Plant Science*, 20(5):318–324, 2015.

[40] Victor Brovkin, Peter M Van Bodegom, Thomas Kleinen, Christian Wirth, Will K Cornwell, J Hans C Cornelissen, and Jens Kattge. Plant-driven variation in decomposition rates improves projections of global litter stock distribution. *Biogeosciences*, 9(1):565–576, 2012.

[41] Brendan M Rogers, Amber J Soja, Michael L Goulden, and James T Randerson. Influence of tree species on continental differences in boreal fires and climate feedbacks. *Nature Geoscience*, 8(3):228–234, 2015.

[42] Dylan W Schwilk and David D Ackerly. Flammability and serotiny as strategies: correlated evolution in pines. *Oikos*, 94(2):326–336, 2001.

[43] Tianhua He, Juli G Pausas, Claire M Belcher, Dylan W Schwilk, and Byron B Lamont. Fire-adapted traits of pinus arose in the fiery cretaceous. *New Phytologist*, 194(3):751–759, 2012.

[44] Juli G Pausas. Bark thickness and fire regime. *Functional Ecology*, 29(3):315–327, 2015.

[45] Jon E Keeley. Ecology and evolution of pine life histories. *Annals of Forest Science*, 69(4): 445–453, 2012.

[46] John W Williams, Bryan N Shuman, Thompson Webb III, Patrick J Bartlein, and Phillip L Leduc. Late-quaternary vegetation dynamics in north america: Scaling from taxa to biomes. *Ecological Monographs*, 74(2):309–334, 2004.

[47] Jill Johnstone, Leslie Boby, Emily Tissier, Michelle Mack, Dave Verbyla, and Xanthe Walker. Postfire seed rain of black spruce, a semiserotinous conifer, in forests of interior alaska. *Canadian Journal of Forest Research*, 39(8):1575–1588, 2009.

[48] Pierre Y Bernier, Sylvie Gauthier, Pierre-Olivier Jean, Francis Manka, Yan Boulanger, André Beaudoin, and Luc Guindon. Mapping local effects of forest properties on fire risk across canada. *Forests*, 7(8):157, 2016.

[49] Sandy P Harrison, I Colin Prentice, Keith J Bloomfield, Ning Dong, Matthias Forkel, Matthew Forrest, Ramesh K Ningthoujam, Adam Pellegrini, Yicheng Shen, Mara Baudena, et al. Understanding and modelling wildfire regimes: an ecological perspective. *Environmental Research Letters*, 16(12):125008, 2021.

[50] Sandy P Harrison, Patrick J Bartlein, Victor Brovkin, Sander Houweling, Silvia Kloster, and I Colin Prentice. The biomass burning contribution to climate–carbon-cycle feedback. *Earth System Dynamics*, 9(2):663–677, 2018.

[51] Ryan Kelly, Melissa L Chipman, Philip E Higuera, Ivanka Stefanova, Linda B Brubaker, and Feng Sheng Hu. Recent burning of boreal forests exceeds fire regime limits of the past 10,000 years. *Proceedings of the National Academy of Sciences*, 110(32):13055–13060, 2013.

[52] Sandy P Harrison and Patrick J Bartlein. *The Future of the World's Climate*, chapter Records from the past, lessons for the future: what the palaeorecord implies about mechanisms of global change, pages 403–436. Elsevier, Amsterdam, 2012.

[53] André Berger and Marie-France Loutre. Insolation values for the climate of the last 10 million years. *Quaternary Science Reviews*, 10(4):297–317, 1991.

[54] William R Peltier and Richard G Fairbanks. Global glacial ice volume and last glacial maximum duration from an extended barbados sea level record. *Quaternary Science Reviews*, 25(23-24): 3322–3337, 2006.

[55] Donald K Perovich, Bonnie Light, Hajo Eicken, Kathleen F Jones, Kay Runciman, and Son V Nghiem. Increasing solar heating of the arctic ocean and adjacent seas, 1979–2005: Attribution and role in the ice-albedo feedback. *Geophysical Research Letters*, 34(19), 2007.

[56] Tao He, Shunlin Liang, Yunyue Yu, Dongdong Wang, Feng Gao, and Qiang Liu. Greenland surface albedo changes in july 1981–2012 from satellite observations. *Environmental Research Letters*, 8(4):044043, 2013.

[57] Jason E Box, Dirk Van As, and Konrad Steffen. Greenland, canadian and icelandic land-ice albedo grids (2000–2016). *GEUS Bulletin*, 38:53–56, 2017.

[58] Jean-Marc Barnola, DYSN Raynaud, Yevgeniy S Korotkevich, and Claude Lorius. Vostok ice core provides 160,000-year record of atmospheric co_2. *Nature*, 329(6138):408–414, 1987.

[59] Jean Jouzel, Valérie Masson-Delmotte, Olivier Cattani, Gabrielle Dreyfus, Sonia Falourd, Georg Hoffmann, Benedicte Minster, Julius Nouet, Jean-Marc Barnola, Jérôme Chappellaz, et al. Orbital and millennial antarctic climate variability over the past 800,000 years. *Science*, 317 (5839):793–796, 2007.

[60] Gunnar Myhre, Eleanor J Highwood, Keith P Shine, and Frode Stordal. New estimates of radiative forcing due to well mixed greenhouse gases. *Geophysical research letters*, 25(14):2715–2718, 1998.

[61] Douglas G Martinson, Nicklas G Pisias, James D Hays, John Imbrie, Theodore C Moore, and Nicholas J Shackleton. Age dating and the orbital theory of the ice ages: Development of a high-resolution 0 to 300,000-year chronostratigraphy$_1$. *Quaternary research*, 27(1):1–29, 1987.

[62] Gerard C Bond and Rusty Lotti. Iceberg discharges into the north atlantic on millennial time scales during the last glaciation. *Science*, 267(5200):1005–1010, 1995.

[63] Peter U Clark, Shawn J Marshall, Garry KC Clarke, Steven W Hostetler, Joseph M Licciardi, and James T Teller. Freshwater forcing of abrupt climate change during the last glaciation. *Science*, 293(5528):283–287, 2001.

[64] Ian R Hall, S. B Moran, Rainer Zahn, Paul C Knutz, Chuan-Chou Shen, and RL Edwards. Accelerated drawdown of meridional overturning in the late-glacial atlantic triggered by transient pre-h event freshwater perturbation. *Geophysical Research Letters*, 33(16), 2006.

[65] Sophia KV Hines, John M Eiler, John R Southon, and Jess F Adkins. Dynamic intermediate waters across the late glacial revealed by paired radiocarbon and clumped isotope temperature records. *Paleoceanography and Paleoclimatology*, 34(7):1074–1091, 2019.

[66] Jerry F McManus, Roger Francois, J-M Gherardi, Lloyd D Keigwin, and Susan Brown-Leger. Collapse and rapid resumption of atlantic meridional circulation linked to deglacial climate changes. *Nature*, 428(6985):834–837, 2004.

[67] Jennifer D Stanford, Eelco J Rohling, Sheldon Bacon, Andrew P Roberts, Francis E Grousset, and Mike Bolshaw. A new concept for the paleoceanographic evolution of heinrich event 1 in the north atlantic. *Quaternary Science Reviews*, 30(9-10):1047–1066, 2011.

[68] Maria AA Rugenstein, Michael Winton, Ronald J Stouffer, Stephen M Griffies, and Robert Hallberg. Northern high-latitude heat budget decomposition and transient warming. *Journal of climate*, 26(2):609–621, 2013.

[69] Nivedita Thiagarajan, Adam V Subhas, John R Southon, John M Eiler, and Jess F Adkins. Abrupt pre-bølling–allerød warming and circulation changes in the deep ocean. *Nature*, 511 (7507):75–78, 2014.

[70] Maria Martin Calvo and I Colin Prentice. Effects of fire and co$_2$ on biogeography and primary production in glacial and modern climates. *New Phytologist*, 208(3):987–994, 2015.

[71] I Colin Prentice, Dominique Jolly, and Biome 6000 Participants. Mid-holocene and glacial-maximum vegetation geography of the northern continents and africa. *Journal of biogeography*, 27(3):507–519, 2000.

[72] Heather Binney, Mary Edwards, Marc Macias-Fauria, Anatoly Lozhkin, Patricia Anderson, Jed O Kaplan, Andrei Andreev, Elena Bezrukova, Tatiana Blyakharchuk, Vlasta Jankovska,

et al. Vegetation of eurasia from the last glacial maximum to present: Key biogeographic patterns. *Quaternary Science Reviews*, 157:80–97, 2017.

[73] Dominic F Ferretti, John B Miller, James WC White, David M Etheridge, Keith R Lassey, David C Lowe, Cecelia M MacFarling, Mark F Dreier, Cathy M Trudinger, Tas D Van Ommen, et al. Unexpected changes to the global methane budget over the past 2000 years. *Science*, 309 (5741):1714–1717, 2005.

[74] Zhihui Wang, Jerome Chappellaz, Key H Park, and John E Mak. Large variations in southern hemisphere biomass burning during the last 650 years. *Science*, 330(6011):1663–1666, 2010.

[75] Piero Zennaro, Natalie Kehrwald, Jennifer Marlon, William F Ruddiman, Tim Brücher, Claudio Agostinelli, Dorthe Dahl-Jensen, Roberta Zangrando, Andrea Gambaro, and Carlo Barbante. Europe on fire three thousand years ago: Arson or climate? *Geophysical Research Letters*, 42 (12):5023–2033, 2015.

[76] Joseph R McConnell, Ross Edwards, Gregory L Kok, Mark G Flanner, Charles S Zender, Eric S Saltzman, J Ryan Banta, Daniel R Pasteris, Megan M Carter, and Jonathan DW Kahl. 20th-century industrial black carbon emissions altered arctic climate forcing. *Science*, 317(5843): 1381–1384, 2007.

[77] Jennifer R Marlon, Patrick J Bartlein, Daniel G Gavin, Colin J Long, R. Scott Anderson, Christy E Briles, Kendrick J Brown, Daniele Colombaroli, Douglas J Hallett, Mitchell J Power, et al. Long-term perspective on wildfires in the western usa. *Proceedings of the National Academy of Sciences*, 109(9):E535–E543, 2012.

[78] Jennifer R Marlon, Ryan Kelly, Anne-Laure Daniau, Boris Vannière, Mitchell J Power, Patrick Bartlein, Philip Higuera, Olivier Blarquez, Simon Brewer, Tim Brücher, et al. Reconstructions of biomass burning from sediment-charcoal records to improve data–model comparisons. *Biogeosciences*, 13(11):3225–3244, 2016.

[79] David J Griggs and Maria Noguer. Climate change 2001: the scientific basis. contribution of working group i to the third assessment report of the intergovernmental panel on climate change. *Weather*, 57(8):267–269, 2002.

[80] Lana D Laird and Ian D Campbell. High resolution palaeofire signals from christina lake, alberta: a comparison of the charcoal signals extracted by two different methods. *Palaeogeography, Palaeoclimatology, Palaeoecology*, 164(1-4):111–123, 2000.

[81] France Oris, Adam A Ali, Hugo Asselin, Laure Paradis, Yves Bergeron, and Walter Finsinger. Charcoal dispersion and deposition in boreal lakes from 3 years of monitoring: Differences between local and regional fires. *Geophysical Research Letters*, 41(19):6743–6752, 2014.

[82] Mikael Ohlson, Auen Korbøl, and Rune H Økland. The macroscopic charcoal record in forested boreal peatlands in southeast norway. *The Holocene*, 16(5):731–741, 2006.

[83] Mikael Ohlson and Elling Tryterud. Interpretation of the charcoal record in forest soils: forest fires and their production and deposition of macroscopic charcoal. *The Holocene*, 10(4):519–525, 2000.

[84] Willy Tinner, Marco Conedera, Brigitta Ammann, Heinz W Gaggeler, Sharon Gedye, Richard Jones, and Beat Sagesser. Pollen and charcoal in lake sediments compared with historically documented forest fires in southern switzerland since ad 1920. *The Holocene*, 8(1):31–42, 1998.

[85] Philip E Higuera, Cathy Whitlock, and Josh A Gage. Linking tree-ring and sediment-charcoal records to reconstruct fire occurrence and area burned in subalpine forests of yellowstone national park, usa. *The Holocene*, 21(2):327–341, 2011.

[86] Mitchell J Power, Jennifer R Marlon, Natalie Ortiz, Patrick J Bartlein, Sandy P Harrison, Francis E Mayle, Aziz Ballouche, Richard HW Bradshaw, Christopher Carcaillet, Carlos E Cordova, et al. Changes in fire regimes since the last glacial maximum: an assessment based on a global synthesis and analysis of charcoal data. *Climate dynamics*, 30(7-8):887–907, 2008.

[87] Anne-Laure Daniau, Patrick J Bartlein, Sandy P Harrison, I Colin Prentice, Scott Brewer, Pierre Friedlingstein, Thomas I Harrison-Prentice, Jun Inoue, Kiwamu Izumi, Jennifer R Marlon, et al. Predictability of biomass burning in response to climate changes. *Global Biogeochemical Cycles*, 26(4), 2012.

[88] Feng He. *Simulating transient climate evolution of the last deglaciation with CCSM 3*. PhD thesis, Univ. Wisconsin-Madison, 2011.

[89] Zhengyu Liu, Bette L Otto-Bliesner, Feng He, Esther C Brady, Robert Tomas, Peter U Clark, Anders E Carlson, Jean Lynch-Stieglitz, William Curry, Edward Brook, et al. Transient simulation of last deglaciation with a new mechanism for bølling-allerød warming. *Science*, 325(5938): 310–314, 2009.

[90] Kendrick J Brown and Richard J Hebda. Ancient fires on southern vancouver island, british columbia, canada: a change in causal mechanisms at about 2,000 ybp. *Environmental Archaeology*, 7(1):1–12, 2002.

[91] Willy Tinner, Priska Hubschmid, Michael Wehrli, Brigitta Ammann, and Marco Conedera. Long-term forest fire ecology and dynamics in southern switzerland. *Journal of Ecology*, 87(2): 273–289, 1999.

[92] Aki Pitkänen, Pertti Huttunen, Högne Jungner, and Kimmo Tolonen. A 10 000 year local forest fire history in a dry heath forest site in eastern finland, reconstructed from charcoal layer records of a small mire. *Canadian Journal of Forest Research*, 32(10):1875–1880, 2002.

[93] Christoper Carcaillet, Heather Almquist, Hans Asnong, Richard HW Bradshaw, Jose S Carrion, Marie-Jose Gaillard, Konrad Gajewski, Jean N Haas, Simon G Haberle, Philippe Hadorn, et al. Holocene biomass burning and global dynamics of the carbon cycle. *Chemosphere*, 49(8):845–863, 2002.

[94] Jennifer R Marlon, Patrick J Bartlein, Anne-Laure Daniau, Sandy P Harrison, Shira Y Maezumi, Mitchell J Power, Willy Tinner, and Boris Vanniére. Global biomass burning: a synthesis and review of holocene paleofire records and their controls. *Quaternary Science Reviews*, 65:5–25, 2013.

[95] Alan N Williams, Scott D Mooney, Scott A Sisson, and Jennifer Marlon. Exploring the relationship between aboriginal population indices and fire in australia over the last 20,000 years. *Palaeogeography, Palaeoclimatology, Palaeoecology*, 432:49–57, 2015.

[96] Yude Pan, Richard A Birdsey, Jingyun Fang, Richard Houghton, Pekka E Kauppi, Werner A Kurz, Oliver L Phillips, Anatoly Shvidenko, Simon L Lewis, Josep G Canadell, et al. A large and persistent carbon sink in the world's forests. *Science*, 333(6045):988–993, 2011.

[97] Merritt R Turetsky, Evan S Kane, Jennifer W Harden, Roger D Ottmar, Kristen L Manies, Elizabeth Hoy, and Eric S Kasischke. Recent acceleration of biomass burning and carbon losses in alaskan forests and peatlands. *Nature Geoscience*, 4(1):27–31, 2011.

[98] Xanthe J Walker, Jennifer L Baltzer, Steven G Cumming, Nicola J Day, Christopher Ebert, Scott Goetz, Jill F Johnstone, Stefano Potter, Brendan M Rogers, Edward AG Schuur, et al. Increasing wildfires threaten historic carbon sink of boreal forest soils. *Nature*, 572(7770):520–523, 2019.

[99] William J de Groot, Michael D Flannigan, and Alan S Cantin. Climate change impacts on future boreal fire regimes. *Forest Ecology and Management*, 294:35–44, 2013.

[100] Jeremiah Marsicek, Bryan N Shuman, Patrick J Bartlein, Sarah L Shafer, and Simon Brewer. Reconciling divergent trends and millennial variations in holocene temperatures. *Nature*, 554 (7690):92–96, 2018.

[101] Ralph M Fyfe, Jessie Woodbridge, and Neil Roberts. From forest to farmland: pollen-inferred land cover change across europe using the pseudobiomization approach. *Global Change Biology*, 21(3):1197–1212, 2015.

[102] David J Ullman, Anders E Carlson, Steven W Hostetler, Peter U Clark, Joshua Cuzzone, Glenn A Milne, Kelsey Winsor, and Marc Caffee. Final laurentide ice-sheet deglaciation and holocene climate-sea level change. *Quaternary Science Reviews*, 152:49–59, 2016.

[103] Andre E Viau, Konrad Gajewski, Michael C Sawada, and Philippe Fines. Millennial-scale temperature variations in north america during the holocene. *Journal of Geophysical Research: Atmospheres*, 111(D9), 2006.

[104] Bryan N Shuman and Jeremiah Marsicek. The structure of holocene climate change in mid-latitude north america. *Quaternary Science Reviews*, 141:38–51, 2016.

[105] Achille Mauri, Basil AS Davis, Pamela M Collins, and Jed O Kaplan. The climate of europe during the holocene: a gridded pollen-based reconstruction and its multi-proxy evaluation. *Quaternary Science Reviews*, 112:109–127, 2015.

[106] Patrick J Bartlein, Sandy P Harrison, Sandra Brewer, Simon Connor, Basil AS Davis, Konrad Gajewski, Joel Guiot, Thomas I Harrison-Prentice, Anna Henderson, Odile Peyron, et al. Pollen-based continental climate reconstructions at 6 and 21 ka: a global synthesis. *Climate Dynamics*, 37(3):775–802, 2011.

[107] John D Jansen, Alexandru T Codilean, Arjen P Stroeven, Derek Fabel, Clas Hättestrand, Johan Kleman, Jon M Harbor, Jakob Heyman, Peter W Kubik, and S Xu. Inner gorges cut by subglacial meltwater during fennoscandian ice sheet decay. *Nature communications*, 5(1):1–7, 2014.

[108] James W Hurrell. Decadal trends in the north atlantic oscillation: Regional temperatures and precipitation. *Science*, 269(5224):676–679, 1995.

[109] Hylke E Beck, Niklaus E Zimmermann, Tim R McVicar, Noemi Vergopolan, Alexis Berg, and Eric F Wood. Present and future köppen-geiger climate classification maps at 1-km resolution. *Scientific data*, 5(1):1–12, 2018.

[110] Sebastian FM Breitenbach, Birgit Plessen, Sarah Waltgenbach, Rik Tjallingii, Jens Leonhardt, Klaus Peter Jochum, Hanno Meyer, Bedartha Goswami, Norbert Marwan, and Denis Scholz. Holocene interaction of maritime and continental climate in central europe: New speleothem evidence from central germany. *Global and Planetary Change*, 176:144–161, 2019.

[111] Thomas Giesecke, Simon Brewer, Walter Finsinger, Michelle Leydet, and Richard HW Bradshaw. Patterns and dynamics of european vegetation change over the last 15,000 years. *Journal of Biogeography*, 44(7):1441–1456, 2017.

[112] Elizabeth A Scharf. A statistical evaluation of the relative influences of climate, vegetation, and prehistoric human population on the charcoal record of five lakes, washington (usa). *Quaternary International*, 215(1-2):74–86, 2010.

[113] Neil Roberts, Ralph M Fyfe, Jessie Woodbridge, M-J Gaillard, Basil AS Davis, Jed O Kaplan, Laurent Marquer, Florence Mazier, Anne Brigitte Nielsen, Shinya Sugita, et al. Europe's lost forests: a pollen-based synthesis for the last 11,000 years. *Scientific reports*, 8(1):1–8, 2018.

[114] Eva Valese, Marco Conedera, Alexander C Held, and Davide Ascoli. Fire, humans and landscape in the european alpine region during the holocene. *Anthropocene*, 6:63–74, 2014.

[115] Juli G Pausas and Jon E Keeley. A burning story: the role of fire in the history of life. *BioScience*, 59(7):593–601, 2009.

[116] Angelica Feurdean, Boris Vannière, Walter Finsinger, Dan Warren, Simon C Connor, Matthew Forrest, Johan Liakka, Andrei Panait, Christian Werner, Maja Andrič, et al. Fire hazard modulation by long-term dynamics in land cover and dominant forest type in eastern and central europe. *Biogeosciences*, 17(5):1213–1230, 2020.

[117] Angelica Feurdean, Siim Veski, Gabriela Florescu, Boris Vannière, Mirjam Pfeiffer, Robert B O'Hara, Normunds Stivrins, Leeli Amon, Atko Heinsalu, Jüri Vassiljev, et al. Broadleaf deciduous forest counterbalanced the direct effect of climate on holocene fire regime in hemiboreal/boreal region (ne europe). *Quaternary Science Reviews*, 169:378–390, 2017.

[118] Philip E Higuera, Linda B Brubaker, Patricia M Anderson, Feng Sheng Hu, and Thomas A Brown. Vegetation mediated the impacts of postglacial climate change on fire regimes in the south-central brooks range, alaska. *Ecological Monographs*, 79(2):201–219, 2009.

[119] Kevin C Ryan. Dynamic interactions between forest structure and fire behavior in boreal ecosystems. *Silva Fennica*, 36(1):13–39, 2002.

[120] Thibaut Fréjaville, Thomas Curt, and Christopher Carcaillet. Tree cover and seasonal precipitation drive understorey flammability in alpine mountain forests. *Journal of Biogeography*, 43 (9):1869–1880, 2016.

[121] Lisa Warden, Matthias Moros, Thomas Neumann, Stephen Shennan, Adrian Timpson, Katie Manning, Martina Sollai, Lukas Wacker, Kerstin Perner, Katharina Häusler, et al. Climate induced human demographic and cultural change in northern europe during the mid-holocene. *Scientific Reports*, 7(1):1–11, 2017.

[122] Tatiana A Blyakharchuk, Nadja M Tchebakova, Elena I Parfenova, and Amber J Soja. Potential influence of the late holocene climate on settled farming versus nomadic cattle herding in the minusinsk hollow, south-central siberia. *Environmental Research Letters*, 9(6):065004, 2014.

[123] Boris Vannière, Olivier Blarquez, Damien Rius, E Doyen, Tim Brücher, Daniele Colombaroli, Simon Connor, Angelica Feurdean, Thomas Hickler, Petra Kaltenrieder, et al. 7000-year human legacy of elevation-dependent european fire regimes. *Quaternary Science Reviews*, 132:206–212, 2016.

[124] Marc Joris Metzger, Robert Gerald Henry Bunce, Rob HG Jongman, Caspar A Mücher, and John W Watkins. A climatic stratification of the environment of europe. *Global ecology and biogeography*, 14(6):549–563, 2005.

[125] Sandy P Harrison, Roberto Villegas-Diaz, Esmeralda Cruz-Silva, Daniel Gallagher, David Kesner, Paul Lincoln, Yicheng Shen, Luke Sweeney, Daniele Colombaroli, Adam Ali, et al. The reading palaeofire database: an expanded global resource to document changes in fire regimes from sedimentary charcoal records. *Earth System Science Data*, 14(3):1109–1124, 2022.

[126] Chiara Molinari, Veiko Lehsten, Richard HW Bradshaw, Mitchell J Power, Peter Harmand, Almut Arneth, Jed O Kaplan, Boris Vannière, and Martin T Sykes. Exploring potential drivers of e uropean biomass burning over the h olocene: a data-model analysis. *Global Ecology and Biogeography*, 22(12):1248–1260, 2013.

[127] Marco Zanon, Basil AS Davis, Laurent Marquer, Simon Brewer, and Jed O Kaplan. European forest cover during the past 12,000 years: a palynological reconstruction based on modern analogs and remote sensing. *Frontiers in plant science*, 9:253, 2018.

[128] William D Collins, Cecilia M Bitz, Maurice L Blackmon, Gordon B Bonan, Christopher S Bretherton, James A Carton, Ping Chang, Scott C Doney, James J Hack, Thomas B Henderson, et al. The community climate system model version 3 (ccsm3). *Journal of Climate*, 19(11):2122–2143, 2006.

[129] The NCAR Command Language. UCAR/NCAR/CISL/TDD, Boulder, Colorado, 2019. URL http://dx.doi.org/10.5065/D6WD3XH5. Version 6.6.2 [Software].

[130] Tyler W Davis, I Colin Prentice, Benjamin D Stocker, Rebecca T Thomas, Rhys J Whitley, Han Wang, Bradley J Evans, Angela V Gallego-Sala, Martin T Sykes, and Wolfgang Cramer. Simple process-led algorithms for simulating habitats (splash v. 1.0): robust indices of radiation, evapotranspiration and plant-available moisture. *Geoscientific Model Development*, 10(2):689–708, 2017.

[131] Patrick J Bartlein and Sarah L Shafer. Paleo calendar-effect adjustments in time-slice and transient climate-model simulations (paleocaladjust v1. 0): Impact and strategies for data analysis. *Geoscientific Model Development*, 12(9):3889–3913, 2019.

[132] Basil AS Davis, Simon Brewer, Anthony C Stevenson, and Joël Guiot. The temperature of europe during the holocene reconstructed from pollen data. *Quaternary Science Reviews*, 22 (15-17):1701–1716, 2003.

[133] I Colin Prentice, Joel Guiot, Brian Huntley, Dominique Jolly, and Rachid Cheddadi. Reconstructing biomes from palaeoecological data: a general method and its application to european pollen data at 0 and 6 ka. *Climate Dynamics*, 12(3):185–194, 1996.

[134] Jessie Woodbridge, Ralph M Fyfe, and Neil Roberts. A comparison of remotely sensed and pollen-based approaches to mapping europe's land cover. *Journal of Biogeography*, 41(11):2080–2092, 2014.

[135] Paula J Reimer, William EN Austin, Edouard Bard, Alex Bayliss, Paul G Blackwell, Christopher Bronk Ramsey, Martin Butzin, Hai Cheng, R Lawrence Edwards, Michael Friedrich, et al. The intcal20 northern hemisphere radiocarbon age calibration curve (0–55 cal kbp). *Radiocarbon*, 62(4):725–757, 2020.

[136] William R Peltier. Global glacial isostasy and the surface of the ice-age earth: the ice-5g (vm2) model and grace. *Annu. Rev. Earth Planet. Sci.*, 32:111–149, 2004.

[137] William R Peltier and Rosemarie Drummond. Rheological stratification of the lithosphere: A direct inference based upon the geodetically observed pattern of the glacial isostatic adjustment of the north american continent. *Geophysical Research Letters*, 35(16), 2008.

[138] Ian Harris, Timothy J Osborn, Phil Jones, and David Lister. Version 4 of the cru ts monthly high-resolution gridded multivariate climate dataset. *Scientific data*, 7(1):1–18, 2020.

[139] Robert J. Hijmans. *raster: Geographic Data Analysis and Modeling*, 2021. URL https://CRAN.R-project.org/package=raster. R package version 3.4-13.

[140] Hiroshi Akima and Albrecht Gebhardt. *akima: Interpolation of Irregularly and Regularly Spaced Data*, 2021. URL https://CRAN.R-project.org/package=akima. R package version 0.6-2.2.

[141] Chris D Clark, Jeremy C Ely, Richard CA Hindmarsh, Sarah Bradley, Adam Ignéczi, Derek Fabel, Colm Ó Cofaigh, Richard C Chiverrell, James Scourse, Sara Benetti, et al. Growth and retreat of the last british–irish ice sheet, 31 000 to 15 000 years ago: the britice-chrono reconstruction. *Boreas*, 51(4):699–758, 2022.

[142] Corey JA Bradshaw and Ian G Warkentin. Global estimates of boreal forest carbon stocks and flux. *Global and Planetary Change*, 128:24–30, 2015.

[143] Christopher Carcaillet, Martine Bouvier, Bianca Fréchette, Alayn C Larouche, and Pierre JH Richard. Comparison of pollen-slide and sieving methods in lacustrine charcoal analyses for local and regional fire history. *The Holocene*, 11(4):467–476, 2001.

[144] Laia Comas-Bru, Sandy P Harrison, Martin Werner, Kira Rehfeld, Nick Scroxton, Cristina Veiga-Pires, et al. Evaluating model outputs using integrated global speleothem records of climate change since the last glacial. *Climate of the Past*, 15(4):1557–1579, 2019.

[145] Jing. Li, John. Reisner, Hieu. Pham, Sigurdur. Olafsson, and Stephen B. Vardeman. Biclustering with missing data. *Information Sciences*, 510:304–316, 2020. URL www.scopus.com.

[146] John Reisner. *biclustermd: Biclustering with Missing Data*, 2021. URL https://CRAN.R-project.org/package=biclustermd. R package version 0.2.3.

[147] Catherine Loader. *locfit: Local Regression, Likelihood and Density Estimation*, 2020. URL https://CRAN.R-project.org/package=locfit. R package version 1.5-9.4.

[148] Ralph Fyfe, Neil Roberts, and Jessie Woodbridge. A pollen-based pseudobiomisation approach to anthropogenic land-cover change. *The Holocene*, 20(7):1165–1171, 2010.

[149] R Core Team. *R: A Language and Environment for Statistical Computing*. R Foundation for Statistical Computing, Vienna, Austria, 2021. URL https://www.R-project.org/.

[150] Tomislav Hengl, Markus G Walsh, Jonathan Sanderman, Ichsani Wheeler, Sandy P Harrison, and I Colin Prentice. Global mapping of potential natural vegetation: an assessment of machine learning algorithms for estimating land potential. *PeerJ*, 6:e5457, 2018.

[151] Bryan Shuman, Patrick Bartlein, Nathaniel Logar, Paige Newby, and Thompson Webb III. Parallel climate and vegetation responses to the early holocene collapse of the laurentide ice sheet. *Quaternary Science Reviews*, 21(16-17):1793–1805, 2002.

[152] R Scott Anderson, Douglas J Hallett, E Berg, Renata B Jass, Jaime L Toney, CS De Fontaine, and A DeVolder. Holocene development of boreal forests and fire regimes on the kenai lowlands of alaska. *The Holocene*, 16(6):791–803, 2006.

[153] Andre E Viau and Konrad Gajewski. Reconstructing millennial-scale, regional paleoclimates of boreal canada during the holocene. *Journal of Climate*, 22(2):316–330, 2009.

[154] Adam A Ali, Olivier Blarquez, Martin P Girardin, Christelle Hély, Fabien Tinquaut, Ahmed El Guellab, Verushka Valsecchi, Aurélie Terrier, Laurent Bremond, Aurélie Genries, et al. Control of the multimillennial wildfire size in boreal north america by spring climatic conditions. *Proceedings of the National Academy of Sciences*, 109(51):20966–20970, 2012.

[155] France Oris, Hugo Asselin, Walter Finsinger, Christelle Hély, Olivier Blarquez, Marie-Eve Ferland, Yves Bergeron, and Adam A Ali. Long-term fire history in northern quebec: implications for the northern limit of commercial forests. *Journal of Applied Ecology*, 51(3):675–683, 2014.

[156] Megan K Walsh, Cathy Whitlock, and Patrick J Bartlein. A 14,300-year-long record of fire–vegetation–climate linkages at battle ground lake, southwestern washington. *Quaternary Research*, 70(2):251–264, 2008.

[157] Olivier Blarquez, Julie Talbot, Jordan Paillard, Lyna Lapointe-Elmrabti, Nicolas Pelletier, and Christian Gates St-Pierre. Late holocene influence of societies on the fire regime in southern québec temperate forests. *Quaternary Science Reviews*, 180:63–74, 2018.

[158] Christopher Carcaillet and Pierre JH Richard. Holocene changes in seasonal precipitation highlighted by fire incidence in eastern canada. *Climate Dynamics*, 16(7):549–559, 2000.

[159] Stephen Shennan, Sean S Downey, Adrian Timpson, Kevan Edinborough, Sue Colledge, Tim Kerig, Katie Manning, and Mark G Thomas. Regional population collapse followed initial agriculture booms in mid-holocene europe. *Nature communications*, 4(1):1–8, 2013.

[160] Anneli Poska and Leili Saarse. Vegetation development and introduction of agriculture to saaremaa island, estonia: the human response to shore displacement. *The Holocene*, 12(5):555–568, 2002.

[161] Christin Jensen. The vegetation history of a coastal stone-age and iron-age settlement at 70°n, norway. *Vegetation history and archaeobotany*, 13(4):269–284, 2004.

[162] Tatiana A Blyakharchuk, Herb E Wright, Pavel S Borodavko, Willem Oscar van der Knaap, and Brigitta Ammann. Late glacial and holocene vegetational changes on the ulagan high-mountain plateau, altai mountains, southern siberia. *Palaeogeography, Palaeoclimatology, Palaeoecology*, 209(1-4):259–279, 2004.

[163] Nadja M Tchebakova, Elena Parfenova, and Amber J Soja. The effects of climate, permafrost and fire on vegetation change in siberia in a changing climate. *Environmental Research Letters*, 4(4):045013, 2009.

[164] Fahu Chen, Zicheng Yu, Meilin Yang, Emi Ito, Sumin Wang, David B Madsen, Xiaozhong Huang, Yan Zhao, Tomonori Sato, H John B Birks, et al. Holocene moisture evolution in arid central asia and its out-of-phase relationship with asian monsoon history. *Quaternary Science Reviews*, 27(3-4):351–364, 2008.

[165] Alexander A Prokopenko, Galina K Khursevich, Elena V Bezrukova, Mikhail I Kuzmin, Xavier Boes, Douglas F Williams, Svetlana A Fedenya, Nataliya V Kulagina, Polina P Letunova, and Anna A Abzaeva. Paleoenvironmental proxy records from lake hovsgol, mongolia, and a synthesis of holocene climate change in the lake baikal watershed. *Quaternary Research*, 68(1):2–17, 2007.

[166] Dieter Demske, Georg Heumann, Wojciech Granoszewski, Małgorzata Nita, Kazimiera Mamakowa, Pavel E Tarasov, and Hedi Oberhänsli. Late glacial and holocene vegetation and regional climate variability evidenced in high-resolution pollen records from lake baikal. *Global and Planetary Change*, 46(1-4):255–279, 2005.

[167] Jack Longman, Vasile Ersek, Daniel Veres, and Ulrich Salzmann. Detrital events and hydroclimate variability in the romanian carpathians during the mid-to-late holocene. *Quaternary Science Reviews*, 167:78–95, 2017.

[168] Martin Schumacher, Wolfram Schier, and Brigitta Schütt. Mid-holocene vegetation development and herding-related interferences in the carpathian region. *Quaternary International*, 415:253–267, 2016.

[169] Tuomo Wallenius. Major decline in fires in coniferous forests - reconstructing the phenomenon and seeking for the cause. *Silva Fennica*, 45(1), 2011.

[170] Jennifer L Clear, Chiara Molinari, and Richard HW Bradshaw. Holocene fire in fennoscandia and denmark. *International Journal of Wildland Fire*, 23(6):781–789, 2014.

[171] Frank Ian Woodward. *Climate and plant distribution*. Cambridge University Press, 1987.

[172] Hadley Wickham, Romain François, Lionel Henry, and Kirill Müller. *dplyr: A Grammar of Data Manipulation*, 2021. URL https://CRAN.R-project.org/package=dplyr. R package version 1.0.7.

[173] Hadley Wickham. *tidyr: Tidy Messy Data*, 2021. URL https://CRAN.R-project.org/package=tidyr. R package version 1.1.3.

[174] Hadley Wickham. Reshaping data with the reshape package. *Journal of Statistical Software*, 21 (12):1–20, 2007. URL http://www.jstatsoft.org/v21/i12/.

[175] Hadley Wickham. *stringr: Simple, Consistent Wrappers for Common String Operations*, 2019. URL https://CRAN.R-project.org/package=stringr. R package version 1.4.0.

[176] David Pierce. *ncdf4: Interface to Unidata netCDF (Version 4 or Earlier) Format Data Files*, 2019. URL https://CRAN.R-project.org/package=ncdf4. R package version 1.17.

[177] Roger Bivand, Tim Keitt, and Barry Rowlingson. *rgdal: Bindings for the 'Geospatial' Data Abstraction Library*, 2021. URL https://CRAN.R-project.org/package=rgdal. R package version 1.5-23.

[178] Edzer Pebesma. Simple Features for R: Standardized Support for Spatial Vector Data. *The R Journal*, 10(1):439–446, 2018. doi: 10.32614/RJ-2018-009. URL https://doi.org/10.32614/RJ-2018-009.

[179] Original S code by Richard A. Becker, Allan R. Wilks. R version by Ray Brownrigg. Enhancements by Thomas P Minka, and Alex Deckmyn. *maps: Draw Geographical Maps*, 2018. URL https://CRAN.R-project.org/package=maps. R package version 3.3.0.

[180] Deepayan Sarkar. *Lattice: Multivariate Data Visualization with R*. Springer, New York, 2008. URL http://lmdvr.r-forge.r-project.org. ISBN 978-0-387-75968-5.

[181] Andy South. *rnaturalearth: World Map Data from Natural Earth*, 2017. URL https://CRAN.R-project.org/package=rnaturalearth. R package version 0.1.0.

[182] Andy South. *rnaturalearthdata: World Vector Map Data from Natural Earth Used in 'rnaturalearth'*, 2017. URL https://CRAN.R-project.org/package=rnaturalearthdata. R package version 0.1.0.

[183] Roger Bivand and Colin Rundel. *rgeos: Interface to Geometry Engine - Open Source ('GEOS')*, 2020. URL https://CRAN.R-project.org/package=rgeos. R package version 0.5-5.

[184] Roger Bivand and Nicholas Lewin-Koh. *maptools: Tools for Handling Spatial Objects*, 2021. URL https://CRAN.R-project.org/package=maptools. R package version 1.1-1.

[185] Erich Neuwirth. *RColorBrewer: ColorBrewer Palettes*, 2014. URL https://CRAN.R-project.org/package=RColorBrewer. R package version 1.1-2.

[186] Sigbert Klinke. *plot.matrix: Visualizes a Matrix as Heatmap*, 2021. URL https://CRAN.R-project.org/package=plot.matrix. R package version 1.6.

[187] William Revelle. *psych: Procedures for Psychological, Psychometric, and Personality Research*. Northwestern University, Evanston, Illinois, 2021. URL https://CRAN.R-project.org/package=psych. R package version 2.1.9.

[188] Ben Hamner and Michael Frasco. *Metrics: Evaluation Metrics for Machine Learning*, 2018. URL https://CRAN.R-project.org/package=Metrics. R package version 0.1.4.

[189] Robert M. Hirsch and Laura A. De Cicco. *User guide to Exploration and Graphics for RivEr Trends (EGRET) and dataRetrieval: R packages for hydrologic data*, chapter A10. U.S. Geological Survey, Reston, VA, 2015. URL https://pubs.usgs.gov/tm/04/a10/.

[190] A Malcolm Gill. Fire and the australian flora: a review. *Australian forestry*, 38(1):4–25, 1975.

[191] James K Agee. *Fire ecology of Pacific Northwest forests*. Island press, 1996.

[192] NOAA US Department of Commerce. Fire weather faq. https://www.weather.gov/jan/fireweatherfaq#:~:text=Fire%20weather%20is%20the%20use,fire%20growth%20and%20smoke%20dispersion. [Online; accessed 3-March-2022].